P

PALEOINTENSITY: ABSOLUTE DETERMINATIONS USING SINGLE PLAGIOCLASE CRYSTALS

Single plagioclase crystals can contain minute magnetic inclusions, capable of recording and preserving a thermoremanent magnetization. Thellier paleointensity experiments using plagioclase feldspars from a historic lava on Hawaii provide a benchmark for the method. The comparison of rock magnetic and Thellier data from feldspars and whole rocks from older lavas indicate that the feldspars are less susceptible to experimental alteration. This resistance is likely related to the lack of clays and protection of the magnetic minerals by the encasing silicate crystals.

Thellier data sets based on single plagioclase crystals are available from continental flood basalt provinces formed during the Cretaceous Normal Polarity Superchron. These data suggest paleomagnetic dipole moments of approximately 12×10^{22} A m^2, significantly higher than the average paleointensity thought to characterize times of frequent geomagnetic reversals. A correlation between intervals of low-reversal frequency and high-geomagnetic field strength is supported, as seen in some numerical simulations of the geodynamo.

On longer timescales, the magnetization held by plagioclase and other silicate crystals can be used to investigate the Proterozoic and Archean field. Data from plagioclase crystals separated from dikes demonstrate how outstanding questions related to growth of the solid inner core and the magnetic field of the young Earth can be addressed in future investigations.

Whole rock paleointensity analyses

The Thellier double heating method (Thellier and Thellier, 1959) is arguably the most rigorous means of learning about past field strength. But when applied to whole rocks, does this approach insure that the past field strength is accurately recovered? In tests using historic lavas, the Thellier method clearly works well because it retrieves the known field strength. Recent studies of lavas formed during the last 5 Ma have applied rigorous selection criteria to detect experimental alteration and nonideal behavior related to magnetic mineral domain state (e.g., Valet, 2003). But in older rocks, the effects of weathering are important. Clay minerals begin to form a progressively larger portion of a whole rock's matrix. Magnetic mineral phenocrysts undergo low-temperature oxidation.

During the successive heating steps required by the Thellier method, fine-grained magnetic minerals can form from clays (Cottrell and Tarduno, 2000). At relatively high, temperature treatments the alteration can be obvious; it is seen in experimental checks when a partial thermoremanent magnetization (TRM) is imparted at a lower temperature to check for the growth of magnetic minerals. The initial stages of alteration, however, are subtle and can be difficult to detect.

Low-temperature oxidation, or maghemitization, results in a fundamental change in the nature of the magnetization (e.g., Özdemir and Dunlop, 1985). Rather than a TRM, the basis of the Thellier approach, the magnetization can become a partial or complete chemical remanent magnetization (CRM). The accuracy of CRM in preserving the original geomagnetic field strength is unclear (Dunlop and Özdemir, 1997).

There are other reasons for concern about paleointensity estimates derived from older rocks. Many of the virtual dipole moments based on Thellier data from the whole rock and submarine glass samples are similar to values that characterize younger geomagnetic excursions and reversal transitions (Tarduno and Smirnov, 2004). Taken at face value, these data imply that the field has been extraordinarily energetic during the last 10 Ma. But factors that could change the magnetic field energy are generally associated with much longer timescales. Natural and experimental alteration of lavas and submarine basaltic glass tends to lower paleointensity values (Smirnov and Tarduno, 2003), suggesting that the apparent difference in field strength before and after 10 Ma is an artifact.

These issues motivate a search for natural paleomagnetic recorders that are less susceptible to alteration in nature and in the laboratory. Single plagioclase crystals are one such alternative recorder of geomagnetic field history.

Plagioclase feldspar paleointensity analyses

Transmission electron microscopy (TEM) analyses of magnetic extracts from plagioclase separated from basaltic lavas indicate that they can contain equal to slightly elongated magnetic particles 50–350 nm in size (Cottrell and Tarduno, 1999, 2000) (see Figure P1). Studies of the directional dependence of magnetic hysteresis indicate little anisotropy in the plagioclase crystals that could adversely affect Thellier analyses (Cottrell and Tarduno, 1999, 2000).

Unblocking temperatures indicate that the magnetic carriers in plagioclase have compositions that match those of the whole rock. Thermal demagnetization through warming of a saturation isothermal remanent magnetization acquired at low temperature has shown the presence of a blurred Verwey transition (the transition from cubic to monoclinic crystalline symmetry; Verwey, 1939) in plagioclase crystals separated from Cretaceous basalts of the Arctic (Tarduno *et al.*, 2002) (see Figure P1). These data, together with the thermal unblocking

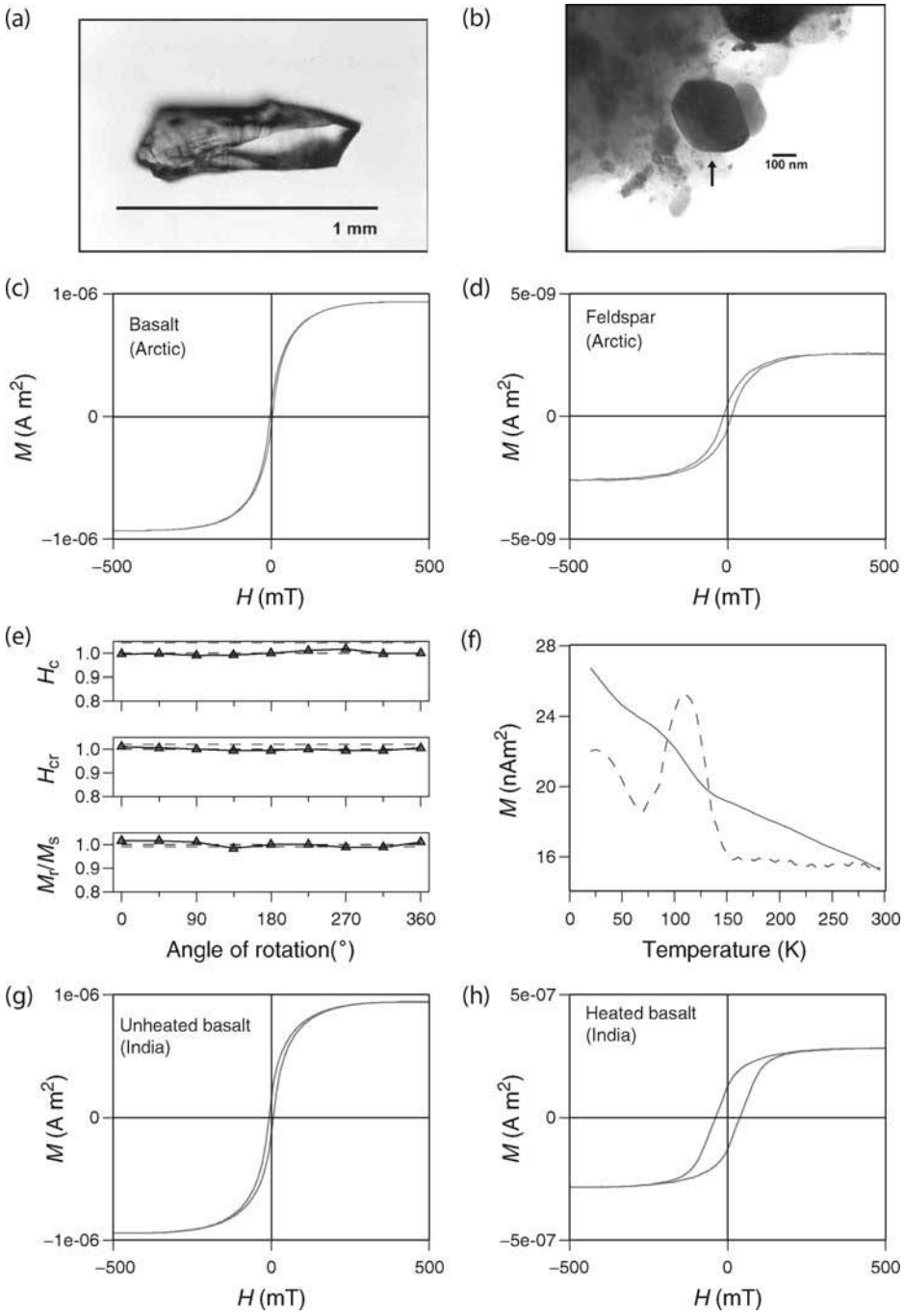

Figure P1 Optical, transmission electron microscope (TEM) and rock magnetic analyses of whole rocks, plagioclase crystals and magnetic separates. (a-f) Examples from the Strand Fiord basalts of the high Arctic after Tarduno *et al.* (2002). (g, h) Examples from the Rajmahal Traps of eastern India after Cottrell and Tarduno (2000). (a) Typical plagioclase crystal used for rock magnetic and paleointensity experiments. (b) TEM image of a magnetic separate from a plagioclase crystal. (c,d) Magnetic hysteresis data (slope corrected) for a whole rock basalt sample and plagioclase feldspar. In general, plagioclase crystals show single domain to pseudo-single domain behavior, while whole rocks display pseudo-single to multidomain characteristics. The former are better suited for Thellier paleointensity analyses. (e) Normalized hysteresis parameters versus rotation angle measured on a plagioclase crystal. The crystal was rotated by 45° increments on the stage of a Princeton Measurements Alternating Gradient Force Magnetometer parallel (solid line and triangles) and perpendicular (dashed line; only mean shown) P1 probes. Abbreviations: M_r/M_s, saturation remanence/saturation magnetization ratio; H_{cr} coercivity of remanence; H_c, coercivity. The lack of systematic variations of these parameters indicates that anisotropy is not a significant concern for Thellier paleointensity experiments. (f) Warming curve of a magnetization (solid line) acquired by a plagioclase crystal at 20 K in a 2.5 T field. Dotted line is the inverse of the derivative. (g,h) Slope corrected magnetic hysteresis curves for unheated and heated whole rock samples. The curve for the heated sample documents the growth of a fine-grained magnetic phase. The heating increments applied were those of a typical Thellier experiment. Magnetic hysteresis curves for plagioclase crystals did not show significant changes after heating (see discussion in Cottrell and Tarduno, 2000).

characteristics and TEM observations, further suggest the plagioclase crystals contain magnetic inclusions of composition similar to that of magnetic grains in the whole rock. In the case of the low-temperature data, the carrier is likely a low Ti titanomagnetite. These observations also suggest that the magnetic particles are inclusions rather than exsolved magnetic particles (Cottrell and Tarduno, 1999, 2000). The latter, which are characteristic of plagioclase in slowly cooled plutonic rocks, typically have end-member mineralogies and distinct shapes, most notably the magnetic "needles", tens of millimeters long, that are sometimes seen oriented along crystallographic axes (e.g., Davis, 1981).

In a test of the method, Thellier analyses of plagioclase crystals separated from a 1955 flow from Kilauea in Hawaii yielded paleointensity estimates that agreed with values reported in detailed comparisons of paleointensity methods based on whole rocks (Coe and Grommé, 1973) and from magnetic observatory data (Cottrell and Tarduno, 1999). The demagnetization of an oriented plagioclase from a Cretaceous lava flow of the Rajmahal Traps demonstrated that the plagioclase recorded the same paleomagnetic record as the whole rock (Cottrell and Tarduno, 2000).

Further comparisons of rock magnetic data from whole rock samples and plagioclase crystals taken from a Rajmahal lava flow demonstrated that the plagioclase crystals were less altered by Thellier heatings (Cottrell and Tarduno, 2000). Specifically, magnetic hysteresis data from heated whole rock samples indicated the formation of a fine-grained magnetic phase; this behavior was not seen in the plagioclase crystals (see Figure P1). This difference in rock magnetic behavior with heating paralleled differences seen in the fidelity and absolute values of paleointensity data. Although whole rock samples meeting paleointensity reliability criteria (e.g., Coe, 1967) yielded paleointensity values that were within error of those derived from single plagioclase crystals, such samples were rare. In general, the whole rocks seldom met reliability criteria and yielded low nominal paleointensity values. The differences can be attributed to the formation of fine-grained magnetite from clays in the groundmass of whole rock samples, resulting in the anomalous acquisition of TRM during Thellier experiments (and a bias toward low values).

Paleointensity during the Cretaceous Normal Polarity Superchron

The experimental alteration, nonideal behavior, and associated high rates of sample reject that typify the Thellier method as applied to whole rocks have generally resulted in a piecemeal approach to the definition of the past geomagnetic field. Directional and paleointensity data are seldom derived from the same rocks. The ability to derive paleointensity values from plagioclase crystals from long lava sequences provides the chance to look at all parts of the time-averaged field. Examining the potential relationships between geomagnetic reversal frequency, secular variation, field morphology and paleointensity is still a daunting task. But if relationships exist, they should be best expressed during superchrons, intervals tens of millions of years long with a few (or no) reversals.

Several continental flood basalt provinces were formed during the Cretaceous Normal Polarity Superchron; these provide an opportunity to gain a more complete view of the past geomagnetic field. For example, Thellier paleointensity analyses of single plagioclase have been derived from distinct lava units of the Rajmahal Traps. The term "lava unit" is used because sometimes it is necessary to combine results from adjacent lava flows that could have been erupted in a very short time. These units were selected from a larger paleomagnetic data set so that they span secular variation. This was gauged in two ways. First, the stratigraphic position of the lava units was considered. Second, the angular dispersion of paleomagnetic directions of the select units (derived from analyses of whole rock samples) simulated that of a complete sampling of the lava sequence. The data allow the calculation of a mid-Cretaceous paleomagnetic dipole moment. The resulting value of $12.5 \pm 1.4 \times 10^{22}$ A m^2 (Tarduno *et al*., 2001) is higher than the present-day field, or estimates of the long term average field during the last 200 Ma.

A similar study has been conducted on lavas of the high Canadian Arctic, which were also erupted during the Cretaceous Normal Polarity Superchron. Plagioclase feldspars separated from these lavas have also yielded Thellier paleointensity estimate from distinct lava units. As in the case of the Rajmahal Traps, the units are thought to average secular variation because geological indicators show the passage of time, and the angular dispersion of paleomagnetic directions recorded by whole rock samples matches that of a larger data set that spans the entire sequence (Tarduno *et al*., 2002). The paleomagnetic dipole moment of $12.7 \pm 0.7 \times 10^{22}$ A m^2 suggested by these data agrees with the value from the Rajmahal Traps and indicates that high paleointensity of the latter rocks was not an isolated event within the Cretaceous Normal Polarity Superchron (see Figure P2) . The data from the Rajmahal Traps and Arctic basalts support a correlation between high field strength and low reversal frequency, as suggested in early models (Cox, 1968; see also discussion by Banerjee, 2001) and in more recent numerical simulations of the geodynamo (Glatzmaier *et al*., 1999).

Precambrian field strength

Mafic dikes of Proterozoic to Archean age are exposed on several continents. These contain feldspars that could carry magnetic inclusions and hence they are potential geomagnetic field recorders. This may provide a means of defining the field during a time interval that may have seen the onset of solid inner core growth. To explore this possibility, Smirnov *et al*. (2003) studied the 2.45 Ga Burakovka intrusion of the Karelian Craton (Russia). Thin mafic border dikes were sampled to minimize the influence of cooling rate. Clear feldspars were selected for study; in other Proterozoic-Archean dike provinces clouded feldspars reflecting exsolution are common (Halls and Zhang, 1998). Magnetic hysteresis parameters indicate multidomain-like behavior of whole rock samples and pseudosingle to single domain (SD) behavior for plagioclase crystals separated from the Karelian dikes. Whole rock samples also show a small anisotropy as recorded by systematic variations in magnetic hysteresis data, presumably recording a flow fabric within the dikes. No significant anisotropy was observed in the plagioclase crystals. The latter observation is important because it indicates that there is not a preferred alignment of elongated particles in the feldspars that could bias TRM acquisition in Thellier experiments.

Transmission electron microscopy analyses suggest that the magnetic inclusions in the plagioclase are equal to slightly elongated and range in size between 50 and 250 nm. Thermal demagnetization data of a saturation remanence imparted on single plagioclase crystals at 10 K are characterized by a well-defined Verwey transition at ~120 K, indicating the presence of stoichiometric magnetite, similar to that reported from whole rock samples.

These rock magnetic data demonstrate the feasibility of the single plagioclase paleointensity approach as applied to select Proterozoic-Archean rocks. Results from only four dikes are available to date from Karelia and it cannot be expected that these adequately record secular variation. Nevertheless, the Thellier paleointensity data are within the range of modern field values. Secular variation and field morphology during this Proterozoic-Archean interval also look amazingly similar to that of the last 5 Ma (Smirnov and Tarduno, 2004).

Discussion and summary

Prévot *et al*. (1990) concluded that geomagnetic reversal rate and paleointensity are decoupled. The contrast between this interpretation and that proposed here arises from differences in data selection. Only a few paleointensity results from rocks older than 10 Ma are based on multiple, independent cooling units that span significant secular variation. Standard paleointensity criteria exclude those lavas with larger multidomain magnetic carriers. A more widespread factor limiting the utility of lavas is weathering. The formation of clays can ultimately

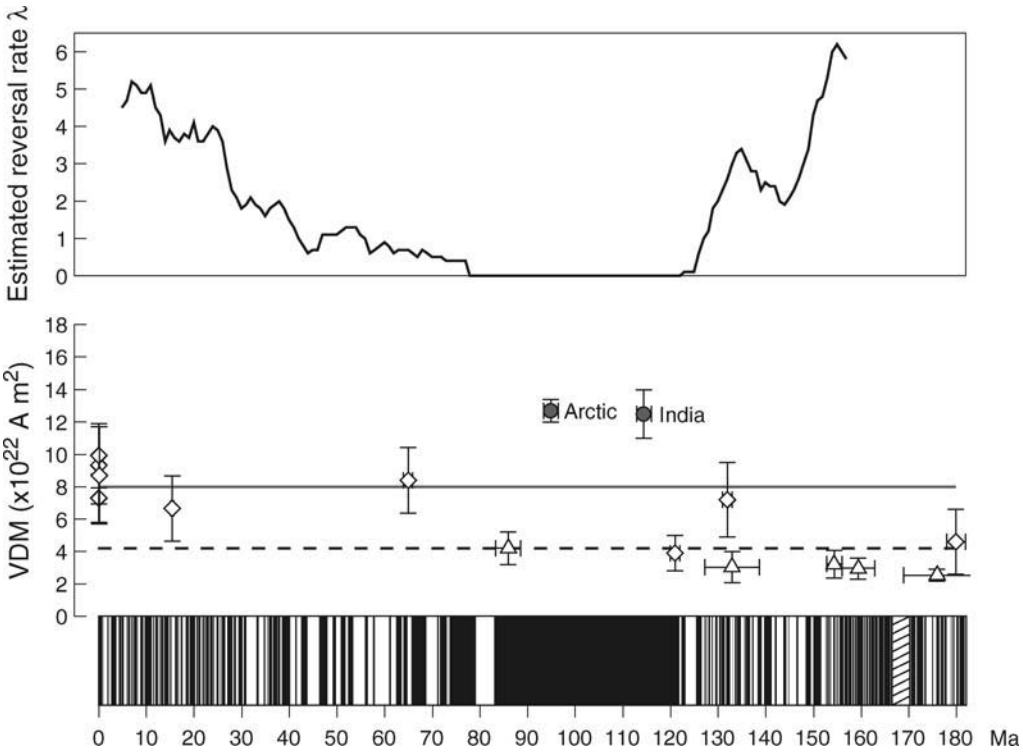

Figure P2 Geomagnetic reversal timescale, select Thellier results (1σ uncertainties shown), and reversal rate (based on a 10-Ma sliding window). Data sources are those selected by Tarduno *et al.* (2001, 2002), with the addition of a new data set from Goguitchaichvili *et al.* (2002). Only studies based on greater than 25 results shown. Data types: triangles, baked contacts; diamonds, basalt whole rocks; circles, plagioclase crystals (Tarduno *et al.*, 2001, 2002). Dashed horizontal line, a proposed mean Cretaceous-Cenozoic value based on Thellier analysis of submarine basaltic glass (Juarez *et al.*, 1998); Solid horizontal line, modern field intensity.

result in the formation of new magnetic minerals during Thellier experiments. In addition, magnetic mineral phenocrysts in the groundmass are transformed by low-temperature oxidation, and CRMs replace TRMs. Some of these effects lead to obvious failures of experimental reliability tests. Others are subtler that have probably led to a bias toward underestimates of field strength.

Because of these limitations, it is premature to apply statistical treatments to the entire basalt virtual dipole moment data set (e.g., Heller *et al.*, 2002) to draw conclusions on the geodynamo. Although there are high-resolution, time-averaged data sets from older lavas (e.g., Kosterov *et al.*, 1997) natural and laboratory alteration will fundamentally limit progress in understanding long-term paleointensity history. This is the prime motivation for a continued pursuit of plagioclase-based Thellier analyses.

Plagioclase feldspar separated from lavas contains minute magnetic inclusions, which appear to have been protected from weathering. Thellier analyses using such crystals have been benchmarked using historic lava. Subsequent tests show that plagioclase crystals are less susceptible to experimental alterations than whole rocks. Because the plagioclase feldspars can be collected from long basalt sequences, they afford a means to obtain joint paleointensity and secular variation data. This further provides the opportunity to investigate relationships between the frequency of geomagnetic reversals and the morphology, secular variation and intensity of Earth's magnetic field. These relationships should be best expressed during superchrons.

Available data from Thellier analyses of plagioclase crystals, coupled with paleomagnetic data from lavas covering various latitude bands, indicate that the time-averaged field during the Cretaceous Normal Polarity Superchron was remarkably strong and stable. A high-field intensity during the Cretaceous Normal Polarity Superchron has also been reported from continued analyses of submarine basaltic glass (Tauxe and Staudigel, 2004). The field was also overwhelmingly dipolar, lacking significant octupole components (Tarduno *et al.*, 2002). These observations suggest that the basic features of the geomagnetic field are intrinsically related. Superchrons may reflect times when the nature of core-mantle boundary heat flux allows the geodynamo to operate at peak efficiency.

Thellier analyses of plagioclase separated from lavas can be used to further examine the reversing field, including times such as the Late Jurassic of peak reversal frequency (McElhinny and Larson, 2003). The approach can also be used to examine the Permian-Carboniferous Kiaman Reversed Polarity Superchron. The Precambrian history of the geomagnetic field bracketing inner core growth is relatively unexplored. Approaches utilizing rigorous Thellier analyses applied to single plagioclase crystals, and other single silicate grains, hold significant promise for revealing this history.

John A. Tarduno, Rory D. Cottrell, and Alexei V. Smirnov

Bibliography

Banerjee, S.K., 2001. When the compass stopped reversing its poles. *Science*, **291**: 1714–1715.

Coe, R.S., 1967. The determination of paleointensities of the Earth's magnetic field with emphasis on mechanisms which could cause nonideal behaviour in Thelliers method. *Journal of Geomagnetism and Geoelectricity*, **19**: 157–179.

Coe, R.S., and Grommé, C.S., 1973. A comparison of three methods of determining geomagnetic paleointensities. *Journal of Geomagnetism and Geoelectricity*, **25**: 415–435.

Cottrell, R.D., and Tarduno, J.A., 1999. Geomagnetic paleointensity derived from single plagioclase crystals. *Earth and Planetary Science Letters*, **169**: 1–5.

Cottrell, R.D., and Tarduno, J.A., 2000. In search of high fidelity geomagnetic paleointensities: A comparison of single crystal and whole rock Thellier-Thellier analyses. *Journal of Geophysical Research*, **105**: 23579–23594.
Cox, A., 1968. Lengths of geomagnetic polarity intervals. *Journal of Geophysical Research*, **73**: 3247–3260.
Davis, K.E., 1981. Magnetite rods in plagioclase as the primary carrier of stable NRM in ocean floor gabbros. *Earth and Planetary Science Letters*, **55**: 190–198.
Dunlop, D.J., and Özdemir, Ö., 1997. *Rock Magnetism, Fundamentals and Frontiers*, Cambridge: Cambridge University Press, 573 pp.
Glatzmaier, G.A., Coe, R.S., Hongre, L., and Roberts, P.H., 1999. The role of the Earth's mantle in controlling the frequency of geomagnetic reversals. *Nature*, **401**: 885–890.
Goguitchaichvili, A., Alva-Valdivia, L.M., Urrutia, J., and Morales, J., 2002. On the reliability of Mesozoic Dipole Low: New absolute paleointensity results from Paraná flood basalts (Brazil). *Geophysical Research Letters*, **29**: 10.1029/2002GL015242.
Halls, H.C., and Zhang, B.X., 1998. Uplift structure of the southern Kapuskasing zone from 2.45 Ga dike swarm displacement. *Geology*, **26**: 67–70.
Heller, R., Merrill, R.T., and McFadden, P.L., 2002. The variation of intensity of earth's magnetic field with time. *Physics of the Earth and Planetary Interiors*, **131**: 237–249.
Juarez, T., Tauxe, L., Gee, J.S., and Pick, T., 1998. The intensity of the Earth's magnetic field over the past 160 million years. *Nature*, **394**: 878–881.
Kosterov, A.A., Prévot, M., and Perrin, M., 1997. Paleointensity of the Earth's magnetic field in the Jurassic: New results from a Thellier study of the Lesotho Basalt, southern Africa. *Journal of Geophysical Research*, **102**: 24859–24872.
McElhinny, M.W., and Larson, R.L., 2003. Jurassic dipole low defined from land and sea data. *Eos, Transactions of the American Geophysical Union*, **84**: 362–366.
Özdemir, Ö., and Dunlop, D.J., 1985. An experimental study of chemical remanent magnetizations of synthetic monodomain titanomaghemites with initial thermoremanent magnetizations. *Journal of Geophysical Research.*, **90**: 11513–11523.
Prévot, M., Derder, M.E., McWilliams, M.O., and Thompson, J., 1990. Intensity of the Earth's magnetic field: Evidence for a Mesozoic dipole low. *Earth and Planetary Science Letters*, **97**: 129–139.
Smirnov, A.V., and Tarduno, J.A., 2003. Magnetic hysteresis monitoring of Cretaceous submarine basaltic glass during Thellier paleointensity experiments: Evidence for alteration and attendant low field bias. *Earth and Planetary Science Letters*, **206**: 571–585.
Smirnov, A.V., Tarduno, J.A., and Pisakin, B.N., 2003. Paleointensity of the early geodynamo (2.45 Ga) as recorded in Karelia: a single crystal approach. *Geology*, **31**: 415–418.
Smirnov, A.V., and Tarduno, J.A., 2004. Secular variation of the Late Archean-Early Proterozoic geodynamo. *Geophysical Research Letters*, **31**, L16607.
Tarduno, J.A., Cottrell, R.D., and Smirnov, A.V., 2001. High geomagnetic field intensity during the mid-Cretaceous from Thellier analyses of single plagioclase crystals. *Science*, **291**: 1779–1783.
Tarduno, J.A., Cottrell, R.D., and Smirnov, A.V., 2002. The Cretaceous Superchron Geodynamo: Observations near the tangent cylinder. *Proceedings of the National Academy of Sciences.* **99**: 14020–14025.
Tarduno, J.A., and Smirnov, A.V., 2004. The paradox of low field values and the long-term history of the geodynamo. In Channell, J.E.T., Kent, D.V., Lowrie, W., and Meert, J.G., (eds.), *Timescales of the Paleomagnetic Field.* American Geophysical Union Geophysical Monograph Series 145. Washington, DC: American Geophysical Union.
Tauxe, L., and Staudigel, H., 2004. Strength of the geomagnetic field in the Cretaceous Normal Superchron: New data from submarine basaltic glass of the Troodos Ophiolite. *Geochemistry, Geophysics and Geosystems*, **5**, Q02H06.
Thellier, E., and Thellier, O., 1959. Sur l'intensité du champ magnétique terrestre dans le passé historique et géologique. *Annales Geophysicae*, **15**: 285–376.
Valet, J.P., 2003. Time variations in geomagnetic intensity. *Reviews of Geophysics*, **41**: 1004.
Verwey, E.J.W., 1939. Electronic conduction of magnetite (Fe_3O_4) and its transition point at low-temperature. *Nature*, **44**: 327–328.

Cross-references

Geodynamo, Numerical Simulations
Geomagnetic Dipole Field
Inner Core
Magnetization, Thermoremanent (TRM)
Paleomagnetism

PALEOINTENSITY, ABSOLUTE, TECHNIQUES

Introduction

The unique possibility to extract the ancient field intensity from magnetic remanence of rocks is to duplicate the acquisition of magnetization by laboratory experiments in presence of a field with a known intensity. This requires a precise knowledge of the mechanisms that govern the magnetization, which is actually the major difficulty inherent to the paleointensity experiments. Acquisition of remanence by strong magnetic fields does not concern natural rocks because the geomagnetic field has a weak intensity (unless they are affected by lightning but this has no interest for paleomagnetism). Another way of magnetizing rocks is by thermal activation, which leads to rotation of some magnetic moments in the direction of the field. The natural magnetization relevant from this process is called a thermoremanent magnetization (TRM). Thermoremanence is acquired by most igneous rocks during cooling from above the Curie temperature (T_c) in the presence of the Earth's magnetic field. Magnetic relaxation, in which remanent magnetization of an assemblage of magnetic grains decays with time, is the most straightforward effect of thermal activation. As temperature decreases through a critical temperature called "blocking temperature" (T_b), an individual magnetic grain experiences a dramatic increase in relaxation time, which will continue down to room temperature. Thus the orientation of the magnetic moment can remain stable at the surface temperature and it will be resistant to effects of magnetic fields after original cooling. Depending on specific parameters inherent to the grain, this magnetic memory can be preserved for billions of years. Rock specimens contain many magnetic grains that can have different characteristics (size, shape etc.) and are thus frequently associated with a distribution of blocking temperatures T_b) from a few tens of degrees up to T_c of the magnetic mineral carrying the magnetization.

Thellier-Thellier technique and derivatives

A very specific characteristic of the total TRM is that it can be separated into the successive magnetizations that were acquired in distinct temperature intervals. For example, TRM of an igneous rock containing magnetite can be broken into portions acquired within successive windows of blocking temperatures from its Curie temperature (T_c) of 580°C down to room temperature. The portion of TRM blocked in any particular T_b window is referred to as "partial TRM," abbreviated pTRM. The total TRM is the vector sum of the pTRMs contributed by all blocking temperature windows. The Individual pTRMs depend only on the magnetic field during cooling through their respective T_b intervals and are not affected by magnetic fields applied during

cooling through lower temperature intervals. This is the law of additivity of pTRM, which is essential for paleointensity experiments.

Indeed, as described above, paleointensity experiments rely on a direct comparison between thermal demagnetization of the natural remanent magnetization (NRM, original magnetization that was acquired during cooling of the material) and acquisition of laboratory partial thermoremanent magnetization (pTRM) in presence of a known field. In principle, NRM and TRM of single domain grains of magnetite retain the same proportionality in the applied field over the entire temperature spectrum (Dunlop and Özdemir, 1993). Thus the NRM/TRM ratio must remain constant. In the opposite situation it is impossible to perform suitable experiments of paleointensity because the response of magnetization to the field is not the same in the laboratory than it was during the initial cooling of the rock. In most cases, this is caused by changes in magnetic mineralogy that either altered the natural remanent magnetization (NRM) or which were produced during the laboratory experiments.

The initial and unique reliable technique for absolute paleointensity was proposed and experimented by Thellier and Thellier (1959). Basically the experiment involves a first heating and cooling of the sample in a known field at say 120C followed by measurement of the total magnetization $M_1 = +\text{TRM}\ (0–120°\text{C}) + \text{NRM}\ (120°\text{C} - T_c)$. The second heating and cooling are performed in presence of a field in the opposite direction and the total magnetization is thus $M_2 = -\text{TRM}\ (0–120°\text{C}) + \text{NRM}\ (120°\text{C} - T_c)$. The residual NRM is obtained by vectorial subtraction (M_1-M_2) while the TRM is given after substitution of the NRM. This operation is repeated at increasing temperatures up to T_c.

Coe (1967) modified the original Thellier protocol and proposed to demagnetize first the NRM in zero field and then to remagnetize the sample. However, measuring the NRM first does not allow one to detect remagnetization components that could be produced during the subsequent heating at the same temperature in presence of the field and carried by grains with high blocking temperatures. In order to solve this problem (see Figure P3), it is preferable to impart the TRM before heating the sample in zero field (Aitken *et al*., 1988; Valet *et al*., 1998; Valet, 2003). The two techniques have their own advantages.

The method of determining the final field value is to calculate the slope of an "Arai" plot (Nagata, 1963), which depicts the amount of NRM lost as a function of pTRM gained for each successive temperature interval (in principle both should keep the same proportion for every temperature interval). The paleointensity is simply obtained after multiplying the slope by the field intensity applied during the experiments. The basic assumption inherent to Thellier experiments is constant proportionality between the NRM lost and the TRM gained after each heating step. Any departure from this behavior cannot be accepted. Unfortunately this ideal situation is not that frequent and linear diagrams over a very wide range of temperatures represent rarely more than 20%–30% of the samples. It is certainly arbitrary to rely on a specific segment of temperature because the quality of the determinations is linked to the amount of NRM involved. We can only be confident if a paleointensity estimate has been derived from a single straight line involving low (say <350°C) and high temperatures (beyond the domain of viscous components). Several indices have been defined (Coe *et al*., 1978) to evaluate the quality of the determinations. They rely on the percent of initial magnetization involved in the segment selected for calculation, quality of the fit and dispersion of the data points.

Limits imposed by magnetomineralogical changes

Apart from their time-consuming aspect, paleointensity experiments are frequently affected by remagnetization caused by alteration of magnetic minerals during heating. It is thus not only essential to detect these changes during the experiments but also to improve the success rate by selecting appropriate samples. Concerning the first aspect, Thellier and Thellier (1959) introduced the pTRM checks that test for duplication of a TRM at one or several previous temperatures. If the new value is different from the previous one, then the magnetic grains were affected during the previous heating steps at higher temperatures. Unfortunately, the pTRM checks increase the number of heatings, making the full experiment more time-consuming, but they are unavoidable and essential to detect alteration. It is quite justified to consider that the absence of pTRM checks unvalidates the quality of a paleointensity experiment.

In some cases remagnetization can produce grains with blocking temperatures higher than the last heating step. In this case, the NRM itself can be affected and partly lost but the corresponding changes will not necessarily be detected by pTRM checks. There is linear relation between the NRM and the TRM; but the directions of the NRM fail to go through the origin of the demagnetization diagrams when plotted in sample coordinates. This is caused by remagnetization in the field direction of the oven. Kosterov and Prévot (1998) made the point that irreversible changes due to alteration can occur even at moderate temperatures. This was observed by measuring hysteresis loops after different heating steps following a previous suggestion by Haag *et al*. (1995). These changes were not always detected by standard pTRM checks, which again emphasizes the need for multiple and complementary verifications, at least for a limited number of samples per

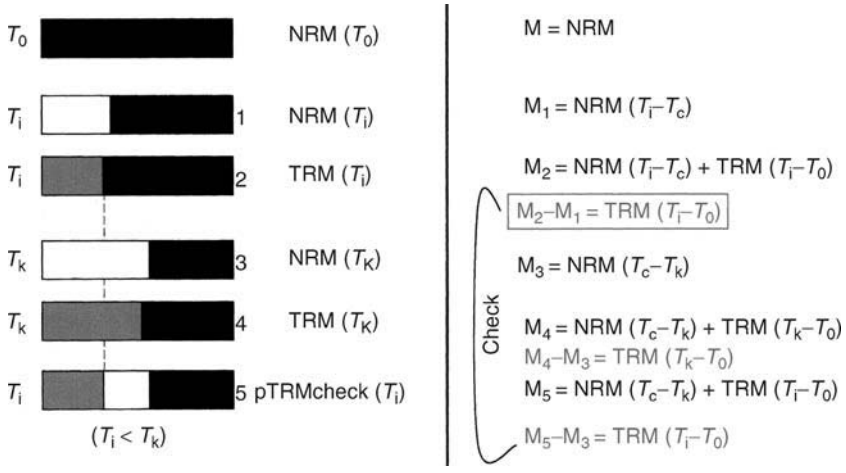

Figure P3 Schematic representation of the procedure for a Thellier-Thellier experiment according to the "modified" Coe protocol. In this case, a TRM is performed first instead of heating in zero field (see text). Black (gray) bars show temperature intervals with remaining NRM (TRM). White bars are for zero magnetization.

lava flow. McCLelland and Briden (1996) and Valet *et al*. (1996) proposed to detect this problem by adding a third heating in zero field, which is particularly appropriate and efficient in the case of the modified Coe version. Indeed if the NRM was affected during the previous heating in presence of field, the repeated experiment will evidently result into a different vector. This approach is possible but more delicate with the standard Thellier-Thellier procedure.

Preselection of the specimens using nontime-consuming techniques rapidly became a critical matter. The problem is that such experiments must necessarily be conducted on adjacent specimens (but from the same core) keeping in mind that there is always a little risk that inhomogeneous magnetic characteristics alter the quality of the selection. Thermomagnetic analyses (measurement of progressive loss of induced susceptibility (K) or saturation remanent magnetization (J_{rs}) while heating up to Curie temperature and its recovery during subsequent cooling) provide useful information about the magnetic minerals and their evolution upon heating. Magnetomineralogical changes have a direct consequence on these two parameters and produce irreversible heating and cooling curves. This test has thus proved very efficient to rule out inappropriate samples, but it does not warranty that those samples which pass the test will necessarily be suitable for paleointensity experiments.

Problems inherent to multidomain grains

Another aspect to consider is the behavior of multidomain (MD) and pseudo-single domain (PSD) grains. Significant progress has been made in this direction. The presence of MD and PSD grains is quite common in lava samples and they can have important consequences. A complete review concerning the theoretical and phenomenological developments on this matter is given by Dunlop and Özdemir (1997). MD and PSD grains do not obey the experimental law of additivity of partial TRMs acquired in nonoverlapping temperature intervals by single domain grains. A direct consequence is the existence of two different slopes in the NRM-TRM plots between low ($<350^\circ$C) and high (350–580°C) temperatures. Such behavior is caused by the difference between the blocking (T_b) temperature required to randomize the orientation of a portion of magnetic grains and thus to create a pTRM during cooling in presence of field and the unblocking (T_{ub}) temperature needed to randomize the orientation of the magnetic grains with magnetization acquired at T_b. Heating at temperature T_i produce a wide range of T_{ub}'s, both lower and higher than T_b, due to repeated domain wall jumps during heating. The anomalous high T_{ub}'s form a tail extending to the Curie point, which has been widely discussed in the literature (Bol'shakov and Shcherbakova, 1979; Worm *et al*., 1988; Halgedahl, 1993; McCLelland and Sugiura, 1987; McCLelland and Shcherbakov, 1995; McCLelland *et al.*, 1996). In a recent paper Dunlop and Özdemir (2000) described how low T_{ub} tails can explain the typical concave shape of the Arai diagrams inherent to multidomain grains. Several theoretical and experimental studies (Bol'shakov and Shcherbakova, 1979; Dunlop and Xu, 1994; Xu and Dunlop, 1994) have shown that demagnetization of the NRM can begin at low temperatures, while a significant part of TRM is acquired at high temperatures. Dunlop and Özdemir (2000) suggested that a significant part of the NRM with low T_{ub} can be easily removed whereas pTRM acquisition is delayed by the presence of high T_b. Thus NRM thermal demagnetization will greatly outweigh pTRM acquisition and this effect persists until the NRM is about half demagnetized.

The presence of MD grains can be detected in curves of continuous or thermal demagnetization by their characteristic tails (Bol'shakov and Shcherbakova, 1979). Following experiments by Vinogradov and Markov (1989), Shcherbakova and Shcherbakov (2000) noticed that TRM acquired between room temperature and 300°C after heating to the Curie temperature cannot be removed completely by heating in the zero field in presence of PSD and MD grains while this is not the case for single domain. The remains of the proportion of magnetization is a measurement of the tail and depends on the amount of MD grains. This approach can thus be recommended provided that standard hysteresis parameters confirm the diagnostic. It is frequent that a part of the NRM-TRM spectrum be touched by multidomain grains, which in this case are not clearly reflected by concave up Arai diagrams. McClelland and Briden (1996), Valet *et al*. (1996) and Dunlop and Özdemir (1997) suggested to compare the NRM measured at T_i before and after heating in presence of field. Riisager and Riisager (2001) recently demonstrated the efficiency of the test (that they renamed "pTRM-tail check") on Paleocene lavas from the Faeroe Islands as well as on baked sediments. All these results indicate that concave diagrams must not be used to extract paleointensity information but it is important to perform appropriate tests to detect MD grains.

Variations in the experimental protocol

In an attempt to reduce the number of heatings, Kono and Ueno (1977) proposed to apply a field perpendicular to the NRM direction in order to extract the NRM and the TRM by performing a single heating at each step. In addition to technical difficulties positioning the sample within the oven, the authors noticed that this approach requires exceptionally stable components and has greater experimental errors. Hoffman *et al*. (1989) suggested that one method of reducing alteration is to split the sample into a number of subsamples (usually about 10), each heated to a particular temperature, once in a zero field and again in a known field. The NRM and the pTRM values are then normalized using the initial intensity of the subsample. This approach relies on the assumption that subspecimens from the same sample are characterized by similar magnetic properties, which is not always true. The natural physical properties of a lava often vary over a few centimeters. Sherwood (1991) evaluated the multispecimen approach and found no improvement with respect to the classical Thellier technique and no evidence for reduced alteration.

Several suggestions have been made to increase the number of determinations. Valet *et al*. (1996) proposed a correction technique taking into account the deviations caused by creation or destruction of magnetization. Corrections rely on the hypothesis that the loss (or gain) of TRM induced by mineralogical transformations is indicated by difference between the pTRM check and the TRM that was initially measured at the same step. In a detailed paper aimed at detecting alteration with high-unblocking temperatures, McClelland and Briden (1996) reached basically the same conclusions. Corrections can be applied if (1) the NRM was not affected and (2) the alteration product has unblocking temperatures lower than the temperature of the last heating. These two conditions can be checked by (1) double demagnetization of the NRM (if NRM demagnetization was performed first) and/or (2) scrutinizing the evolution of the NRM in sample coordinates. The suitability of corrections was tested on contemporaneous lava flows. The technique was reasonably successful and gave field determinations within a typical error between 10% and 20% inherent to paleointensity studies. However, it is frequently questioned because there is no clear indication about the reliability of field determinations. For this reason corrections remain speculative particularly in the absence of determinations without corrections for the same flow.

A complete different track was followed by Tanaka *et al*. (1995) who performed continuous direct measurements of the total vector at high temperatures. They defended that this approach can give reliable determinations whereas the standard method does not. The sample was heated in a cryogenic magnetometer with a small furnace installed immediately outside one of the access holes and the measurements were done within the magnetometer. The authors noticed that the drop in temperature did not exceed 1°C at 400°C when moving the sample from the furnace into the magnetometer. The technique involves two successive heatings (with and without field) over successive temperature intervals and does not require cooling the sample to room temperature except at T_{i-1}. The operation is repeated at incremental steps

and allows determination of the NRM lost and the TRM gained within each successive temperature interval rather than in a cumulative manner.

A very similar approach has been developed recently by LeGoff and Gallet (2004) with a vibrating magnetometer. The system called "Triaxe" vibrates horizontally along a single direction and comprises three orthogonal sets of pickup coils. Heating is produced by a 2.5 kHz alternating current in a bifilaresistor, avoiding electromagnetic interference in the pickup coils. Heating and cooling rates can be adjusted up to a maximum of 60 °C min^{-1}. The sensor and heating-cooling systems are centered inside three perpendicular Helmholtz coils coaxial with the magnetometer axes. Thus a major advantage of this system is that the TRM can be produced in any direction and in particular along the same direction as the initial NRM, avoiding any problems related to anisotropy of the TRM. The same system is used also to produce a zero field. This equipment has been tested with success on archeological material and compared to results obtained with the classical Thellier experiments. Given the gain in precision in rapidity and the versatility provided by this apparatus, there is no doubt that it will be extensively used in future for archeo- and paleointensity studies.

Recent improvements using alternative materials

Pick and Tauxe (1993a) proposed that submarine basaltic glasses would be an ideal material for absolute paleointensity. The magnetic population of submarine volcanic glasses is consistent with very fine Ti-magnetite grains in the superparamagnetic or SD state. There was some concern about the primary origin of the magnetization because of the very fine grain sizes but consistent determinations were obtained from nicely linear Arai plots by Pick and Tauxe (1993a; 1993b), Meija *et al*. (1996), Carlut and Kent (2000), which rules out this possibility. These results must be considered along with recent studies by Zhou *et al*. (1999, 2000) using electron microscope analysis, which indicate that submarine glasses do not seem to be sensitive to alteration on a timescale of a few million years.

Volcanic glasses could thus be ideal candidates for studies of absolute paleointensity. However some aspects still prevent basaltic glasses from several paleomagnetic applications. In most if not all studies published so far, the glass samples were not oriented and the direction of the magnetic field could not be recovered. It is thus impossible to deal with the full vector (which somehow is a paradox after having measured directions without intensity for a very long period). This is even more critical in the case of submarine volcanics since there is a technical problem linked to the difficulty of collecting submarine samples (Cogné *et al*., 1995) oriented with respect to the geographic coordinates. In this case it is impossible to check the consistency of the magnetic polarity of the glass samples with the underlying crustal magnetic anomaly. This may change in future with the development of new collecting tools. Another limitation is the weak remanent magnetization of the small glassy fragments containing very few crystals. The total moment being on the order of some 10^{-9} A m^2 or less and the measurements are frequently noisy. The irregular size of small chips of glass requires special mounting to allow accurate orientation of the samples for the measurements. Carlut and Kent (2000) proposed a new mounting technique (based on potassium silicate instead of salt encapsulation) to measure magnetic moments as low as 5×10^{-10} A m^2. Below this value, measurements are seldom possible and thus the material cannot be used for paleointensity. Lastly lavas enriched in magnetic oxides along ridge segments can induce high magnetic anomalies and thus add a significant contribution to the main magnetic field. There is no doubt that volcanic glasses are promising to study long-term changes in the average field intensity. It is interesting that the time-averaged field value derived so far from the experiments conducted with this material is lower than the one derived from lava flows.

Cottrell and Tarduno (1999) suggested that the use of plagioclase crystals may provide a viable source of paleointensity data. The major argument is that these crystals are less affected by alteration during heating experiments. The plagioclase grains are picked after crushing the samples, but the direction can be obtained from other specimens taken from the same core. The paleointensity results for 10 plagioclase crystals taken from a sample drilled in the 1955 Kilauea lava flow (Hawaii) indicates a mean paleofield value of 33.8 μT, 5% lower than the expected field of about 36 μT measured at the Honolulu magnetic observatory. Since no field measurement has been performed directly above the flow this could be explained by local anomalies (Coe and Gromme, 1973; Baag *et al*., 1995; Valet and Soler, 1999). It is important to report that the field determinations have been obtained from low temperature intervals. At higher temperatures, remanence decay was rapid and measurement errors became significant. Such difficulties for measuring extremely low intensities (sometimes $<5 \times 10^{-12}$ A m^2) may be a limiting factor on a wider use of this technique. In a subsequent study, Cottrell and Tarduno (2000) studied 113-Ma-old basalts from the Rajmahal traps using whole rocks and single plagioclase crystals. The paleointensity determinations derived from the whole rock measurements were of lower quality and gave lower values than the plagioclase crystals, which according to the authors was caused by a fine-grained magnetic phase formed during the Thellier-Thellier heating experiments.

Two recent studies indicate that these new materials, plagioclases and volcanic glasses may converge but actually being complementary. Tarduno *et al*. (2001) reported 56 experiments on plagioclase crystals from basalts that formed during the quiet period of the Cretaceous polarity chron and found a strong time-averaged dipole moment, three times greater than during periods with reversals. Similar strong paleointensity was obtained independently by Tauxe and Staudigel (2004) who measured submarine Cretaceous basaltic glasses from the Trodos Ophiolite.

Conclusion

Paleointensity studies remain extremely delicate and time-consuming. However the past two decades of research have seen many developments, which will improve the selection of the samples and the success rate of the determinations. Another important factor is that the conjugation of techniques but also the possibility of using different materials makes now possible a critical evaluation of the data and thus an estimate of their degree of confidence.

Jean-Pierre Valet

Bibliography

Aitken, M.J., Adrian, A.L., Bussell, G.D., and Winter, M.B., 1989. Geomagnetic intensity variation during the last 4000 years. *Physics of the Earth and Planetary Interiors*, **56**: 49–58.

Baag, C., Helsley, C.E., Xu, S.Z., and Lienert, B.R., 1995. Deflection of paleomagnetic directions due to magnetization of the underlying terrain. *Journal of Geophysical Research* **100**(B7): 10013–10027.

Bol'shakov, A.S., and Sherbakova, V.V., 1979. A thermomagnetic criterion for determining the domain structure of ferrimagnetics. *Izvestia Academia of Science, USSR Physics. Solid Earth, Engl. Transl.*, **15**: 111–117.

Carlut, J., and Kent, D.V., 2000. Paleointensity record in zero-age submarine basalt glass: Testing a new dating technique for recent MORBS. *Earth and Planetary Science Letters*, **183**: 389–401.

Coe, R.S., 1967. Paleointensities of the Earth's magnetic field determined from Tertiary and Quaternary rocks. *Journal of Geophysical Research*, **72**: 3247–3262.

Coe, R.S., and Gromme, C.S., 1973. A comparison of three methods of determining geomagnetic paleointensities. *Journal of Geomagnetism and Geoelectricity*, **25**: 415–435.

Coe, R.S., Gromme, S., and Mankinen, E.A., 1978. Geomagnetic intensities from radiocarbon-dated lava flows on Hawaii and the

question of the Pacific nondipole low. *Journal of Geophysical Research*, **83**: 1740–1756.
Cogné, J.P., Francheteau, J., and Courtillot, V., 1995. Large rotation of the easter microplate as evidenced by oriented paleomagnetic samples from the sea-floor. *Earth and Planetary Science Letters*, **136**: 213–222.
Cottrell, R.D., and Tarduno, J.A., 1999. Geomagnetic paleointensity derived from single plagioclase crystals. *Earth and Planetary Science Letters*, **169**: 1–5.
Cottrell, R.D., and Tarduno, J.A., 2000. In search of high-fidelity geomagnetic paleointensities: a comparison of single plagioclase crystals and whole rock Thellier-Thellier analyses. *Journal of Geophysical Research*, **105**: 23579–23594.
Dunlop, D.J., and Xu, S., 1994. Theory of partial thermoremanent magnetization in multidomain grains. 1. Repeated identical barriers to wall motion single microcoercivity. *Journal of Geophysical Research*, **99**: 9005–9023.
Dunlop, D.J., and Özdemir, Ö., 1993. Thermal demagnetization of VRM and pTRM of single domain magnetite: no evidence for anomalously high unblocking tempertaures. *Geophysical Research Letters*, **20**: 1939–1942.
Dunlop, D.J., and Özdemir, Ö., 1997. *Rock Magnetism.* Cambrige: Cambridge University Press, 573 pp.
Dunlop, D.J., and Özdemir, Ö., 2000. Effect of grain size and domain state on thermal demagnetization tails. *Geophysical Research Letters*, **27**: 1311–1314.
Haag, M., Dunn, J.R., and Fuller, M., 1995. A new quality check for absolute paleointensities of the earth magnetic field. *Geophysical Research Letters*, **22**: 3549–3552.
Halgedahl, S.L., 1993. Experiments to investigate the origin of anomalously elevated unblocking temperatures. *Journal of Geophysical Research*, **98**: 22443–22460.
Hoffman, K.A., Constantine, V.L., and Morse, D.L., 1989. Determination of absolute paleointensity using a multi-specimen procedure. *Nature*, **339**: 295–297.
Kono, M., and Ueno, N., 1977. Paleointensity determination by a modified Thellier method. *Physics of the Earth and Planetary Interiors*, **13**: 305–314.
Kosterov, A.A., and Prévot, M., 1998. Possible mechanisms causing failure of paleointensity experiments in some basalts. *Geophysical Journal International*, **134**: 554–572.
Le Goff, M., and Gallet, Y., 2004. A new three-axis vibrating sample magnetometer for continuous high-temperature magnetization measurements: applications to paleo- and archeointensity determinations. *Earth and Planetary Science Letters*, **229**: 31–43.
McClelland, E., and Briden, J.C., 1996. An improved methodology for Thellier-type paleointensity determnation in igneous rocks and its usefulness for verifying primary thermoremanence. *Journal of Geophysical Research*, **101**(B10): 21995–22013.
McClelland, E., Muxworthy, A.R., and Thomas, R.M., 1996. Magnetic properties of the stable fraction of remanence in multidomain (MD) magnetite grains: single-domain or MD? *Geophysical Research Letters*, **23**: 2831–2834.
McClelland, E., and Sugiura, N., 1987. A kinematic model of pTRM acquisition in multidomain magnetite. *Physics of the Earth and Planetary Interiors*, **46**: 9–23.
McClelland, E., and Shcherbakov, V.P., 1995. Metastability of domain state in multi-domain magnetite: consequences for remanence acquisition. *Journal of Geophysical Research*, **100**: 3841–3857.
Mejia, V., Opdyke, N.D., and Perfit, M.R., 1996. Paleomagnetic field intensity recorded in submarine basaltic glass from the East Pacific Rise, the last 69 KA. *Geophysical Research Letters*, **23**: 475–478.
Nagata, T., Arai, Y., and Momose, K., 1963. Secular variation of the geomagnetic total force during the last 5000 years. *Journal of Geophysical Research*, **68**: 5277–5281.
Pick, T., and Tauxe, L., 1993a. Geomagnetic paleointensities during the Cretaceous normal superchron measured using submarine basaltic glass. *Nature*, **36**: 238–242.
Pick, T., and Tauxe, L., 1993b. Holocene paleointensities: Thellier experiments on submarine basaltic glass from the east pacific Rise. *Journal of Geophysical Research*, **98**(B10): 17949–17964.
Sherwood, G.J., 1991. Evaluation of a multispecimen approach to paleointensity determination. *Journal of Geomagnetism and Geoelectricity*, **43**: 341–349.
Tanaka, H., Athanassopoulos, J.D.E., Dunn, J.R., and Fuller, M., 1995. Paleointensity determinations with measurements at high temperature. *Journal of Geomagnetism and Geoelectricity*, **47**: 103–113.
Tarduno, J.A., Cotrell, R.D., and Smirnov, A.V., 2001. High geomagnetic intensity during the mid-Cretaceous fromThellier analyses of single plagiocalse crystals. *Science*, **291**: 1779–1780.
Tauxe, L., and Staudigel, H., 2004. Strength of the geomagnetic field in the Cretaceous Normal Superchron: New data from submarine basaltic glass of the Troodos Ophiolite, *Geochemistry, Geophysics, and Geosystems*, **5**: Q02H06, doi:10.1029/2003GC000635.
Thellier, E., and Thellier, O., 1959. Sur l'intensité du champ magnétique terrestre dans le passé historique et géologique. *Annales Geophysicae*, **15**: 285–376.
Valet, J.P., 2003. Time variations in geomagnetic intensity, *Reviews of Geophysics*, **41**(1): 1004.
Valet, J.P., Brassart, J., Le Meur, I., Soler, V., Quidelleur, X., Tric, E., and Gillot, P.Y., 1996. Absolute paleointensity and magnetomineralogical changes. *Journal of Geophysical Research*, **101**: 25029–25044.
Valet, J.P., Tric, E., Herrero-Bervera, E., Meynadier, L., and Lockwood, J.P., 1998. Absolute paleointensity from Hawaiian lavas younger than 35ka. *Earth and Planetary and Science Letters*, **161**: 19–32.
Valet, J.P., Brassart, J., Le Meur, I., Soler, V., Quidelleur, X., Tric, E., and Gillot, P.Y., 1996. Absolute paleointensity and magnetomineralogical changes. *Journal of Geophysical Research*, **101**: 25029–25044.
Valet, J.P., and Soler, V., 1999. Magnetic anomalies of lava fields in the Canary islands. Possible consequences for paleomagnetic records. *Physics of the Earth and Planetary Interiors*, **115**: 109–118.
Worm, H.U., Jackson, M., Kelso, P., and Banerjee, S.K., 1988. Thermal demagnetization of partial thermoremanent magnetization. *Journal of Geophysical Research*, **96**: 12196–12204.
Xu, S., and Dunlop, D.J., 1994. The theory of partial thermoremanent magnetization in multidomain grains. 2. Effect of microcoercivity distribution and comparison with experiment. *Journal of Geophysical Research*, **99**: 9025–9033.
Zhou, W., Van der Voo, R., and Peacor, D.R., 1999. Preservation of pristine titanomagnetite in older ocean-floor basalts and its significance for paleointensity studies. *Geology*, **27**: 1043–1046.
Zhou, W., Van der Voo, R., Peacor, D., and Zhang, Y., 2000. Variable Ti-content and grain size of titanomagnetite as a function of cooling rate in very young MORB. *Earth and Planetary Science Letters*, **179**: 9–202000.

Cross-references

Archeology, Magnetic Methods
Archeomagnetism
Baked Contact Test
Magnetic Domain
Magnetic Mineralogy, Changes Due to Heating
Magnetization, Natural Remanent (NRM)
Magnetization, Thermoremanent (TRM)
Magnetization, Thermoremanent, in Minerals
Paleointensity, Absolute, Determination

PALEOINTENSITY, RELATIVE, IN SEDIMENTS

What is "relative" paleointensity?

The intensity of depositional remanent magnetization (DRM) in sediments is not absolute, that is, DRM intensity is not solely a function of the ambient field strength at the time of deposition (see Magnetization, depositional remanent, DRM). The intensity of DRM recorded in sediments, when treated with a normalization process, is termed "relative paleointensity." The term "relative" is used because, although the ratio of two intensity values is considered an accurate measure of the percent difference in field strength, a single intensity value is not a stand-alone measure of the Earth's geomagnetic dipole moment (see Figure P4). Sedimentary records must be calibrated against absolute intensity measurements derived from volcanic samples or archeological baked clays (see Magnetization, thermoremanent; Archeomagnetism).

This situation exists because the intensity of DRM is dependent on the amount of ferrimagnetic material present in the sediment sample, the magnetic domain-state of the ferrimagnetic particles, and the mineralogy of the recording assemblage. For example, a package of sediment deposited in the presence of a weak magnetic field may acquire a strong remanence if the sediment contains a large amount of magnetite. In contrast, a package of sediment deposited in a strong field may have a very weak signal if the sediment contains very little magnetite, such as in deep-sea carbonates or biosiliceous ooze (see Figure P5). These nonfield effects must be removed in order to isolate the dependence of DRM on the ambient field intensity. Typically, the intensity of the natural remanent magnetization (see Magnetization, natural remanent, NRM) is divided by a correction factor that is sensitive to the amount of remanence-carrying grains present in the sample. The parameter NRM/(correction factor) yields the intensity of NRM per amount of remanence carrying grains.

The need to correct for nonfield effects has long been recognized. Johnson *et al*. (1948) suggested dividing DRM by isothermal remanent magnetization (IRM) to account for differences in the "magnetization potential" of the sediment (see Magetization, isothermal remanent, IRM). They further suggested that a DRM versus applied field curve derived from redeposition experiments could be used to calibrate NRM intensity in natural sediments. Kent (1973) explored this idea by carrying out a laboratory redeposition experiment in which natural deep-sea sediments were stirred in the presence of an applied field to simulate bioturbation. The resulting deposits were free of inclination error and the intensity of remanence was linearly proportional to the applied field over the range 20–120 μT. This elegant experiment demonstrated that a linear relationship between DRM intensity and ambient field strength existed when an invariant sediment assemblage was repeatedly redeposited. However, invariant sediment assemblages rarely exist in nature. Natural sediment assemblages vary with time as a consequence of environmental processes controlling sediment supply, transport, and deposition. This makes sediments interesting and valuable for their ability to monitor environmental processes and climate change (see Environmental magnetism). This is also responsible for the complexity of the magnetic recording processes in sediment.

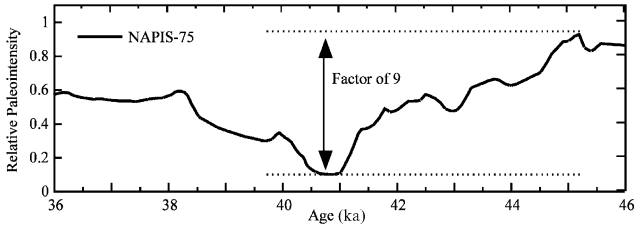

Figure P4 The interval 36–46 ka from the North Atlantic Paleointensity Stack (NAPIS-75) (Laj *et al.*, 2000). The data set has been divided by its mean value, so that the mean is equal to 1. The Laschamp geomagnetic excursion, referred to as the Laschamp Event, is manifested as a 1–2 ka interval of very low intensity at 40–41.5 ka. The Laschamp Event is preceded by an intensity peak at ~45 ka, at which time the geomagnetic field was nine times stronger than during the Laschamp Event. Relative paleointensity records such as NAPIS-75 can reveal the percent change in the geomagnetic field intensity, but not the absolute field strength.

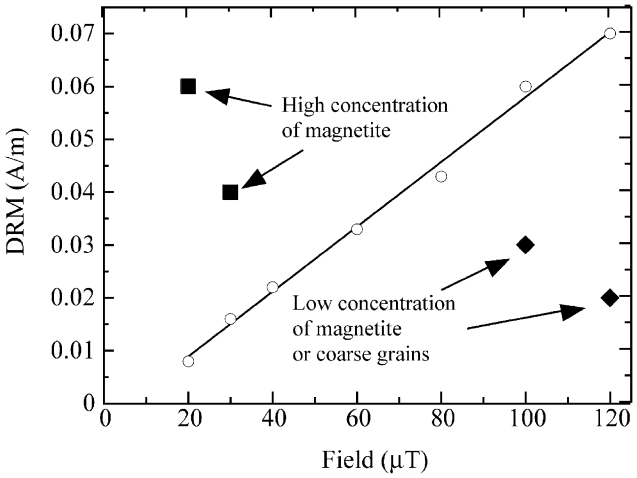

Figure P5 Conceptual model of the intensity of depositional remanent magnetization (DRM) as a function of ambient field strength. Ideally, DRM would be linearly dependent on the amplitude of the ambient field (open circles). In sediments, DRM intensity is dependent on the concentration of remanence carrying grains and the magnetic domain state of the particles. Solid squares represent sediment deposited in the presence of a weak field, but carry a strong DRM due a high concentration of magnetite. Diamonds represent sediment deposited in a strong ambient field, but carry a weak DRM due to low concentration of magnetite, or inefficient recorders (coarse grains, hematite) (After Tauxe, 1993).

Normalization parameters and processes

King *et al*. (1983) proposed a set of guidelines to place limitations on the acceptable amount of sedimentological variability, and limit paleointensity studies to sediments most likely to yield reliable data. The "King Criteria," later modified by Tauxe (1993), attempt to ensure the homogeneity of the magnetic mineral assemblage. If the sedimentary sequence being studied is homogeneous, then one can be confident that any observed features in the geomagnetic field record represent true field behavior, rather than artifacts due to the sedimentology. The uniformity criteria were originally developed to test the suitability of sediments for normalization using anhysteretic remanent magnetization (see Magnetization, anhysteretic remanent, ARM). Hence, the concentration dependence of ARM and the grain-size dependence of ARM observed in magnetite strongly influenced the development of these criteria. These criteria have since become a general set of guidelines, regardless of the normalization method chosen.

First, the sediments should record a strong, stable, single component of remanence whose orientation is appropriate for the site latitude. If the orientation of the remanence vector is inaccurate, then intensity is likely to be inaccurate. Second, the carrier of the NRM should be magnetite. Any mineral with a spontaneous magnetic moment will experience a torque in the presence of an ambient magnetic field.

The stronger the particle's moment, the stronger the torque, and presumably the greater the efficiency of aligning with the field. Magnetite, Fe_3O_4, has the strongest spontaneous moment of the commonly occurring iron-bearing minerals. Further, magnetite and titanomagnetite ($Fe_{3-x}Ti_xO_4$) are the most abundant magnetic minerals in sediments. Therefore magnetite and titanomagnetite are important carriers of DRM in most sediments. Accessory minerals such as hematite, maghemite, greigite and pyrrhotite have been shown to be carriers of a stable DRM in a few rare cases (Kodama, 1982; Tauxe and Kent, 1984; Hallam and Maher, 1994). Generally, hematite has a very low-saturation magnetization and therefore it experiences a weak magnetic torque. Thus its ability to align accurately with the ambient field is questionable. Further, hematite may form in situ long after deposition, such as in redbeds, thus acquiring a chemical remanence (see Magnetization, chemical remanent, CRM) rather than DRM. Maghemite and greigite are more commonly associated with low-temperature oxidation and iron-sulfur diagenesis, respectively (e.g., Roberts and Turner, 1993; Reynolds *et al*., 1994; Snowball and Torri, 1999), implying the alteration of the primary magnetization and acquisition of a CRM at some unknown time after deposition. Ideally, magnetite should be the only magnetic mineral present in the sediment, to avoid the possibility that the normalization method will activate grains that do not carry DRM.

Third, the magnetite particle size should be 1–10 μm. Superparamagnetic particles (SP, <30 nm for magnetite) are thermally unstable at room temperature and do not carry DRM. Stable single domain (SSD) grains (≈30 nm–1 μm for magnetite) have strong moments and experience a strong torque in an ambient field, in addition to weaker viscous drag due to their smaller size. However, fine SSD grains are susceptible to the influence of Brownian motion (Stacey, 1972). Lu *et al*. (1990) also suggested that fine SSD grains adhere to clay minerals and are rotated out of alignment with the ambient field when the clays are compacted into horizontal orientations. Multi-domain (MD) grains have low magnetization and therefore experience a weaker magnetic torque. Larger grains are more strongly influenced by the gravitational force than by the magnetic force (see Magnetic domain). PSD grains, corresponding to the 1–10 μm size range in magnetite, are assumed to be the most efficient recorders of DRM.

Fourth, the concentration of magnetite should not vary by more than a factor of 10. This limitation on concentration variability is based on the effects of particle interaction during ARM acquisition. The concentration of magnetic material is typically monitored using magnetic susceptibility (k), saturation isothermal remanent magnetization (SIRM), or saturation magnetization (M_S).

The normalization parameters currently in use are k, anhysteretic remanent magnetization (ARM), and (SIRM). Two other methods, the pseudo-Thellier method (Tauxe *et al.,* 1995) and the integral method (Brachfeld *et al*., 2003), are normalization procedures that have been explored, but not widely used at present. There is not one single normalization parameter that is applicable to all sedimentary records. In selecting the most appropriate normalization parameter for a given sedimentary record, it is necessary to thoroughly characterize the composition, concentration, and grain size of the magnetic recording assemblage, which may be a small subset of the entire magnetic mineral assemblage.

Magnetic susceptibility is logistically and economically the most easily measured magnetic parameter. Susceptibility is a routine measurement conducted on sediment cores collected by ocean research vessels. The ease of measurement is one reason for the continued use of k as a normalization parameter. However, k is measured in the presence of an applied alternating field, whereas DRM is a remanent magnetization. MD and SP grains that do not contribute to DRM contribute strongly to k and lead to "over-correction." The ratio DRM/k is artificially low if these grains are present (Brachfeld and Banerjee, 2000). In addition, several studies have shown strong correspondence between k and $\delta^{18}O$. The presence of Milankovitch periodicities in k profiles from oceanic, lacustrine, and loess records (e.g., Bloemendal and deMenocal, 1989; deMenocal *et al*., 1991; Peck *et al*., 1994; Bloemendal *et al*., 1995), suggests that climatic factors influence the supply of magnetic material to marine, lacustrine, and aeolian sediment. In such cases there is a risk that the climatically induced variability in k, or any potential normalization parameter, could be transferred to the normalized intensity record (e.g., Kok, 1990; Schwartz *et al*., 1996; 1998; Lund and Schwartz, 1999; Guyodo *et al*., 2000).

Levi and Banerjee (1976) laid out the arguments in favor of ARM as a normalization parameter. Levi and Banerjee (1976) analyzed a sedimentary record from Lake St. Croix, Minnesota. They compared the alternating field (AF) coercivity spectra of the NRM, ARM, and SIRM. The coercivity spectra of NRM and ARM were nearly identical, while that of a SIRM was much softer (Figure P6). They argued that ARM activated the same grains that carried the NRM, which is the critical factor for selecting a normalization parameter. In addition, since the coercivity spectra of NRM and ARM were identical, the ratio NRM/ARM did not vary with AF demagnetization level, whereas the ratio NRM/IRM (and hence the assumed paleointensity) varied strongly with the demagnetization level.

Complications with ARM normalization arise from strong grain-size and concentration dependencies. Below 1 μm (approximately), small changes in grain-size result in large changes in ARM acquisition (Dunlop and Özdemir, 1997). Above 1 μm, ARM acquisition is less dependent on grain size (Dunlop and Özdemir, 1997). This is the basis for uniformity criterion 3, which states that sediments suitable for paleointensity studies contain magnetite in the 1–10 μm size range. Sediments in which 0.1–1 μm magnetite is the carrier of remanence would be susceptible to miscorrection using ARM. Even relatively small changes in the grain-size of DRM carriers could translate into very large changes in ARM acquired.

ARM acquisition is strongly dependent on the concentration of magnetic material in a sample. Sugiura (1979) imparted ARM to synthetic sediments with varying volume fractions of magnetite. A sample with 2.5-ppm (parts per million) magnetite acquired an ARM that was four times stronger than a sample with 2.3% magnetite. At high magnetite

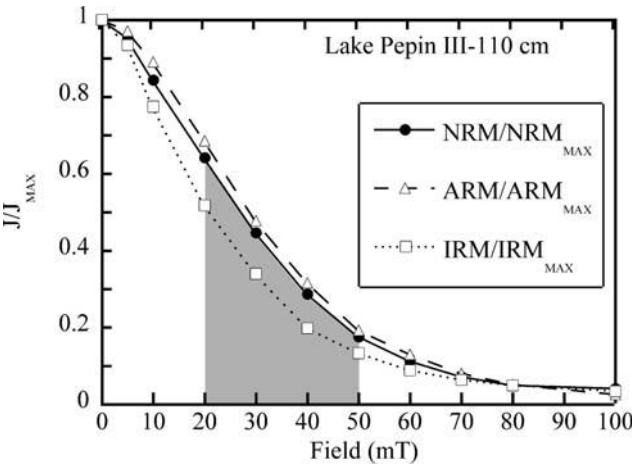

Figure P6 Stepwise alternating field demagnetization of NRM, ARM, and IRM carried by a sediment sample from Lake Pepin, Minnesota (Brachfeld and Banerjee, 2000). Levi and Banerjee (1976) suggested that the most appropriate normalization parameter is the one that activates the same grains that carry the NRM. This is assessed using the alternating field (AF) demagnetization coercivity spectrum. For this sample, the coercivity spectrum of the ARM is nearly identical to the NRM, while the IRM spectrum is softer. ARM is the most appropriate normalization parameter for this sediment sample. The shaded region denotes the area under the NRM demagnetization curve, which is the basis for the integral normalization method (see text).

concentrations, ARM acquisition is less efficient due to particle interactions, which tend to demagnetize the assemblage. The criterion that magnetite concentration vary by no more than a factor of 10 was designed to ensure that the mechanism of ARM acquisition, be it efficient or inefficient, is at least consistent throughout the entire sediment sequence.

Isothermal remanent magnetization (IRM) is imparted by exposing a sample to a steady field for several seconds, then reducing the field nearly instantaneously to zero. By applying stepwise increasing fields and measuring the remanence after each step, one can obtain an IRM acquisition curve. At some field strength the sample acquires its maximum possible signal, at which point the sample has acquired a saturation isothermal remanent magnetization. SIRM and the magnitude of the saturating field vary for different minerals. Magnetite saturates in fields of 100–300 mT. Hematite and goethite requires fields in excess of several tesla to achieve saturation (Dunlop and Özdemir, 1997). SIRM acquisition is less sensitive to grain interactions than ARM acquisition because the applied field which is very strong can overcome the demagnetizing effect of grain interactions. The danger in using SIRM is that—at high fields, nearly all of the magnetic minerals will acquire an IRM or SIRM, even those grains that do not contribute to the DRM. In particular, MD grains that do not contribute to DRM will contribute disproportionately to SIRM.

Tauxe *et al*. (1995) proposed the pseudo-Thellier method of relative paleointensity normalization. The pseudo-Thellier method is an analog of the Thellier. Thellier double heating experiment that is applied to absolute intensity samples. In the pseudo-Thellier method, one plots NRM lost at each AF demagnetization level versus ARM gained at that AF demagnetization level. Relative paleointensity is calculated as the slope of the best-fit line fit to the data (see Figure P7). This method is particularly useful for identifying viscous components of magnetization, which are typically removed after the 5–20 mT demagnetization step. Viscous components are manifested as a line segment with a slightly steeper slope. One can identify these components from the pseudo-Thellier plot, and avoid these intervals when calculating the best-fit line.

Brachfeld *et al*. (2003) proposed an integration method of normalization. This method expands on Levi and Banerjee (1976) who argued that the coercivity spectrum of the normalization parameter should match the coercivity spectrum of the NRM. The integral method involves integrating the area under the NRM/NRM_{MAX} demagnetization curve over an optimal AF range, for example 20–50 mT. The normalization parameter, ARM/ARM_{MAX} is integrated over the same interval. Relative paleointensity is calculated as

$$\frac{\int_{20\ \mathrm{mT}}^{50\ \mathrm{mT}} \mathrm{NRM}(H_{\mathrm{AF}})\mathrm{d}H_{\mathrm{AF}}}{\int_{20\ \mathrm{mT}}^{50\ \mathrm{mT}} \mathrm{ARM}(H_{\mathrm{AF}})\mathrm{d}H_{\mathrm{AF}}}$$

(see Figure P6). The goal of this method is to ensure that the same coercivity spectrum is reflected in both the NRM and the normalization parameter.

There are several ways to assess the quality and accuracy of a normalized intensity record. The simplest and most common method is to apply several normalization parameters. It has traditionally been assumed that if several normalization parameters yield similar profiles, then the sediment is homogeneous and any of the parameters is an adequate normalizer. Normalized intensity records can be judged by comparison with records from other sites, for example other sedimentary records, absolute intensity records, or records of cosmogenic isotopes (^{10}Be, ^{36}Cl), whose production rates are modulated by geomagnetic field intensity (Frank *et al*., 1997; Frank, 2000; Baumgartner *et al*., 1998; Wagner *et al*., 2000a,b).

Normalized intensity records from the same geographic region should yield similar patterns and amplitudes if properly normalized. Unfortunately, the amplitude of normalized intensity features can be quite different depending on the normalization method used (Schwartz *et al*., 1996, 1998; Lund and Schwartz, 1999; Brachfeld and Banerjee, 2000). Several workers have suggested that the variable amplitudes of crests and troughs as a function of normalization method are the result of subtle grain-size variations that are not removed during normalization (Amerigian, 1977; Sprowl, 1985; Lehman *et al*., 1994, 1998; Schwartz *et al*., 1996; Williams *et al*., 1998; Brachfeld and Banerjee, 2000).

An internal check on the quality of a normalized intensity record is to examine correlations between rock magnetic parameters and normalized intensity. Harrison and Somayajulu (1966) pointed out that the paleointensity estimate should not be correlated with rock magnetic parameters, which they assessed using a linear regression correlation coefficient. Tauxe and Wu (1990) brought this test into the frequency domain by calculating coherence spectra for the normalized paleointensity and the normalization parameters. This permits the identification of frequency bands where paleointensity and rock-magnetic parameters are responding to the same external influence, climatic or otherwise. Tauxe and Wu (1990) proposed that true normalized intensity should not be coherent with its specific normalization parameter. Coherence is typically tested between NRM/k and k, NRM/ARM and ARM, and NRM/SIRM and SIRM. The best relative paleointensity record is the one that shows no coherence with its normalization parameter. Brachfeld and Banerjee (2000) recommended that normalized intensity also be tested for coherence with grain-size parameters such as the median destructive field of the NRM (NRM_{MDF}) or the coercivity of remanence (H_{CR}).

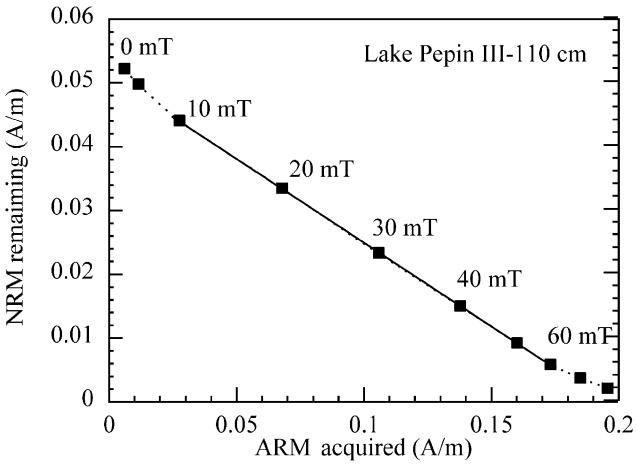

Figure P7 The pseudo-Thellier plot for a sediment sample from Lake Pepin, Minnesota. Tauxe *et al*. (1995) devised this alternate normalization method to simulate the Arai diagram obtained through the Thellier. Thellier absolute intensity analysis. NRM remaining at each demagnetization level is plotted against ARM gained at the same AF level. Viscous components of remanence are identified by the change in slope of the trend line. This sample has a viscous component of remanence that is removed after AF demagnetization at the 10 mT level. Relative paleointensity for this sample is calculated as the slope of the trend line from 20–60 mT.

Paleointensity as a correlation and dating tool

Until the late 1980s, the study of geomagnetic field behavior recorded in sediments was largely undertaken for magnetostratigraphy and to study the geodynamo (see Magnetostratigraphy; Paleomagnetism). Beginning in the late 1980s-early 1990s, several researchers noticed the globally coherent pattern of geomagnetic field paleointensity variations over the last 50 ka–100 ka years (Constable and Tauxe, 1987; Tauxe and Valet, 1989; Tauxe and Wu, 1990; Tric *et al*., 1992; Meynadier *et al*., 1992). Soon thereafter, advances in instrumentation enabling the rapid measurement of continuous u-channel subsamples

(Tauxe *et al*., 1983; Weeks *et al*., 1993; Nagy and Valet 1993) led to a large increase in the number of long, continuous, sedimentary records analyzed for geomagnetic paleointensity variations. The resulting database of globally distributed records enabled the construction of stacks (weighted averages of many records), which are now used as millennial-scale correlation and dating tools.

The dipole component of the geomagnetic field exhibits temporal variations in its intensity on timescales of hundreds to millions of years. Variations in the geomagnetic dipole are synchronously experienced everywhere on the globe. Therefore, a specific geomagnetic field paleointensity feature represents the same "instant" in time everywhere on Earth. Sedimentary records of geomagnetic field paleointensity from nearly all of Earth's shallow seas, deep ocean basins, and large lakes demonstrate the global coherence of features with wavelengths of 10^4–10^5 years (Figure P8, Tric *et al*., 1992; Meynadier *et al*., 1992; Schneider, 1993; Yamazaki *et al*., 1995; 1999; Guyodo and Valet, 1996, 1999; Laj *et al*., 1996, 2000, 2004; Lehman *et al*., 1996; Peck *et al*., 1996; Verosub *et al*., 1996; Channell *et al*., 1997; 2000; Roberts *et al*., 1997; Schwartz *et al*., 1998; Stoner *et al*., 1998, 2000, 2002; Kok and Tauxe, 1999; Channell and Kleiven 2000; Guyodo *et al*., 2001; Nowaczyk *et al*., 2001; Sagnotti *et al*., 2001; Mazaud *et al*., 2002; Thouveny *et al*., 2004; Valet *et al*., 2005). A common characteristic of these records is the presence of several intervals of very low intensity during the past 800 ka. These are interpreted as geomagnetic excursions, which often involve large but short-lived directional changes (>45° deviation of the virtual geomagnetic pole from its time-averaged position) followed by a return of the vector to its previous state (see *Geomagnetic excursion*). Several of the sedimentary records listed above suggest that excursions are associated with a reduction in field strength to less than 50% of its present day value, but are not always associated with a directional change.

These intervals of weak geomagnetic field intensity are partly responsible for peaks in radionuclide production rates. Peaks in ^{10}Be and ^{36}Cl concentration interpreted as the Mono Lake Event and the Laschamp Event have been observed in the Vostok, Dome C, Byrd, Camp Century, and GRIP ice cores (Beer *et al*., 1984, 1988, 1992; Yiou *et al*., 1985, 1997; Raisbeck *et al*., 1987; Baumgartner *et al*., 1997, 1998; Wagner *et al*., 2000b). Excursions, whether detected through paleomagnetism or cosmogenic isotopes, are marker horizons that can be used to correlate records from widely separated regions. However, an excursion is one single tie point. A more powerful correlation and dating tool uses time series of geomagnetic paleointensity variations and cosmogenic nuclide production rates for stratigraphic correlation.

Correlation and dating using geomagnetic paleointensity is a "tuning" method. The paleointensity record from the site of interest is compared to a well-dated reference curve. By matching peaks and troughs between the two records, one can import the reference curve ages to the study area. This method has been used to construct chronologies for sites that lacked materials for radiocarbon dating and lacked calcite for oxygen-isotope stratigraphy (Stoner *et al*., 1998; Sagnotti *et al*., 2001; Brachfeld *et al*., 2003).

Any single record of geomagnetic field variability is not suitable for a reference curve. Any single record may contain errors in its chronology or contamination of its remanent magnetization. Guyodo and Valet (1996) proposed using a "stack" to combine many records, thereby enhancing the signal to noise ratio, averaging out any flaws present in the individual records, and extracting the broadscale global features of the geomagnetic field. Guyodo and Valet (1996) showed that a distinctive pattern of geomagnetic field paleointensity was observable in deep-sea sedimentary records from around the globe (see Figure P8). They produced a 200 ka global stack of 19 paleointensity records, named Sint-200, which they suggested could be used as a millennial-scale correlation and dating tool. Each of the 19 constituent records in Sint-200 had its own oxygen-isotope stratigraphy. By correlating paleointensity variations in an undated sediment core with the Sint-200 target curve, one could import the SPECMAP oxygen isotope stratigraphy to the core site.

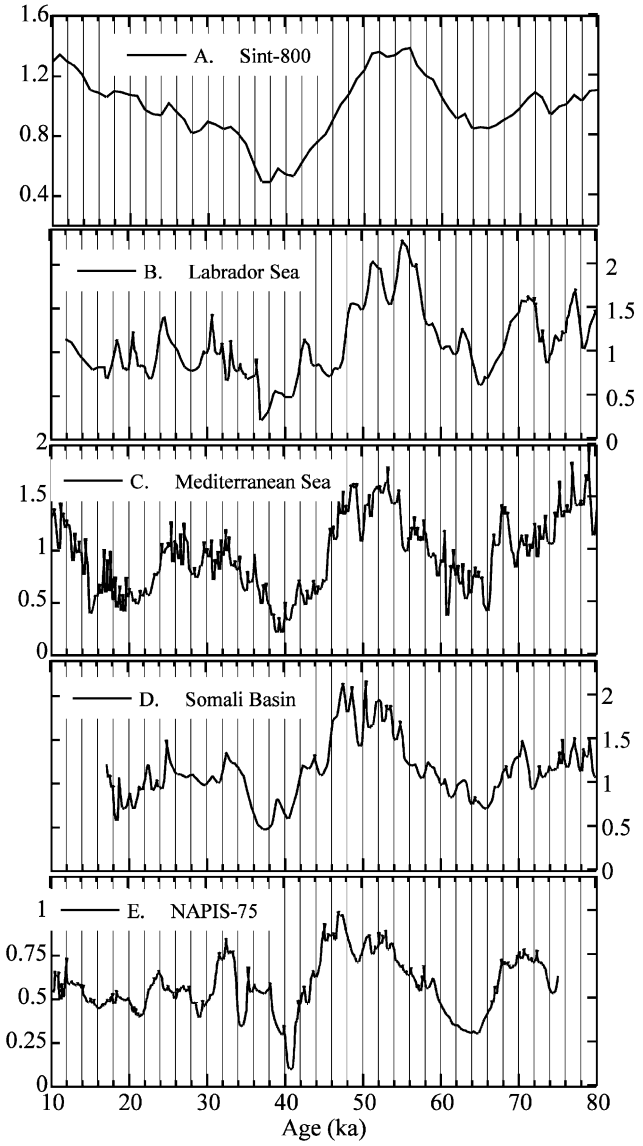

Figure P8 A comparison of globally distributed paleointensity records for the interval 10–80 ka. (A) Sint-800 (Guyodo and Valet, 1999) is a stack comprised of 33 records. Short wavelength features are not preserved in this low-resolution stack. (B) Labrador Sea (Stoner *et al*., 1998), (C) Mediterranean Sea (Tric *et al*., 1992), (D) Somali Basin (Meynadier *et al*., 1992), (E) NAPIS-75 (Laj *et al*., 2000). Features with wavelengths of 5–10 ka can be recognized and correlated from the Labrador Sea south to the Somali Basin.

The constituent records of Sint-200, and its subsequent extension to the 800 ka Sint-800 (Guyodo and Valet, 1999) were all deep-sea sediment cores with relatively low-sedimentation rates. Therefore, short wavelength features are not preserved in Sint-800. Two newer stacks with higher temporal resolution, the 75 ka North Atlantic paleointensity stack (NAPIS-75) and the South Atlantic paleointensity stack (SAPIS), were constructed from high-sedimentation rate records from sediment drifts in the North Atlantic and the South Atlantic, respectively (Laj *et al*., 2000; Stoner *et al*., 2002). NAPIS-75 is a stack of six individual high-resolution records (sedimentation rates = 20 to 30 cm/ka) from cores recovered from the Nordic seas and the North Atlantic. The stacks cover the time interval 10–75 ka, providing

overlap with the radiocarbon timescale. The NAPIS-75 chronology is linked to the GISP2 ice core chronology. First, Heinrich layers and a volcanic ash were used as tie points to correlate the six cores. Second, a fine scale correlation was achieved by matching magnetic susceptibility oscillations and ARM oscillations, which put all six cores on a common depth scale (Kissel *et al*., 1999). The resulting stack was placed on the GISP2 age model of Grootes and Stuiver (1997) by correlating the planktonic foraminifera $\delta^{18}O$ record in one of the sediment cores with the $\delta^{18}O$ record in the GISP2 ice core (Voelker *et al*., 1998; Kissel *et al*., 1999).

There are striking similarities between NAPIS-75 and a synthetic geomagnetic field record calculated from ^{36}Cl and ^{10}Be data obtained from the GRIP/GISP2 ice cores (Baumgartner *et al*., 1997, 1998; Finkel and Nishiizumi, 1997; Yiou *et al*., 1997; Wagner *et al*., 2000a,b), which suggests a common geomagnetic origin. Features with a 1000 to 2000-year wavelength can be recognized in both records. The millennial scale features of NAPIS-75, coupled to the precise GISP2 timescale, constitutes a highly efficient tool for correlating and dating cores in different oceans basins around the world (Stoner *et al*., 2000, 2002), particularly in the Arctic Ocean and southern Ocean, where $\delta^{18}O$ stratigraphy is not available. The extension of NAPIS-75 to NAPIS-300, a 300 ka stack, is now in progress (C. Laj and C. Kissel, personal communication).

SAPIS was constructed from five cores from the South Atlantic (Stoner *et al*., 2002). The five cores were placed on a common depth scale by correlating magnetic susceptibility, oxygen isotope stratigraphy, geomagnetic inclination, and relative paleointensity. The age model for SAPIS comes largely from one core, Ocean Drilling Program (ODP) Site 1089, whose oxygen isotope stratigraphy was correlated to a nearby core with 14 radiocarbon dates, and by correlating the oxygen isotope stratigraphy to SPECMAP (Stoner *et al*., 2003).

NAPIS and SAPIS display remarkable similarities over the interval 30–65 ka. The two records display similar peak-to-trough amplitudes, and features with 5-ka wavelengths can be recognized and correlated between the two records. Some differences were present, which the authors ascribed to subtle flaws in chronology—uncorrected environmental influences on the magnetic mineral assemblage, or genuine differences in the nondipole geomagnetic field behavior at these two sites. Nevertheless, the excellent correspondence between the two stacks over key intervals, for example 30–45 ka, illustrates the potential to use geomagnetic field paleointensity as a global, millennial-scale correlation and dating tool.

A high resolution global paleointensity stack (GLOPIS-75, Laj *et al*., 2004) is a stacked record consisting of 24 paleointensity records distributed world wide, and all with sedimentation rates exceeding 7 cm/ka. The 24 paleointensity records were each individually correlated to NAPIS-75, which was used as the master curve. Each record was resampled every 200 years, normalized to a mean value of 1, and stacked arithmetically (Laj *et al*., 2004). An iterative process was applied to successively remove discrete intervals in the individual records that may be unreliable, followed by recalculation of the stack using the remaining points. The resulting GLOPIS-75 record covers the interval 10–75 ka.

GLOPIS-75 was calibrated to absolute virtual apparent dipole moment values (VADM) using the archeomagnetic dataset of Yang *et al*. (2000) and globally distributed volcanic data spanning 0–20 ka (Laj *et al*., 2002). The main trends in this calibrated global stack are very similar to NAPIS-75. There are several noteworthy features. The Mono Lake Event and the Laschamp Event are dated at 34.6 ka and 41 ka, respectively, precise ages that are tied to the GISP2 ice core age model. The duration of these excursions are 1100 years for the Mono Lake Event and 1000–1900 years for the Laschamp Event (Laj *et al*., 2004). Refinements to GLOPIS-75 can be expected as the number and distribution of paleointensity records increases, particularly with the addition of new records currently under construction from the North Atlantic, Arctic and Antarctic, and with the addition of records spanning 0–20 ka.

Summary

The intensity of DRM recorded by sediments is influenced by the concentration, domain state, and composition of the magnetic mineral assemblage. These nonfield effects on the DRM are removed by normalizing the DRM with a laboratory-derived correction factor such as *k*, ARM, or SIRM. No single normalization parameter is appropriate for all sediments. The magnetic mineral assemblage of each sedimentary record must characterized in order to select the most appropriate normalization parameter. High-quality sedimentary geomagnetic paleointensity records are now being used as global correlation and dating tools. Features with wavelengths of 5 ka, and possibly shorter, can be recognized and correlated between the Northern and Southern hemispheres. By synchronizing geomagnetic intensity records, we may now have the ability to determine millennial-scale leads and lags in Earth's climate systems. Ongoing studies are extending paleointensity stacks further back through time (Valet *et al*., 2005), and investigating the extent to which finescale features can be recognized and correlated. This includes marine, estuarine, and lacustrine records, with the goal of expanding the temporal and spatial distribution of records, particularly in the Southern Hemisphere (Gogorza *et al*., 2000, 2002; Stoner *et al*., 2002, 2003; Brachfeld *et al*., 2003) and the Arctic (Nowaczyk *et al*., 2001; St. Onge *et al*., 2003, 2005; King *et al*., 2005; Stoner *et al*., 2005).

Acknowledgments

I thank Carlo Laj, Catherine Kissel, Yohan Guyodo, Joe Stoner, and Laure Meynadier for providing their datasets.

Stefanie Brachfeld

Bibliography

Amerigian, C., 1977. Measurement of the effect of particle size variation on the DRM to ARM ratio in some abyssal sediments. *Earth and Planetary Science Letters*, **36**: 434–442.

Baumgartner, S., Beer, J., Suter, M., Diitrich-Hannen, B., Synal, H.-A., Kubik, P.W., Hammer, C., and Johnsen, S., 1997. Chlorine-36 fallout in the Summit Greenland Ice Core Project ice core. *Journal of Geophysical Research*, **102**: 26659–26662.

Baumgartner, S., Beer, J., Masarik, J., Wagner, G., Meynadier, L., and Synal, H.-A., 1998. Geomagnetic modulation of the ^{36}Cl flux in the GRIP ice core, Greenland. *Science*, **279**: 1330–1332.

Beer, J., Andrée, M., Oeschger, H., Siegenthaler, U., Bonani, G., Hofmann, H., Morenzoni, E., Nessi, M., Suter, M., Wölfli, W., Finkel, R., and Langway, C., Jr. 1984. The Camp Century ^{10}Be record: implications for long-term variations of the geomagnetic dipole moment. *Nuclear Instruments and Methods in Physics Research*, **B5**: 380–384.

Beer, J., Siengenthaler, U., Bonani, G., Finkel, R.C., Oeschger, H., Suter, M., and Wölfi, W., 1988. Information on past solar activity and geomagnetism from ^{10}Be in the Camp Century ice core. *Nature*, **331**: 675–679.

Beer J., Bonani, G.S., Dittrich, B., Heller, F., Kubik, P.W., Tungsheng, L., Chengde, S., and Suter, M., 1992. ^{10}Be and magnetic susceptibility in Chinese loess. *Geophysical Research Letters*, **20**: 57–60.

Bloemendal, J., Liu, X.-M., and Rolph, T.C., 1995. Correlation of the magnetic susceptibility stratigraphy of Chinese loess and the marine oxygen isotope record: Chronological and palaeoclimatic implications. *Earth and Planetary Science Letters*, **131**: 371–380.

Bloemendal, J., and deMenocal, P.B., 1989. Evidence for a change in the periodicity of tropical climate cycles at 2.4 Myr from whole core magnetic susceptibility measurements. *Nature*, **342**: 897–900.

Brachfeld, S.A., Domack, E.W., Kissel, C., Laj, C., Leventer, A., Ishman, S.E., Gilbert, R., Camerlenghi, A., and Eglinton, L.B., 2003. Holocene history of the Larsen Ice Shelf constrained by geomagnetic paleointensity dating. *Geology*, **31**: 749–752.

Brachfeld, S., and Banerjee, S.K., 2000. A new high-resolution geomagnetic relative paleointensity record for the North American Holocene: A comparison of sedimentary and absolute intensity data. *Journal of Geophysical Research*, **105**: 821–834.

Channell, J.E.T., Hodell, D.A., and Lehman, B., 1997. Relative geomagnetic paleointensity and delta ^{18}O at ODP site 983 (Gardar Drift, North Atlantic) since 350 ka. *Earth and Planetary Science Letters*, **153**: 103–118.

Channell, J.E.T., and Kleiven, H.F., 2000. Geomagnetic palaeointensity and astrochronological ages for the Matuyama-Brunhes boundary and boundaries of the Jaramillo subchron: palaeomagnetic and oxygen isotope records from ODP Site 983. *Philosophical Transactions of the Royal Society London A*, **358**: 1027–1047.

Channell, J.E.T., Stoner, J.S., Hodell, D.A., and Charles, C.D., 2000. Geomagnetic paleointensity for the last 100 kyr from the sub-Antarctic South Atlantic: a tool for interhemispheric correlation. *Earth and Planetary Science Letters*, **175**: 145–160.

Constable, C.G., and Tauxe, L., 1987. Paleointensity in the pelagic realm: Marine sediment data compared with archeomagnetic and lake sediment records. *Geophysical Journal of the Royal Astronomical Society*, **90**: 43–59.

deMenocal, P., Bleomendal, J., and King, J.W., 1991. A rock-magnetic record of monsoonal dust deposition to the Arabian Sea: Evidence for a shift in the mode of deposition at 2.4 Ma. *Proceedings of the Ocean Drilling Program- Scientific Results*, **117**: 389–407.

Dunlop, D.J., and Özdemir, Ö., 1997. *Rock Magnetism*, Cambridge: Cambridge University Press.

Finkel, R.C., and Nishiizumi, N., 1997. Beryllium-10 concentrations in the Greenland Ice Sheet Project 2 ice core. *Journal of Geophysical Research*, **102**: 26,699–26,706.

Frank, M., 2000. Comparison of cosmogenic radionuclide production and geomagnetic field intensity over the last 200000 years. *Philosophical Transactions of the Royal Society London A*, **358**: 1089–1107.

Frank, M., Schwarz, B., Baumann, S., Kubik, P.W., Suter, M., and Mangini, A., 1997. A 200 kyr record of cosmogenic radionuclide production rate and geomagnetic field intensity from ^{10}Be in globally stacked deep-sea sediments. *Earth and Planetary Science Letters*, **149**: 121–129.

Gogorza, C.S.G., Sinito, A.M., Lirio, J.M., Nuñez, H., Chaparro, M., and Vilas, J.F., 2002. Paleosecular variations 0–19000 years recorded by sediments from Escondido Lake (Argentina). *Physics of the Earth and Planetary Interiors*, **133**: 35–55.

Gogorza, C.S.G., Sinito, A.M., Tommaso, I.D., Vilas, J.F., Creer, K. M., and Nuñez, H., 2000. Geomagnetic secular variations 0–12 kyr as recorded by sediments from Lake Moreno (southern Argentina). *Journal of South American Earth Sciences*, **13**: 627–645.

Grootes, P.M., and Stuiver, M., 1997. $^{18}O/^{16}O$ variability in Greenland snow and ice with 10^3 to 10^5 year time resolution. *Journal of Geophysical Research*, **102**: 26455–26470.

Guyodo, Y., Acton, G.D., Brachfeld, S., and Channell, J.E.T., 2001. A sedimentary paleomagnetic record of the Matuyama chron from the western Antarctic margin (ODP Site 1101). *Earth and Planetary Science Letters*, **191**: 61–74.

Guyodo, Y., Gaillot, P., and Channell, J.E.T., 2000. Wavelet analysis of relative geomagnetic paleointensity at ODP Site 983. *Earth and Planetary Science Letters*, **184**: 109–123.

Guyodo, Y., and Valet, J.-P., 1999. Global changes in intensity of the Earth's magnetic field during the past 800 kyr. *Nature*, **399**: 249–252.

Guyodo, Y., and Valet, J.-P., 1996. Relative variations in geomagnetic intensity from sedimentary records: the past 200000 years. *Earth and Planetary Science Letters*, **143**: 23–36.

Hallam, D.F, and Maher, B.A., 1994. A record of reversed polarity carried by the iron sulphide greigite in British Early Pleistocene sediments. *Earth and Planetary Science Letters*, **121**: 71–80.

Harrison, C.G.A., and Somayajulu, B.L.K., 1966. Behavior of the Earth's magnetic field during a reversal. *Nature*, **212**: 1193–1195.

Johnson, E.A., Murphy, T., and Torreson, O.W., 1948. Pre-history of the Earth's magnetic field, *Terrestrial Magnetism and Atmospheric Electricity* **53**: 349–372.

Kent, D.V., 1973. Post depositional remanent magnetization in deep sea sediments. *Nature*, **198**: 32–34.

King, J., Banerjee, S.K., and Marvin, J., 1983. A new rock-magnetic approach for selecting sediments for geomagnetic paleointensity studies: application to paleointensity for the last 4000 years. *Journal of Geophysical Research*, **88**: 5911–5921.

King, J.W., Heil, C., O'Regan, M., Moran, K., Gattacecca, J., Backman, J., Jakobsson, M., and Moore, T., 2005. Paleomagnetic results from the Pleistocene sediments of Lomonosov Ridge, Central Arctic Ocean, IODP Leg 302, *Eos, Transactions, American Geophysical Union* **86**(52), Fall Meet. Suppl. Abstract GP44A-04.

Kissel, C., Laj, C., Labeyrie, L., Dokken, T., Voelker, A., and Blamart, D., 1999. Rapid climatic variations during marine isotopic stage 3: magnetic analysis of sediments from nordic seas and North Atlantic. *Earth and Planetary Science Letters*, **171**: 489–502.

Kok, Y.S., 1999. Climatic influence in NRM and ^{10}Be-derived geomagnetic paleointensity data. *Earth and Planetary Science Letters*, **166**: 105–119.

Kok, Y.S., and Tauxe, L., 1999. A relative geomagnetic paleointensity stack from Ontong-Java plateau sediments for the Matuyama. *Journal of Geophysical Research*, **104**: 25401–25413.

Kodama, K.P., 1982. Magnetic effects of maghemitization of Plio-Pleistocene marine sediments, northern California. *Journal of Geophysical Research*, **87**: 7113–7125.

Laj, C., Kissel, C., Garnier F., and Herrero-Bervera, E., 1996. Relative geomagnetic field intensity and reversals for the last 1.8 My from a central equatorial Pacific core. *Geophysical Research Letters*, **23**: 3393–3396.

Laj, C., Kissel, C., Mazaud, A., Channell, J.E.T., and Beer, J., 2000. North Atlantic Paleointensity Stack since 75 ka (NAPIS-75) and the duration of the Laschamp event. *Philosophical Transactions of the Royal Society London Series A*, **358**: 1009–1025.

Laj, C., Kissel, C., Mazaud, A., Michel, E., Muscheler, R., and Beer, J., 2002. Geomagnetic field intensity, North Atlantic Deep Water circulation and atmospheric $\Delta^{14}C$ during the last 50 kyr. *Earth and Planetary Science Letters*, **200**: 179–192.

Laj, C., Kissel, C., and Beer, J., 2004. High resolution paleointensity stack since 75 kyr (GLOPIS-75) calibrated to absolute Values. In Channell, J.E.T., Kent, D.V., Lowrie, W., and Meert, J., (eds.), *Timescales of the Internal Geomagnetic Field*. American Geophysical Union Geophysical Monograph, **145**: 255–265.

Lehman, B., Laj, C., and Kissel, C., 1998. Relative paleointensity determinations from marine sediments: an empirical correction for grain size variations. *Annales Geophysicae, Supplement I*, **16,** 206. European Geophysical Society,

Lehman, B., Laj, C., Kissel, C., Mazaud, A., Paterne, M., and Labeyrie, L., 1996. Relative changes of the geomagnetic field intensity during the last 280 kyear from piston cores in the Açores area. *Physics of the Earth and Planet. Interios*, **93**: 269–284.

Lehman, B., Laj, C., and Kissel, C., 1994. Improvements in selection criteria for geomagnetic paleointensity determinations based on magnetic hysteresis analysis of sediments from the central North Atlantic Ocean. *Eos, Transactions, American Geophysical Union*, **75**: 192.

Levi, S., Banerjee, S.K., and 1976. On the possibility of obtaining relative paleointensities from lake sediments. *Earth and Planetary Science Letters*, **29**: 219–226.

Lu, R., Banerjee, S.K., and Marvin, J., 1990. Effects of clay mineralogy and the electrical conductivity of water on the acquisition of depositional remanent magnetization in sediments. *Journal of Geophysical Research*, **95**: 4531–4538.

Lund, S.P., and Schwartz, M., 1999. Environmental factors affecting geomagnetic field palaeointensity estimates from sediments, In Maher, B.A., and Thompson, R., (eds.), *Quaternary Climates,*

Environments and Magnetism. Cambridge: Cambridge University Press, pp. 323–311.

Mazaud, A., Sicre, M.A., Ezat, U., Pichon, J.J., Duprat, J., Laj, C., Kissel, C., Beaufort, L., Michel, E., and Turon, J.L., 2002. Geomagnetic-assisted stratigraphy and sea surface temperature changes in core MD94-103 (Southern Indian Ocean): possible implications for North-South climatic relationships around H4. *Earth and Planetary Science Letters*, **201**: 159–170.

Nagy, E., and Valet, J.-P., 1993. New advances for paleomagnetic studies of sediment cores using u-channels. *Geophysical Research Letters*, **20**: 671–674.

Nowaczyk, N.R., Frederichs, T.W., Kassens, H., Norgaard-Pedersen, N., Spielhagen, R.F., Stein, R., and Weiel, D., 2001. Sedimentation rates in the Makarov Basin, Central Arctic Ocean—A paleo—and rock-magnetic approach. *Paleoceanography*, **16**: 368–389.

Peck, J.A., King, J.W., Colman, S.M., and Kravchinsky, V.A., 1996. An 84-kyr record from the sediments of Lake Baikal, Siberia. *Journal of Geophysical Research*, **101**: 11365–11385.

Peck, J.A., King, J.W., Colman, S.M., and Kravchinsky, V.A., 1994. A rock-magnetic record from Lake Baikal, Siberia: Evidence for late Quaternary climate change. *Earth and Planetary Science Letters*, **122**: 221–238.

Raisbeck, G.M., Yiou, F., Bourles, D., Lorius, C., Jouzel, J., and Barkov, N.I., 1987. Evidence for two intervals of enhanced ^{10}Be deposition in Antarctic ice during the last glacial period. *Nature*, **326**: 273–277.

Reynolds, R.L., Tuttle, M.L., Rice, C.A., Fishman, N.S., Karachewski, J.A., and Sherman, D.M., 1994. Magnetization and geochemistry of greigite-bearing Cretaceous strata, North Slope Basin, Alaska. *American. Journal of Science*, **294**: 485–528.

Roberts, A.P., Lehman, B., Weeks, R.J., Verosub, K.L., and Laj, C., 1997. Relative paleointensity of the geomagnetic field over the last 200000 years from ODP Sites 883 and 884, North Pacific Ocean. *Earth and Planetary Science Letters*, **152**: 11–23.

Roberts, A.P., and Turner, G.M., 1993. Diagenetic formation of ferrimagnetic iron sulphide minerals in rapidly deposited marine sediments, South Island, New Zealand. *Earth and Planetary Science Letters*, **115**: 257–273.

Sagnotti, L., Macrí, P., Camerlenghi, A., and Rebessco, M., 2001. Antarctic environmental magnetism of Antarctic Late Pleistocene sediments and interhemispheric correlation of climatic events. *Earth and Planetary Science Letters*, **192**: 65–80.

Schwartz, M., Lund, S.P., and Johnson, T.C., 1996. Environmental factors as complicating influences in the recovery of quantitative geomagnetic field paleointensity estimates from sediments. *Geophysical Research Letters*, **23**: 2,693–2,696.

Schwartz, M., Lund, S.P., and Johnson, T.C., 1998. Geomagnetic field intensity from 71 to 12 ka as recorded in deep-sea sediments of the Blake Outer Ridge, North Atlantic Ocean. *Journal of Geophysical Research*, **103**: 30407–30416.

Schneider, D.A., 1993. An estimate of Late Pleistocene geomagnetic intensity variation from Sulu Sea sediments. *Earth and Planetary Science Letters*, **120**: 301–310.

Snowball, I.F., and Torii, M. 1999. Incidence and significance of ferrimagnetic iron sulphides in Quaternary studies, In Maher, B.A., and Thompson, R. (eds.), *Quaternary Climates and Magnetism.* Cambridge: Cambridge University Press, pp. 199–230.

Sprowl, D.R., 1985. The paleomagnetic record from Elk Lake, MN, and its implications, PhD Dissertation thesis, University of Minnesota.

Stacey, F.D., 1972. On the role of Brownian Motion in the control of detrital remanent magnetization of sediments. *Pure and Applied Geophysics.*, **98**: 139–145.

St-Onge, G., Stoner, J.S., and Hillaire-Marcel, C., 2003. Holocene paleomagnetic records from the St. Lawrence Estuary, eastern Canada: centennial- to millennial scale geomagnetic modulation of cosmogenic isotopes. *Earth and Planetary Science Letters*, **209**: 113–130.

St.Onge, G., Stoner, J., Rochon, A., and Channell, J.E., 2005. High resolution Holocene paleomagnetic secular variation records from the Eastern and Western Canadian Arctic. *Eos, Transactions, American Geophysical Union*, **86**(52), Fall Meet. Suppl. Abstract GP44A-03.

Stoner, J.S., Channell, J.E.T., and Hillaire-Marcel, C., 1998. A 200 ka geomagnetic chronostratigraphy for the Labrador Sea: Indirect correlation of the sediment record to SPECMAP. *Earth and Planetary Science Letters*, **159**: 165–181.

Stoner, J.S., Channell, J.E.T., Hillaire-Marcel, C., and Kissel, C., 2000. Geomagnetic paleointensity and environmental record from Labrador Sea core MD95–2024: global marine sediment and ice core chronostratigraphy for the last 110 kyr. *Earth and Planetary Science Letters*, **183**: 161–177.

Stoner, J.S., Laj, C., Channell, J.E.T., and Kissel, C., 2002. South Atlantic and North Atlantic geomagnetic paleointensity stacks (0–80 ka): implications for inter-hemispheric correlation. *Quaternary Science Reviews*, **21**: 1141–1151.

Stoner, J.S., Channell, J.E.T., Hodell, D.A., and Charles, C.D., 2003. A ∼580 kyr paleomagnetic record from the sub-Antarctic South Atlantic (Ocean Drilling Program Site 1089). *Journal of Geophysical Research,* **108**, doi:10.1029/2001JB001390.

Stoner, J.S., Francus, P., Bradley, R.S., Patridge, W., Abbott, M.A., Retelle, M.J., Lamoureux, S., and Channell, J.E.T., 2005. Abrupt shifts in the position of the north magnetic pole from Arctic lake sediments: Relationship to archeomagnetic jerks. *Eos, Transactions, American Geophysical Union* **86**(52), Fall Meet. Suppl. Abstract GP44A-02.

Sugiura, N., 1979. ARM, TRM, and magnetic interactions: concentration dependence. *Earth Planetary and Science Letters*, **42**: 451–455.

Tauxe, L., LaBreque, J.L., Dodson, R., Fuller, M., and Dematteo, J., 1983. "U"-channels—a new technique for paleomagnetic analysis of hydraulic piston cores. *Eos, Transactions, American Geophysical Union*, **64**: 219.

Tauxe, L., and Kent, D.V., 1984. Properties of a detrital remanence carried by hematite from study of modern river deposits and laboratory redeposition experiments. *Geophysical Journal of the Royal Astronomical Society*, **77**: 543–561.

Tauxe, L., and Valet, J.-P., 1989. Relative paleointensity of the Earth's magnetic field from marine sedimentary records: A global perspective. *Physics of the Earth and Planetary Interiors*, **56**: 59–68.

Tauxe, L., and Wu, G., 1990. Normalized remanence in sediments of the western equatorial Pacific; Relative paleointensity of the geomagnetic field. *Journal of Geophysical Research*, **95**: 12337–12350.

Tauxe, L, 1993. Sedimentary records of relative paleointensity and the geomagnetic field: theory and practice. *Reviews of Geophysics*, **31**: 319–354.

Tauxe, L., Pick, T., and Kok, Y.S., 1995. Relative paleointensity in sediments: a pseudo-Thellier approach. *Geophysical Research Letters*, **22**: 2885–2888.

Thouveny, N., Carcaillet, J., Moreno, E., Leduc, G., and Nérini, D., 2004. Geomagnetic moment variation and paleomagnetic excursions since 400 kyr B.P.: a stacked record from sedimentary sequences of the Portuguese margin. *Earth and Planetary Science Letters*, **219**: 377–396.

Tric, E., Valet, J.-P., Tucholka, P., Paterne, M., La Beyrie, L., Guichard, F., Tauxe, L., and Fontugne, M., 1992. Paleointensity of the geomagnetic field during the last 80000 years, *Journal of Geophysical Research*, **97**: 9,337–9,351.

Valet, J.-P., Meynadier, L., and Guyodo, Y., 2005. Geomagnetic dipole strength and reversal rate over the past two million years. *Nature*, **435**: 802–805.

Verosub, K.L., Herrero-Bervera, E., and Roberts, A.P., 1996. Relative geomagnetic paleointensity across the Jaramillo subchron and the Matuyama/Brunhes boundary. *Geophysical Research Letters*, **23**: 467–470.

Voelker, A., Sarnthein, M., Grootes, P.M., Erlenkeuser, H., Laj, C., Mazaud, A., Nadeeau, M.J., and Schleicher, M., 1998. Correlation of marine ^{14}C ages from the Nordic Sea with GISP2 isotope record: implication for ^{14}C calibration beyond 25 ka B.P. *Radiocarbon*, **40**: 517–534.

Weeks, R., Laj, C., Endignoux, L., Fuller, M., Roberts, A., Manganne, R., Blanchard, E., and Goree, W., 1993. Improvements in long-core measurement techniques: applications in palaeomagnetism and palaeoceanography. *Geophysical Journal International*, **114**: 651–662.

Wagner, G., Masarik, J., Beer, J., Baumgartner, S., Imboden, D., Kubik, P.W., Synal, H.-A., and Suter, M., 2000a. Reconstruction of the geomagnetic field between 20 and 60 kyr B.P from cosmogenic radionuclides in the GRIP ice core. *Nuclear Instruments and Methods In Physics Research Section B*, **172**: 597–604.

Wagner, G., Beer, J., Laj, C., Kissel, C., Masarik, J., Muscheler, R., and Synal, H.-A., 2000b. Chlorine-36 evidence for the Mono Lake event in the Summit GRIP ice core. *Earth and Planetary Science Letters*, **181**: 1–6.

Williams, T., Thouveny, T.N., and Creer, K.M., 1998. A normalised intensity record from Lac du Bouchet: geomagnetic palaeointensity for the last 300 kyr. *Earth and Planetary Science Letters*, **156**: 33–46.

Yamazaki, T., 1999. Relative paleointensity of the geomagnetic field during Brunhes Chron recorded in North Pacific deep-sea sediment cores: orbital influence? *Earth and Planetary Science Letters*, **169**: 23–35.

Yamazaki, T., Ioka, N., and Eguchi, N., 1995. Relative paleointensity of the geomagnetic field during the Brunhes chron. *Earth and Planetary Science Letters*, **136**: 525–540.

Yang, S., Odah, H., and Shaw, J., 2000. Variations in the geomagnetic dipole moment over the last 12000 years. *Geophysical Journal International*, **140**: 158–162.

Yiou, F., Raisbeck, G.M., Bourles, D., Lorius, C., and Barkov, N.I., 1985. ^{10}Be in ice at Vostok Antarctica during the last climatic cycle. *Nature*, **316**: 616–617.

Yiou, F., Raisbeck, G.M., Baumgartner, S., Beer, J., Hammer, C., Johnsen, S., Jouzel, J., Kubik, P.W., Lestringuez, J., Stiévenard, M., Suter, M., and Yiou, P., 1997. Beryllium-10 in the Greenland Ice Core Project ice core at Summit, Greenland. *Journal of Geophysical Research*, **102**: 26,783–26,794.

Cross-references

Archeomagnetism
Environmental Magnetism
Geomagnetic Excursion
Magnetic Domain
Magnetic Susceptibility
Magnetization, Anhysteretic Remanent (ARM)
Magnetization, Chemical Remanent (CRM)
Magnetization, Depositional Remanent (DRM)
Magnetization, Isothermal Remanent (IRM)
Magnetization, Natural Remanent (NRM)
Magnetization, Thermoremanent (TRM)
Magnetostratigraphy
Paleomagnetism
Rock-Magnetism

PALEOMAGNETIC FIELD COLLECTION METHODS

The primary aim of paleomagnetic research is to reconstruct the orientation of the Earth's magnetic field at a given location from the study of a rock unit of known age. For this purpose, it is required to collect samples from the unit to be studied with the purpose of determining their magnetization and magnetic mineralogy in the laboratory. In order to conduct consistency tests of the direction of magnetization of the unit of interest, it is advisable to sample the unit at several localities as widely as possible. This procedure helps to avoid biasing effects introduced by undetected tectonic complications or other, probably more local alteration effects. In return, more effort is required in collecting samples in the field and the adoption of a well-defined hierarchy that needs to be followed during sampling is also needed.

In paleomagnetic parlance, a site refers to the location of each place where a particular sedimentary bed, or cooling igneous unit (i.e., one lava flow or one dyke) is exposed and samples are collected. A sample refers to each oriented piece of rock separately that is retrieved from the outcrop, whereas a specimen refers to smaller pieces of rock, which are well-determined in shape and dimensions obtained from one sample. Commonly, six to eight samples are required within 5–10 m of outcrop at a single site to average out the nonsystematic errors possibly made during sample orientation. At the laboratory, each sample will be split in specimens that can be inserted in the holder of the available instrument that is used for the measurement of magnetization and other laboratory tests. In practice, it is a good idea to have samples large enough to provide multiple specimens, even when only one specimen per sample is all that is required for the measurement of magnetization. This is the case because if more than one specimen per sample is measured at each site, the averaging of the orientation errors will not be unbiased unless the specimens measured for each sample is equal in number. In any case, little is gained in accuracy if more than three specimens from each sample are measured in one site.

Although this hierarchy is easy to follow in general, there are some aspects that require closer examination. For example, if the only access to the rock is through a long drill core (for example those obtained in exploration wells), then following the above definitions we would be limited to only one sample per site (unless more than one core is retrieved at the same location), as little would be gained in terms of accuracy of orientation by measuring more than one specimen per rock-unit traversed by the core. In thick enough units, however, it might prove to be convenient to measure six to eight specimens from the same unit to get a more representative estimation of the magnetization of the unit at that site (core). Certainly, in these conditions the error in the reconstructed magnetization (even when it might only refer to the inclination as the horizontal orientation of the core might not be available) introduced by the error in the orientation of the core will not be averaged out, but at least some internal checks for consistency and homogeneity of the magnetic properties of each rock unit can be made in this form.

As for the actual samples, these can be grouped in three main types depending on the procedure followed for their collection. The most common type of paleomagnetic sample is collected by using a portable drill with a water-cooled diamond bit. The drill is commonly powered by a gasoline engine, but in some occasions it might be necessary to use an electric drill that uses a rechargeable battery. The diameter of the cores drilled in this form is commonly $\sim$2.5 cm and the length depends on the hardness of the rock, the type of drill-bit used and the expertise of the operator. After coring the outcrop to the desired depth and the drill apparatus has been retrieved, an orientation devise is introduced in the space left by the bit. The orientation devise consists of a long tube that has a slot extending from one of its extremes, and a swiveling surface with some type of level attached to the other. The devise is rotated until the surface on the outer extreme becomes horizontal, allowing the correct orientation of the core before retrieving it from the outcrop. The slot in the lower end of the orienting devise (now inserted in the rock) is used to mark the sample, commonly with a brass rod. The orientation is made using a magnetic or a solar compass (or both) attached to the orientation devise, and by reading the angle of the core relative to either the horizontal or the vertical plane. The accuracy of orientation with this method is about $\pm 2^\circ$. After the completion of orientation, the orienting devise is retrieved and the core is broken from the outcrop, labeled, and packed.

Another type of paleomagnetic sample is collected by the simpler method of orienting a block of the outcrop that is later broken and labeled. These types of samples are commonly collected when the lithology is not suitable for coring. There are logistic complications for transporting the coring equipment (including water and gasoline) to the outcrop, there are laws forbidding the use of coring equipment (as for example in some national parks or reserve areas), or in desperation when the coring equipment breaks down in the middle of a field season. Although simpler in logistics, this method of sample collection is not as good as the coring method because of the limitations in the accuracy of orientation and on the need of collecting joint blocks that are more likely to have been affected by weathering than the massive portions of the outcrop. It also requires carrying of an excess material that has to be thrown away after specimens have been sliced out of the sample in the laboratory.

The third main type of paleomagnetic sample is collected in the form of core sample obtained from lake- or sea-bottom cores or from exploration wells. These samples are typically ~10 cm diameter and can be from a few meters to some hundreds of meters and even kilometers long. There are two main types of coring techniques in this category: piston coring (in which the bit is introduced forcefully into the sediment) and rotary drills (similar in all respects to the first type of samples discussed above, but with drills that are much larger and not likely to be handled by just one bare-handed operator). Both types of cores are commonly azimuthally unoriented and the direction of the core is assumed to be vertical. Evidently, these types of samples provide less reliability in terms of accuracy of orientation, which often involve the operation of expensive machinery and may not yield recovery of the entire core, but as already mentioned they can be the only access to one particular rock unit.

In some particular situations, paleomagnetic samples can be collected by using very specific (and sometimes very ingenious) methods that often combine some aspects of the three main types just mentioned. For example, loose sediments that are accessible in outcrop cannot be suitable for drilling or for block sampling. In this case, samples can be collected by inserting small plastic boxes in the sediment and orienting them before removing the material around to retrieve the box. Some degrees of impregnation with an epoxic resin might also be used for this purpose, or any other method that allows the operator to retrieve a reasonably well oriented sample.

In summary, the most important aspect to have in mind when collecting samples for any paleomagnetic work is the ability to orient the samples. Although in some circumstances the orientation must be necessarily limited to a distinction between the up and down directions, therefore limiting the utility of such samples.

Edgardo Cañón-Tapia

Cross-references

Paleomagnetism

PALEOMAGNETIC SECULAR VARIATION

The source of the Earth's magnetic field has been the subject of scientific study for more than 400 years (e.g., Gilbert, 1600). At present we believe that most of the field measured at the Earth's surface is of internal origin, generated by hydromagnetic dynamo action in the liquid-iron outer core. Historic measurements of the geomagnetic field have documented its primarily dipolar spatial structure at the Earth's surface and its temporal variability, which is termed as secular variation. One notable characteristic of the Earth's magnetic field and secular variation is its full vector nature, with significant space-time variability in both directions and intensity. Recent historic secular variation (HSV) studies (e.g., Thompson and Barraclough, 1982; Bloxham and Gubbins, 1985. Olson *et al*., 2002) have characterized the global pattern of short-term secular variation and have related its variability to the core dynamo process.

Paleomagnetic studies make it clear, however, that the Earth's magnetic field has undergone a wider range of temporal and spatial variability than has been seen in historic times. Geomagnetic field polarity reversals have occurred intermittently in time (e.g., Cande and Kent, 1995) and the intervening time intervals of stable dipole polarity contain paleomagnetic secular variation (PSV) larger in amplitude and broader in frequency content than HSV. PSV studies have also documented occasional excursions (Watkins, 1976; Verosub and Banerjee, 1977), which are anomalous PSV fluctuations that may be aborted polarity reversals or represent a fundamentally different multipolar state of the geomagnetic field (Lund *et al*., 1998, 2001).

PSV is estimated from the paleomagnetic study of archeological materials, unconsolidated sediments, and rocks. The paleomagnetic methods used to recover PSV data are well documented (e.g., Butler, 1992. Tauxe, 1993. Merrill *et al*., 1998; Dunlop and Özdemir, 2001), and everyone noticed that rather different methods are normally used to recover estimates of paleomagnetic field direction and intensity. Therefore, historically, PSV directional data usually do not have associated paleointensity estimates and vice versa. However, over the last decade that tendency has finally been balanced by the development of numerous high-resolution full-vector PSV records.

This article surveys our current knowledge of PSV; it will provide an overview of PSV data sources, methods of PSV analysis, long-term characteristics of PSV, and models for PSV behavior. The survey will discuss both intensity and directional variability. Special attention will be paid to the relationship between PSV and HSV, the evidence for or against long-term stationarity of PSV, the relationship of PSV to excursions, and the characteristics of PSV that may be useful in dynamo studies.

PSV data

PSV data come from a wide variety of paleomagnetic studies that can be separated into three groups based on the type of sediment or rock measured, the degree of detail in stratigraphic sampling, and the degree of age control for each study. The three resulting PSV data groups are (1) studies of Quaternary-aged sequences of unconsolidated sediments, lava flows, or archeological materials, which can be dated in detail by radiocarbon methods or oxygen isotope stratigraphy, and which are sampled in detail sufficient to resolve the temporal pattern of PSV variability (termed waveform information); (2) studies of older sediment or lava flow sequences that have waveform information but no detailed age control; and (3) studies of any aged rock or sediment sequences that have poor within sequence age control and no waveform information (sequential data are not serially correlated). The first type of PSV study can be used for a full spectrum of time series analyses (waveform, spectral, or statistical analyses); the second type of study can be used for waveform and statistical analyses; the third type of study is only suitable for statistical analysis.

The materials normally used for detailed paleomagnetic studies of PSV are archeological materials (kilns, fire pits, etc.), lava flows, and lake or marine sediment sequences. Each of these materials has inherent advantages and disadvantages for the accurate recording of PSV and the accumulation of paleomagnetic records from all three materials in parallel is the ideal way to establish regional patterns of PSV. Figure P9 illustrates the use of multiple PSV records derived from multiple

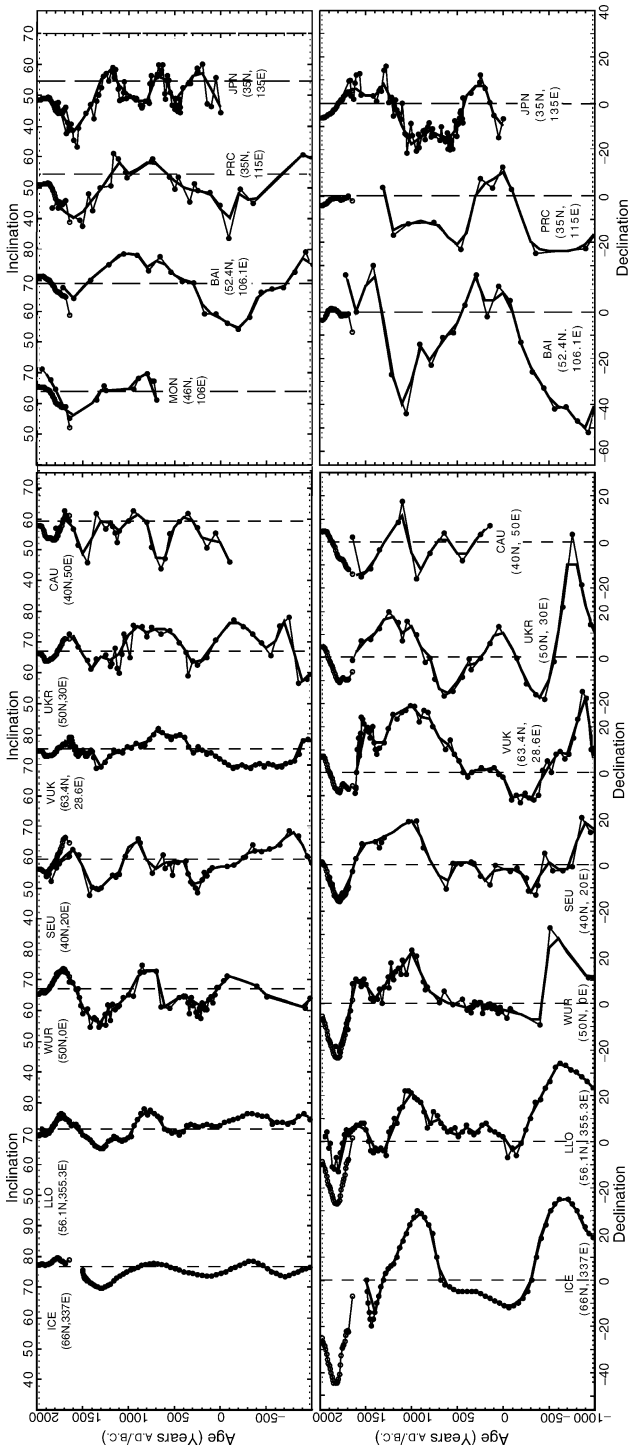

Figure P9 Comparison of paleomagnetic and historic secular variation directional data from Eurasia. Composite PSV records, summarized in Constable *et al.* (2000), extend from Iceland (ICE) to Japan (JPN). Solid dots are original paleomagnetic data, heavy solid lines are interpolated time-series (PSVMOD1.0 available at http://earth.usc.edu/~slund), and open circles in the last 400 years are estimated historical field variations based on spherical harmonic analysis.

data sources (data summarized in Constable *et al.*, 2000) to reconstruct the paleomagnetic directional variability across Eurasia for the last 3 ka. PSV records ICE, Loch Lomand, Scotland (LLO), Lake Vukonjarvi, Finland (VUK), and Lake Baikal, Russia (BAI) are derived from lake sediment sequences, while the other six PSV records are based on archeological and lava-flow measurements. The solid dots in Figure P9 are the actual paleomagnetic measurements, the heavy solid lines are interpolated equi-spaced time series (PSVMOD1.0, available at http://earth.usc.edu/~slund), and open circles in the most recent 400 years are estimated historical secular variation based on spherical harmonic analysis.

Lava flows and archeological materials have the advantage that their natural remanent magnetization (NRM) is normally a thermoremanent magnetization (TRM). A TRM is acquired over time intervals of less than a few minutes to days by heating a material to high temperatures and cooling it in the presence of the geomagnetic field. Therefore, the TRM retains a truly "instantaneous" record of PSV. The primary disadvantage of archeological materials is their scarcity prior to about 2000 years B.P. The primary disadvantage of lava flows is the difficulty in finding sufficient radiocarbon dated flows within a region to develop a long duration, composite PSV record; only a few such studies are currently available in the whole world (e.g., Champion, 1980. Holcomb *et al.*, 1986; Kissel and Laj, 2004).

Sediments acquire their NRM, termed as depositional or post-depositional remanent magnetization (DRM/PDRM), due to mechanical alignment of magnetic grains with the geomagnetic field while they are in the water column or in interstitial spaces just below the sediment-water interface. The grains are subsequently locked into that orientation by grain-grain contacts during dewatering, normally within 10–20 cm of the sediment-water interface. The primary advantage of sediment sequences is their potential to provide continuous, high-resolution PSV records far back in time from many sites around the world. The primary drawback to sediments, however, is the lower resolution of the DRM/PDRM recording process due to some degree of inherent smoothing of the PSV signal during remanence acquisition near the sediment-water interface. In most high-resolution sediment records, the smoothing interval can be estimated to be less than 100 years in duration, but further study is necessary to establish the role of smoothing in a better manner in the acquisition process of DRM/PDRM.

An added complexity associated with all PSV data is the limited extent to which they can be compared to HSV data. This difficulty in correlation occurs because (1) PSV data does not have the broad spatial (global) sampling distribution of HSV data, (2) the inherent vector resolution of PSV data (2° to 4° $\alpha 95$ at best) is significantly lower than the resolution of HSV data (typically 1° $\alpha 95$ or better), and (3) the radiometric ages associated with PSV have relatively large errors (ca. $\pm$100 years or greater). PSV records derived from sediments have the added disadvantage, noted previously, of not recovering instantaneous estimates of secular variation due to inherent DRM/PDRM smoothing. Because of these differences, it is difficult to compare the space-time structures of HSV and PSV data in detail, even though site measurements of PSV and HSV may agree within the limit of data resolution (e.g., Figure P9). What we can hope is that analysis of PSV data will yield spatial and/or temporal characteristics that relate, in some way, to observed HSV characteristics.

Three examples of total-vector PSV records are shown in Figures P10-P12. Figure P10 is a Holocene PSV record from wet lake sediments of Lake St. Croix (Lund and Banerjee, 1985; Lund and Schwartz, 1999), Figure P11 is a late-Pleistocene PSV record from uplifted (dry) lake sediments surrounding Mono Lake (Liddicoat and Coe, 1979; Lund *et al.*, 1985), and Figure P12 is a late-Pleistocene PSV record recovered from deep-sea sediments of the western North Atlantic Ocean (Lund *et al.*, 2001, 2005).

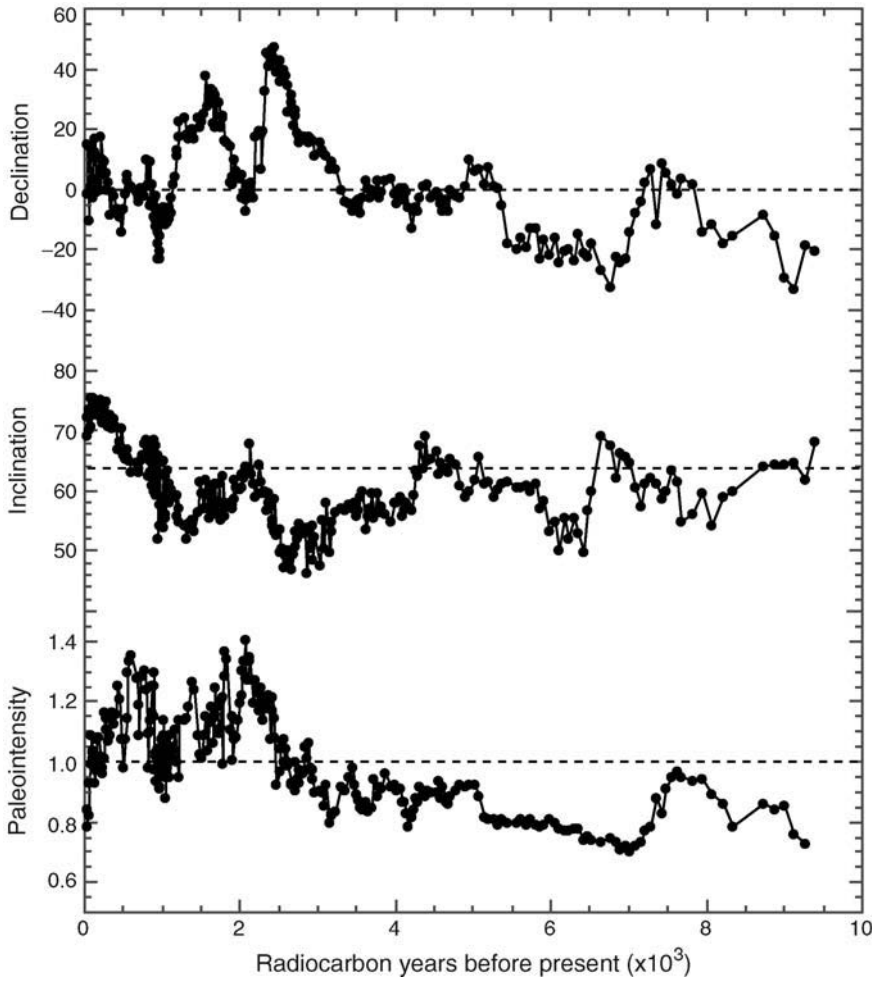

Figure P10 Holocene full-vector paleomagnetic secular variation record recovered from Lake St. Croix, Minnesota (USA) (Lund and Banerjee, 1985; Lund and Schwartz, 1999).

Time-series analysis of PSV

The conceptual framework for analysis of PSV data is based on the fact that HSV records are too short in duration to adequately characterize the totality of temporal field variability, while PSV records are too scattered spatially to routinely describe the prehistoric spatial field variability. We can hope, however, to identify spatial and short duration temporal components of the HSV that may relate to long-term temporal components of the PSV. We can also attempt to improve the spatial estimates of PSV by, perhaps, appealing to analogs in HSV. Such a coordinated analysis of PSV and HSV can perhaps address a key to an unresolved question in secular variation studies: What is the mapping function between the observed spatial and temporal variations of the geomagnetic field? Only with a coherent view of the total spatiotemporal variability of the historic and prehistoric geomagnetic field can we properly evaluate models of the core dynamo process, which is the source of the field variability.

Analysis of PSV data uses a variety of time-series and modeling techniques in order to delineate the spatial and temporal characteristics of PSV. Time-series techniques that can be applied to PSV data will be considered in this section; modeling techniques will be considered in the next section. Time-series techniques are classified into three broad categories: waveform analysis, spectral analysis, and statistical analysis. Each of these techniques has unique advantages for characterizing a particular type of PSV data and thereby providing a point of comparison with HSV data.

Waveform analysis

PSV records that display good serial correlation between adjacent data points (e.g., Figures P9-P12) can be used to assess the actual time evolution of geomagnetic field variability. This time evolution can be characterized either by evaluating simple PSV features, such as maxima or minima of inclination, declination, or paleointensity, or more distinctive sets of features termed vector waveforms (Lund, 1996). One type of vector waveform that may have fundamental importance for dynamo studies is the vector-looping pattern termed circularity (Runcorn, 1959. Skiles, 1970) often exhibited by HSV and PSV records (e.g., Bauer, 1895. Creer, 1983. Lund, 1996). Comparisons of simple features or vector waveforms may take place (1) within individual paleomagnetic records, (2) between records of different sites, and (3) between PSV and HSV records (where they overlap in time), and can be used to assess the temporal evolution of secular variation. Comparisons of the amplitudes and phase relationships of PSV features or waveforms with their spatial counterparts(?) in global maps of the present-day field may be used to assess the spatial-temporal mapping of secular variation. Below we discuss three different types of waveform comparison that document distinctive PSV characteristics.

The first type of waveform comparison that should be considered is between PSV records and HSV records from the same sites. For example, Figure P9 shows a transect of PSV records for the last 3 ka across Eurasia. Open circles in the interval A.D. 1600 to A.D. 2000 estimate the historic secular variation for each site based on spherical

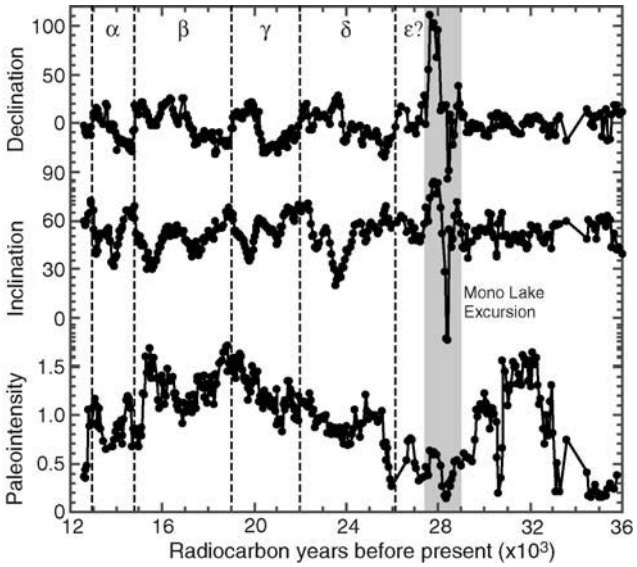

Figure P11 Late Pleistocene full-vector paleomagnetic secular variation record recovered from uplifted lake sediments exposed at Mono Lake, California (USA) (Liddicoat and Coe, 1979; Lund *et al.*, 1988). Note the presence of the Mono Lake excursion near 28000 radiocarbon years B.P. and indication of at least four cycles of a complex repeating vector waveform (α-ε?) associated with the excursion.

harmonic analyses. Such comparisons indicate that only the largest amplitude, longest period (~200–400 years) HSV features can be correlated with the PSV variability (indicated by solid circles in Figure P9). This limited correlation is due to the fact that PSV records only resolve features greater than about 4° in amplitude and a few hundred years in duration. Even then, this correlation shows that high-resolution PSV records can accurately record and extend the long-term temporal variation only hinted at in HSV records.

The second type of comparison, between different high-resolution PSV records from the same region (e.g., Europe or East Asia), can be used to assess the spatial extent of PSV features. For example, Figure P9 shows late Holocene PSV records from seven different sites in Europe (Iceland, ICE to CAU) spread over 70° of longitude (~7000 km) and four different sites in East Asia (MON to Japan, JPN) spread over 30° of longitude (~3000 km). Within each of these regions, it is readily apparent that a large number of directional features can be correlated among the records. (i.e., not to say that the records are identical, but variations in sampling rate and signal to noise ratios or errors in data acquisition and analysis probably can explain most of the differences in single records). One interpretation of these observations is that PSV features with periods longer than a few hundred years must correspond to spatial features that are observable in historic maps of the geomagnetic field and have spatial domains of several 1000 km.

A similar comparison between PSV records from different geographic regions is more problematic. For example, the comparison between European and East Asian PSV records in Figure P9 indicates that there is no simple correlation between directional records from the two regions that preserves phase relationships or long-term trends in the directional data. Similarly, there is no simple vector pattern that

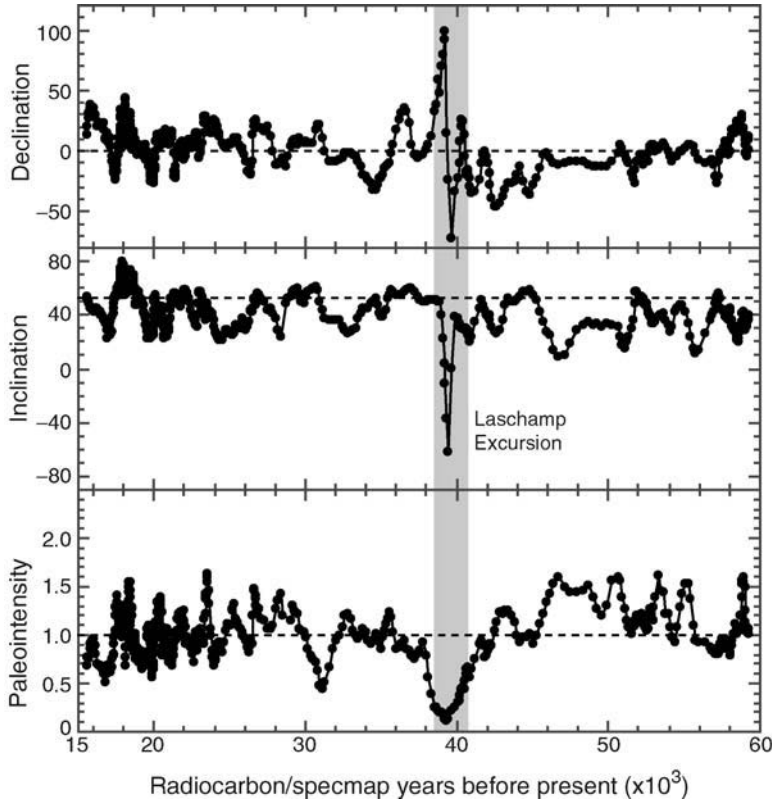

Figure P12 Late Pleistocene full-vector paleomagnetic secular variation record from deep-sea piston core JPC-14, western north Atlantic Ocean (Lund *et al.*, 2001, 2005). Note the presence of the Laschamp excursion near ~40000 years B.P.

can be traced all the way across Eurasia for the last 3000 years. It thus appears that straightforward PSV vector correlations break down beyond perhaps 5000 km. Thompson (1984) noted a similar scale of spatial coherence in the correlation of HSV waveforms. He determined that HSV could be broken down into about nine different regions over the Earth's surface. Within each region, HSV waveforms are broadly correlative, but between regions the patterns are significantly different (and uncorrelated except for an overall vector average approximating the axial dipole expectation). This lack of global-scale correlation appears to be present in directional PSV records as well and indicates that there is no persistent westward (or eastward) drift of distinctive geomagnetic features over thousands of years, as has been suggested most recently by Merrill *et al*. (1998).

Paleointensity, on the other hand, does show clear evidence of global-scale coherence in its variability. Comparisons of paleointensity records from around the world (e.g., Guyodo and Valet, 1999; Laj *et al*., 2000; Stoner *et al*., 2003) show clear evidence that most long-term (>1000 years) paleointensity variability is correlatable on a global scale. For example, Figure P13 shows two high-resolution relative paleointensity records recovered from deep-sea sediments on almost opposite sides of the Earth (Stott *et al*., 2002). The records identify 30 paleointensity features that are synchronous in age (~500 years resolution) based on oxygen isotope age determinations, including a distinctive paleointensity low associated with directional records of the Laschamp Excursion at each site. One future task of PSV studies is to rationalize how significantly different patterns of directional variability can exist around the world in the presence of such globally coherent paleointensity variability.

A third type of waveform comparison can be made between PSV features or vector waveforms within individual paleomagnetic records. Such comparisons have occasionally identified distinctive vector

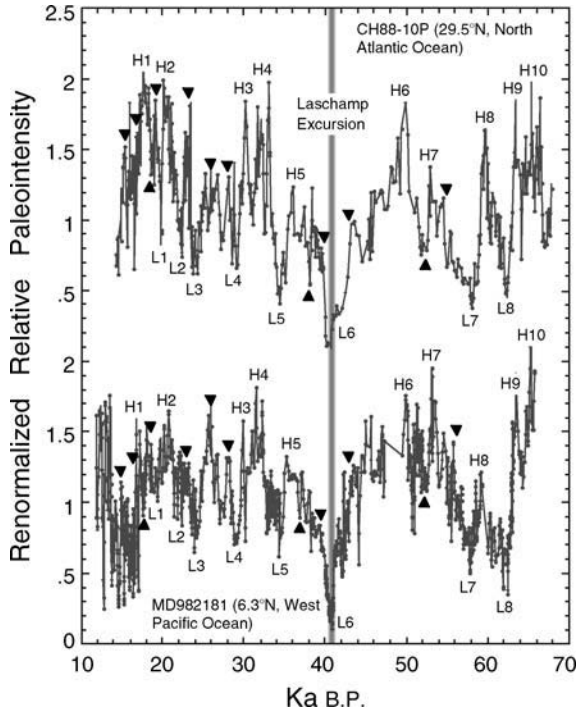

Figure P13 Late-Pleistocene paleointensity comparison between sediment PSV records from the North Atlantic Ocean and western Equatorial Pacific Ocean (Stott *et al.,* 2002). A number of distinctive and correlatable paleointensity features are noted in the two records; independent oxygen isotope stratigraphies suggest that these features are synchronous (~500 year uncertainty).

waveforms that seem to recur every 2500 to 4000 years. The PSV record from Mono Lake, shown in Figure P11, illustrates this recurrence pattern. At least four recurrences (α-δ) of basically the same complex waveform can be noted (Lund *et al*., 1988). With each recurrence, the waveform is slightly altered; however, the general pattern persists for more than 16 ka. It is likely that this distinctive waveform has evolved out of the Mono Lake excursion (waveform ϵ? in Figure P11). Similar recurring patterns have been noted in the Holocene PSV record from Lake St. Croix (Figure P10; Lund and Banerjee, 1985) in a late Pleistocene PSV record from Russia (Ekman *et al*., 1987), and after the Summer Lake Excursion recorded in lake sediments from Oregon (Negrini *et al*., 1994).

Recurring vector waveforms can also be identified by their distinctive sequences of vector looping (circularity). Such looping patterns (Runcorn, 1959) are characteristic of both PSV (e.g., Creer, 1983) and HSV (e.g., Bauer, 1895) and have been suggested (Skiles, 1970) to be an indicator of westward or eastward drift of the geomagnetic field (although there is no significant evidence of long-term persistent drift of the field as noted above). However, the correlation between observed looping and drift is not unique (Dodson, 1979). Large amplitude loops, often associated with recurring vector waveforms, last about 1000 to 1400 years; small amplitude loops have also been noted that last about 500–800 years. Looping intervals might be used as an indicator of the simplest temporal scale for PSV coherence at individual sites.

Excursions

One type of vector waveform deserves special note—magnetic field excursions, which are anomalous PSV fluctuations defined by virtual geomagnetic poles (VGPs) located more than 45° away from the geographic pole. It is clear that excursions do occur; it is often not clear, however, what is their waveform morphology or whether some excursions are really artifacts of field-laboratory measurement errors. There is growing evidence (e.g., Lund *et al*., 2001, 2005) that at least seventeen excursions have occurred in the Brunhes Epoch (0–780000 years B.P.). One distinctive element of all these excursions is that they occur within intervals of anomalously low global-scale paleointensity (see Figures P11-P13). Most excursion records are difficult to correlate around the world because of uncertainties in their age estimates. But, three of the most recent excursions are becoming better understood: the Mono Lake excursion (CA. 28000 years B.P.; Denham and Cox, 1971; Liddicoat and Coe, 1979; Figure P11), The Laschamp excursion (CA. 41000 years B.P.; Bonhommet and Zahringer, 1969; Figures P12 and P13) and the Blake Event (CA. 125000 years B.P.; Smith and Foster, 1969). For each of these excursions, there are now multiple independent records from around the world, which are sufficiently well dated to correlate the records and estimate that individual excursion records are synchronous to ~500-year resolution. There are also a number of high-resolution excursion records (e.g., Liddicoat and Coe, 1979; Lund *et al*., 2005.rpar; that assess the local waveform patterns of excursions and the surrounding normal PSV. However, there are still not enough high-resolution excursion records to be certain about their global pattern of field variability or relationship to normal PSV or magnetic field reversals.

Spectral analysis

Spectral analysis describes the frequency content of PSV over timescales of 10^2–10^5 years. Traditional ideas suggest that PSV should be a band limited process. That is, that the spectral power of PSV should markedly diminish beyond some cutoff period on the order of 10^4 years. PSV records longer than the cutoff period should then be stationary in a statistical sense and have an average field vector direction that is constant through time for a given site. The axial dipole hypothesis, a cornerstone of plate tectonic reconstructions, assumes that the PSV process is stationary and that each site's average field vector (during intervals of normal polarity) satisfies the formula,

$\tan I = 2\tan\lambda$, $D = 0°$, where λ is the site paleolatitude. One important goal of PSV studies is to test the long-term validity of the axial dipole hypothesis and the notion of a stationary PSV spectrum with limited power at $>10^4$ years.

Spectral analysis also describes the characteristic distribution of continuous spectral power within the overall PSV process (Barton, 1982, 1983) and identifies whether there are distinct frequency bands within the continuous spectrum that have higher than average spectral power. Knowledge of the PSV power spectrum and its potential changes in time and space is critical for better understanding the relationship between PSV and the core dynamo process that generates it.

The primary limitation in recovering detailed estimates of the PSV spectrum is the quality of age estimates associated with the PSV records. Records dated using radiocarbon methods over the last 40 ka or so may have systematic errors with respect to "true" time due to radiocarbon reservoir effects. They may also have random errors on the order of 10^2 years or worse due to random dating errors. Older PSV records can also be dated using oxygen isotope stratigraphies, but such age estimates have random uncertainties on the order of 10^3 years.

Despite these limitations, important and convincing spectral estimates of late-Quaternary PSV have been recovered from several regions around the world: Europe, North America, the Far East, Australia, and South America. Figure P14 shows the stacked PSV spectrum of unit-vector (RMS of scalar inclination and declination spectra) and paleointensity results from three deep-sea sediment PSV records in the western North Atlantic Ocean that are >50 ka in duration. These results provide a good overview of the long-term PSV spectrum. The unit-vector and paleointensity spectra are continuous in their power distribution, with the largest amplitude secular variation occurring at periods much greater than 10^3 years (far beyond the range of HSV). Both spectra are red (power-law relationship between frequency and power) for periods <5 ka–12 ka, and white (~constant power as a function of frequency) for longer periods with no indication of a marked decrease in spectral power at the longest observed periods (~50 ka). These characteristics suggest that the geomagnetic field is not stationary (band-limited) over timescales of less than about 10^5 years. The corner frequencies (boundaries between dominantly red and white spectra, indicated by arrows in Figure P14), are about 5 ka for the unit-vector spectrum and about 12 000 years for the paleointensity spectrum. One interpretation of the corner frequency is that the red spectrum describes the intrinsic dynamics of field variability associated with the dynamo process, while the white spectrum describes random perturbations of that process or longer-term external forces acting on that process (e.g., Channell *et al*., 1998). In this scenario, the corner frequency in paleointensity of ~12 ka defines the longest time constant of normal dynamo activity. The fact that the unit-vector corner frequency is only ~5 ka is due to the observation that vector variations only reflect nonaxial dipole field variability, not total field variability. It is probably not coincidental that the longest repeating vector waveforms noted in individual PSV records approach the unit-vector corner frequency of ~5 ka. There is also evidence of selected spectral bands in the red portion of the spectra with larger than average spectral power. That is the pattern noted in most other PSV spectra determined from shorter duration records (e.g., Barton, 1982, 1983). These spectral bands probably define the detailed pattern of dynamo activity in a region at any one time, but none of these components are probably periodic on a long-term spatial or temporal scale and they should tend to smear out when spectra from different time intervals or spatial regions are stacked.

Most of these spectral characteristics have no temporal analog in HSV because of the short time span of historic measurement. One might, however, attempt to relate the long-term PSV spectral characteristics to the present day geomagnetic field spatial spectrum. The spatial field due to core sources has a cutoff near spherical harmonic degree 12 and the spectral power decreases quickly from a maximum at harmonic degree 1 (dipole terms). Only spatial terms of about degree 6 or less have vector amplitudes large enough to be recorded in PSV., One might therefore hypothesize that the long-term PSV spectrum must be

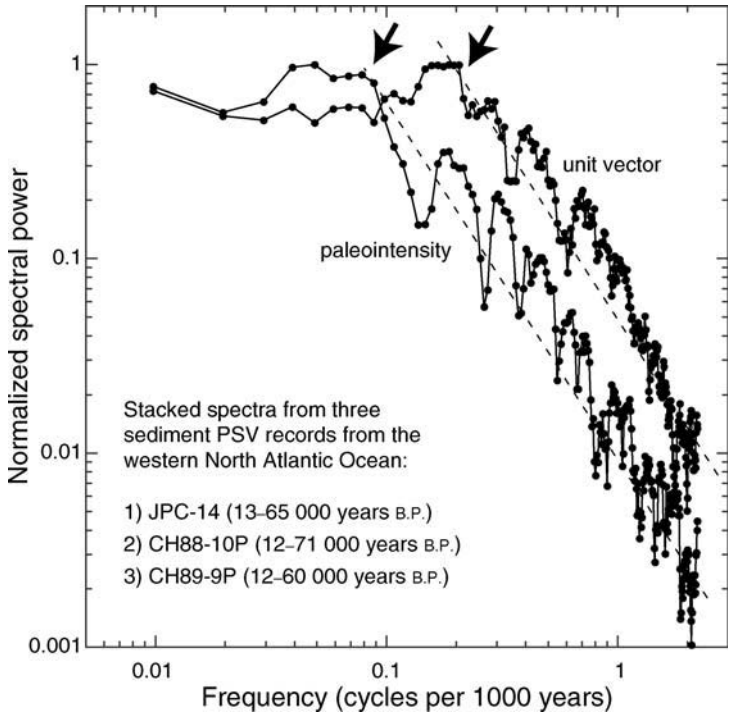

Figure P14 Paleointensity and unit-vector spectra for a stack of three long-term deep-sea sediment PSV records from the western North Atlantic Ocean. One of the records, JPC-14, is shown in Figure P12. Arrows indicate corner frequencies, which separate "white" and "red" portions of the spectra.

due to temporal variations of spatial components of the present-day field with spherical harmonic degree 5–6, under normal conditions.

Statistical analysis

The aspect of PSV that is easiest to analyze is its statistical behavior averaged over some interval of time. For this reason, statistical properties of PSV, within time windows in the order of 10^5 or 10^6 years, were the first PSV characteristics to be compared spatially, and even today they are the only PSV characteristics that can be easily compared on a global scale. Such comparisons provide the strongest evidence relating to possible long-term stationarity of geomagnetic field behavior, the axial dipole hypothesis, and the potential global pattern of selected PSV characteristics. Statistical study of PSV follows two very different paths on the basis of sampling frequency and age control of the paleomagnetic measurements. In the first approach, paleomagnetic field directions in undated rock sequences are measured under the assumption that the age difference of successive rock units is large compared to the longest period of PSV (often assumed to be about 10000 years). Each data point is therefore assumed to be an independent random value picked from an assumed frequency-band-limited PSV process. Data sets from small regions, averaged over 10^5 or 10^6 years, are then statistically analyzed and compared with some global model of the expected statistical behavior. (Even if the underlying assumptions of spectral content are wrong, as they likely are, results from this type of statistical analysis should not be seriously biased if the data are truly randomly spaced in time.) The second approach is to measure well-dated (either by radiocarbon or oxygen isotope methods) paleomagnetic sequences where the sampling interval is less than the shortest period of PSV (about 30 years). It is not often feasible to find sequences with such short time spacing, but useful information can be obtained with sample intervals up to perhaps 250 years (and even longer under special circumstances). Statistics are estimated from equispaced time-series derived from the dated paleomagnetic records. This method permits spatial comparison of statistical parameters averaged over much shorter time intervals, on the order of 10^3–10^5 years. In such studies, it is likely that the statistics does not represent a "stationary" estimate of space-time field variability but rather a "statistical snapshot" of an evolving space-time field structure.

Statistical analyses of the probability distributions of both field vectors and their equivalent VGPs from single sites indicate that neither distribution is typically Fisherian (Fisher, 1953; spherical analog of the Gaussian or normal distribution). For example, Brock's (1971) results from equatorial Africa (Figure P15) show that both field vectors and VGPs tend to have somewhat elliptical distributions. Engebretson and Beck (1978) have summarized the statistical parameters normally used to characterize the shape of the probability distribution. It is probable that shape statistics vary systematically as a function of latitude (and longitude?) and future studies of shape statistics may provide important added characteristics of the Earth's long-term PSV. As a starting point, it is worth noting that the range of vector variability (as a function of latitude) noted in historic maps of the geomagnetic field is comparable to the range of vector variability noted in individual PSV records from the late Quaternary. This suggests that, even though secular variation changes on timescales far beyond the range of historic measurements, the normal range of its spatial variability is completely present in the observed historic field. A similar observation has been made for the long-term pattern of PSV angular dispersion by McFadden *et al*. (1988).

Currently, the two statistical parameters most often measured in PSV studies are the ΔI anomaly, which is the site mean inclination minus the expected axial dipole field inclination and the angular dispersion associated with a site's vector (or equivalent VGP) variability. The global pattern of the ΔI anomaly estimates how well the axial dipole hypothesis, the cornerstone of plate tectonic reconstructions, fits the actual geomagnetic field behavior. The global pattern of angular dispersion should provide some measure of the spatial pattern of intrinsic "energy" or "dynamics" in the core dynamo process. This variability may be due to differing proportions of dipole versus nondipole field variability (see summary in Merrill *et al*., 1998) or it could be interpreted as the relative importance of primary versus secondary family spherical harmonic components (McFadden *et al*., 1988), two orthogonal components of the geomagnetic field that may have fundamental relationships to dynamo theory (Roberts and Stix, 1972).

The ΔI anomaly was perhaps first quantified by Wilson in 1970 who noticed that the average paleomagnetic pole positions associated with individual geographic regions (e.g., Australia, Europe, North America) were always farther from the sampled region than the known geographic pole. This offset, termed the farsided effect, is due to paleomagnetic inclinations that are systematically more negative than their axial dipole expectation (negative ΔI anomaly), on average. McElhinny *et al*. (1996) have determined the global ΔI anomaly for the last 5 Ma (see Figure P16), on average, and noted that the ΔI anomaly is mostly negative with a maximum anomaly near the Equator and a latitudinal variation that is symmetric about the Equator and

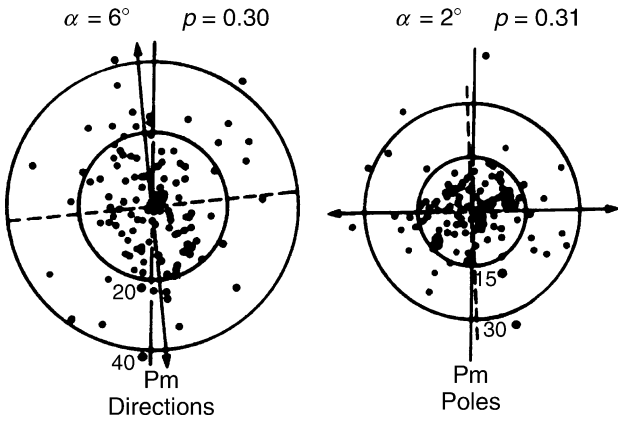

Figure P15 Statistical distribution of PSV directions and virtual geomagnetic poles (VGPs) from Equatorial Africa (Brock, 1971).

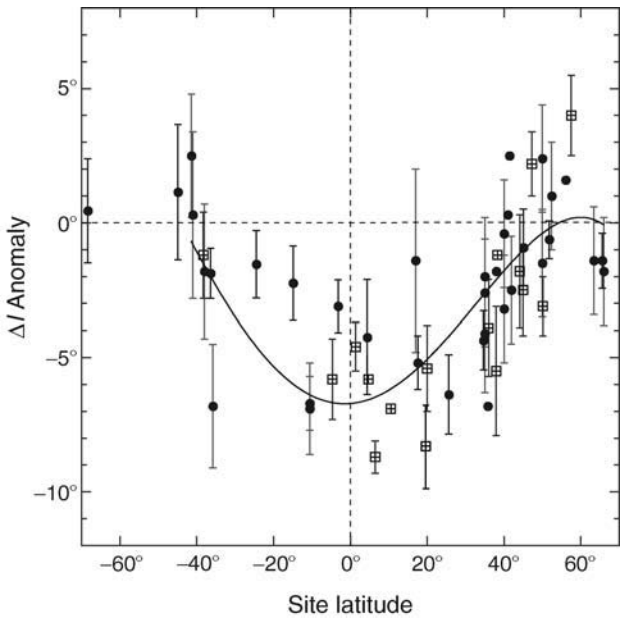

Figure P16 ΔI anomaly as a function of latitude for selected time intervals: solid symbols—last 5 Ma average, open circles last few thousand years average, open squares, last ~10–20 ka average.

zonal (any site along a line of latitude will have the same magnitude of ΔI anomaly). Their analysis also indicated that ΔI anomaly has persisted with the same general pattern and magnitude for the last 5 Ma during both normal and reversed polarity. Other workers (e.g., Coupland and Van der Voo, 1980; Livermore *et al*., 1984; Schneider and Kent, 1990) have noted that a similar pattern of ΔI anomaly has persisted for at least the last 100 million years, but with slow variations in the maximum anomaly magnitude. Statistical studies of shorter-term equispaced PSV time-series (e.g., Lund, 1985; Lund *et al*., in review) indicate that the ΔI anomaly averaged over 10^3 years (see open circles in Figure P16) and 10^4 years (see open squares in Figure P16) also show the same general ΔI anomaly pattern noted in the longer-term data. However, Constable and Johnson (2000) have argued that nonzonal components of the ΔI anomaly are significant and have persisted for the last several million years, with some Equatorial regions having more significant ΔI anomalies than other regions and some high-latitude regions actually having positive ΔI anomalies. These observations all suggest that the spatial pattern of the ΔI anomaly is persistent but nonstationary in its detailed pattern over timescales greater than $\sim 10^4$ years. The implication of the ΔI anomaly for plate tectonic studies is that paleolatitude estimates derived from paleomagnetic studies may be in error by as much as 8° depending on time and paleolatitude. Similar analyses of declination have shown no significant deviations in declination values from 0° over the last several million years.

Analysis of PSV angular dispersions (either directions or their equivalent virtual geomagnetic poles, VGPs) has established that this parameter also displays a distinctive zonal pattern of amplitude variation with latitude. The average latitudinal pattern of VGP angular dispersion for the last 5 Ma (McFadden *et al*., 1988) is shown in Figure P17. Lund (1985) and Lund *et al*. (in review) have noted, however, that VGP angular dispersion averaged over 10^3 and 10^4 year intervals (open circles and open squares in Figure P17) using equispaced PSV time-series is significantly lower than the 5 Ma average, and Merrill and McFadden (1988) have shown that it can vary on much longer (10^7 year) timescales as well. A variety of parametric models, summarized in Merrill *et al*. (1998), have been developed to attempt to explain the observed spatial pattern of angular dispersion in an *ad hoc* manner. More recently, McFadden *et al*. (1988) were able to relate the long-term average pattern of VGP angular dispersion to historical field observations and developed model G, based on the relative importance of primary versus secondary family magnetic field components (Roberts and Stix, 1972), to explain the latitude dependence.

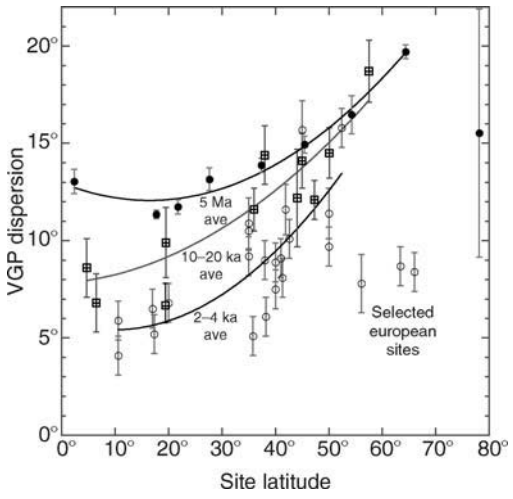

Figure P17 VGP angular dispersion as a function of latitude for selected time intervals: solid symbols—last 5 Ma average, open circles last few thousand years average, open squares, last ~10–20 ka average.

These statistical observations indicate clearly that PSV varies in a nonstationary manner over a variety of timescales, a pattern consistent with the PSV spectrum described above, and may be related to the continuing time evolution of regional PSV waveforms. One discordant note in this discussion of PSV nonstationarity is the qualitative sense that, even though PSV statistics may vary quantitatively in a nonpredictable manner over time, the PSV vector mean for any site is heavily "attracted" to its axial dipole expected direction. This may be due to the symmetry associated with the Earth's rotation, one of the driving forces of the dynamo. But, whatever be the cause, it seems prudent, perhaps, to think of PSV as "quasi-stationary" in its behavior based on the overall sense of "attraction" to such a "fixed point" (the axial dipole expectation) in time and space.

Models of PSV

An alternative method for the analysis of PSV is to develop models for the observed field variability. Such models may be conceptual in nature with their primary purpose being to qualitatively estimate the style of variability that a potential dynamo source might generate, or the models may be more quantitative (essentially mathematical simulation models), with their primary purpose being to replicate observed PSV. The mathematical simulation models may be developed from more conceptual models, with sources that may have some basis in reality, or purely from empirical (unrealistic) inputs. A third group of models that characterize the actual hydromagnetic process that generates the Earth's core field is beyond the scope of this survey.

Conceptual models

Previously, various conceptual models have been proposed to qualitatively explain characteristic features of HSV. Three models that have been discussed most often are (1) dipole wobble, (2) westward (or eastward) drift of the total nondipole field, and (3) standing and drifting nondipole fields. These conceptual models have also been called upon to qualitatively explain specific components of PSV or to justify and physically explain specific mathematical simulation models of PSV.

Dipole wobble has been suggested as one component of HSV and PSV based on the presence of an 11.5° offset in the present day dipole field, its persistence during historic time, and the indication from paleomagnetic data that the field has an average declination of 0° over timescales of 10^4 years or longer. Therefore, the average dipole field direction must have moved prehistorically and perhaps it has "wobbled" irregularly.

The paleomagnetic evidence for dipole wobble is problematic because of non uniqueness. PSV at a single site is really the nonaxial dipole variation (dipole wobble plus true nondipole variation) at that site. The proportion of dipole wobbles versus true nondipole contributions to PSV can only be assessed by analyzing globally distributed paleomagnetic data. Merrill and McElhinny (1983) carried out such an analysis of Northern Hemisphere archeomagnetic data for the last 2000 years and suggested that a significant dipole wobble component does exist. Dipole wobble contributions have also been estimated from the statistical analysis of angular dispersion (e.g., McFadden *et al*., 1988); however, the proportion of dipole wobble depends upon the proposed model of dipole wobble variability.

Westward drift has been suggested as an important element of HSV based on the observation that temporal changes in nondipole field components at the Earth's surface are due primarily to the westward drift in time of the spatial nondipole field components. The cause of westward drift has been related to differential rotation of the fluid outer core, where the field is generated, versus the overlying lithosphere. The importance of westward drift is complicated by the fact that some areas of the Earth have exhibited eastward drift and other areas have exhibited no drift at all during historic times (e.g., Thompson, 1984). Paleomagnetic evidence for westward drift comes from a variety of

PSV observations, of which a few are unique. The circularity of PSV data has long been associated with westward or eastward drift of the paleomagnetic field, although other nonaxial dipole variations could produce the same effect. The recurring waveforms, noted earlier, may indicate westward (or eastward) drift of a complex nondipole waveform that changes very slowly in time compared to the time it takes for the waveform to drift entirely around the Earth (2500–4000 years). In such a model, similar waveform and spectral characteristics should be noted at all sites along a line of latitude. The Holocene waveform comparisons noted earlier, however, do not appear to be compatible with this model. Regional PSV comparisons within Europe, East Asia, or North America separately display waveform correlations that are consistent with a westward drift model; however, no simple correlation can apparently be made between the three regional data sets. Such a correlation between regional PSV records is necessary if persistent westward (or eastward) drift is a predominant aspect of PSV.

Standing nondipole field components have been proposed to improve the fit of drifting nondipole field components to the total HSV. If truly present, their origin might be related to standing components of fluid flow near the core mantle boundary caused by irregularities in the boundary conditions. The presence of standing nondipole components in the paleomagnetic record, however, is very difficult to evaluate because of problems of nonuniqueness and the uncertainties of spatial PSV behavior. To the extent that standing nondipole components might produce nonzonal components of I and D, their importance must be below the level of noise associated with parametric statistical analyses of long-term PSV (average I, D; AI; angular dispersion), for all of these parameters are apparently zonal in their spatial distribution. However, in the study of late Quaternary PSV waveforms, standing nondipole sources have been suggested as reasonable (but nonunique) alternatives to westward drift to explain the observed waveform variability within individual paleomagnetic records.

Mathematical simulation models

Models that are more quantitative have also been applied to HSV and PSV. Spherical harmonic models separate the field into dipole and nondipole components and may include secular change coefficients for predicting short-term temporal variations. The primary drawback to spherical harmonic models is their general lack of relevance to the underlying physical causes of the Earth's internal magnetic field. (The exception to this may be the separation of spherical harmonic coefficients into primary and secondary family field components.) Models based on the variability of multiple localized sources in the outer core have occasionally been used as alternatives to spherical harmonic models. These models, which may use a distribution of dipoles, current loops, or wave patterns in their formulation, are more appealing in that those sources may mimic that part of the core process associated with observed nondipole foci observed at the Earth's surface (e.g., Thompson, 1984).

Spherical harmonic models are hard to apply to PSV because of the inherent timing uncertainties associated with PSV data and because of the poor spatial distribution of most PSV data. Even so, several recent summaries of PSV for the last few thousand years (e.g., Hongre *et al*., 1998; Constable *et al*., 2000; Korte and Constable, in press), based on worldwide (but poorly distributed) sites, have begun to give us a low-degree spherical harmonic view of PSV. Figure P18, for example, shows the geomagnetic field radial flux (Br) and non-axial dipole radial flux (Br-anomaly) at the core-mantle boundary for two prehistoric epochs based on SHA of PSV time-series (Constable *et al*., 2000). The advantage of PSV derived SHA data sets is that they can be tied to HSV derived SHA data sets and used to extend our view of the true global-space-time pattern of secular variation back thousands of years beyond the range of HSV. In this way, we can finally begin to address the global space-time pattern of secular variation on scales appropriate to the dynamics of PSV and the geodynamo.

Historically, time-averaged PSV statistical parameters, such as the ΔI anomaly and vector dispersion, have been more amenable to time-averaged spherical harmonic analysis. For example, the ΔI anomaly can be modeled by an axial dipole with added quadrupolar and octupolar components; the long-term changes in ΔI can then be modeled as changes in the quadrupole-octupole (or primary-secondary family) amplitude ratio. (See Merrill and McElhinny (1983) for more detailed discussion.)

Localized dipole-current-loop models, with either standing or drifting sources, have been applied to individual high-resolution PSV records, as well as to statistical PSV records. An example of a drifting radial dipole model for the Lake St. Croix PSV record (Figure P10; Lund and Banerjee, 1985) is shown in Figure P19. Two drifting radial dipoles plus an axial dipole are able to model almost all of the

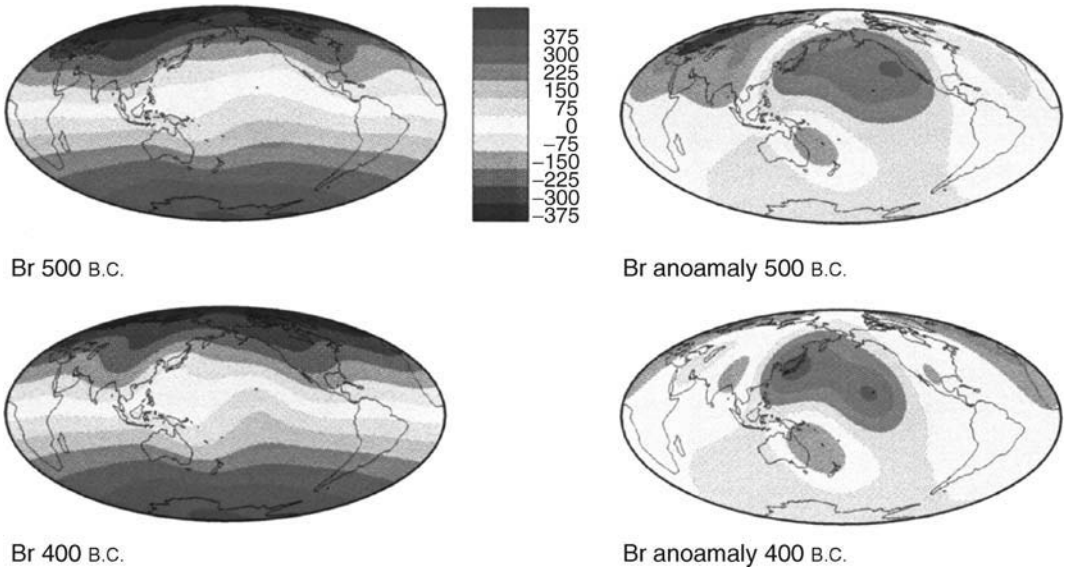

Figure P18 Models of geomagnetic field radial flux (Br) and nonaxial dipole radial flux (Br-nad) at the core-mantle boundary for two prehistoric epochs, 500 B.C. and 400 B.C. The models are the result of downward continuation of spherical harmonic models of PSV data from Constable *et al*. (2000).

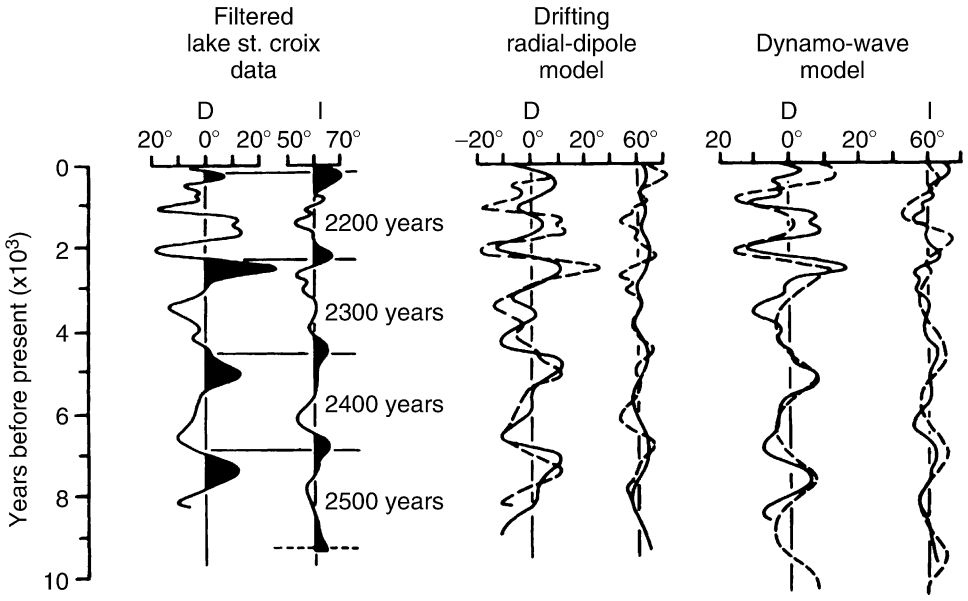

Figure P19 Radial-dipole and dynamo-wave models of the Lake St. Croix PSV record.

observed variability at Lake St. Croix for the last 9 ka. Unfortunately, more complicated standing radial dipole models could also fit the data. But, these models would require more sources in order to fit the characteristic phase relationships of the Lake St. Croix PSV data. The drifting radial dipole model for Lake St. Croix predicts similar PSV behavior for other sites on Lake St. Croix's latitude; the standing radial dipoles model will only produce regional coherence. The difficulty in correlating the Lake St. Croix PSV record with other global records outside of North America argues that a drifting radial dipole model is probably not appropriate to explain recurring waveforms. However, the complex recurrent waveforms noted in several PSV records are very difficult to model with standing sources due to the number of sources required and the detailed timing of recurrent intensity variations that each source must maintain relative to the other sources.

An alternative model of PSV, based on poleward migrating dynamo waves in the Earth's outer core, has been developed by Olson and Hagee (1987). Figure P19 shows the results of their model applied to the observed Lake St. Croix PSV. It is apparent that the poleward-migrating dynamo-wave model does just as good a job of fitting the observed variability as the drifting radial-dipole model. The dynamo wave model, however, only requires regional coherence in waveform correlations, but not a global-scale correlation. Hagee and Olson (1989) have also applied this dynamo wave model to a global set of Holocene PSV records and shown that the same general pattern of dynamo-wave variability noted to Lake St. Croix, can also explain all other Holocene PSV around the world.

Steve P. Lund

Bibliography

Barton, C.E., 1983. Analysis of paleomagnetic time series-techniques and applications. *Geophysical Surveys*, **5**: 335–368.

Bauer, L.A., 1895. On the distribution and the secular variation of terrestrial magnetism, No. III. *American Journal of Sciences*, **50**: 314.

Bloxham, J., and Gubbins, D., 1985. The secular variation of Earth's magnetic field. *Nature*, **317**: 777–781.

Bloxham, J., and Roberts, P., 1991. The geomagnetic main field and the geodynamo. *Reviews of Geophysics*, **29**: 428–432.

Bonhommet, N., and Zahringer, J., 1969. Paleomagnetism and potassium-argon age determinations of the Laschamp geomagnetic polarity event. *Earth and Planetary Science Letters*, **6**: 43s.

Brock, A., 1971. An experimental study of paleosecular variation. *Geophysical Journal of Royal Astronomical Society*, **24**: 303.

Butler, R., 1992. *Paleomagnetism: Magnetic Domains to Geologic Terranes*, London: Blackwell Publishers, 321 pp.

Cande, S.C., and Kent, D.V., 1995. Revised calibration of the geomagnetic polarity timescale or the late Cretaceous and Cenozoic. *Journal of Geophysical Research*, **100**: 6093–6095.

Champion, D.E., 1980. Holocene geomagnetic secular variation in the western United States: implications for the global geomagnetic field (Open file report 80–824), U.S. Geological Survey, 314 pp.

Channell, J., Hodell, D., McManus, J., and Lehman, B., 1998. Orbital modulation of geomagnetic paleointensity. *Nature*, **394**: 464–468.

Clement, B.M., and Kent, D.V., 1987. Short polarity intervals within the Matuyama: transitional field records from hydraulic piston cored sediments from the North Atlantic. *Earth and Planetary Science Letters*, **81**: 253–264.

Clement, B., and Constable, C., 1991. Polarity transitions, excursions, and paleosecular variation of the Earth's magnetic field. *Reviews of Geophysics*, **29**: 433–442.

Constable, C., Johnson, C., and Lund, S., 2000. Global geomagnetic field models for the last 3000 years. *Philosophical Transactions of the Royal Society of London* A, **358**: 991–1008.

Creer, K.M., 1983. Computer synthesis of geomagnetic paleosecular variations. *Nature*, **304**: 695–699.

Denham, C.E., and Cox, A., 1971. Evidence that the LAschamp polarity event did not occur 13300–30400 years ago. *Earth and Planetary Science Letters*, **13**: 181–190.

Dodson, R.E., 1979. Counterclockwise precession of the geomagnetic field vector and westward drift of the nondipole field. *Journal of Geophysical Research*, **84**: 637.

Dunlop, D., and Ozdemir, O., 2001. *Rock Magnetism*, Cambridge: Cambridge University Press, 596 pp.

Ekman, I., Bakhmutov, V., and Zagniy, G., 1987. Stratification and correlation of varved clays in terms of the fine paleostructures of the Earth's magnetic field, In Kabailiene, M. (ed.), *Methods for the Investigation of Lake Deposits: Paleoecological and Paleoclimatological Aspects,* Academy of the Sciences of the Lithuanian SSR, Vilnius.

Engebretson, D.C., and Beck, M.E., 1978. On the shape of directional data sets. *Journal of Geophysical Research*, **83**: 5979–5982.
Fisher, R.A., 1953. Dispersion on a sphere. *Proceedings of the Royal Society of London*, **A**, **217**: 295.
Gilbert, W., 1600. *De Magnete*, reprinted New York: Dover Publications, 368 pp. 1958.
Guyodo, Y., and Valet, J., 1999. Global changes in intensity of the Earth's magnetic field during the last 800 kyr. *Nature*, **399**: 249.
Holcomb, R., Champion, D., and McWilliams, M., 1986. *Geological Society of America Bulletin*, **97**: 829–839.
Hongre, L., Hulot, G., and Khokhlov, A., 1998. An analysis of the geomagnetic field over the last 3000 years. *Physics of the Earth and Planetary Interiors*, **106**: 311–335.
King, J.K., 1983. Geomagnetic secular variation curves for northeastern North America for the last 9000 years, unpublished PhD dissertation. Minneapolis: University of Minnesota.
Kissel, C., and Laj, C., 2004. Improvements in procedure and paleointensity selection criteria for Thellier-Thellier determinations: application to the Hawaii basaltic long core. *Physics of the Earth and Planetary Interiors*, **45**: 155–169.
Korte, M., and Constable, C., 2003. Continuous global geomagnetic field models for the past 3000 years, *Physics of the Earth and Planetary Interiors;* **140**: 73–89.
Laj, C., Kissel, C., Mazoud, A., Channell, J., and Beer, J., 2000. North Atlantic paleointensity stacksince 75 ka (NAPIS-75) and the duration of the Laschamp event. *Philosophical Transactions of the Royal Society of London, Series* **A**, **358**: 1009.
Liddicoat, J., and Coe, R., 1979. Mono Lake geomagnetic excursion. *Journal of Geophysical Research*, **84**: 261–271.
Lund, S.P., 1985. A comparison of the statistical secular variation recorded in some late Quaternary lava flows and sediments, and its implications. *Geophysical Research Letters*, **12**: 251–254.
Lund, S.P., 1996. A comparison of Holocene paleomagnetic secular variation records from North America. *Journal of Geophysical Research*, **101**(B4): 8007–8024.
Lund, S.P., and Banerjee, S.K., 1985. Late Quaternary paleomagnetic field secular variation from two Minnesota lakes. *Journal of Geophysical Research*, **90**: 803–825.
Lund, S.P., Liddicoat, J.C., Lajoie, K.L., 1988. Henyey and Steve W. Robinson. Paleomagnetic evidence for long-term (10^4 year) memory and periodic behavior in the Earth's core dynamo process. *Geophysical Research Letters*, **15**: 1101–1104.
Lund, S.P., Acton, G. Clement, B. Okada, M. Williams, T., 1998. Initial paleomagnetic results from ODP Leg 172: high resolution geomagnetic field behavior for the last 1.2 Ma. *EOS, Transactions, American Geophysical Union*, **79**: 178–179.
Lund, S., and Schwartz, M., 1999. Environmental factors affecting geomagnetic field intensity estimates from sediments. In Maher, B., and Thompson, R. (eds.), *Quaternary Climates, Environments, and Magnetism.* Cambridge: Cambridge University Press, pp. 323–351.
Lund, S.P., Williams, T., Acton, G., Clement, B., and Okada, M., 2001. Brunhes Epoch magnetic field excursions recorded in ODP Leg 172 sediments. In Keigwin, L., Rio, D., and Acton, G. (eds.), Proceedings of the Ocean Drilling Project, Scientific Results Volume **172**, Ch. 10, 2001.
Lund, S.P., Schwartz, M., Keigwin, L., and Johnson, T., 2005. High-resolution records of the Laschamp geomagnetic field excursion. *Journal of Geophysical Research*, **110**: B04101.
McFadden, P.L., Merrill, R.T., and McElhinny, M.W., 1988. Dipole/quadrapole family modeling of paleosecular variation. *Journal of Geophysical Research*, **93**: 11583–11588.
Merrill, R.T., and McElhinny, M.W., 1977. Anomalies in the time-averaged paleomagnetic field and their implications for the lower mantle. *Reviews of Geophysics and Space Physics*, **15**: 309.
Merrill, R., McElhinny, M., and McFadden, P., 1998. *The Magnetic Field of the Earth.* San Diego, CA: Academic Press, 531 pp.
Merrill, R.T., and McFadden, P.L., 1988. Secular variation and the origin of geomagnetic field reversals. *Journal of Geophysical Research*, **93**: 11589–11598.
Negrini, R., Erbes, D., Roberts, A., Verosub, K., Sarna-Wojcicki, A., and Meyer, C., 1994. Repeating waveform initiated by a 180–190 ka geomagnetic excursion in western North America: implications for field behavior during polarity transitions and subsequent secular variation. *Journal of Geophysical Research*, **99**: 24105–24119.
Olson, P., Sumita, I., and Aurnou, J., 2002. Diffusive magnetic images of upwelling patterns in the core. *Journal of Geophysical Research*, **107**: 2348.
Olson, P., and Hagee, V.L., 1987. Dynamo waves and paleomagnetic secular variation. *Geophysical Journal of the Royal Astronomical Society*, **88**: 139–159.
Runcorn, K., 1959. On the theory of geomagnetic secular variation. *Annales Geophysicae*, **15**: 87.
Schneider, D.A., and Kent, D.V., 1990. The time-averaged paleomagnetic field. *Reviews of Geophysics*, **28**: 71–96.
Skiles, D., 1970. A method of inferring the direction of drift og the geomagnetic field from paleomagnetic data. *Journal of Geomagnetism and Geoelectricity*, **22**: 441.
Smith, J.D., and Foster, J., 1969. Geomagnetic reversal in Brunhes normal polarity epoch. *Science*, **163**: 565–567.
Stoner, J., Channell, J., Hodell, D., and Charles, C., 2003. A 580 kyr paleomagnetic record from the sub-Antarctic South Atlantic (ODPSite 1089). *Journal of Geophysical Research*, **108**: 2244.
Tauxe, L., 1993. Sedimentary records of relative paleointensity of the geomagnetic field: theory and practice. *Reviews of Geophysics*, **31**: 319–354.
Thompson, R., 1984. Geomagnetic evolution: 400 years of change on planet. *Physics of the Earth and Planetary Interiors*, **36**: 61–77.
Thompson, R., and Barraclough, D.R., 1982. Geomagnetic secular variation based on Spherical Harmonic and Cross Validation analyses of historical and archaeomagnetic data. *Journal of Geomagnetism and Geoelectricity*, **34**: 245–263.
Verosub, K.L., and Banerjee, S.K., 1977. Geomagnetic excursions and their paleomagnetic record. *Journal of Geophysical Research*, **15**: 145–155.
Watkins, N., 1976. Polarity group sets up guidelines, *Geotimes*, **21**: 18–20.

PALEOMAGNETISM

Introduction

Most people, certainly mariners and explorers since at least the 15th century, are aware of the value of a compass as a navigational aid. This works because the Earth generates a magnetic field, which, at the Earth's surface, is approximately that of a geocentric axial dipole (GAD). By geocentric we mean that this dipolar field is centered at the center of the Earth and by axial we mean that the axis of the dipolar field aligns with the spin axis of the Earth. This means that a magnetic compass will align approximately in the north-south direction. It also means that a magnetic dip circle will give the inclination of the magnetic field (the angle the direction the magnetic field makes with the horizontal) which, together with a knowledge of the structure of a dipole field, gives the approximate latitude. If the field were precisely that of a GAD then the north-south direction and the latitude could be obtained accurately. The deviation of magnetic north from geographical or true north is called the magnetic declination and was known to the Chinese from about A.D. 720. In 1600, William Gilbert published the results of his experimental studies in the treatise *De Magnete* and confirmed that the geomagnetic field is primarily dipolar.

The properties of lodestone—now known to be magnetite—were known in ancient times to the Chinese, who invented the earliest

known form of magnetic compass as early as the 2nd century B.C. This compass consisted of a lodestone spoon rotating on a smooth board. Magnetic inclination (or dip) was discovered by Georg Hartmann in 1544. Hence it has been known for some time that natural rock can behave as a compass needle and align itself along what is now recognized as being the direction of the magnetic field.

At the end of the 18th century, it was recognized that deviation of magnetic compasses could occur because of nearby strongly magnetized rocks. Delesse and Melloni were the first to observe that the magnetization in certain rocks was actually parallel to the Earth's magnetic field. Folgerhaiter extended their work and studied the magnetization of bricks and pottery. He argued that when a brick or pot was fired in the kiln then the remanent magnetization it acquired on cooling provided a record of the direction of the Earth's magnetic field. With the wisdom of hindsight, specifically a better understanding of the physics of magnetization and the mineralogy of rocks, it is fairly obvious that this would be the case. Volcanic rocks are heated well above the Curie point so the magnetization is free to align with the external magnetic field and becomes locked in as the rock cools. This is known as a *thermoremanent magnetization* (*TRM*) (*q.v.*). In sedimentary rocks the magnetic particles will act just like a compass needle and align themselves with the external magnetic field as they settle and then become mechanically locked in as the rock is formed. This is known as a *depositional remanent magnetization* (*DRM*) (*q.v.*).

This is the essence of paleomagnetism that the rock will lock in a fossil record of the ancient (or paleo) magnetic field. The fossil magnetism naturally present in a rock is termed the *natural remanent magnetization* (*NRM*) (*q.v.*). The primary magnetization is the component of the NRM that was acquired when the rock was formed, and may represent all, part, or none of the total NRM. After formation the primary magnetization may decay either partly or completely and additional components, referred to as secondary magnetizations, may be added by several processes. A major task in all paleomagnetic investigations is to identify and separate the magnetic components in the NRM, using a range of demagnetization and analysis procedures. Typically there is also significant effort put in to date the magnetizations so that not only the direction of the magnetic field at that particular sampling site is known but also the time when the field was in that direction. Many of the successful applications of paleomagnetism have derived from an effective partnership with geochronology.

David in 1904 and Brunhes in 1906 reported the first discovery of NRM that was roughly opposite in direction to that of the present field and this led to the speculation that the Earth's magnetic field had reversed its polarity in the past. In 1926 Mercanton pointed out that if the Earth's field had in fact reversed itself in the past, then reversely magnetized rocks should be found in all parts of the world. He demonstrated that this was indeed the case for Quaternary-aged rocks around the world. The speculation gained further support when Matuyama in 1929 observed reversely magnetized lava flows from the past one or two million years in Japan and Manchuria. However, doubts about the validity of the field reversal hypothesis surfaced during the 1950s after Néel presented theory that showed it was possible for samples to acquire a magnetization antiparallel to the external field during cooling, a process referred to as self-reversal. Shortly thereafter Nagata and Uyeda found the first laboratory-reproducible self-reversing rock, the Haruna dacite. Subsequently it was recognized that self-reversal is relatively rare and by the early 1960s it was accepted that the Earth's magnetic field has indeed reversed and that the phenomenon of field reversal has occurred many times. An excellent history of this subject has been given by Glen (1982).

By 1960 the study of the magnetic properties of minerals and rocks and the use of magnetization in rocks to infer the properties of the Earth's past magnetic field had evolved into two separate but related disciplines, respectively referred to as rock magnetism and paleomagnetism. By providing information about the location and orientation of continents relative to the Earth's magnetic pole, paleomagnetism has played a significant role in our understanding of Earth processes, particularly with regard to continental drift and polar wander and the development of plate tectonics.

As currently practiced, paleomagnetism includes topics such as age determination, stratigraphy, magnetic anomaly interpretation and paleoclimatology, as well as the traditional paleomagnetic topics of tectonics, polar wander, and studies of the evolution and history of the Earth's magnetic field.

Determining a paleomagnetic pole

A central assumption for much of paleomagnetism is that if the field directions at any given locality are averaged over an appropriate time interval then the resulting direction is the same as that for a geocentric axial dipole. If that is the case then the inclination I is related to the paleolatitude λ by

$$\tan I = 2 \tan \lambda \qquad \text{(Eq. 1)}$$

Hence it is possible to determine the angular distance (paleocolatitude $p = 90 - \lambda$) of the sampling site from the pole at the time that the magnetization was acquired. Using the declination D and the paleocolatitude of this time-average field direction it is then possible to determine the latitude and longitude (λ_p, ϕ_p) of the time-average magnetic pole, known as the *paleomagnetic pole*, relative to the latitude and longitude (λ_s, ϕ_s) of the sampling site. The spherical geometry needed for this can be visualized with the help of Figure P20. If the continent has moved and/or rotated since the magnetization was acquired, then the paleomagnetic pole will not coincide with the current north pole, leading to the concept of apparent polar wander (see polar wander). Paleomagnetic poles for magnetizations with different ages, but from the same continent, will plot in different positions, providing an apparent polar wander path (APWP) for the continent.

Alternatively, it is a simple matter to place the continent on the globe such that the paleomagnetic pole coincides with the north pole. This then places the continent correctly on the globe with regard to its latitude and orientation at the time the magnetization was acquired. It does not, unfortunately, give any longitudinal information.

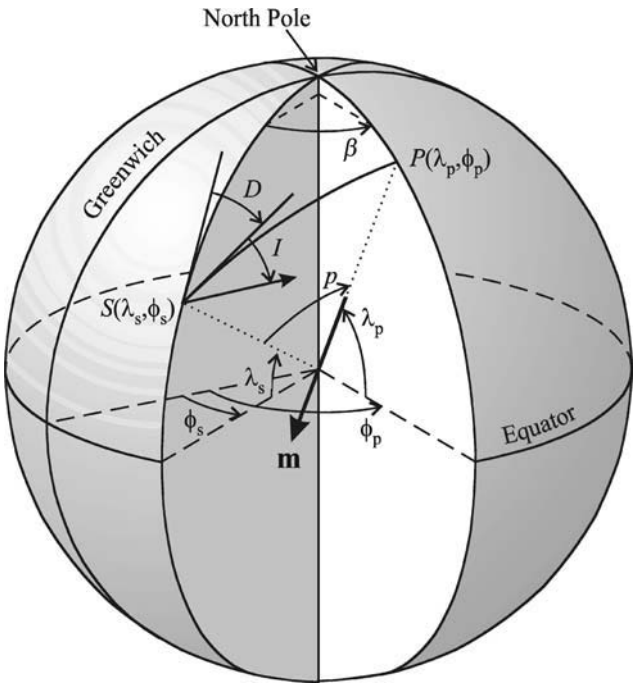

Figure P20 Position of the paleomagnetic pole *P* relative to the sampling site *S*. Modified after Merrill *et al.* (1996).

In addition to geochronology, various geological field tests are used to provide additional evidence on the nature and timing of the acquisition of the magnetization. The three traditional, and most common, tests are known as the fold test (see Magnetization, remanent, fold test), the conglomerate test, and the *baked contact test* (*q.v.*). The field relationships for these classical tests are shown in Figure P21. If the *in situ* directions of magnetization in a folded rock-unit differ from place to place, but agree after "unfolding" the rock-unit to its original pre-folding structure, then the magnetization must predate the folding and must have been stable since that time. Conversely, if the *in situ* directions agree then the magnetization must postdate the folding. If cobbles from the rock formation under investigation can be found in a conglomerate then, because the orientations of the cobbles will have been randomized, the magnetization of these cobbles should have no preferred direction if their original magnetization has been stable. If the direction of magnetization in the baked contact zone surrounding an intrusion is parallel to that observed in the intrusion, but differs from that of the unbaked country rock, then the magnetization of the intrusion has been stable since cooling. It is also important to determine the paleohorizontal of the rock-unit accurately so that the inclination I used in Eq. (1) is meaningful.

It has already been noted that it is necessary to use the time-average field to determine a paleomagnetic pole. This is because the Earth's present magnetic field, and most probably Earth's past field at any particular time, is not that of a simple geocentric axial dipole. Only about 75% of the present field intensity is attributed to a dipole field, a percentage that was about 82% or 83% at the beginning of the 20th century. This dipolar field is not static and is currently tilted about 10.7° from the rotation axis. The remainder of the field is referred to as the nondipole field, which characteristically exhibits more rapid spatial and temporal variations than the dipole field. Consequently it is necessary to average out these variations. Some rocks, for example thin lava flows, can acquire their primary magnetization in less than a year and so that primary magnetization often reflects the instantaneous field and not the time-average field. Thus it becomes necessary to use a sampling scheme that will average out these variations in order to give a reliable paleomagnetic pole.

A hierarchical scheme is typically used to obtain an estimate of a paleomagnetic pole position from a given location. Oriented samples are taken throughout the rock formation of interest. Specimens obtained from these samples are used to investigate rock magnetic properties. Statistical analysis of sample directions provides an estimate of the ancient field direction and its variance for the rock-unit. The mean magnetic direction for this unit is then used in Eq. (1) to determine a *virtual geomagnetic pole* (*VGP*). It is referred to as a "virtual" pole because at this level in the hierarchy it is unlikely that the field would have been averaged to that of a GAD. This makes it possible to average a "sufficient" number of VGP from widely dispersed sampling sites as a final step in the hierarchy to obtain an estimate of the paleomagnetic pole position. Alternatively, if it is apparent from the geology that sampling localities spatially close to each other will provide coverage of a sufficient time interval, then it is possible to average the magnetic field directions and use this mean direction in Eq. (1) to estimate the paleomagnetic pole position. It is presumed that at this level in the hierarchy the geocentric axial dipole assumption is satisfied and that the paleomagnetic pole position provides a reliable estimate of the paleogeographic pole position. There are no hard and fast rules and the procedures used in collecting samples and analyzing them vary depending on such factors as the properties of the site, the nature of the rocks sampled, the goals of the investigation and, to some extent, on the nature of the investigators. Detailed procedures on how this is done are described elsewhere in this volume.

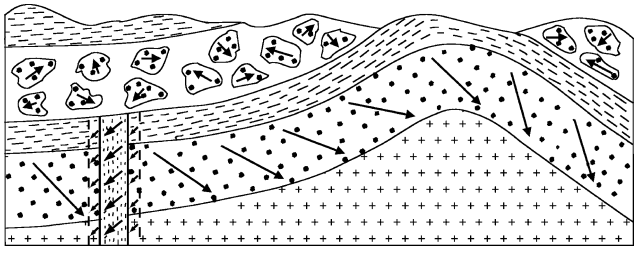

Figure P21 Field relationships for the fold, conglomerate, and baked contact tests. From Merrill and McElhinny (1983).

Buried within this process is the question of how much time is required to obtain a good approximation of the time-average field so that the GAD assumption is in fact reasonable. If a very short interval is used, then the averaging will be incomplete and this can produce significant errors. Conversely, if too long an interval is used then, for example, global tectonic processes can become significant and the sampling locality may have moved a substantial amount relative to the geographic pole. There is no widespread agreement on the optimum time interval for averaging but a minimum of 10 ka is generally viewed as necessary. The GAD assumption appears to be excellent for the time-average magnetic field over the past 5 Ma, although a small nondipole component may also be present. It is difficult to determine whether the GAD assumption has been valid throughout most of geological time but there is reasonable evidence to indicate that the assumption is very good to first order for the last few hundred million years. The evidence is less compelling for times prior to about 300 Ma ago.

Paleomagnetic field

Probably the best-documented fact stemming from paleomagnetism is that Earth's magnetic field has reversed polarity many times. By this it is meant that the north and south geomagnetic poles (the two locations where a line through the geocentric dipole intersects the Earth's surface) have traded places. The duration of a polarity transition is imperfectly known but it is probably in the order of 10^3 to 10^4 years, a time during which the intensity drops to a minimum of around a quarter of its normal value. The field is said to have normal polarity when the north geomagnetic pole is above 45° north latitude, reverse polarity when this pole lies below 45° south latitude, and transitional for all other latitudes. Hundreds of reversals have now been documented and for the past 160 Ma there is now a fairly reliable geomagnetic polarity timescale (GPTS). From this timescale it is evident that reversals do not occur with a simple periodicity but instead appear to occur randomly in time. The underlying rate at which reversals occur seems to vary on a timescale of about 10^8 year, probably reflecting changes in the lower mantle.

The very nature of the generative process of the geomagnetic field—a dynamo operating in the iron-rich liquid outer core—demands that the field is ever changing. The resulting gradual change in the magnetic field with time is referred to as *secular variation* (*q.v.*) which, as already discussed, must be averaged out in order to obtain a paleomagnetic pole. This secular variation occurs over a wide range of timescales, the shortest period that can be observed being around a year. This is because of the shorter period variations screened out by the semiconducting mantle. It is generally felt that the characteristic times of dynamo processes are less than 10^6 years, so variations due to internal processes in the dynamo typically occur in less than 10^6 years. Longer timescale variations, such as in the reversal rate, probably reflect changes in boundary conditions on the core. Apart from reversals, the largest changes in the Earth's magnetic field are known as excursions short intervals of time (of the order 10^4 years) when VGP deviate unusually far from the geographic pole.

The intensity of the field also changes with time. However, because of rock magnetic problems, these changes are more difficult to determine than the changes in direction. Direct measurements of the Earth's magnetic field from magnetic observatories indicate that that the dipole intensity decreased by about 5% during the 20th century.

Indirect measurements from archeomagnetism and paleomagnetism (there are several different absolute and relative paleointensity methods) indicate that the intensity of the Earth's field has varied significantly on a timescale that is geologically short. For example, 2 ka ago the intensity appears to have been 30%–40% greater than the present value but 6 ka ago it was found to be 30% less. Good relative paleointensity data from marine sediments provide a reasonable estimate of the intensity variation for the most recent several hundred thousand years. Intensities from times prior to this come from so-called absolute paleointensity methods, which seemingly should provide more accurate estimates than relative estimates. However, absolute intensity estimates are obtained from lava flows, which provide estimates that represent essentially an instantaneous estimate of the magnetic field rather than a time-average value. Typically there are large spatial and temporal gaps between such estimates. Although there is an incomplete agreement on what constitutes a reliable absolute paleointensity estimate, most paleomagnetists would agree that there are only about 1000 reliable estimates for all of geological time prior to about 5 Ma ago. A consequence is that several models have been advanced to describe the intensity variation over the past few hundred million years and there is little agreement on which model should be preferred.

Tectonics

In the 1950s it was not immediately clear whether apparent polar wander was indeed due to polar wander itself or to movement of the continents. However, because the apparent polar wander paths were different for different continents, paleomagnetists argued that continental drift had occurred. For example, the APWPs from 350 Ma to present for North America and Europe (including Russia west of the Ural Mountains) can effectively be made to coincide by removing the Atlantic Ocean and closing up the continents. This is consistent with Wegener's pioneering suggestion of continental drift to explain various geographic and geologic features—but not magnetic. Nevertheless the claims by paleomagnetists were often dismissed prior to the mid-1960s by other scientists, primarily because of concerns about the reliability of the geocentric axial dipole field assumption, questions concerning the fidelity of rocks as recorders of the primary remanent magnetization and because of the apparent absence of a driving mechanism for continental drift.

Today, paleomagnetic poles are widely used to locate the past positions of continents, particularly when marine magnetic anomaly data are not available. Indeed, as the oldest marine rocks are slightly less than 200 Ma old, paleomagnetic poles and APWPs are the primary quantitative tools for locating land masses prior to 200 Ma. In addition, paleomagnetic poles provide valuable information on tectonics on a smaller scale. For example, a substantial part of north-western North America appears to have been added to the craton in pieces, referred to as displaced terranes, during the Cenozoic.

Marine magnetic anomalies (variations in the intensity of the magnetic field that are usually measured at the sea surface) played a prominent role in the establishment of seafloor spreading and plate tectonics. It was noticed that these magnetic anomalies formed stripes parallel to and symmetric about the mid-ocean ridges. Vine and Matthews and Morley and Larochelle independently recognized that these magnetic stripes were caused by alternating blocks of normally and reversely magnetized volcanic rocks in the upper part of the oceanic crust. According to their model, crust is formed at the mid-ocean ridge, spreads away on both sides of the ridge and cools. As the rock cools at the Curie temperature it acquires a thermoremanent magnetization parallel to the ambient direction of the Earth's magnetic field. Reversals of the Earth's magnetic field will then produce blocks of alternate polarity. Hence the spreading crust acts like a magnetic tape recorder by recording the reversals of Earth's magnetic field, producing the observed stripes. It is now recognized that this magnetization is recorded in Layer 2 of the oceanic crust, an igneous layer of pillow basalts and dikes that lies beneath Layer 1, a sedimentary layer that was deposited later. Because this field varies over Earth's surface, the geocentric axial dipole field assumption is invoked and marine magnetic anomalies are transformed to the poles in order to make comparisons between anomalies from different localities. Because polarity contrast is used, undetected nondipole components will not have a significant effect on the final result. These marine magnetic anomalies have played a major role in the development of a geomagnetic polarity timescale for the last 170 Ma and in our understanding of the motions of tectonic plates during this recent time interval.

In a strict interpretation of plate tectonics, all deformation is confined to three types of plate boundaries: divergent plate boundaries (spreading centers)—where new material is produced; convergent plate boundaries (subduction zones)—where material descends back into the Earth, and transform faults where no new material is produced or removed. Support for this approximation comes from many sources including that the vast majority of energy released by earthquakes occurs at plate boundaries. However, there are places where this strict interpretation must be modified. For example, much of the Tibetan Plateau has experienced uplift of more than 5 km since the collision of India with the rest of Eurasia, which occurred about 50–65 Ma ago. Even such cases as this where interplate tectonics is important, paleomagnetism has proven to be a valuable tool in determining the character of the deformation.

The final tectonic example we give involves an ongoing controversy concerning features known as hot spots. These features are associated with interplate basaltic volcanism characterized by linear volcanic chains that grow older in the direction of plate motion. For more than a quarter of a century, it was believed that hot spots were maintained by material rising from the lower mantle through lower mantle plumes that formed part of the upward flow of a long-lived stable pattern of whole-mantle convention. Furthermore, it was supposed that these plumes do not change their relative positions. As already noted, given a single APWP, it is not immediately apparent whether this is due to polar wander or continental motion, and this is because it is difficult to find a fixed reference frame. Consequently a fixed hot spot reference frame was an enormously attractive concept. The fixed hot spot model implies that all islands and seamounts along a particular hot spot chain are formed at the same latitude and longitude. However, recent inclination data obtained by drilling seamounts from the northern end of the Hawaiian Emperor Seamount chain suggests that this is not the case. The magnetic inclinations of drilled samples from the Emperor Seamounts at the northern end of this chain seem to indicate the seamounts formed at significantly higher latitudes than that of the present hot spot, which lies beneath the island of Hawaii. If the paleomagnetic data from the Emperor Seamounts are sufficient to average out secular variation, if the paleohorizontal has been accurately obtained, and if the primary magnetization has been properly obtained, then the fixed hot spot model is not obeyed, at least for the Hawaiian-Emperor hot spot chain. In 1998 Steinberger and O'Connell showed how it was possible for hot spot plumes under a single plate to show less relative motion while at the same time it was moving relative to plumes under a different plate. This suggests it is unlikely that plumes can be effectively anchored in a convecting mantle and it seems that the weight of evidence is currently against the idea of a fixed hot spot reference frame.

Magnetostratigraphy and paleoclimate studies

Because there is an excellent first-order reversal chronology for most of the Mesozoic and all of the Cenozoic and because reversals occur randomly in time, sequences of reversals can be used for age dating and stratigraphic control. For example, a distinctive reversal pattern found in sediments in one area can sometimes be correlated with the same pattern in a different area. Sedimentation rates will typically be different in the two areas and so some stretching of the record from one area is required to make a correlation. This makes the match

nonunique and so the correlation is more convincing the more distinctive the local pattern of reversals is. Absolute ages can be assigned to the sediment sections involved when the pattern of reversals can be identified in the reversal chronology. In addition, rock magnetic properties, such as magnetic susceptibility are sometimes used for correlation of marine cores taken in the same general location. Details on how magnetostratigraphy is done in practice are provided in books such as Opdyke and Channell (1996).

Often the detailed characteristics of a sediment will vary with depth because the source of the sediments has changed with time or because of physical, biological, or chemical alteration of the sediments after deposition. This provides a record that can be used for paleoclimate and environmental studies. Typically, although the magnetic properties will often vary with depth in sediments, this does not usually provide primary information on paleoclimatic changes. However, magnetic properties such as magnetic susceptibility can frequently be correlated with primary proxies for paleoclimate such as the variation in oxygen isotopes. Thus susceptibility, which can be measured relatively quickly, provides valuable data when there are gaps in the isotope record.

Paleomagnetism also plays a key role in testing global paleoclimatic hypotheses. For example, in 1969 Mikhail Budyko proposed a model for ice sheets that could lead to a runaway situation in which the whole Earth becomes covered in ice. The possibility of one or more glaciations that led to an entirely, or mostly, ice-covered Earth around 600 Ma ago is referred to as the snowball earth hypothesis. Paleomagnetism has provided significant support to this hypothesis by showing that, for example, Precambrian igneous rocks associated with glacial deposits in Namibia exhibit shallow magnetic inclinations, providing a clear implication that glacial deposits were formed at tropical latitudes in the Late Precambrian.

Concluding remarks

In essence, paleomagnetism provides three types of information: first, it provides a record of the Earth's magnetic field, which is a proxy for processes deep within the Earth; second, with some assumptions about the structure of the magnetic field, it provides information on the past location of rock-units; and, third, having calibrated the magnetic information, it provides the possibility to use APWPs and the geomagnetic polarity timescale as dating tools. Each of these types of information will contribute to our ongoing quest to understand our planet and its processes.

A major question to be addressed is whether global tectonics early in the Earth's history had a substantially different character from today. Hence paleomagnetism must develop the capacity to provide reliable location information for rocks formed early in the Earth's history.

The geomagnetic polarity timescale for the past 160 Ma is reasonably well developed and provides significant information on processes deep within the Earth with characteristic times in the order of 10^8 years. However, this timescale continues to evolve and it is necessary to invest the effort to obtain a complete and accurate record. The plate tectonic process has ensured that seafloor older than about 160 Ma has been recycled and so there is no well-ordered "tape recording" of reversals older than this. Instead, it is necessary to develop the reversal chronology for times before this through a painstaking process of dating, correlation, and assembly of information from continental rocks. Although the reversal chronology has been extended back into the Paleozoic, large gaps in coverage remain and there are a few data for the Precambrian. This timescale will provide valuable information on internal Earth processes and will also itself become a valuable dating tool.

Reliable paleointensity data for almost all times are needed. The resulting information is required to understand the long-term evolution of the Earth's magnetic field. In turn, this is likely to provide better understanding of the evolution of the Earth's inner core.

At this stage there is insufficient evidence regarding the structure of the time-average field for times earlier than about 300 Ma. This is an impediment to accurate reconstruction of earlier land masses. To some extent this creates a circular problem: a GAD field is assumed and paleoreconstructions are performed; inconsistencies in the paleoreconstructions are then attributed to non-GAD structure in the ancient geomagnetic field. If the structure of the field is actually known then it is possible to obtain an accurate paleoreconstruction. Conversely, if the paleolocations of the continental masses are known then it is possible to get information about the structure of the paleofield. It is going to require substantial innovation to achieve both of these without independent evidence.

Acknowledgments

This article is published with the permission of the Chief Executive Officer, Geoscience Australia.

Ronald T. Merrill and Phillip L. McFadden

Bibliography

Cox, A., and Doell, R.R., 1960. Review of paleomagnetism. *Geological Society of America Bulletin*, **71**: 645–768.

Evans, M., and Heller, F., 2003. *Environmental Magnetism: Principles and Applications of Enviromagnetics*, San Diego, CA: Academic Press.

Glen, W., 1982. *The Road to Jaramillo.* Stanford: Stanford University Press.

McElhinny, M.W., and McFadden, P.L., 2000. *Paleomagnetism: Continents and Oceans.* San Diego CA: Academic Press.

Merrill, R.T., and McElhinny, M.W., 1983. *The Earth's Magnetic Field: its History, Origin and Planetary Perspective.* London: Academic Press.

Merrill, R.T., McElhinny, M.W., and McFadden, P.L., 1996. *The Magnetic Field of the Earth: Paleomagnetism, the Core, and the Deep Mantle.* San Diego, CA: Academic Press.

Morley, L.W., and Larochelle, A., 1964. *Paleomagnetism as a Means of Dating Geological Events*. In Osborne, F.F. (ed.), Geochronology in Canada., The Royal Society of Canada Special Publications, Toronto: University of Toronto Press, **8**: 39–51.

Opdyke, N.D., and Channell, J.E.T., 1996. *Magnetic Stratigraphy.* San Diego, CA: Academic Press.

Steinberger, B., and O'Connell, R.J., 1997. Changes in the Earth's rotation axis owing to advection of mantle density heterogeneities. *Nature*, **387**: 169–173.

Vine, F.J., and Matthews, D.H., 1963. Magnetic anomalies over oceanic ridges. *Nature*, **199**: 947–949.

Cross-references

Baked Contact Test
Dipole Moment Variation
Geocentric Axial Dipole Hypothesis
Geodynamo
Geomagnetic Dipole Field
Geomagnetic Polarity Timescales
Geomagnetic Secular Variation
Harmonics, Spherical
Inner Core
Magnetic Susceptibility
Magnetization, Natural Remanent (NRM)
Magnetization, Remanent, Fold Test
Magnetization, Thermoremanent (TRM)
Nondipole Field
Paleointensity
Reversals, Theory
Statistical Methods for Paleovector Analysis
Time-averaged Paleomagnetic Field
True Polar Wander

PALEOMAGNETISM, DEEP-SEA SEDIMENTS

Introduction

Deep-sea (pelagic) sediments, deposited remotely from sources of continental detritus, have been a very important source for learning about the direction and intensity of the ancient geomagnetic field (paleomagnetism) because they often carry a primary natural remanent magnetization (NRM) acquired at the time of deposition, or shortly thereafter. The age of a primary magnetization can be determined from the accompanying biostratigraphy or isotope stratigraphy. The magnetization directions of known age have been used to assess plate motion (continental drift) or to record the characteristics of the ancient geomagnetic field, such as the sequence of polarity reversal in the geologic past. The record of geomagnetic polarity reversal (magnetostratigraphy) in deep-sea sediments, first practiced by Opdyke *et al*. (1966), has become important in paleoceanography and biostratigraphy, and in geologic timescale construction. The geomagnetic polarity time scale (GPTS), based on the sequence of polarity reversal through time, is the central thread to which the other facets of geologic time (radiometric, isotopic, biostratigraphic) are correlated in the construction of geologic timescales for the last 150 Ma (see Opdyke and Channell, 1996). Prior to ~150 Ma, the GPTS is less well defined, due to the lack of *in situ* oceanic crust and hence marine magnetic anomaly records, and is not adequately correlated to the biozonations that define geologic stages. The global synchronicity of polarity reversals (of the main axial dipole field) means that magnetic polarity stratigraphies can be used to correlate environmental (isotopic) and biostratigraphic events among contrasting environments and remote locations. The stochastic (unpredictable) occurrence of polarity reversal, and our inability to distinguish one normal (reverse) polarity chron from another, means that precise correlation through magnetic polarity stratigraphy is only possible at polarity reversals, with interpolation between these tie points. Within individual polarity chrons (time intervals between polarity reversals) magnetic records can be used for correlation if geomagnetic directional "secular" variation and/or paleointensity are adequately recorded. The conditions for adequate recording of secular variation and geomagnetic paleointensity are more stringent than for the recording of polarity reversals as contamination (overprint) of primary magnetization is less crippling for polarity records (~180° directional changes) than for the more subtle changes that define secular variation and paleointensity.

Origin of primary magnetizations

What makes deep-sea sediments efficient recorders of the geomagnetic field at time of deposition? Sediments can acquire a detrital remanent magnetization (DRM) at the time of deposition by mechanical orientation of fine grained magnetite (Fe_3O_4) or titanomagnetite ($xFeTiO_4$ [$1 - x$] Fe_3O_4) into line with the ambient geomagnetic field at the sediment-water interface. The natural remanent (permanent) magnetization (NRM) of ferrimagnetic (titano) magnetite results in a torque that statistically orients the magnetic moment of the grain population into line with the ambient geomagnetic field. The mechanical orientation of grains may be achieved either at the sediment-water interface (DRM) or in the uppermost few centimeters or decimeters of the sediment in which case the resulting remanence is referred to as pDRM (post-depositional detrital remanent magnetization).

Following introduction of the concept by Irving and Major (1964), progressive acquisition of postdepositional detrital remanent magnetization (pDRM) has been modeled as an exponential or cubic function of progressive lock-in with depth (Hyodo, 1984; Mazaud, 1996; Meynadier and Valet, 1996; Roberts and Winklhofer, 2004). Teanby and Gubbins (2000) used an 8 cm uniform mixed layer (magnetization = 0) to simulate the bioturbated surface layer, underlain by an exponential lock-in function. Channell and Guyodo (2004) have used a sigmoidal pDRM function based on tanh(x). The function can be defined by a surface mixing layer depth (M) at which 5% of the magnetization is acquired, and a lock-in depth (L) that is the depth below M at which 50% of the magnetization is acquired (see Figure P22). The assumption of a well-mixed layer (M), in which the sediment is thoroughly consumed by sipunculid or echiuran worms and other benthos, is valid in deep-sea sediments where the mixing coefficient exceeds the product of mixed layer depth and sedimentation rate (Guinasso and Schink, 1975). In deep-sea sediments, isotopic tracers indicate mean mixed layer thicknesses of about 10 cm (values vary by an order of magnitude from 3–30 cm) that is largely independent of sedimentation rate (Boudreau, 1994). Using ^{14}C of the bulk carbonate fraction as the isotopic tracer, Thomson *et al*. (2000) estimated mixed layer thicknesses of 10–20 cm in box cores collected close to the Rockhall Plateau. These values are greater than the 2–13 cm mixed layer thicknesses obtained from further south in the North Atlantic using ^{14}C in foraminifera (Trauth *et al*., 1997; Smith and Rabouille, 2002). Estimates of mixed layer thickness are grain size sensitive (see Bard, 2001) and would be expected to be lower for the coarse fraction (foraminifera) than for the bulk carbonate (nannofossils). For this reason, mixed layer thickness estimates based on ^{14}C and other isotopic tracers should be considered as minimum estimates for the fine (PSD) grains that carry stable magnetization. The main control on the mixed layer thickness appears to be organic carbon flux derived from surface water productivity (Trauth *et al*., 1997; Smith and Rabouille, 2002). A recent redeposition study has suggested that, at least for some lithologies, intergranular interactions overcome the magnetic aligning torque so that bioturbation would not enhance, but rather disrupt, the remanent magnetization (Katari *et al*., 2000). This proposition is in agreement with Tauxe *et al*. (1996) who, based on an analysis of the position of the Matuyama-Brunhes boundary relative to oxygen isotope records, concluded that magnetization lock-in depth is insignificant in marine sediments. Other studies (DeMenocal *et al*., 1990; Lund and Keigwin, 1994; Kent and Schneider, 1995; Channell and Guyodo, 2004) invoked pDRM, and hence a finite (decimeter-scale) lock-in depth, to explain reversal-isotope correlations and observed attenuation of secular variation records.

Magnetite and titanomagnetite grains carrying DRM or pDRM in marine sediments may be of detrital or biogenic origin. Titanomagnetite is likely to have a detrital origin from the weathering of igneous rocks (such as mid-ocean ridge or oceanic island basalts) or from volcanic ash falls. A magnetic remanence known as thermal remanent magnetization (TRM) is acquired as the (titano)magnetite grain cools through a blocking temperature spectrum within its igneous host. The detrital grains retain this TRM during erosion, transport, and subsequent incorporation into the deep-sea sediment. The interaction of the TRM of individual grains with the ambient geomagnetic field

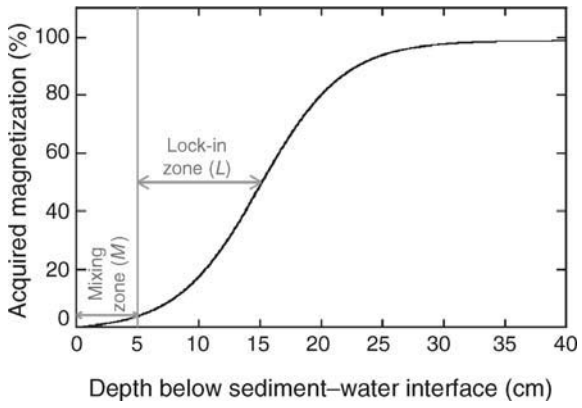

Figure P22 The sigmoidal function based on tanh(x) used to model the mixing zone (thickness M) and the underlying lock-in zone (thickness L) (after Channell and Guyodo, 2004).

at the time of sediment deposition generates the orienting torque that produces DRM or pDRM.

Magnetite (Fe_3O_4), with low or insignificant Ti (titanium) substitution, is commonly associated with biogenic sources. Magnetotactic bacteria are ubiquitous in freshwater and marine environments (e.g., Kirschvink and Chang, 1984; Petersen *et al*., 1986; Vali *et al*., 1987). They inhabit aerobic and anaerobic sediments and form intracellular chains of fine-grained (single domain) "magnetosomes" of magnetite (Blakemore and Blakemore, 1990) or, less commonly, goethite (Mann *et al*., 1990; Heywood *et al*., 1990). Magnetite and goethite magnetosomes have been observed to coexist within the same bacterium (Bazylinski *et al*., 1995). The intracellular magnetite and goethite crystals are formed by a process referred to as biologically controlled mineralization (BCM) (Lowenstam and Weiner, 1989; Bazylinski and Frankel, 2003). Intracellular magnetite and goethite are usually structurally well ordered and have a narrow (single domain) size distribution that is optimal for the retention of magnetic remanence in ferrimagnetic minerals such as magnetite and goethite (Figure P23).

Other Fe(III)-reducing bacteria secrete magnetite, and a range of other iron minerals, outside the cell by a process referred to as biologically induced mineralization (BIM) (Lowenstam and Weiner, 1989; Frankel and Bazylinski, 2003). Magnetite and other iron minerals produced by BIM are often poorly crystalline, fine-grained, and not structurally ordered. In the case of *Geobacter metallireducens* (also referred to as bacterium strain GS-15), magnetite is produced outside the cell as fine (superparamagnetic) grains produced by the oxidation of organic matter and Fe(III) reduction (Lovley, 1990). Unlike magnetotactic bacteria, these iron reducers are nonmagnetotactic (nonmotile), unconcerned about the size, shape, or composition of the iron mineral product, and can produce a range of iron minerals depending on the nature of the surrounding medium.

Magnetotactic bacteria apparently utilize the internal magnetite-goethite chains to navigate along geomagnetic field lines (magnetotaxis) to find optimal redox conditions in the near-surface sediment. In the absence of sensitivity to gravity due to neutral buoyancy in seawater, the ambient magnetic field provides up-down orientation, either in the Northern or Southern hemisphere (Kirschvink, 1980). The single-domain grain size typical for magnetite and goethite produced by BCM indicates that magnetic remanence is central to magnetosome function. Living magnetotactic bacteria tend to be concentrated at depths of few tens of centimeters below the sediment-water interface at the transition from iron-oxidizing to iron-reducing conditions (Karlin *et al*., 1987). The conditions under which BIM and BCM of magnetite takes place, and the depth in the sediment column to which these microbes are active (see Liu *et al*., 1997), are clearly of great importance in understanding the origin of the magnetic signature in sediments. Magnetic methods for the recognition of magnetosome chains, and individual magnetosomes, have been proposed by Moskowitz *et al*. (1988, 1994).

Apart from bacteria, other biogenic marine sources of magnetite are chiton (mollusk) teeth, fish, whales, and turtles. The role of magnetite in fish and marine mammals is thought to be navigational (Kirschvink and Lowenstam, 1979; Kirschvink *et al*., 2001; Walker *et al*., 2003). As for bacterial magnetite, these biogenic magnetite grains are often in the SD grain size range, the optimal grain size range for a stable magnetic remanence and are usually pure magnetite. The grains acquire a so-called chemical remanent magnetization (CRM) as they grow through their "critical" volume within the host organism.

Biogenic magnetite has been commonly observed in marine sediments on the basis of particle shape and size (e.g., Kirschvink and Chang, 1984; Petersen *et al*., 1986; Vali *et al*., 1987). The small elongate (SD) grain size of biogenic magnetite, typically $\sim 0.2 \pm 0.05$ μm across (Figure P23), and the resulting high surface area to volume ratio makes these grains susceptible to diagenetic dissolution. A large proportion of the biogenic magnetite in surface sediment may not survive sediment burial. Detrital magnetite (often titanomagnetite) appears to have greater survivability perhaps due to larger initial grain size and/or less intimate contact with pore waters. Stable primary NRMs in deep-sea sediments are commonly associated with PSD, rather than SD or MD, magnetite. Larger multidomain (MD) magnetite, with dimensions in excess of a few microns, carry a lower coercivity magnetization (than PSD or SD grains) that is more prone to remagnetization during the history of the sediment or sedimentary rock.

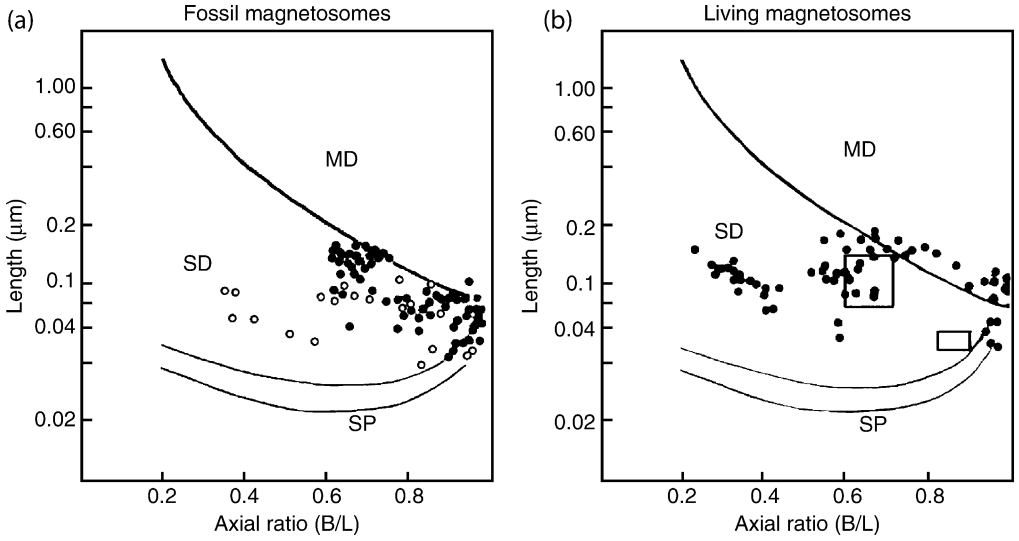

Figure P23 (a) Size and axial ratio (breadth/length) of fossil magnetite magnetosomes observed in Mesozoic and Tertiary sediments (open circles) and Quaternary sediments (closed circles). (b) Size and axial ratio (breadth/length) of magnetite magnetosomes from living bacteria (modified after Vali *et al*., 1987). Boxed regions in (b) from observations of Kirschvink (1983). Size distribution of multidomain (MD), single-domain (SD) and superparamagnetic (SP) magnetite grains after Butler and Banerjee (1975).

Origin of secondary magnetizations

Reduction diagenesis

CRM acquired during sediment diagenesis is the principal process that generates secondary magnetizations in marine sediments. The other important secondary magnetization is viscous remanent magnetization (VRM), the time-dependent acquisition of magnetization by the ambient (usually Brunhes Chron) geomagnetic field. A CRM postdates sediment deposition (usually by an unknown amount of time) and must be differentiated from the primary magnetization if sedimentary magnetic data are to be correctly interpreted. The primary and secondary magnetizations are differentiated in the laboratory by stepwise, progressive, demagnetization using either temperature or alternating fields. The differentiation can be successful if the two magnetization components respond differently to the demagnetization process (see Dunlop and Ozdemir, 1997).

A wide range of reactions, many of which are mediated by microbes, occur during deep-sea sediment diagenesis. Studies of pelagic pore waters indicate a sequence of electron acceptors used in the oxidation of sedimentary organic matter: O_2, nitrate NO_3^-, manganese (Mn^{3+}), iron (Fe^{3+}) then sulfate SO_4^{2-} (see Burdige, 1993). The utilization of sulfate has been found to be particularly important in the dissolution of magnetite grains in pelagic sediments. Microbial reduction of pore water sulfate (usually derived from seawater) yields sulfide ions that combine with the most reactive iron phase often magnetite to produce iron sulfide (Canfield and Berner, 1987). In most marine sedimentary environments, authigenic iron sulfides are dispersed throughout the sediment or associated with organic-rich burrows. In visual core descriptions of deep-sea sediments recovered during the 20-year duration of the Ocean Drilling Program, "pyrite" and amorphous iron sulfides are widespread and these iron sulfides probably originated through microbial sulfate reduction. The initial products are iron monosulfides (FeS), such as mackinawite, and further diagenesis may produce greigite (Fe_3S_4), pyrite (FeS_2) and pyrrhotite (FeS_{1+x} where $x = 0$–0.14). Pyrite is paramagnetic and therefore does not carry magnetic remanence. Pyrrhotite (e.g., Fe_7S_8) and greigite, on the other hand, are ferrimagnetic and capable of carrying a stable magnetization.

A secondary magnetization (CRM) carried by authigenic pyrrhotite often develops at the expense of a primary magnetization carried by magnetite. The dissolution of magnetite will be accentuated where sufficient pore water sulfate and labile organic matter support microbial sulfate-reducing communities. In organic rich, reducing, diagenetic conditions, such as the Japan Sea, pyrite and pyrrhotite are readily formed (Kobayashi and Nomura, 1972), at the expense of magnetite and other forms of reactive iron. Iron sulfide formation in marine sediments is limited either by the availability of pore-water sulfate (usually derived from sea-water) or the availability of organic carbon to sustain sulfate-reducing bacteria (Canfield and Berner, 1987). On the Ontong-Java Plateau, increased C_{org} in glacial isotopic stages has led to enhanced magnetite dissolution (Tarduno, 1994). In Taiwan, Pleistocene sediments contain detrital magnetite, authigenic greigite and pyrrhotite (Horng *et al*., 1998). Authigenic gregite has been detected in lake sediments (Giovanoli, 1979; Snowball and Thompson, 1988; Roberts *et al*., 1996) and in marine environments (Tric *et al*., 1991; Reynolds *et al*., 1994; Lee and Jin, 1995; Roberts and Weaver, 2005).

The dissolution of magnetite within the upper few decimeters of hemipelagic sediments has been documented by a reduction in coercivity and magnetization intensity as finer grains undergo preferential dissolution (Karlin and Levi, 1983; Leslie *et al*., 1990). In pelagic, high sedimentation rate, "drift" sediments from the Sub-Antarctic South Atlantic (see Figure P24a) and Iceland Basin (see Figure P24b), the pore water profiles indicate steady sulfate depletion with depth. At both sites, a primary magnetization records the polarity stratigraphy (Channell and Lehman, 1999; Channell, 1999; Channell and Stoner, 2002; Stoner *et al*., 2003) although there is abundant visual evidence that authigenic iron sulfide formation accompanies pore-water sulfate depletion. In the case of the Sub-Antarctic South Atlantic site (Figure P24a), NRM intensity decreases with depth, together with reduction in the ratio of anhysteretic susceptibility (k_{arm}) to susceptibility (k). This ratio (k_{arm}/k) is a magnetite grain-size proxy where higher values indicate finer grains. In the Iceland Basin record, the depletion of sulfate is not accompanied by marked changes in these magnetic parameters (Figure P24b). This may be due to the presence of a more reactive iron phase than magnetite at the Iceland Basin site and /or to the presence of a particularly reactive *magnetite* phase (e.g., fine-grained biogenic magnetite) at the Sub-Antarctic South Atlantic site.

Two additional profiles from the sub-Antarctic South Atlantic indicate a marked decrease in NRM intensity and k_{arm}/k at 150–200 cm depth (see Figures P25 and P26). This denotes a marked *increase* in grain size of magnetite at this depth relative to surface sediment (Figure P25) due to preferential dissolution of fine-grained magnetite due to the higher surface area to volume ratio. This dissolved fine-grained magnetite fraction carries NRM but is not an important contributor to volume susceptibility (Figure P25). Its fine grain size (k_{arm}/k values >6 are consistent with magnetite grain sizes of less than 0.1 μm) imply that the magnetite may be partly biogenic in origin. We conclude that the fine-grained (biogenic) magnetite is often lost during early diagenesis due to its small grain size and hence high reactivity. Note that k_{arm}/k values $>\sim 3$ are absent in the Iceland Basin record (Figure P24b) implying that biogenic magnetite is a less important component of the total magnetite budget at this site.

At some deep-sea sites, the concentration of sulfate in pore waters remains high to the base of the recovered section indicating (in the absence of a sulfate source at depth) that sulfate reduction is not a continuing process, even in the presence of a few percent organic carbon. This has been observed in siliceous sediments from the South Atlantic (ODP Leg 177), NW Pacific (ODP Leg 145), equatorial Pacific (ODP Leg 138) where magnetostratigraphic records indicate preservation of a primary magnetization (Channell and Stoner, 2002; Weeks *et al*., 1995; Schneider, 1995). We speculate that the organic carbon associated with diatomaceous (siliceous) oozes may be too refractory, or otherwise unavailable due to adsorption or encapsulation in/on siliceous surfaces, to be utilized by sulfate reducing microbes. Under these conditions of arrested sulfate reduction, a primary magnetization carried by magnetite will often be preserved.

Dissolution of magnetite by combination with sulfide ions, released by microbial reduction of pore water sulfate, is the most important process that accounts for the degradation of the magnetic signal in deep-sea sediments. In the presence of an iron phase that is more reactive than magnetite (e.g., goethite), the formation of iron sulfides may occur without appreciable magnetite dissolution.

Oxidation diagenesis

In contrast to the role of reduction diagenesis on magnetite dissolution, the primary magnetic signal in deep-sea sediments can be destroyed by oxidation of magnetite to maghemite. Kent and Lowrie (1974) and Johnson *et al*. (1975) documented this process in the so-called red clay facies that occurs over a large part of the mid-latitude Pacific (Davies and Gorsline, 1976). Henshaw and Merrill (1980) showed that the magnetic signal in these sediments is also affected by the authigenic growth of ferromanganese oxides and oxyhydroxides. The red clays are devoid of calcareous and siliceous microfossils and accumulated below the CCD (calcium compensation depth) at rates of ~25 cm/Ma, more than an order of magnitude slower than "average" pelagic sedimentation rates. The primary magnetization in the red clay facies is lost at depths of a few meters below the sediment-water interface, and the loss of magnetization often coincides with the later part of the Gauss Chron, close to the time of onset of Northern Hemisphere glaciation. The reduced grain size of eolian detrital magnetite, due to lower prevailing wind velocities prior to the onset of Northern Hemisphere glaciation, may influence the degradation of the magnetic signal in these sediments (Yamazaki and Katsura, 1990).

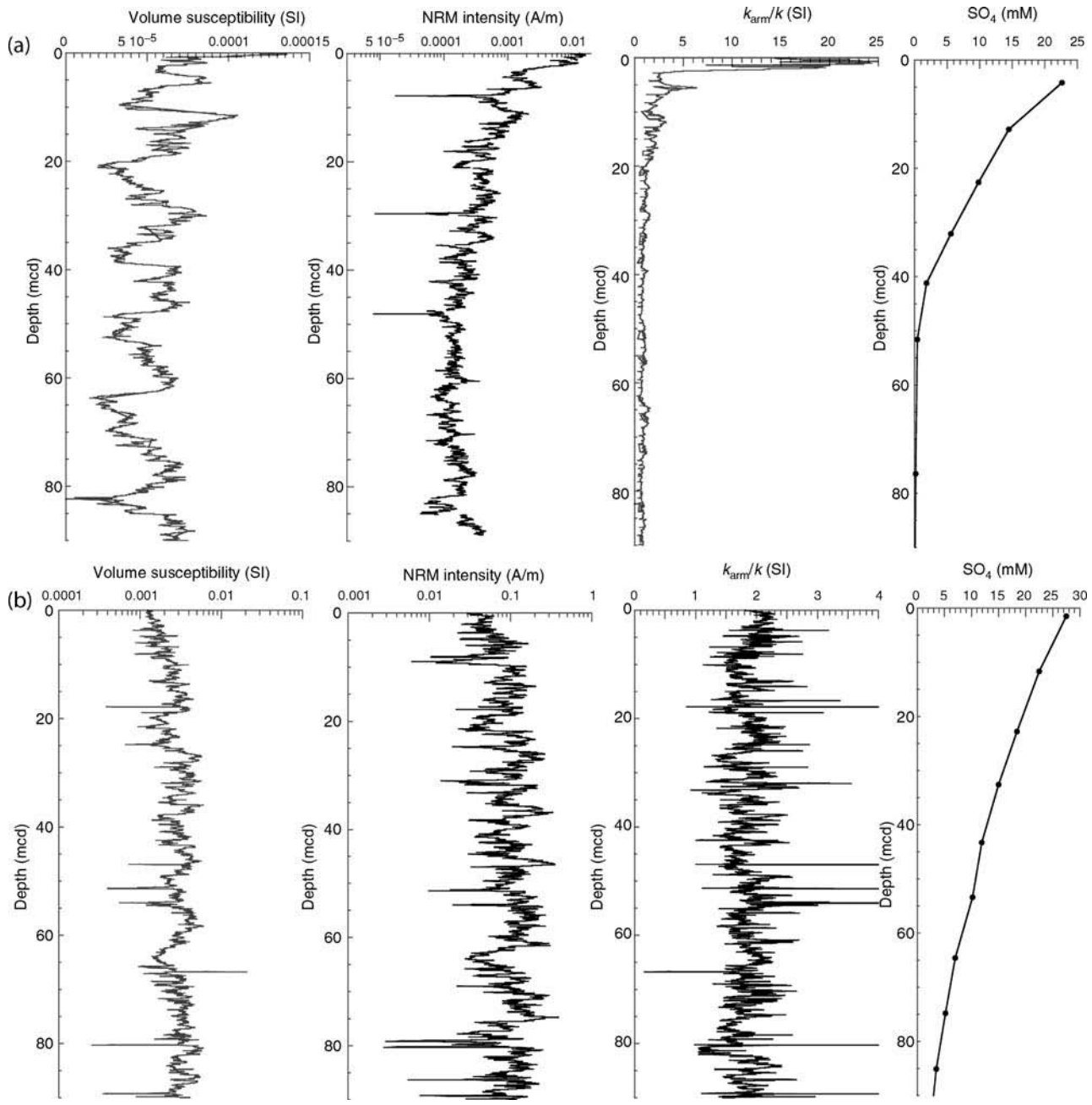

Figure P24 Volume susceptibility, NRM intensity after demagnetization at peak fields of 25 mT, anhysteretic susceptibility divided by susceptibility (k_{arm}/k), and pore water sulfate concentrations: (a) ODP Site 1089 (sub-Antarctic South Atlantic at 40.9°S, 9.9°E, 4620 m water depth) and (b) ODP Site 984 (Iceland Basin at 61.4°N, 24.1°W, 1648 m water depth). Data from Stoner *et al.* (2003), Channell (1999), and Shipboard Scientific Party (1996, 1999). At both sites, the 90 m composite depths (mcd) shown here represent ~600 ka, at mean sedimentation rates of 15 cm/ka.

Other origins of secondary magnetizations

Florindo *et al.* (2003) attribute low susceptibilities at some deep-sea drilling sites to dissolution of magnetite to form smectite in the presence of high concentrations of dissolved silica. Although authigenic smectite is widespread in deep-sea sediments, there are a number of different pathways for its formation and magnetite is one of a number of different possible precursors.

Degradation of the primary magnetic signal in deep-sea sediment cores can be attributed to factors associated with drilling and recovery. For example, magnetite in calcareous oozes from ODP Leg 154 (Ceara Rise, equatorial Atlantic) carry a secondary magnetization imposed by drilling that is apparently oriented radially in the core cross-section (Curry *et al.*, 1997). No primary magnetization was resolved in these sediments. Magnetite grains are, however, not apparently greatly affected by sulfate reduction as pore water sulfate remains high (>20 mM) to ~200 m depth and magnetic susceptibility does not decrease with depth (Curry *et al.*, 1997; Richter *et al.*, 1997). Low activity of sulfate reducing microbes may be due to low levels of (labile) organic matter in these sediments. The magnetic susceptibility record is not affected by diagenetic dissolution or authigenesis of

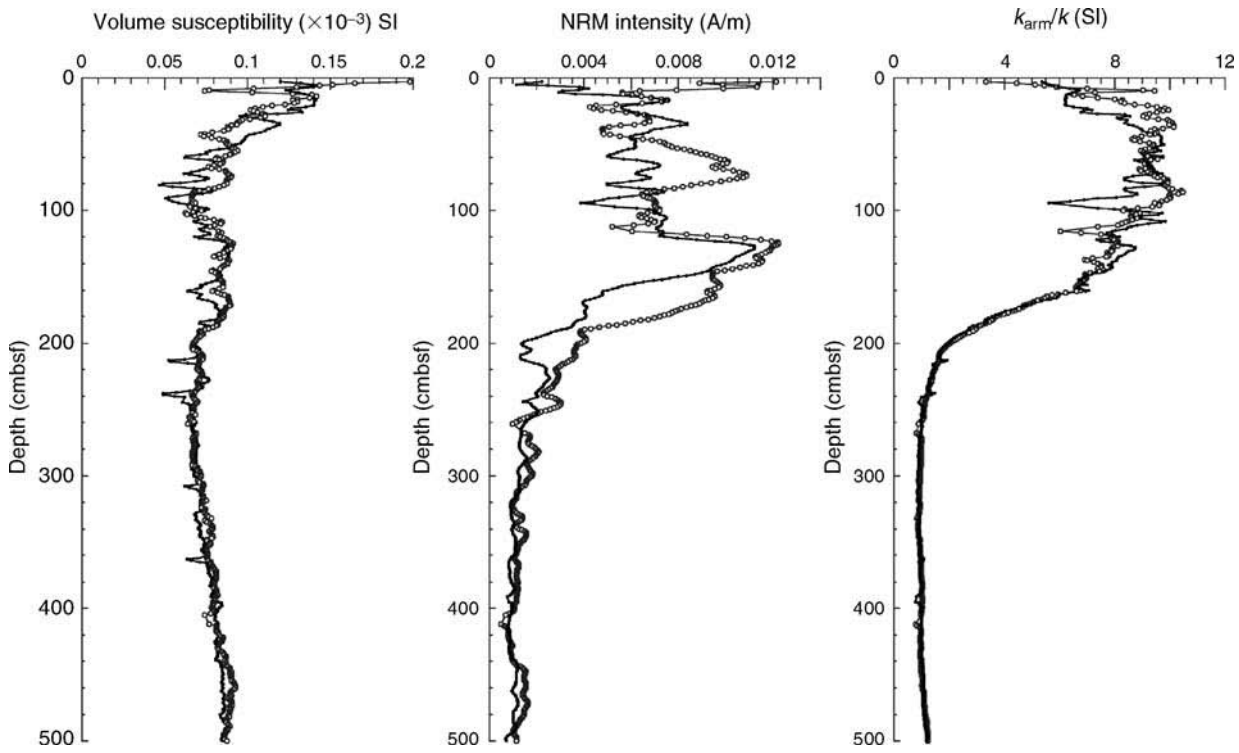

Figure P25 Volume susceptibility, NRM intensity after demagnetization at peak fields of 25 mT, anhysteretic susceptibility divided by susceptibility (k_{arm}/k) for two piston cores (4-PC03 and 5-PC01) collected during cruise TTN-057 in the sub-Antarctic South Atlantic at 40.9°S, 9.9°E and 41.0°S, 9.6°E, respectively, and 4620 m water depth. The 500 cm record shown here represents ~25 ka at a mean sedimentation rate of 20 cm/ka. Data from Channell *et al.* (2000).

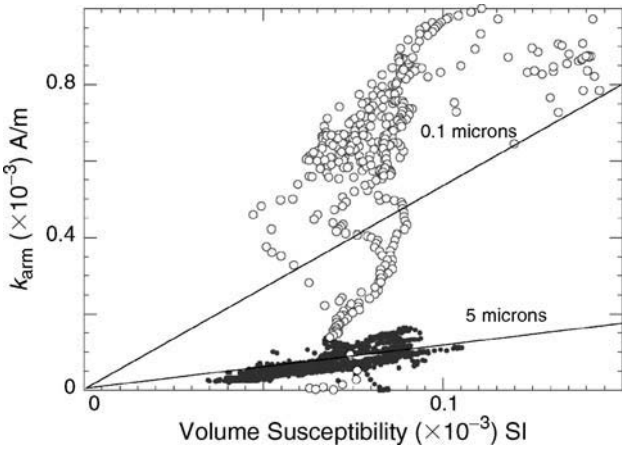

Figure P26 Anhysteretic susceptibility (k_{arm}) plotted against susceptibility (k) for Cores 4-PC03 and 5-PC01, from the sub-Antarctic South Atlantic. The measurements represent the last ~25 ka. Open symbols indicate Holocene samples. Data from Channell *et al.* (2000). The lines corresponding to magnetite grain size estimates of 0.1 μm and 5 μm after King *et al.* (1983).

magnetic minerals, and the cycles in susceptibility, produced by variations in surface water productivity, have provided a robust astrochronology (Shackleton *et al.*, 1999). The fidelity of the cyclostratigraphy supports other rock magnetic data (Richter *et al.*, 1997), indicating that magnetite has remained unaltered in ODP Leg 154 sediments. The magnetite grains are at least partially in the pseudo-single domain (PSD) size range (Richter *et al.*, 1997) and therefore capable of carrying stable primary magnetization. The observed radial (re)magnetization is attributed to an isothermal remanence (IRM) imposed by the coring procedure (Curry *et al.*, 1997).

In pelagic and volcaniclastic sediments of ODP Leg 157, from close to the Canary Islands, PSD magnetite appears to carry an inward-directed radial magnetization (Herr *et al.*, 1998; Fuller *et al.*, 1998). The coercivity of this radial remagnetization is greater than the more commonly observed downward-directed remagnetization associated with drilling, that can often be eliminated in peak alternating fields of ~20 mT. The coercivity of the radial remagnetization is greater than that of a simple IRM acquired in the few tens of mT fields associated with the steel core barrels and the remagnetization is more pronounced in poorly lithified sediments (Fuller *et al.*, 1998). We speculate that the nonmagnetic matrix in these sediments, when disturbed or shocked by drilling, allows physical re-orientation of magnetite grains in ambient magnetic fields emanating from the core barrels, bottom hole assembly or cutting shoe.

At any time during the history of the sediment or sedimentary rock, secondary magnetizations may be acquired (as CRMs) by chemical alteration of existing magnetic minerals, or by growth of new magnetic minerals.. Apart from the diagenetic changes noted above, events such as uplift, weathering, and deformation can all trigger the development of secondary CRMs. For example, much of the Paleozoic sequence of North America and Europe was remagnetizated coeval with the Hercynian (Late Carboniferous) orogenic pulse. This "orogenic" remagnetization is very widespread in North America, extending thousands of kilometers into the continental interior from the Appalachian margin. In carbonate rocks in North America and Europe, the Hercynian remagnetization is a CRM carried by magnetite. Authigenesis of magnetite may be triggered by orogenic activity in the Appalachians and the migration of hydrocarbon rich fluids into the hinterland (McCabe *et al.*, 1983, 1989; McCabe and Channell, 1994). Weathering and

uplift can result in the growth of magnetic iron oxides and oxyhydroxides (such as hematite and goethite) from preexisting Fe-bearing minerals such as clays or iron sulfides. The high coercivity of CRMs carried by hematite and goethite makes them difficult to remove by alternating field demagnetization techniques.

Conclusions

On the basis of a survey of the global distribution of high-quality magnetic stratigraphies in deep-sea sediments, Clement *et al*. (1996) concluded that terrigeneous sediment input is a factor that contributes to data quality. Sediments from the North Atlantic and the North Pacific, and the Indian Ocean, often contain terrigeneous material that appears to have aided preservation of a primary magnetization in these sediments and hence enhanced the magnetostratigraphic records from these regions. Although biogenic magnetite is ubiquitous in modern deep-sea sediments, fine SD particles are particularly susceptible to dissolution due to their high surface area to volume ratio. Much of this biogenic magnetite fraction does not appear to survive early diagenesis. The detrital magnetite component is more likely to survive, and record the direction and intensity of the geomagnetic field at the time of deposition. Diagenetic dissolution of magnetite in deep-sea sediments often occurs by reaction with sulfide ions to form iron sulfides. The formation of sulfide ions is generally a result of microbially mediated reduction of seawater sulfate in pore waters. The resulting sulfide ions in pore water react with magnetite or, if present, a more reactive iron phase, to produce iron sulfides that may carry a secondary CRM. The process is limited by the availability of sulfate and labile organic matter required by sulfate-reducing bacteria. Even in the presence of abundant pore water sulfate, high-quality magnetic records (preservation of primary magnetization) in siliceous sediments may be due to the low activity of sulfate-reducing microbes due to the role of tests of siliceous organisms in shielding labtile organic matter from sulfate-reducing microbes.

James E.T. Channell

Bibliography

Bard, E., 2001. Paleoceanographic implications of the difference in deep-sea sediment mixing between large and fine particles. *Paleoceanography*, **16**: 235–239.

Bazylinski, D.A., Frankel, R.B., Heywood, B.R., Mann, S., King, J.W., Donaghay, P.L., and Hanson, P.K., 1995. Controlled biomineralization of magnetite (Fe_3O_4) and greigite (Fe_3S_4 in a magnetotactic bacterium. *Applied and Environmental Microbiology*, **61**: 3232–3239.

Bazylinski, D.A., and Frankel, R.B., 2003. Biologically controlled mineralization in Prokaryotes. In Biomineralization, P.M., Dove, J.J., De Yoreo, and Weiner, S. (eds.), *Reviews in Mineralogy and Geochemistry*, **54**: 217–247. Washington, DC: The Mineralogical Society of America.

Blakemore, R.P., and Blakemore, N.A. Magnetotactic magnetogens. In Frankel, R.B., and Blakemore, R.P. (eds.), *Iron Biominerals*. New York: Plenum Press, pp. 51–67.

Boudreau, B.P., 1994. Is burial velocity a master parameter for bioturbation? *Geochimica et Cosmochimica Acta*, **58**: 1243–1249.

Burdige, D.J., 1993. The biogeochemistry of manganese and iron reduction in marine sediments. *Earth Science Reviews*, **35**: 249–284.

Butler, R.F., and Banerjee, S.K., 1975. Theoretical single-domain grain-size range in magnetite and titanomagnetite. *Journal of Geophysical Research*, **80**: 4049–4058.

Canfield, D.E., and Berner, R.A., 1987. Dissolution and pyritization of magnetite in anoxic marine sediments. *Geochimica et Cosmochimica Acta*, **51**: 645–659.

Channell, J.E.T., 1999. Geomagnetic paleointensity and directional secular variation at Ocean Drilling Program (ODP) Site 984 (Bjorn Drift) since 500 ka: Comparisons with ODP Site 983 (Gardar Drift). *Journal of Geophysical Research*, **104**: 22937–22951.

Channell, J.E.T., and Lehman, B., 1999. Magnetic stratigraphy of Leg 162 North Atlantic Sites 980–984. In Jansen, E., Raymo, M.E., Blum, P., and Herbert, T. (eds.), Proceedings of the Ocean Drilling Program-Scientific Results, College Station, TX (Ocean Drilling Program), **162**: 113–130.

Channell, J.E.T., and Guyodo, Y., 2004. Magnetic stratigraphy of the Matuyama Chronozone at ODP Site 982 (Rockall Bank), evidence for finite magnetization lock-in depths. In *Timescales of the Internal Geomagnetic Field*. *American Geophysical Union* Geophysical Monograph, **145**: 205–219.

Channell, J.E.T., and Stoner, J.S., 2002. Plio-Pleistocene magnetic polarity stratigraphies and diagenetic magnetite dissolution at Ocean Drilling Program Leg 177 Sites (1089, 1091, 1093 and 1094). *Marine Micropaleontology*, **45**: 269–290.

Channell, J.E.T., Stoner, J.S., Hodell, D.A., and Charles, C., 2000. Geomagnetic paleointensity for the last 100 kyr from the subantarctic South Atlantic: a tool for interhemispheric correlation. *Earth and Planetary Science Letters*, **175**: 145–160.

Clement, B.M., Kent, D.V., and Opdyke, N.D., 1996. A synthesis of magnetostratigraphic results from Pliocene-Pleistocene sediments cored using the hydraulic piston corer. *Paleoceanography*, **11**: 299–308.

Curry, W.B., Shackleton, N.J., and Richter, C., *et al*., 1997. Proceedings of the Ocean Drilling Program, Initial Reports, **154**: College Station, Texas (Ocean Drilling Program).

Davies, T.A., and Gorsline, D.S., 1976. Oceanic sediments and sedimentary processes. In Riley, J.P., and Chester, R., (eds.), *Chemical Oceanography.* New York: Academic Press, pp. 1–80.

DeMenocal, P.B., Ruddiman, W.F., and Kent, D.V., 1990. Depth of post-depositional remanence acquisition in deep-sea sediments: a case study of the Brunhes-Matuyama reversal and oxygen isotopic stage 19.1. *Earth and Planetary Science Letters*, **99**: 1–13.

Dunlop, D.J., and Ozdemir, O., 1997. *Rock Magnetism.* Cambridge: Cambridge University Press, 573 pp.

Florindo, F., Roberts, A.P., and Palmer, M.R., 2003. Magnetite dissolution in siliceous sediments. *Geochemistry, Geophysics, Geosystems*, **4**(7), 1053, doi:10.1029/2003GC000516.

Frankel, R.B., and Bazylinski, D.A., 2003. Biologically induced mineralization by bacteria. In Biomineralization. Dove, P.M., De Yoreo, J.J., and Weiner, S. (eds.), *Reviews in Mineralogy and Geochemistry*, **54**: 95–114. Washington, DC: The Mineralogical Society of America.

Fuller, M., Hastedt, M., and Herr, B., 1998. Coring-induced magnetization of recovered sediment. In Weaver, P.E.E., Schmincke, H-U., Firth, J.V., and Duffield, W. (eds.), Proceedings of the Ocean Drilling Program-Scientific Results, 157: College station, Texas (Ocean Drilling Program), pp. 47–56.

Giovanoli, F., 1979. A comparison of the magnetization of detrital and chemical sediments from Lake Zurich. *Geophysical Research Letters*, **6**: 233–235.

Guinasso, N.L., and Schink, D.R., 1975. Quantitative estimates of biological mixing rates in abyssal sediments. *Journal of Geophysical Research*, **80**: 3032–3043.

Henshaw, P.C., and Merrill, R.T., 1980. Magnetic and chemical changes in marine sediments. *Reviews of Geophysics and Space Physics*, **18**: 483–504.

Herr, B., Fuller, M., Haag, M., and Heider, F., 1998. Influence of drilling on two records of the Matuyama/Brunhes polarity transition in marine sediment cores near Gran Canaria. In Weaver, P.E.E., Schmincke, H-U., Firth, J.V., and Duffield, W. (eds.), Proceedings of the Ocean Drilling Program-Scientific Results, **157**: College station, Texas (Ocean Drilling Program), pp. 57–69.

Heywood, B.R., Bazylinski, D.A., Garratt-Reed, A.J., Mann, S., and Frankel, R.B., 1990. Controlled biosynthesis of greigite (Fe_3S_4) in magnetotactic bacteria. *Naturwiss*, **77**: 536–538.

Horng, C.-S., Torii, M., Shea, K.-S., and Kao, S.-J., 1998. Inconsistent magnetic polarities between greigite- and pyrrhotite/magnetite-bearing marine sediments from the Tsailiao-chi section, southwestern Taiwan. *Earth and Planetary Science Letters*, **164**: 467–481.

Hyodo, M., 1984. Possibility of reconstruction of the past geomagnetic field from homogeneous sediments, *Journal of Geomagnetism and Geoelectricity*, **36**: 45–62.

Irving, E., and Major, A., 1964. Post-depositional detrital remanent magnetization in a synthetic sediment. *Sedimentology*, **3**: 135–143.

Jansen, E., Raymo, M.E., Blum, P., *et al*., 1996. Proceedings of The Ocean Drilling Program, Initial Reports, **162**: College Station, Texas (Ocean Drilling Program).

Johnson, H.P., Lowrie, W., and Kent, D.V., 1975. Stability of anhysteretic remanent magnetization in fine and coarse magnetite and maghemite particles. *Geophysical Journal of the Royal Astronomical Society*, **41**: 1–10.

Karlin, R., and Levi, S., 1983. Diagenesis of magnetic minerals in recent hemipelagic sediments. *Nature*, **303**: 327–330.

Karlin, R., Lyle, M., and Heath, G.R., 1987. Authigenic magnetite formation in suboxic marine sediments. *Nature*, **6**: 490–493.

Katari, K., Tauxe, L., and King, J., 2000. A reassessment of post-depositional remanent magnetism: preliminary experiments with natural sediments. *Earth and Planetary Science Letters*, **183**: 147–160.

Kent, D.V., and Lowrie, W., 1974. Origin of magnetic instability in sediment cores from the central north Pacific. *Journal of Geophysical Research*, **79**: 2987–3000.

Kent, D.V., and Schneider, D.A., 1995. Correlation of paleointensity variation records in the Brunhes/Matuyama polarity transition interval. *Earth and Planetary Science Letters*, **129**: 135–144.

King, J.W., Banerjee, S.K., and Marvin, J., 1983. A new rock-magnetic approach to selecting sediments for geomagnetic paleointensity studies: application to paleointensity for the last 4000 years. *Journal of Geophysical Research*, **88**: 5911–5921.

Kirschvink, J.L., 1980. South-seeking magnetic bacteria. *Journal of Experimental Biology*, **86**: 345–347.

Kirschvink, J.L., 1983. Biogenic ferrimagnetism: A new biomagnetism. In Williamson, S.J., Romani, G.-L., Kaufman, L., and Modena, I. (eds.), *Biomagnetism.* New York: Plenum Press, pp. 501–531.

Kirschvink, J.L., and Chang, S.B.R., 1984. Ultrafine-grained magnetite in deep-sea sediments: possible bacterial magnetofossils. *Geology*, **12**: 559–562.

Kirschvink, J.L., and Lowenstam, H.A., 1979. Mineralization and magnetization of chiton teeth: paleomagnetic, sedimentologic, and biologic implications of organic magnetite. *Earth and Planetary Science Letters*, **44**: 193–204.

Kirschvink, J.L., Walker, M.M., and Deibel, C.E., 2001. Magnetite-based magnetoreception. *Current Opinion in Neurobiology*, **11**: 462–467.

Kobayashi, K., and Nomura, M., 1972. Iron sulfides in the sediment cores from the Sea of Japan and their geophysical implications. *Earth and Planetary Science Letters*, **16**: 200–208.

Lee, C.H., and Jin, J.-H., 1995. Authigenic greigite in mud from the continental shelf of the Yellow Sea, off the southwestern Korean peninsula. *Marine Geology*, **128**: 11–15.

Leslie, B.W., Lund, S.P., and Hammond, D.E., 1990. Rock magnetic evidence for the dissolution and authigenic growth of magnetic minerals within anoxic marine sediments of the California continental borderland. *Journal of Geophysical Research*, **95**: 4437–4452.

Liu, S.V., Zhou, J., Zhang, C., Coile, D.R., Gajdarziska-Josifovska, M., and Phelps, T.J., 1997. Thermophilic Fe (III)-reducing bacteria from the deep subsurface: the evolutionary implications. *Science*, **277**: 1106–1109.

Lovley, D.R., 1990. Magnetite formation during microbial dissimilatory iron reduction. In Frankel, R.B., and Blakemore, R.P. (eds.), *Iron Biominerals*, New York: Plenum Press, pp. 151–166.

Lowenstam, H.A., and Weiner, S., 1989. *On Biomineralization.* New York: Oxford University Press.

Lund, S., and Keigwin, L., 1994. Measurement of the degree of smoothing in sediments paleomagnetic secular variation records: an example from late Quaternary deep-sea sediments of the Bermuda rise, western North Atlantic Ocean. *Earth and Planetary Science Letters*, **122**: 317–330.

Mann, S., Sparks, N.H.C., Frankel, R.B., Bazylinski, D.A., and Jannasch, H.W., 1990. Biomineralization of ferrimagnetic greigite (Fe_3S_4) and iron pyrite (FeS_2) in a magnetotactic bacterium. *Nature*, **343**: 258–260.

Mazaud, A., 1996. Sawtooth variation in magnetic intensity profiles and delayed acquisition of magnetization in deep sea cores. *Earth and Planetary Science Letters*, **139**: 379–386.

McCabe, C., and Channell, J.E.T., 1994. Late Paleozoic remagnetization in limestones of the Craven Basin (northern England) and the rock magnetic fingerprint of remagnetization secondary carbonates. *Journal of Geophysical Research*, **99**: 4603–4612.

McCabe, C., Van der Voo, R., Peacor, D.R., Scotese, C.R., and Freeman, R., 1983. Diagenetic magnetite carries ancient yet secondary remanence in some Paleozoic sedimentary carbonates. *Geology*, **11**: 221–223.

McCabe, C., Jackson, M., and Saffer, B., 1989. Regional pattern of magnetic authigenesis in the Appalachian Basin: implications for the mechanism of late Paleozoic remagnetization. *Journal of Geophysical Research*, **94**: 10429–10443.

Meynadier, L., and Valet, J.-P., 1996. Post-depositional realignment of magnetic grains and asymetrical saw-toothed pattern of magnetization intensity. *Earth and Planetary Science Letters*, **140**: 123–132.

Moskowitz, B.M., Frankel, R.B., Flanders, P.J., Blakemore, R.P., and Schwartz, B.B., 1988. Magnetic properties of magnetotactic bacteria. *Journal of Magnetism and Magnetic Materials*, **73**: 273–288.

Moskowitz, B.M., Frankel, R.B., and Bazylinski, D.A., 1994. Rock magnetic criteria for the detection of biogenic magnetite. *Earth and Planetary Science Letters*, **120**: 283–300.

Opdyke, N.D., Glass, B., Hays, J.P., and Foster, J., 1966. Paleomagnetic study of Antarctica deep-sea cores. *Science*, **154**: 349–357.

Opdyke, N.D., and Channell, J.E.T., 1996. *Magnetic Stratigraphy.* London: Academic Press, 346 pp.

Petersen, N., von Dobeneck, T., and Vali, H., 1986. Fossil bacterial magnetite in deep-sea sediments from the South Atlantic Ocean. *Nature*, **320**: 611–615.

Reynolds, R.L., Tuttle, M.L., Rice, C.A., Fishman, N.S., Karachewski, J.A., and Sherman, D.M., 1994. Magnetization and geochemistry of greigite-bearing Cretaceous strata, north slope basin. Alaska, *American Journal of Science*, **294**: 485–528.

Richter, C., Valet, J.-P., and Solheid, P.A., 1997. Rock magnetic properties of sediments from Ceara Rise (Site 929): implications for the origin of the magnetic susceptibility signal. In Shackleton, N.J., Curry, W., and Bralower, T.J. (eds.), Proceedings of the Ocean Drilling Program-Scientific Results, 154: College station, Texas (Ocean Drilling Program), pp. 169–179.

Roberts, A.P., Reynolds, R.L., Verosub, K.L., and Adam, D.P., 1996. Environmental magnetic implications of greigite (Fe_3S_4) formation in a 3 Ma lake sediment record from Butte Valley, northern California. *Geophysical Research Letters*, **23**: 2859–2862.

Roberts, A.P., and Winklhofer, M., 2004. Why are geomagnetic excursions not always recorded in sediments? Constraints from post-depositional remanent magnetization lock-in modeling. *Earth and Planetary Science Letters,* **227**: 345–359.

Roberts, A.P., and Weaver, R., 2005. Multiple mechanisms of remagnetization involving sedimentary greigite (Fe_3S_4). *Earth and Planetary Science Letters*, **231**: 263–277.

Schneider, D.A., 1995. Paleomagnetism of some Leg 138 sediments: Detailing Miocene magnetostratigraphy, In Pisias, N.G., Mayer, L.A., Janecek, T.R., Palmer-Julson, A., and van Andel, T.H. (eds.), Proceedings of The Ocean Drilling Program—Scientific Results, 138: College Station Texas (Ocean Drilling Program), pp. 59–72.

Shackleton, N.J., Crowhurst, S.J., Weedon, G., and Laskar, L., 1999. Astronomical calibration of Oligocene-Miocene time. *The Royal Society London Philosophical Transactions*, **357**: 1909–1927.

Shipboard Scientific Party, Site 984, In Jansen, E., M. Raymo, P. Blum, *et al*. (eds.), 1996. Proceedings of The Ocean Drilling Program, Initial Reports, College Station, Texas (Ocean Drilling Program), **162**: 169–222.

Shipboard Scientific Party, Site 1089. In Gersonde, R., Hodell, D.A., Blum, P. *et al*., 1999. Proceedings of The Ocean Drilling Program, Initial Reports, **177**, 1–97, [CD ROM]. Available from Ocean Drilling Program, Texas A&M University, College Station, Texas 77845–9547, USA.

Smith, C.R., and Rabouille, C., 2002. What controls the mixed-layer depth in deep-sea sediments? The importance of POC flux. *Limnology and Oceanography*, **47**: 418–426.

Snowball, I., and Thompson, R., 1988. The occurrence of greigite in sediments from Loch Lomond. *Journal of Quaternary Science*, **3**: 121–125.

Stoner, J.S., Channell, J.E.T., Hodell, D.A., and Charles, C., 2003. A 580 kyr paleomagnetic record from the sub-Antarctic South Atlantic (ODP Site 1089). *Journal of Geophysical Research*, **108**: 2244, doi:10.1029/2001JB001390.

Tarduno, J.A., 1994. Temporal trends of magnetic dissolution in the pelagic realm: Gauging paleoproductivity. *Earth and Planetary Science Letters*, **123**: 39–48.

Tauxe, L., Herbert, T., Shackleton, N.J., and Kok, Y.S., 1996. Astronomical calibration of the Matuyama-Brunhes boundary: consequences for the magnetic remanence acquisition in marine carbonates and Asian loess sequences. *Earth and Planetary Science Letters*, **140**: 133–146.

Teanby, N., and Gubbins, D., 2000. The effect of aliasing and lock-in processes on paleosecular variation records from sediments. *Geophysical Journal International*, **142**: 563–570.

Thomson, J., Brown, L., Nixon, S., Cook, G.T., and McKenzie, A.B., 2000. Bioturbation and Holocene sediment accumulation fluxes in the north-east Atlantic Ocean (Benthic Boundary Layer experiment sites). *Marine Geology*, **169**: 21–39.

Trauth, M.H., Sarnthein, M., and Arnold, M., 1997. Bioturbational mixing depth and carbon flux at the seafloor. *Paleoceanography*, **12**: 517–526.

Tric, E., Laj, C., Jéhanno, C., Valet, J-P., Kissel, C., Mazaud, A., and Iaccarino, S.,1991. High resolution record of the Olduvai transition from Po valley (Italy) sediments: support for dipolar transition geometry. *Physics of the Earth and Planetary Interiors* **65**: 319–336.

Vali, H., Förster, O., Amarantidis, G., and Petersen, N., 1987. Magnetotactic bacteria and their magnetofossils in sediments. *Earth and Planetary Science Letters*, **86**: 389–400.

Walker, M.M., Diebel, C.E., and Kirschvink, J.L., 2003. Detection and use of the Earth's magnetic field by aquatic vertebrates. In Collin, S.P., and Marshall, N.J. (eds.), *Sensory Processing in Aquatic Environments.* New York: Springer-Verlag, pp. 53–74.

Weeks, R.J., Roberts, A.P., Verosub, K.L., Okada, M., and Dubuisson, G.J., 1995. Magnetostratigraphy of upper Cenozoic sediments from Leg 145, North Pacific Ocean. In Rea, D.K., Basov, I.A., Scholl, D.W., and Allan, J. (eds.), Proceedings of The Ocean Drilling Program—Scientific Results, 145: College Station, Texas (Ocean Drilling Program), pp. 209–302.

Yamazaki, T., and Katsura, T., 1990. Magnetic grain size and viscous remanent magnetization of pelagic clay. *Journal of Geophysical Research*, **95**: 4373–4382.

Cross-references

Biomagnetism
Geomagnetic Polarity Timescales
Iron Sulfides
Magnetization, Chemical emanent (CRM)
Magnetization, Depositional Remanent (DRM)
Magnetization, Isothermal Remanent (IRM)
Magnetization, Natural Remanent (NRM)
Magnetization, Thermoremanent (TRM)
Magnetization, Viscous Remanent (VRM).
Magnetostratigraphy
Paleomagnetism

PALEOMAGNETISM, EXTRATERRESTRIAL

With the advent of the space age, a rich paleomagnetic record has been discovered in the inner solar system. The various bodies of the solar system differ in their interactions with the solar wind, depending upon their size, the presence or absence of active dynamos, remanent magnetic fields, and atmospheres. Observations of these interactions have shown that like Earth, Mercury appears to have an active dynamo, whereas Venus, the Moon, Mars, and those asteroids studied do not.

In a planet with an active dynamo, magnetic fields arise from magnetic material because of the induced magnetism in the ambient field and their earlier acquired remanent magnetism. Magnetic fields observed on the Moon and Mars in the absence of an active dynamo must be due to remanent magnetism only. These fields due to remanent magnetization, or paleomagnetic fields, have been investigated on the Moon and Mars with satellite-based surveys. In addition, samples brought to Earth by the Apollo missions from the Moon and those that have come to Earth from the Moon, Mars, and asteroids in the form of meteorites provide additional paleomagnetic data. Other meteorites include primitive material from the early solar system and even presolar grains.

This extraterrestrial paleomagnetic record may offer a fascinating glimpse of the magnetic fields in the early solar system, providing we are clever enough to interpret it correctly.

Lunar paleomagnetism

Observations from spacecraft prior to Apollo established limits on any lunar dipole moment should be at least five orders smaller than the geomagnetic dipole, but to the surprise of many, the Apollo-returned basalts and breccias carried stable natural remanent magnetization (NRM). With the advent of surface magnetometers on Apollo 12, 14, 15 and 16, subsatellites in low orbits on Apollo 15 and 16, and the more recent Lunar Prospector, it also became clear that the substantial volumes of the lunar crust are magnetized.

Apollo samples

The Apollo samples were collected from the lunar regolith and consisted of igneous rocks, breccias, and soil. Their rock magnetism is very different from that of terrestrial samples. The dominant magnetic phases in the lunar samples are metallic iron and iron-nickel as shown in Figure P27 (Strangway *et al*., 1970; Nagata *et al*., 1972). The Fe-Ni is in the form of the Ni poor alpha phase kamacite. Kamacite has an irreversible thermomagnetic curve with a Curie point between 740°C–770°C, whereas taenite has a range of Curie points dependent upon Ni content. On heating, kamacite converts to taenite with a sluggish return transition on cooling, whose temperature is dependent upon Ni content. This inversion is responsible for the irreversible thermomagnetic curve illustrated in Figure P27b. The mare basalts recovered from the regolith had iron as the dominant remanence carrying phase, whereas the breccias contained the Fe-Ni. In some breccias

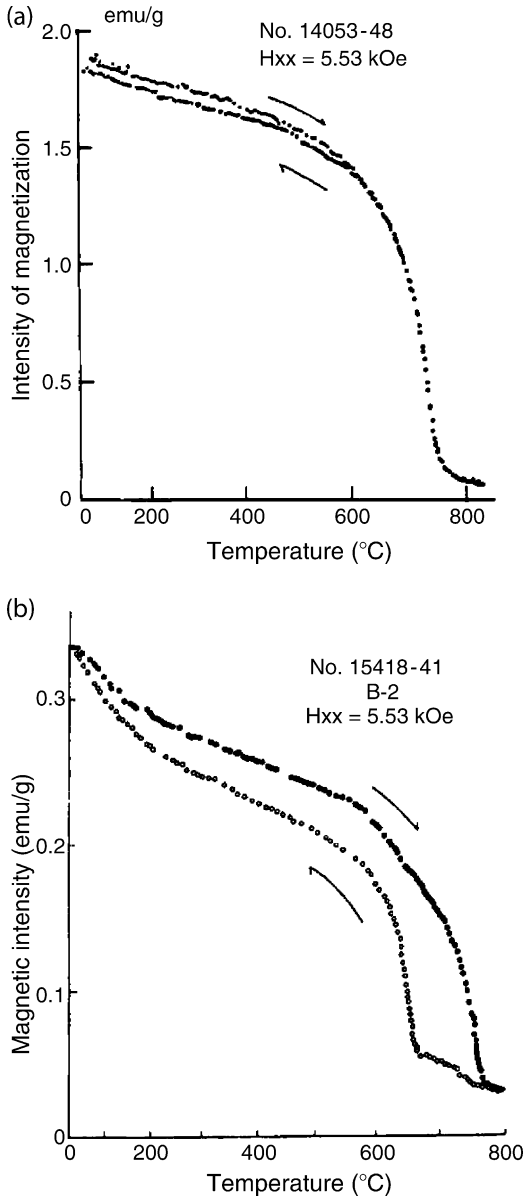

Figure P27 Magnetic phases in lunar rocks: (a) Apollo 14 mare basalt showing reversible thermomagnetic curve demonstrating presence of metallic iron and (b) Apollo 15 breccia, illustrating the effect of kamacite-taenite transition (Nagata *et al.*, 1972).

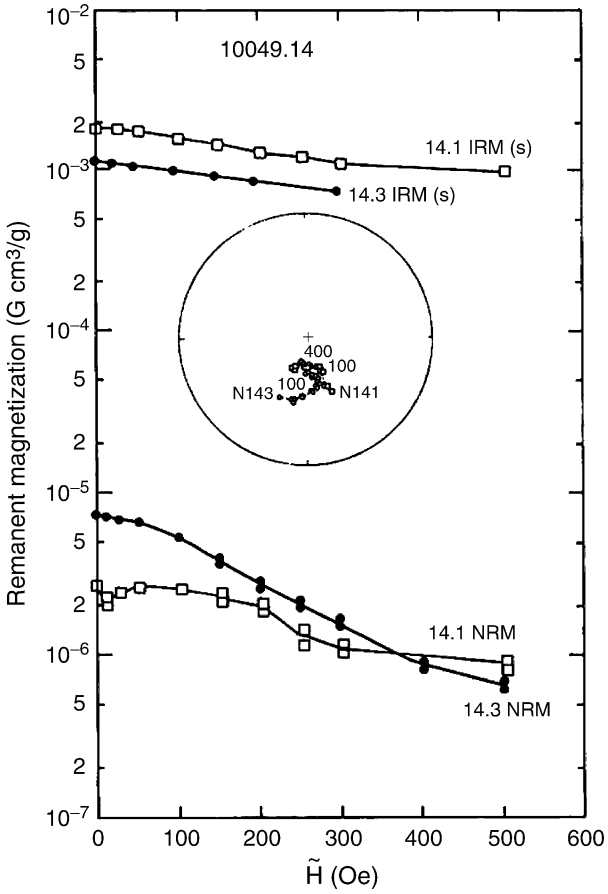

Figure P28 AF demagnetization of natural remanent magnetization (NRM) and saturation isothermal remanent magnetization (IRMs) of an Apollo 11 mare basalt. Note the directional similarity of the two samples after demagnetization to 100 Oe (10 mT).

with extreme coercivity the mineral "tetrataenite" may be present (Wasilewski, 1988).

The rock magnetism of the soils presented an immediate problem because they contained more ferromagnetic iron than the basalts from which they were principally derived. This iron is predominantly superparamagnetic as demonstrated by Nagata (1972). Three possible explanations of the origin of the excess iron were suggested: (1) by reduction of paramagnetic iron-rich silicates in the presence of solar wind hydrogen in the uppermost surface layer of the soil (Houseley *et al.*, 1973), (2) by reduction in the thermal blankets of ejecta material (Pearce *et al.*, 1972), and (3) by shock decomposition of iron rich silicates (Cisowski *et al.*, 1973). To some extent these processes overlap and all may contribute to the excess metallic iron, but the first mechanism appears to be dominant and may have relevance elsewhere in the solar system, for example on asteroids. The paramagnetic and ferromagnetic iron content of soils forms a useful classification scheme for soils and serves an indicative of provenance (Wasilewski and Fuller, 1975). The magnetic properties of the breccias vary according to their subgroups. The regolith breccias are similar to the soil from which they are derived by varying degrees of shock metamorphism. The fragmental breccias contain clasts in a porous matrix. The melt breccias, which consist of clasts in an igneous textured matrix, have properties similar to the igneous rocks.

The lunar paleomagnetic record comes primarily from the mare basalts and the melt breccias (see Figure P28). The plutonic rocks that are largely unsuitable for paleomagnetism are in the form of clasts in breccias. The paleomagnetism of the breccias is frequently hard to interpret, but in the melt breccias thermoremanent magnetization (TRM) appears to dominate, so that their mode of magnetization is similar to that of the mare basalts. The samples had experienced some degree of shock, exposure to radiation, and thermal cycling on the lunar surface.

The role of shock as a possible source of magnetization in the presence of a magnetic field, or demagnetization in the absence of such a field, was investigated in a number of experimental studies (Cisowski *et al.*, 1973, 1976). Flying plate experiments in which soil samples were encapsulated in the plate demonstrated that shock levels of a few GPa (tens of kilobars) in fields of tens of microteslas were sufficient to induce magnetization in lunar soil comparable in intensity with that found in the regolith breccias samples. In the absence of the

magnetic field, shock was shown to harden thermoremanent magnetization by preferentially demagnetizing the softer magnetic phases. A flying plate impact at a velocity of 17 km/s into a block of terrestrial basalt in an ambient field of 1 mT field demonstrated shock magnetization and the generation of a plasma that displaced and compressed the ambient field (Figure P29, Srnka *et al*., 1986). Effects of radiation and thermal cycling were also investigated and are unlikely to be important factors in the origin of lunar magnetism.

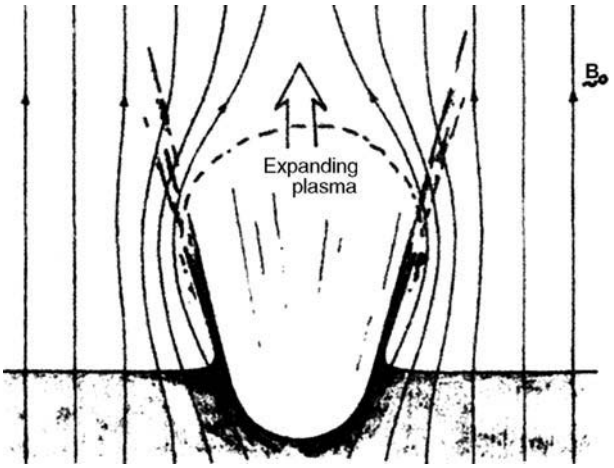

Figure P29 Model of field compression by impact in flying plate experiment. The plate was traveling at 17 km/s and impacted a block of basalt. The ambient field was 10 Oe (1 mT). The block was magnetized by the event and pick up coils demonstrated the formation of a plasma and field compression consistent with the model shown.

Later it became clear that at least some stable primary magnetization was preserved from the initial cooling of samples on the moon as igneous rocks. In the absence of any knowledge of the orientation,—in which the samples acquired their magnetization—the interest focused in on the intensity of magnetization they carry and the possibility of finding the history of the intensity of ancient lunar magnetic fields. Despite some success, classical methods of determining intensity involving heating the sample to give a TRM in a known field in the laboratory, were confounded by irreversible changes brought about by heating the samples. Various other methods including using ARM as a proxy for TRM (Shaw Stephenson and Collinson, 1974), heating by microwave radiation (Hale *et al.*, 1978) and IRM normalization (Cisowski and Fuller, 1986) were utilized. The IRM normalization method is admittedly a poor substitute for classical intensity determination methods, but because of the availability of data from a large number of samples it had a value as a rough indicator. Such a distinctive result followed that even the poor accuracy likely for IRM normalization was useful. From all of the intensity work it emerged that there was a high field with a surface intensity comparable to the Earth's surface field between 3.85 and 3.65 Ga (Figure P30). Two discussions of the subsequent history were that the field intensities gradually decreased over a period of about 1 Ga (Collinson, 1984; Runcorn, 1994). In contrast, Cisowski and Fuller (1986) suggested that there was a relatively brief period of high intensity from about 3.85 to 3.65 Ga and that outside of this period intensities could not be distinguished from background noise. Additional work is needed to clarify this point.

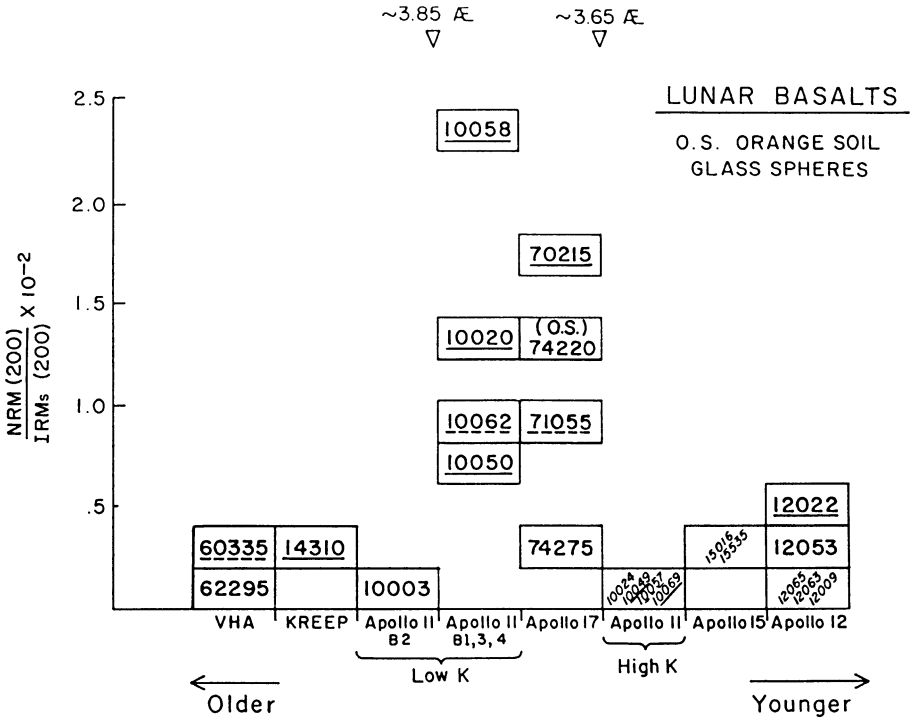

Figure P30 Paleointensity estimates from Apollo mare basalts by the IRMs normalization method. Calibration of the method by thermoremanent magnetism (TRM) experiments suggest that values of NRM(200)/IRMs(200) are equivalent to field intensities of 0.5 Oe. Note that only some of the Apollo 11 and 17 basalts with ages between approximately 3.85 and 3.65 Ga show values of NRM(200)/IRMs(200) greater than 0.5 suggesting that only in this age range were fields comparable to or greater than the geomagnetic surface field at present.

Magnetization of the lunar crust observed with surface and subsatellite magnetometers and electron reflectance experiment

The Apollo surface magnetometers (e.g., Dyall, 1972) revealed fields from a few tens of gammas (nT) at the Mare sites to 100 nT at the Fra Mauro Apollo 14 site and hundreds of nanoteslas at the Apollo 16 highland site. The stronger magnetizations could be explained by the strong magnetization of basin ejecta of the Fra Mauro and Cayley formations (Strangway *et al*., 1973). The scale length of coherence appeared to be relatively short –from 100 m to km. The results from the subsatellite magnetometers (Coleman *et al*., 1972; Russell *et al*., 1975) and the electron reflectance experiments (Lin *et al*., 1988) confirmed the results from the surface magnetometers in finding stronger fields over the highlands than over the Mare. They also showed stronger fields over the older eastern Mare than the younger western Mare. The high resolution of the electron reflectance experiment demonstrated that cratered regions were not systematically more strongly, or weakly, magnetized than surrounding regions (Lin, 1979). It is also confirmed from the observation of the subsatellite magnetometer surveys that the strongest magnetic anomalies were antipodal to the younger large impact basins. This suggested that a lunar field was required at the time of the younger giant impacts to account for the field compression and magnetization at the antipodes proposed by (Hood and Huang, 1991) as well as to account for the strong magnetization of mare basalts of this age. The sites of the strongest anomalies include regions of swirls similar to the Reiner gamma feature. These features are probably caused by the strong fields of the magnetic anomalies that stand off the radiation that otherwise darkens the albedo of the lunar surface.

The magnetometer/electron reflectometer experiment on Lunar Prospector has greatly improved the resolution and coverage of the magnetic mapping of the Moon, so that the entire surface is now mapped. The results were not only confirmed but also extended the earlier results that showed that the fields over the highlands were strong compared with those over the Mare despite the fact that the dominant occurrence of iron is of course in the Mare (Lucey *et al*., 1995). The electron reflectance results (Mitchell *et al*., 2004) also confirmed the ubiquitous presence of small-scale anomalies with dimensions of order tens of kilometers. This is consistent with the small scale of surface anomalies observed with the Apollo surface magnetometers. The absence of fringing anomalies around craters of up to 50 km in diameter (Halekas *et al*., 2003) indicates that there cannot be coherent magnetization in the upper tens of kilometers of the crust. Moreover, since the Curie point of iron is soon reached in deeper regions, it appears that the crust does not contain large volumes of uniform magnetization. Thus the elegant theorem of Runcorn (1975), which proved that the field recorded in a spherical shell from cooling in the field of an internal dipole source is not be detectable from the outside, may not be relevant to the interpretation of lunar crustal magnetism. Following the assumption of shallow sources, Mitchell *et al*. (2003) developed a simple model for the magnetism of the lunar crust. They reconstructed the field by sequentially applying the magnetizing and demagnetizing effects of the known basin forming events to give the field illustrated in Figure P31. They found that the model was much improved by adding 1 nT background field. It therefore appears that the magnetization of the lunar crust is basically due to the effects of large basin forming events and that a relatively stronger field is required at the age of the proposed strong field era to explain the anomalies over the antipodes of the young basins.

Origin of lunar magnetism

After attempts to explain the magnetization of the Moon and of returned samples by exotic models had been investigated and found wanting, Runcorn's initial suggestion of a lunar dynamo (e.g., Runcorn, 1975) was generally accepted. The history of this dynamo was less clear and two rival ideas emerged corresponding to the two views of the field intensity records. One invoked a lunar dynamo that operated from about 3.9 Ga, giving a surface field comparable to the Earth's surface field and gradually lost intensity over about a billion years (Collinson, 1984; Runcorn 1994). In contrast, Cisowski and Fuller (1986) argued for a relatively brief period of high intensity between about 3.9 and 3.6 Ga with intensity outside of this interval indistinguishable from background noise. But still, it is not clear which of these suggestions were correct. With either model, the strongly magnetized mare and highland samples would have acquired their NRM as they get cooled in the dynamo field and the strongest anomalies antipodal to the younger giant basins could have acquired their magnetization in an enhanced antipodal field by shock magnetization as suggested by Hood *et al*. (1991). Recently, a short period of dynamo action has been proposed to be associated with a major overturn of the lunar mantle that made the core cool rapidly. This could have generated a magnetic field between 3.85 and 3.65 Ga, during a brief period of convection (Stegman *et al*., 2003).

In conclusion, it should be remembered that the lunar dipole moment required to give a particular surface field on the Moon is smaller than the geomagnetic dipole moment required to give a comparable surface field on Earth because the radius of the Moon is smaller than the Earth's. Moreover, since we do not know how dynamo fields scale with the size of the region in which they are generated, we should not assume that the ratio of lunar to terrestrial dipole moments varies as the volume (Stevenson, 2002), or as the cube of the radii of the cores. Only in this case, does the cube of the core dimension cancel with the inverse cube of the dipole field fall off, so that the decrease in moment of the core is canceled by the decrease in the distance to source. In contrast, if the lunar dynamo had given the same moment as the geodynamo, which is admittedly unlikely given the small size of the lunar core, the lunar surface field would be two orders stronger than the surface field on the Earth. Admittedly, this is a rough and ready argument, but dynamo action in the lunar core with a dipole moment weaker than that of the geodynamo could still have generated surface fields similar to those interpreted from the paleomagnetic studies.

Martian paleomagnetism

Studies of Martian magnetism consist of direct observations of the magnetism of the soil by Viking, the magnetic surveys of the crustal field carried out by Mars Surveyor, and the paleomagnetic record of the Shergotite, Nahklite, and Chassignite (SNC) meteorites.

Viking and Pathfinder: soil and dust magnetic experiments

The Viking Magnetic Properties Experiment (Hargraves *et al*., 1977, 1979) provided an estimate of the amount of magnetic material in the martian soil at a few percent. Moreover, the magnet experiments demonstrated that some 80% of the magnetic material was strongly magnetic suggesting that it was magnetite, titanomagnetite, or their more oxidized equivalents maghemite and titanomaghemite. Their preferred interpretation was that the mineral was maghemite and that its occurrence was in the form of a pigment dispersed throughout the soil.

Pollack *et al*. (1977) analyzed the airborne dust from the Martian images and found that the best match they achieved to their derived imaginary refractive indices was for fine-grained magnetite. Additional analysis of the airborne dust particles including Pathfinder data indicated that fine magnetite rather than titanomagnetite was required to explain the high-saturation magnetization.

The Mars Pathfinder lander carried similar magnetic experiments to those on Viking with the important addition of a multispectral imager (Hargaves *et al*., 2000). Despite difficulties, the results of these analyses confirmed the earlier suggestion that there is a strongly magnetic phase present either as coatings, or nanoparticles. The phase is either magnetite or maghemite. Again, maghemite was the preferred choice.

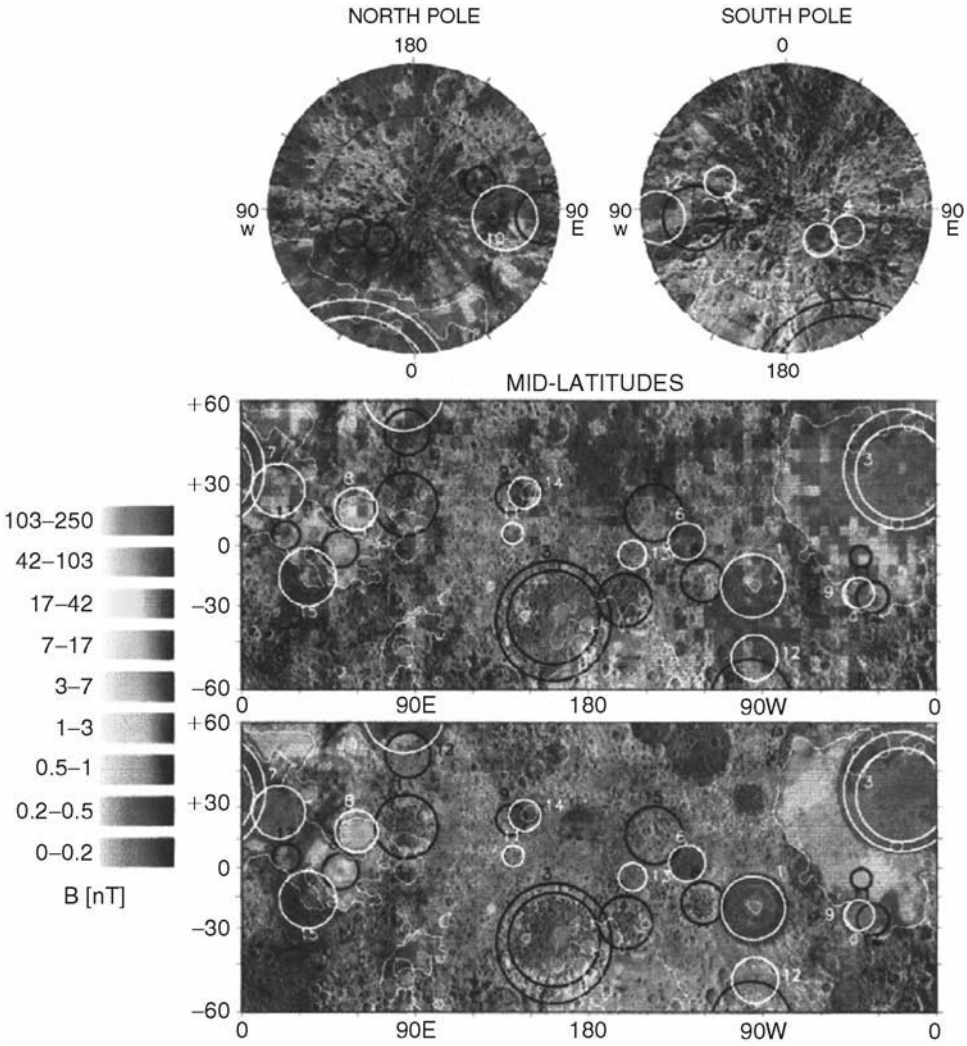

Figure P31 Model for lunar crustal magnetization; the top panel for mid-latitudes shows the magnetic anomaly data and the bottom panel shows the model reconstruction (With permission, Halekas, 2003).

On the missions presently at Mars, there are Mössbauer experiments that should identify the phases present. Such identification of the magnetic phases in the soil will be important in distinguishing an origin by direct weathering from surface basalts, or something more exotic. In the former case, titanium would be expected to be present, whereas pure magnetite, or maghemite, would suggest the latter.

Viking had also measured the composition of the martian atmosphere, which turned out to be a key piece of information demonstrating that the meteorites Shergottites, Nahklites, and Chassignites (SNC) did indeed come from Mars. The main discussion of them will therefore be given in this martian section.

Shergottites, Nahklites, and Chassignites (SNC) meteorites: the Martian meteorites

As noted above, the primary evidence for the martian origin of the SNC meteorites is that they contain noble gases that match the present martian atmosphere. In particular, it was found that the trapped noble gases in impact glass melt in EETA79001 were a perfect match for those measured by the Viking lander. Moreover, the ages of all except ALH84001 are young enough (200–1300 Ma) that given their volcanic nature they must have come from an evolved body with recent volcanic activity. Histories have been established for the various meteorites with estimates of the age of their initial formation on Mars, the age of the event that blasted them from the martian surface, their time in transit, and finally the age of arrival on Earth.

The rock magnetism of the SNC meteorites is much more like that of terrestrial samples than is that of the lunar samples, or indeed of other meteorites. The dominant carriers of the paleomagnetic record in these martian samples are magnetite and low Ti titanomagnetites and pyrrhotite. The paleomagnetism of the SNC meteorites has yielded a possible record of the surface magnetic field of Mars. Estimates of the order of 1 μT have come from microwave intensity determinations with Nakhla (Shaw *et al*., 2001).

ALH84001 has played such a special role because of the claims of the presence of life forms in it (McKay *et al*., 1997) that a separate discussion is given here. ALH84001 is a cataclastic orthopyroxenite. It initially crystallized at 4.5 Ga, was involved in a major impact event at 4.0 Ga, was excavated from the Martian surface by another event at approximately 16 Ma, and eventually landed in Antarctica 13 ka ago. It contains secondary carbonate of controversial origin within which magnetite also of controversial origin is found. The carbonate has been dated at approximately 4.0 Ga. This magnetite played a critical role in the controversy over the evidence for life because it was

interpreted to be biogenic having been formed in martian bacteria analogously to the magnetite formed in terrestrial bacteria (Thomas-Keprta, 2000, 2001). However, the demonstration of a topotactic relationship of both the magnetite in iron-rich carbonate and periclase in magnesium-rich carbonate strongly suggests that most of the magnetite was formed by breakdown of the iron-rich carbonate during the impact event at 4.0 Ga (Barber and Scott, 2002). Whether there is other magnetite of biogenic origin remains to be seen, although Barber and Scott (2002) see no requirement for it.

The natural remanent magnetization (NRM) of ALH84001 is predominantly carried by the fine magnetite (Collinson, 1997; Cisowski, 1986). Collinson's initial study of mutually oriented samples of ALH84001 (Collinson 1997) indicated that individual subsamples had soft magnetizations whose directions were dissimilar, but that a harder magnetization, which demagnetized between 20 and 40 mT, was similar in different samples. His interpretation of the magnetization gave an estimate of the Martian field of one order smaller than the geomagnetic field.

Isolated NRM in two neighboring pyroxene grains of ALH84001 was reported by Kirschvink *et al*. (1997) to differ by some 70°. The magnetization was interpreted to have been acquired during cooling after the 4.0 Ga impact event and now differed due to subsequent differential rotation of the grains during brittle deformation. Given this interpretation, Kirschvink *et al*. (1997) argued that the differing magnetizations in the neighboring grains leads to an upper temperature limit, since magnetization on Mars of 110C (the maximum temperature the sample was exposed to during sample preparation). Using exquisite technique with high-resolution SQUID magnetometers, Weiss *et al*. (2000) discovered that the magnetization was inhomogeneous on the scale of the individual carbonate blebs. They suggested that the magnetization was probably carried by pyrrhotite and magnetite in association with the carbonate. In this work, observations of partial thermal demagnetization of small regions of millimeter size with the high-resolution SQUIDs further reduced the constraints on heating, since the time that the magnetization was acquired on the Martian surface, to 40C (Figure P32).

Antretter *et al*. (2003) confirmed the observation by Collinson (1997) that despite soft magnetization, which differed from one subsample to another, at higher intermediate harder magnetization from different subsamples agreed in direction. Assuming that the magnetite was formed from the carbonate in the major impact event at 4.0 Ga, as petrological evidence suggests, the NRM will record this field.

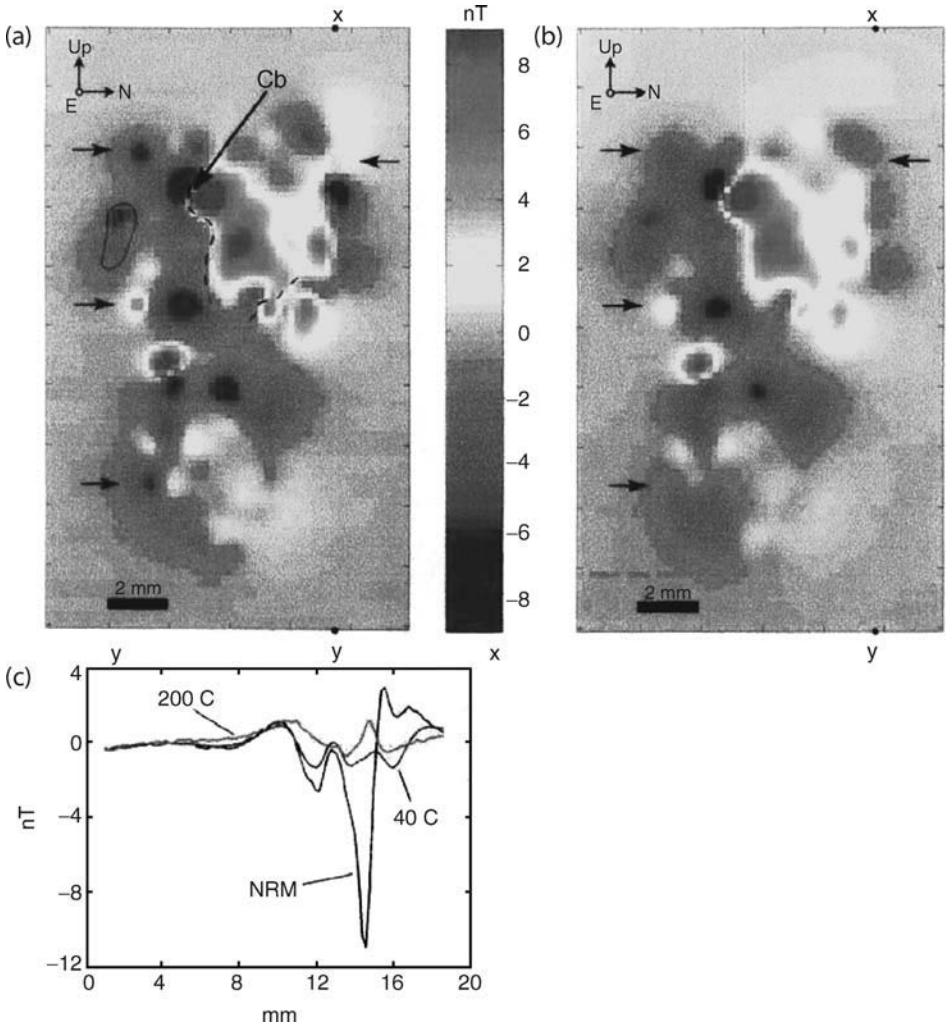

Figure P32 Results of partial thermal demagnetization of a region within ALH 84001 measured with high-resolution SQUID measurements. Note that the magnetization is changed upon heating to 40°C. Hence assuming that the NRM was acquired entirely on Mars, the material cannot have been heated subsequently above 40°C (With permission; Weiss *et al.*, 2000).

Normalizing the intensity of the NRM by the saturation isothermal remanence (IRMs) then gives an estimate for the 4.0 Ga martian field one order smaller than the present geomagnetic field. If the magnetization is heterogeneous due to magnetization at different times, or due to subsequent misalignment as suggested by Kirschvink *et al.* (1997), this may be a minimum field value.

Crustal magnetic field of Mars

Just as the paleomagnetic record discovered by the Apollo missions was one of the bigger surprises of the lunar exploration, so the magnitude and distribution of the martian magnetic anomalies has proved a major surprise in martian exploration. The magnetic crustal field on Mars differs from the terrestrial crustal field in its intensity and distribution (Acuna *et al*., 1999; Connerney *et al*., 2001). On Earth, the magnetic features are distributed more or less uniformly over the planet. On Mars, the strong features are largely confined to a band that covers two-thirds of the southern highlands (Figure P33). They also reach an order of magnitude stronger than substantial terrestrial anomalies. An $n = 90$ spherical harmonic model (Cain *et al*., 2003) gave an upper limit for the martian dipole six orders smaller than the geomagnetic dipole moment and close to the noise in the martian coefficients. However, between $n = 20$ and 40 the martian power spectrum is 40 times stronger than that of the Earth.

There have been discussions of the linear nature of the anomalies and the possibility that they record a seafloor-spreading-like mechanism on Mars (Acuna *et al*., 1999) or terrane accretions (Fairen *et al*., 2002). However, the evidence for seafloor-like anomalies has been questioned by Harrison (Harrison, 2000) and even the linear nature of the features has been disputed by Arkhani-Hamed (2001a). The possibility of reversals of the Martian dynamo is supported by calculations of paleomagnetic poles from isolated anomalies that turned out to be in similar locations, but of both polarities (Arkhani-Hamed, 2001b). More recent analyses have increased the resolution of the surveys and drawn attention to the presence of smaller anomalies in the northern plains and the possibility of the role of shock demagnetization associated with the major basin of Utopia (Halekas, 2003).

Discussion

The origin of the martian anomalies and the explanation of their distribution and strength remain unclear. However, it appears that there must have been a relatively strong surface magnetic field, at least comparable with that of the geomagnetic surface field, when the strong anomalies of the southern highlands were formed. The caveat discussed in reference to the lunar dynamo and the strength of the surface fields it may generate must also be remembered here. Hence, if the dipole moments generated by the martian and geodynamos are similar, say to order of magnitude, then the surface martian field would be stronger than terrestrial surface field simply due to the ratio of the radii of the planets. The strongest observed anomalies are about an order larger than those on Earth.

Numerous magnetic phases have been suggested to help in understanding the high remanent magnetization of the Martian crust: e.g., hematite (Dunlop and Kletetschka, 2001, Kletetschka *et al*., 2000a, Özedmir and Dunlop, 2002), hematite-ilmenite solid solution (Kletetschka *et al*., 2002, Robinson *et al*., 2000), and low-temperature oxidation, or weathering to give maghemite, or hematite (Özdemir, 2000). Cooling experiments with iron-rich basalts were carried out and revealed the presence of titanium-rich cruciform titanomagnetites that were modeled as the source of the martian crustal anomalies (Hammer *et al*., 2003). The role of pyrrhotite has been emphasized by Rochette *et al*. (2001). The most potent magnetic material that might give rise to these strongly magnetized rocks is generally recognized to be SD magnetite (e.g., Kletetschka *et al*., 2000b).

Given the saturation magnetization of magnetite of 4.9×10^5 A/m, the saturation remanent magnetization of a 0.5% dispersion of uniaxial, SD magnetite will be between 1×10^3 A/m and 2×10^3 A/m. Assuming a surface field intensity an order of magnitude greater than the geomagnetic field, the TRM, or indeed the chemical remanent magnetization

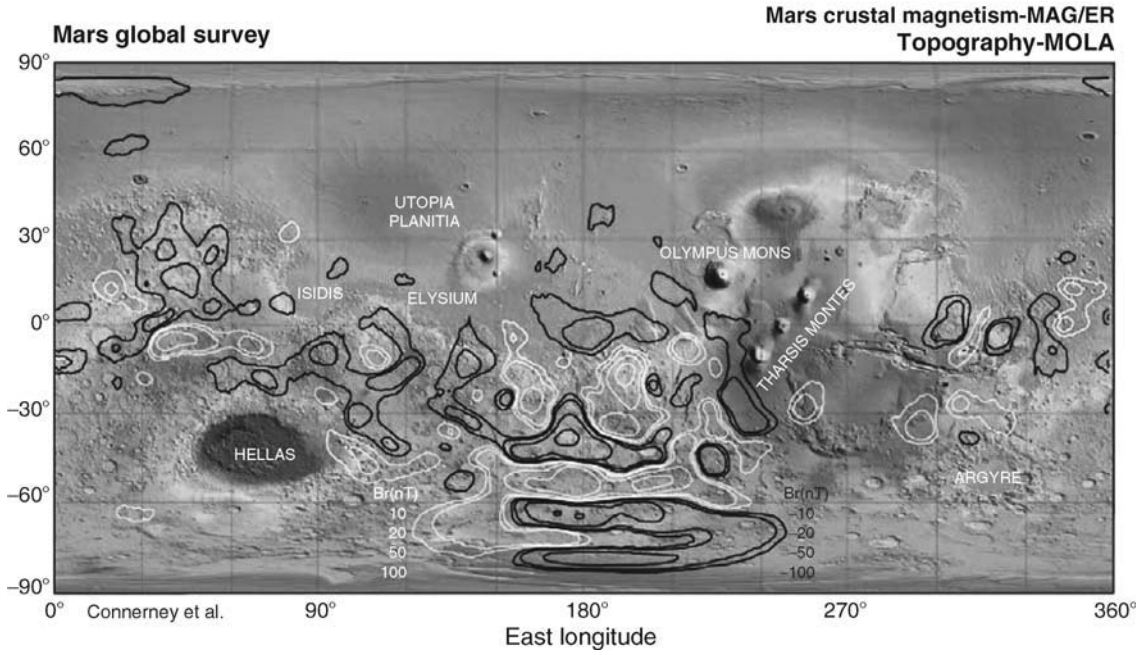

Figure P33 Mars crustal magnetic anomalies from Connerney *et al.* (2001). Note that the strongest anomalies are in a band stretching some 60° of latitude, which is centered equatorially near 0° longitude and expands to cover most of the Southern Hemisphere near 180° longitude. Within the Southern Hemisphere, the anomalies are weak in Hellas and Argyre, and over the Tharsis region (With permission, Purucker).

(CRM), will give the ~10–20 A/m required by the models for the Martian crustal fields. With a surface field comparable to the geomagnetic field, 0.5% of SD magnetite may be sufficient to give the required to depths of ~10 km in parts of the Southern Hemisphere to meet the requirements of the models. The key point is that this magnetite must be in a SD state.

No matter what proves to be the explanation of the intensity of the martian anomalies, their distribution and in particular their confinement to a band largely in the Southern Hemisphere remains a puzzle (Figure P31). Moreover, there is strong evidence that beneath the younger surface material of the northern plains, there is cratered older material similar to that found in the Southern Highlands (Frey, 2003), so that the superficial difference in appearance of the two regions is not a sufficient explanation.

To explain the lack of strong anomalies in the north, hydrothermal activity has been invoked to demagnetize the features in the northern basin (Solomon *et al*., 2002). Another possibility is that the strong magnetic anomalies are never formed in the Northern Hemisphere, but only in the Southern Highlands (Scott and Fuller, 2004). This idea is based on: (1) an early carbon dioxide rich atmosphere in which weak acids formed, dissolved iron from igneous rocks, depositing iron rich carbonates in the upper crust and (2) the fine magnetite that was then formed by decomposition of the siderite on subsequent heating due to intrusions. Given the observed correlation between water channels and magnetic anomalies in the Southern Highlands (Harrison and Grimm, 2000), this suggestion is consistent with the disposition of the anomalies. Only in these regions water was found to be present in the appropriate amounts to permit the necessarily intermittent dissolution and deposition processes to take place.

Another factor that has emerged with the newer analyses is the possible role of demagnetization caused by the impacts that formed the large basins in the Northern Hemisphere. In this view, it appears that just as in the absence of strong magnetization in the major basins on the Moon permits a simple model of magnetization of the lunar crust, so on Mars, the same absence of strong anomalies in Argyre, Hellas, and Utopia basin suggest a similar role of shock demagnetization on Mars. Indeed Hood *et al*. (2000) have argued that the size of the demagnetized region around Hellas corresponds to the region that would have experienced 2 GPa, the shock value required for pyrrhotite to pass through a transition into a nonmagnetic phase. If shock does play a dominant role of in determining not only the lack of anomalies associated with Argyre and Hellas, but also with even bigger features of Utopia in the Northern Hemisphere, then important aspects of the Martian crustal magnetic field may be modeled by similar demagnetizing effects to those utilized in the lunar model of Mitchell *et al*. (2003).

Conclusion

The martian crustal anomalies, the magnetization of ALH840001, and other SNC meteorites suggest that a martian dynamo generated a global magnetic field early in martian history, but that it shut off sometime soon after 4.0 Ga. The strength of the surface anomalies may be partially explained by the smaller distance from the sources in the martian core to the surface, but their distribution on the martian surface requires an explanation. Clearly the role of shock demagnetization associated with large basin-forming events has played an important role in determining the observed distribution, but there appears to be a need for some additional explanation of the absence of anomalies in the Northern Hemisphere.

Asteroid paleomagnetism

Prior to the 1990s our knowledge of the asteroids was from telescopic observations and interpretations of the sources of certain meteorites. With advent of the space era of exploration, observations by spacecraft with magnetometers onboard permitted estimates of the magnetic fields and ultimately of the magnetization of a sampling of asteroids. Beginning with the flyby of 9969 Braille in 1991 by Deep Space 1 (DS1) (Richter *et al*., 2001), there have been flybys of 951 Gaspra (Kivelson *et al*., 1993) and 243 Ida by Galileo on its way to Jupiter, and of 433 Eros and of 253 Mathilde by the Near Earth Rendezvous Mission (NEAR) which subsequently landed on 433 Eros (Acuna *et al*., 2001). With the exception of the observations on 433 Eros, estimates of the magnetic fields of the various asteroids rely on the interpretation of the interaction of the solar wind with these bodies. The nature of this interaction can reveal whether it is strongly and coherently magnetized, weakly and incoherently magnetized, or whether it is without remanent magnetization and simply has an induced magnetization dependent on the solar wind field. The results of such measurements constrain the origin and history of the asteroid and potentially have important bearing on the origin of the solar system.

The closest approach of DS1 of 28 km was achieved at 1.3 AU. Despite the strong magnetic noise from the ion propulsion unit of DS1, magnetic field measurements were made of 9969 Braille and yielded an estimate of its magnetic moment of 2.1×10^{11} A m^2 (Richter *et al*., 2001). The magnetometer on Galileo observed a disturbance of the solar wind field during the flyby of Gaspra consistent with the asteroid having a remanent magnetization (Figure P34). The intensity of magnetization was comparable with that of chondritic meteorites (Kivelson *et al*., 1993; Baumgartel *et al*., 1994). A similar effect was observed on the flyby of 243 Ida, although it was weaker. In contrast to these results, the magnetometer on the NEAR spacecraft on its approach to 433 Eros and after landing failed to detect a global magnetic field (Acuna *et al*., 2002). The upper limit on the field value was reported 0.005 A/m, giving a remanent magnetization of 1.9×10^{-6} A m^2/kg. This is orders of magnitude smaller than those reported for 951 Gaspra and 9969 Braille and for meteorites likely to have come from this type of asteroid.

Taken at face value these results suggest that Gaspra and Ida have relatively strong coherent magnetization comparable in intensity to that seen in strongly magnetized chondrites (see below) to which they are most closely linked spectroscopically. This would be consistent with their S-type classification. Such a magnetization might have been acquired by initial cooling in a substantial magnetic field, or as a result of some subsequent event. On the other hand, the results from Eros, also an S-type, suggest cooling in the absence of a field, or random magnetization, such as might be acquired in a cold accretion process. The puzzling results from the asteroid magnetic field observations led to suggestions of random magnetization within 433 Eros (Wasilewski *et al*., 2002) and to reconsideration of the possibility that the magnetization of chondritic meteorites might be randomly oriented. The latter will be discussed below.

Conclusion

The results from 9969 Braille, 951 Gaspra, and to a lesser extent 243 Ida suggest homogenous magnetization and hence magnetization recording the field of the planetesimal in which it was formed or some subsequent event in a field. In contrast, the results from 433 Eros suggest that its constituent magnetic phases either carried little intrinsic magnetization, or that they were not strongly heated in the accretion process.

Meteorite paleomagnetism

Introduction

Meteorites provide a sampling of the oldest material in the solar system and even pre-solar grains. In addition they sample the moon, planets, and asteroids. Recently, the number of meteorites available for analysis has more than doubled because of the remarkable Antarctic meteorite collections obtained by recent Japanese and US expeditions, in which Prof. William Cassidy of the University of Pittsburgh played a key role. We thus have the possibility of studying the paleomagnetism,

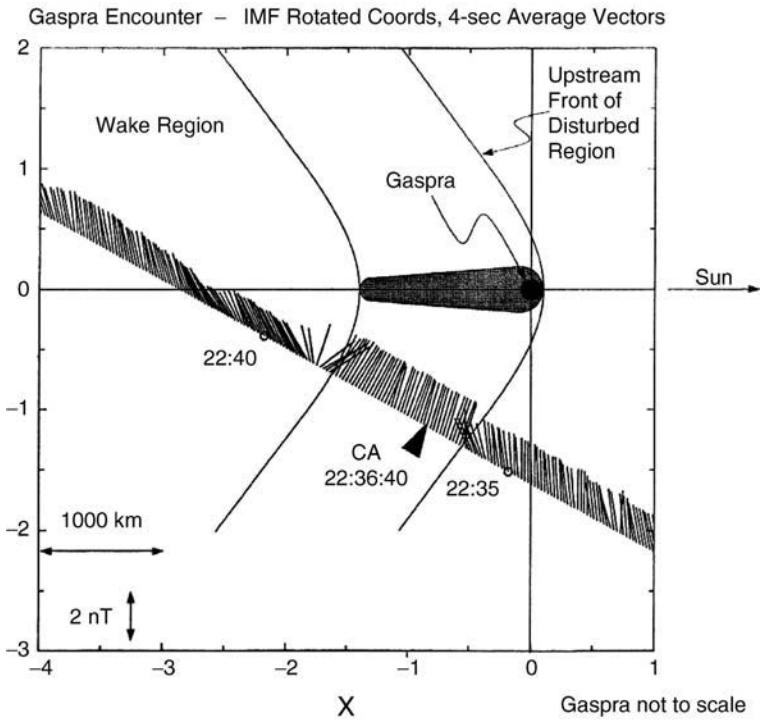

Figure P34 Disturbance of solar wind field during Gaspra flyby and a model for its magnetosphere (With permission; Kivelson *et al.,* 1993).

as well as the petrology, chemical, and isotopic composition and age of this material, so fortuitously brought to Earth and preserved in a relatively pristine state. Meteorites are divided into chondrites, achondrites, stoney-irons, and irons. The irons are separated because they are metal rich. The chondrites and achondrites are separated according to the presence, or absence of chondrules, which are small spherules, 0.1–2 mm in size. The achondrites are differentiated, in contrast to the chondrites. McSween (1999) provides an excellent modern introduction to meteorites.

Chondrites are heterogeneous aggregates with radiogenic ages of 4.56 Ga, which is consistent with the presence in chondrites of products of short-lived radioactive isotopes such as ^{26}Al, and the similarity of their composition to that of the sun. Among the inclusions in chondrites are the refractory calcium aluminum inclusions (CAI). They formed between 1400 and 1100°C as condensates, or evaporative residues, or more complex mixtures of thermally processed material. As such, they are of great interest as a means of glimpsing early solar system magnetic fields, although the magnetic material in them formed somewhat later than the earliest condensates. The chondrule population in the chondrites, is the next most primitive material available to us, which probably formed a few million years after the CAIs, although their origin remains somewhat controversial. Unfortunately, the CAIs and chondrules have suffered either the varying degrees of aqueous alteration especially in the various carbonaceous chondrites, or the thermal metamorphism especially in the ordinary chondrites.

The achondrites in principle are simpler to understand than the chondrites because they are derived from the products of igneous differentiation similar to processes seen on the Earth. However, achondrites are also frequently brecciated, so that we find rarely anything like a pristine igneous rock. They crystallized at approximately 4.5 Ga.

The paleomagnetism of meteorites has been a major research area for more than half a century since the pioneering work of Stacey *et al.* (1961) and a comprehensive review appeared in the 1980s (Cisowski, 1987), as well as a very useful discussion in the *Rock Magnetism* text by Dunlop and Özdemir (1999). It is a rich field with the possibility of giving information about early solar system magnetic fields, and in addition key magnetic data for asteroids, the moon, and Mars. There are however major difficulties in the interpretation of the paleomagnetic record of meteorites that must be addressed before the data can be used with confidence (e.g., Wasilewski *et al*., 2002). Magnetic studies have focused upon the chondrites, their inclusions, and achondrites. Yet, the complicated histories of these meteorites make the interpretation of their paleomagnetic record particularly tricky.

Magnetic properties of different categories of meteorites

Irons contain dominantly Fe-Ni, in the form of the Ni poor alpha phase kamacite, and the Ni-rich gamma phase taenite. Irons have been classified according to their composition and the dimensions of the Widmanstatten pattern, which is related to their Ni content and cooling rate. Kamacite has an irreversible thermomagnetic curve with a Curie point of between 740 C and 770 C, whereas taenite has a range of Curie points dependent upon Ni content. As we noted in the discussion of the magnetic properties of the Apollo samples, on heating kamacite inverts to taenite with a sluggish return transition on cooling. This temperature is dependent upon Ni content. A plot of the fraction of the saturation magnetization due to the alpha Fe-Ni phase kamacite against the temperature of the gamma to alpha transition separates the various subgroups (Figure P35a) (Strangway *et al*., 1970; Nagata *et al.,* 1972).

Because many chondrites contain metallic Fe-Ni, whereas achondrites do not, the subdividision into chondrites, or achondrites, has a natural magnetic expression. This is best seen if the fraction of the total saturation magnetization due to the alpha phase, or kamacite, is plotted against the total saturation magnetization of the meteorite (Figure P35b, P35c). Kamacite and taenite, alpha and gamma phases of NiFe dominate the magnetic properties of most meteorites. It is tetrataenite, the stable form of NiFe below 320°C that is seen for the most part in ordinary chondrites as was first pointed out by Wasilewski

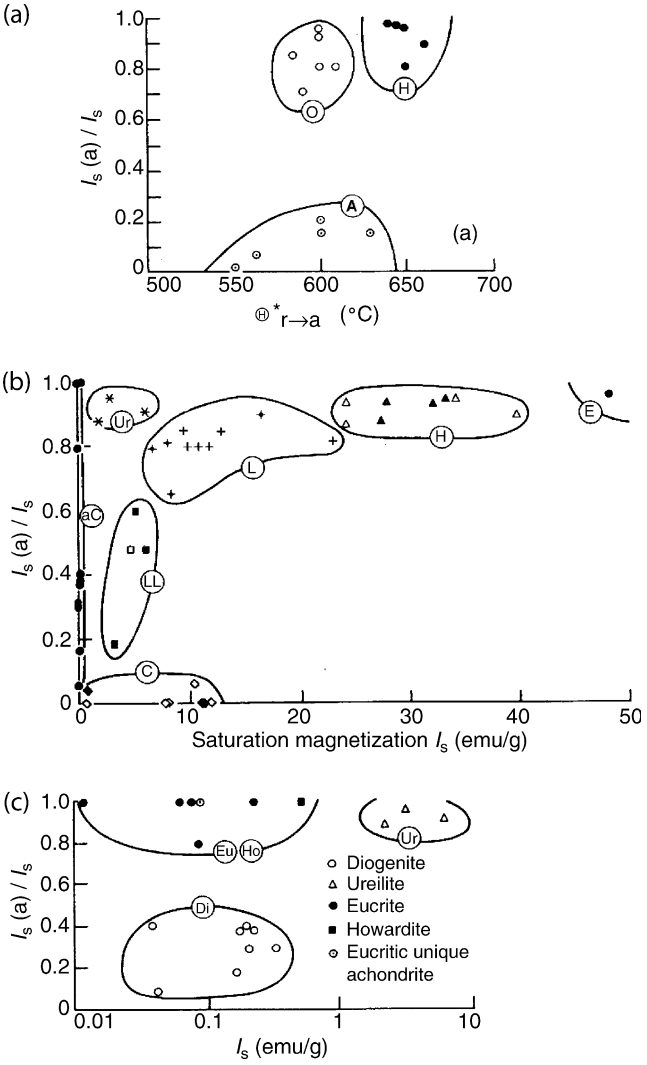

Figure P35 Magnetic classification of meteorites (a) the ratio of the saturation magnetization of the alpha phase to the total saturation magnetization plotted against the temperature of the gamma to alpha transition defines the various group of the irons H—hexahedrites, O—octahedrites, and A—ataxites. (b) the same ratio plotted against saturation magnetization defines the various groups of chondrites and (c) also separates the various groups of achondrites (Strangway *et al.*, 1970; Nagata *et al.*, 1972; Cisowski, 1987).

(e.g., 1988). Tetrataenite is remarkable for its extreme anisotropy and coercivity that can reach as much as 100 mT. The carbonaceous chondrites have multiple magnetic phases that are not yet completely understood.

Achondrites are the products of igneous differentiation and have in general much less metallic content than the chondrites. As Cisowski (1987) notes, they are somewhat analogous to lunar samples with eucrites and diogenites being similar to monomict lunar breccias. They too are conveniently divided in the same parameters as those used for the chondrites (Figure P35c).

The SNCs (Shergotites, Nahklites, and Chassignites) are a special group of meteorites from an evolved body with relatively recent volcanic activity that has been shown to be Mars. They contain magnetite, titanomagnetites, and pyrrhotite and have been discussed above in the section on Mars.

A lunar origin has been demonstrated for certain meteorites. These have the characteristic mixes of metallic Fe and Fe-Ni found in lunar samples.

Paleomagnetic record of meteorites

The prime interest in meteorite paleomagnetic studies is in the intensity of the fields in which the NRM was acquired and the possibility of gaining insight to early solar system magnetic fields, or in the martian and lunar meteorites to the history of the magnetic field of Mars and the Moon. Meteorites may be exposed to shock effects in their assembly or in their subsequent history, to radiation, and to temperature changes in space, and finally to heating as they come through the atmosphere. All these factors can have an effect on their paleomagnetic record, but they do not eliminate the possibility of some primary magnetization acquired at the time of their formation.

Iron meteorites can carry stable NRM, but the microstructure of the kamacite taenite intergrowths has been shown to control the direction of TRM, while the intensity of the TRM was not found to depend upon the field in which it was acquired (Brecher and Albright, 1977). For these reasons the paleomagnetic record of the irons has not been pursued strongly.

The paleomagnetic record of the chondrites and achondrites has been energetically investigated. Unfortunately, many of the meteorites collected in earlier times were contaminated by magnets used to recognize them as meteorites. Recently, and particularly with the Antarctic collections, care has been taken to maintain the meteorites in as pristine a condition as possible. In earlier work, plots of NRM versus IRMs were used to aid in the detection of contamination and in the interpretation of the origin of the NRM (Sugiura and Strangway, 1988). Wasilewski and Dickinson (2000) have recently suggested using the ratio of NRM:IRMs (or REM as they call it) as a preliminary indication of contamination, with values greater than 0.1 being indicative of exposure to a strong magnet.

The carbonaceous chondrites are some of the most intensely investigated of all meteorites with studies of individual CAIs, chondrules, and of bulk samples. The individual refractory inclusions and other chondrules are of particular interest because they may contain a record of solar system magnetic fields extant prior to the assembly of the meteorite. A necessary test for this is the demonstration that their magnetization was acquired before aggregation of the parent meteorites randomly oriented in the sample. This is an application of the classical conglomerate test of paleomagnetism, in which the clasts within a conglomerate are shown to be magnetized randomly within the conglomerate, whereas the matrix is coherently magnetized. Thus their magnetization may have been acquired prior to assembly into the conglomerate because they do not exhibit the coherent magnetization that might have been acquired during, or since the conglomerate was assembled. Unfortunately, this very direct test has been confounded by the random nature of the magnetization of the matrix and its virtual absence as a significant carrier of homogeneous NRM in some chondrites.

Paleomagnetic analyses of CAIs in Allende have been reported (Smethurst and Herrero-Bervera, 2002) and gave consistent values of 5.2–5.4 μT by the Shaw method (Shaw, 1974) for the intensity of the field they record. Results from Allende chondrules are inconsistent: values range from hundreds of millitesla (Lanoix *et al.*, 1978) to 70 and 130 mT (Nagata and Sugiura, 1977). Moreover, Nagata and Sugiura (1977) obtained similar results from the matrix and from bulk samples as they had from chondrules in double heating experiments from 20 to 300 °C. This of course strongly suggests that the magnetization was a low-temperature overprint. Such information may be of interest as a means of estimating the temperature to which the meteorite was heated at the time of acquisition of the low-temperature overprint. In ALH 76009, 13 chondrules were found to have random orientation despite the matrix samples showing an overprint (Nagata and Funaki, 1981). Stepwise thermal demagnetization suggested

that the chondrules may have acquired their magnetization in a steady field within which they were rotating slowly.

The interpretation of the magnetization of carbonaceous chondrites, as opposed to the inclusions that they contain, is complicated by the discovery that the paleomagnetic record of the matrix is randomly oriented within some of these meteorites (e.g., Brecher, Stein, and Fuhrman, 1977). The magnetization of some carbonaceous chondrites such as Coolidge, Murray, and Yamato fall off slowly with AF demagnetization and exhibit directional stability. Investigations of multiple oriented samples from these meteorites to check for random magnetization would be of great interest. The presence of tetrataenite is suggested by extreme stability against AF demagnetization. Other carbonaceous chondrites show quite different behavior with NRM that falls off rapidly with the NRM decreasing by as much as an order of magnitude with AF to 10 mT. e.g., Tysnhes Island and Bushof (Gus'kova, 1963). Results are also available for samples that have been cycled through the low-temperature transition of magnetite at ~120 K (Brecher and Arrhenius, 1974). Classical double heating intensity determinations have been carried out for Orgueil, Murchison, Leoville, with multiple determinations for Allende. The results fall in the range of tens and hundreds of microtesla. However, the bulk of the magnetization is blocked below 200°C and one must question how well such magnetization is likely to reflect fields more than 4 Ga old.

The magnetization of ordinary chondrites suffers from the same problem of the heterogeneity of the magnetization that is encountered with the carbonaceous chondrites. The phenomenon was investigated systematically by Morden and Collinson (1992). They demonstrated that the magnetism of subsamples of 8LL chondrites and 3L chondrites was randomly oriented down to the scale of millimeters, which was the smallest for which they could be confident of maintaining accurate orientation of subsamples (Figure P36). They also discovered a magnetic fabric, which they considered to be a primary structure formed during the final lithification of the various chondrites. The random paleomagnetic result was therefore interpreted as primary. However, this interpretation is not consistent with the strong metamorphic heating of some of these meteorites, unless magnetization took place before final aggregation. Subsamples of Bjurbole including were also found to be randomly magnetized (Wasilewski *et al*., 2002). This once again raises a general question of how homogeneous the magnetization of chondrite is and hence what size of sample can be regarded as giving an indication of any possible primary magnetization. Nevertheless numerous dual heating intensity determinations on bulk samples have been carried out. They have yielded values a little lower than the carbonaceous chondrites with values falling between a few μT and nearly 200 μT. The blocking temperatures are rather higher than in the carbonaceous chondrites with the pTRM acquired and the NRM demagnetized linearly related up to steps near to 400°C.

The interpretation of the magnetization of achondrites is in principle simpler than that of chondrites because achondrites originated by crystallization from a magma, or in the case of primitive achondrites, as the residues of partial melting. Therefore they are formed above the Curie points of any magnetic minerals they contain and should have acquired a primary NRM of thermal origin on the evolved body in which they were formed. However, unfortunately only very few achondrites appear to be unbrecciated igneous rocks. Rather achondrites mostly compare with the lunar suite of breccias with igneous clasts, whereas just a few may be true igneous rocks. The crystallization ages of the howardite, eucrite, diogenite clan (HED) are between 4.40 and 4.55 Ga

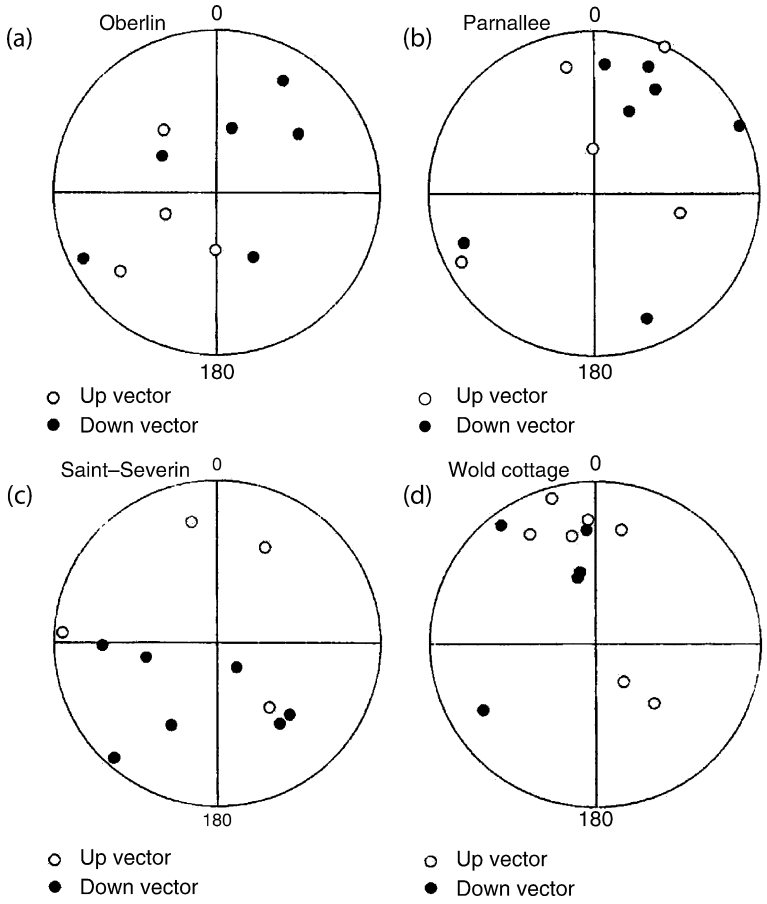

Figure P36 Demonstration of randomly directed remanent magnetization in ordinary chondrites (Morden and Collinson, 1992).

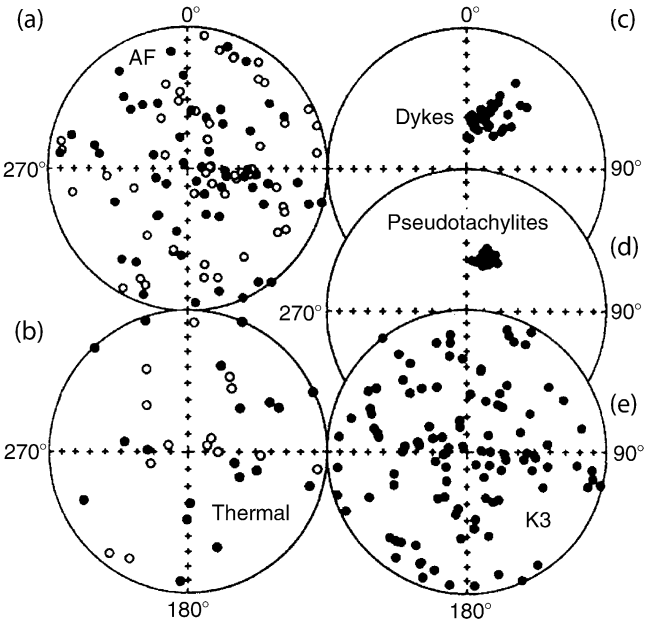

Figure P37 Magnetization of Vredefort impact crater samples. Strong random magnetization of shocked basement after (a) AF demagnetization, and (b) thermal demagnetization. (c) and (d) TRM like magnetization in dykes and melt rock recording earth's field, (e) orientation of minimum susceptibility axes (Carporzen *et al.*, 2005).

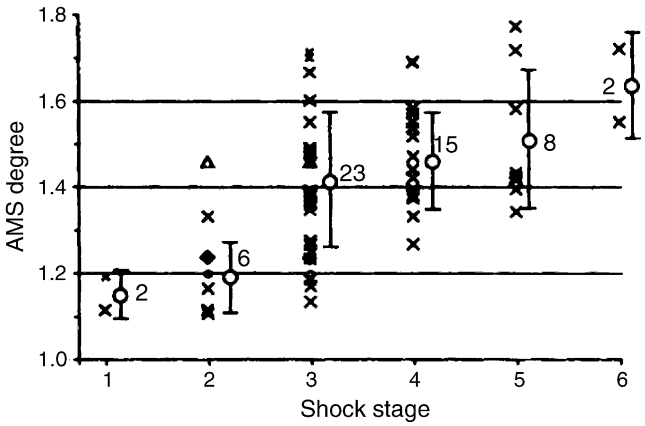

Figure P38 The relation between fabric and shock demonstrated by the correlation of magnetic anisotropy with shock level (Gattaccea *et al.*, 2005).

and thus appear to have come from a parent body that had a brief and active history. The shergottites, nahklites, and chassignites (SNC) meteorites, although achondrites were discussed above because of their demonstrated martian origin.

Not a lot of paleomagnetism has been done on the achondrites other than the SNC meteorites. Some exhibit directionally stable NRM that is resistant to AF demagnetization and to some degree against thermal demagnetization. Some have ratios of NRM:IRMs so high that according to the criterion suggested by Wasilewski *et al*. (2002) contamination must be suspected. One dual heating intensity determination has been done on an Antarctic achondrite (Yamato 7038) and yielded a field intensity of less than 10 μT.

Recent work has produced important results, which bear on the studies of randomly directed remanent magnetization in meteorites and on the role of shock in many meteorites. The first result comes from a study of the Vredefort meteorite impact crater by Carporzen *et al*. (2005). Rocks such as the dykes and pseudotachylites carrying TRM are acquired during cooling after the impact was magnetized coherently with small scatter between samples (Figure P37c,d). In contrast, shocked granitoid basement rocks are magnetized randomly (Figure P37a, b). These shocked rocks also have anomalously high intensities of magnetization. This magnetization of the shocked rocks is interpreted to have been acquired in the intense fields of the plasmas generated by the shock event. The anisotropy of these samples was also determined and the minimum susceptibility axes found to be randomly oriented. In individual samples the anisotropy was related to the remanence direction, indicating that both were caused by the shock events. In other related work, it has been demonstrated that the foliation of chondrites does indeed have an impact origin. Gattacecca *et al*. (2005) showed that the magnitude of the susceptibility anisotropy is correlated with shock level (Figure P38). These two results call in to doubt again the use of randomly directed magnetization as an indication of magnetization acquired prior to meteorite assembly, demonstrate that foliation can be shock generated, and make the interpretation of paleointensities obtained from meteorites more problematical.

Discussion

The paleomagnetic record of meteorites is probably the most difficult of all paleomagnetic records to interpret. In particular, the record in CAIs and chondrules is difficult because they are later incorporated in chondrites and so one must separate the history prior to accretion from postaccretion history in the meteorite. Nevertheless there are standard techniques for doing this and progress is being made, despite the difficulties discussed above. In some cases, CAIs and chondrules may carry a record of the fields experienced prior to accretion, but much of the magnetization is probably a postaccretional low-temperature overprint. The magnetization of carbonaceous chondrites and ordinary chondrites may well have been acquired on the surface of the parent body and yielded, respectively, fields of hundreds and tens of microtesla. The NRM of achondrites and primitive achondrites may have been acquired at different depths on an evolved parent body. Only a single double heating experiment was available that yielded a value in the single microtesla range.

The interpretation of these results in terms of early solar system fields is not easy. The fields in which CAIs and chondrules were formed must have been very early solar system fields and Strangway *et al*. (1988) suggested that these may have been strong fields associated with T-Tauri winds. However, as we have seen that care needs to be taken in while interpreting these field estimates. The fields recorded by carbonaceous and ordinary chondrites are presumably due to surface processes on the parent bodies and modern studies are increasingly recognizing the difficulty of interpreting these results (Gattacceca *et al*., 2003). Achondrites and primitive achondrites may yield values for different depths in short-lived parent bodies in the form of planets or planetesimals, that might had active dynamos. The question of parent bodies of meteorites a major research area discussed in McSween (1999). For the present purposes, we simply note that S-type asteroids have similar spectra, but not identical to ordinary chondrites, whereas C-type asteroids have features in their spectra characteristic of hydrated minerals typical of the aqueous alteration exhibited by carbonaceous chondrites. It is therefore interesting that S-type asteroid Gaspra appears to have an intensity of magnetization comparable with chondrites, but puzzling that Eros, which is also an S-type asteroid, has a very low magnetization.

Conclusion

A remarkable extraterrestrial paleomagnetic record has been found to be associated with the Moon, Mars, the asteroids, and the meteorites. Observations from spacecraft provide evidence that suggests that just as the Earth and Mercury have dynamos generating magnetic fields at the present, the Moon and Mars may have had similar dynamos in the past

that generated comparable fields. They also suggest that there were magnetic fields in the solar system at the time of origin of chondrites and achondrites, but the records of the chondrules in carbonaceous chondrites and of the primitive CAIs remain hard to interpret in these observations.

Michael D. Fuller

Bibliography

Acuña, M.H., Anderson, B.J., Russell, C.T., Wasilewski, P., Kletetschka, G., Zanetti, L., and Omidi, N., 2002. NEAR Magnetic field observations at eros: first measurements from the surface of an asteroid. *Icarus*, **155**: 220–228.

Acuña, M.H., Connerney, J.E.P., Ness, N.F., Lin, R.P., Mitchell, D., Carlson, C.W., McFadden, J., Anderson, K.A., Reme, H., Mazelle, C., Vignes, D., Wasilewski, P., and Cloutier, P., 1999. Global distribution of crustal Mars Global Surveyor MAG/ER experiment. *Science*, **284**: 790–793.

Arkani-Hamed, J., 2001a. A 50-degree spherical harmonic model of the magnetic field of Mars. *Journal of Geophysical Research*, **106**: 23197–23208.

Arkani-Hamed, J., 2001b. Paleomagnetic pole positions and pole reversals of Mars. *Geophysical Research Letters*, **28**: 3409–3412.

Arkani-Hamed, J., 2002. Magnetization of the martian crust, JGR,107E5, 10, 1029/2001JE001496.

Barber, D.J., and Scott, E.R.D., 2003. Transmission electron microscopy of minerals in the martian meteorite Allan Hills 84001. *Meteoritics and Planetary Science*, **38**(6): 831–848.

Baumgartel, K., Sauer, K., and Bogdanov, A., 1994. A magnetohydrodynamic model of solar wind interaction with asteroid Gaspra. *Science*, **263**: 653–655.

Brecher, A., and Arrhenius, G., 1974. The paleomagnetic record of carbonaceous chondrites: natural remanence and magnetic properties. *Journal of Geophysical Research*, **79**: 2081–2106.

Brecher, A., Stein, J., and Fuhrman, M., 1977. The magnetic effects of brecciation and shock in meteorites. *The Moon*, **17**: 205–216.

Cain, J.C., Ferguson, B.B., and Mozzoni, D., 2003. An $n = 90$ internal potential function of the Martian crustal field, *Journal of Geophysical Research*, **108E2**: 5008, doi 10, 1029/2000JEE001487, 2003.

Carporzen, L., Gilder, S.A., and Hart, R.J., 2005. Paleomagnetism of the Vredefort meteorite crater and implications f or craters on Mars. *Nature*, **435**: 198–201.

Cisowski, S.M., 1987. Magnetism of meteorites. In Jacobs, J.A. (ed.) *Geomagnetism*, **2**: 525–560.

Cisowski, S.M., and Fuller, M., 1986. Lunar paleointensities via the IRM(s) normalization method and the early magnetic history of the moon. In Hartmann, W.K., Phillips, R.J., and Taylor, G.J. (eds.), *The Origin of the Moon.* Houston: Lunar and Planetary Science Institute, pp. 411–424.

Cisowski, S.M., Fuller, M., Rose, M., and Wasilewski, P.J., 1973. Magnetic effects of experimental shocking of lunar soil. *Proceedings of The Fourth Lunar Science Conference*, 3003–3017.

Cisowski, S.M., Fuller, M., Rose, M.F., and Wasilewski, P.J., 1976. Magnetic effects of shock and their implications for magnetism of lunar samples. *Proceedings of the Sixth Lunar Science Conference*, 3123–3141.

Cisowski, S.M., Collinson, D.W., Runcorn, S.K., Stephenson, A., and Fuller, M.,1986. A review of lunar paleointensity data and implications for the origin of lunar magnetism, *Proceedings of the Thirteenth Lunar and Planetary Science Conference*. *Journal of Geophysical Research*, **88**: A691–A704.

Collinson, D.W., 1997. Magnetic properties of Martian meteorites: Implications for an ancient Martian magnetic field. *Meteoritics and Planetary Science*, **32**: 803–811.

Connerney, J.E.P., Acuña, M.H., Wasilewski, P.J., Kletetschka, G., Ness, N.F., Reme, H., Lin, R.P., and Mitchell, D.L., 2001. The global magnetic field of Mars and implications for crustal evolution. *Geophysical Research Letters*, **28**: 4015–4018.

Dunlop, D.J., and Ozdemir, O., 1997. *Rock Magnetism.* Cambridge: Cambridge University Press.

Dunlop, D.J., and Kletetschka, G., 2001. Multi-domain hematite: A source of planetary magnetic anomalies? *Geophysical Research Letters*, **28**: 3345–3348.

Dyall, P., and Parkin 1971. The magnetism of the Moon. *Scientific American*, **225**: 62–73.

Fairén, A.G., Ruiz, J., and Anguita, F., 2002. An origin for the linear magnetic anomalies on Mars through accretion of terranes; Implications for dynamo timing. *Icarus*, **160**: 220–223.

Frey, H.V., 2003. Large diameter visible and buried impact basin on Mars: Implications for the age of the highlands and (buried) lowlands and turnoff of the global magnetic field, Abstract, *Lunar and Planetary Sciences*, XXXIV, 1838pdf.

Fuller, M., Rose, F., and Wasilewski, P.J., 1973. Preliminary results of an experimental study on the magnetic effects of shocking lunar soil. *Proceedings of the Fourth Lunar Science Conference*, pp 58–61.

Fuller, M., 1974. Lunar magnetism. *Reviews of Geophysics*, **12**: 23–70.

Fuller, M., 1987. Lunar paleomagnetism. In Jacobs, J.A. (ed.), *Geomagnetism*, **2**: 307–456.

Fuller, M., 1998. Lunar magnetism—a retrospective view of the Apollo sample magnetic studies. *Physics, Chemistry and Earth Sciences*, **23**(78): 725–735.

Gattacceca, J., Rochette, P., and Bourot-Denise, M., 2003. Magnetic properties of a freshly fallen LL ordinary chondrite: the Bensour meteorite. *Physics of the Earth and Planetary Interiors*, **140**: 345–358.

Gattacceca, J., Rochette, P., Denise, M., Cosolmagno, G., and Folco, L., 2005. An impact origin for the foliation of chondrites. *Earth and Planetary Science Letters*, **234**: 351–368.

Gus'kova, Y.G., 1963. Investigation of natural remanent magnetization of stoney meteorites. *Journal of Geomagnetism and Aeronomy*, **3**: 308–313.

Hale, C.J., Fuller, M., and Bailey, R.C., 1978. On the application of microwave heating to lunar paleointensity determination. *Proceedings of the Ninth Lunar Science Conference*, 3165–3179.

Halekas, J.S., 2003. The origins of Lunar Crustal Magnetic Fields, PhD Thesis, Berkeley: University of California.

Halekas, J.S., Lin. R.P., and Mitchell, D.L., 2003. Magnetic effects of impacts on the moon (2003), ABS, *Eos, Transcations, American Geophysical Union* **84**(46): GP22A-04.

Harrison, C.G.A., 2000. Questions about magnetic lineations in the ancient crust of Mars. *Science*, **287**: 547a.

Harrison, K.P., and Grimm, R.E., 2002. Controls on Martian hydrothermal systems: Application to valley network and magnetic anomaly formation. *Journal of Geophysical Research*, **107**(E5) 10.1029/2001JE001616.

Hammer, J.E., Brachfield, S., and Rutherford, M.J., 2003. An igneous origin for martian magnetic anomalies?, Abstract, *Lunar Planetary Science*, XXXIV #1918, CD-ROM.

Hargraves, R.B., Collinson, D.W., Arvidsen, R.E., and Spitzer, C.R., 1977. Viking magnetic properties experiment: primary mission results. *Journal of Geophysical Research*, **82**: 4547–4558.

Hargraves, R.B., Collinson, D.W., Arvidsen, R.E., 1979. Viking magnetic properties experiment: extended mission results. *Journal of Geophysical Research*, **84**: 8379–8384.

Hargraves, R.B., Knudsen, J.M., Bertelsen, P., Goetz, W., Gunnlaugsson, H.P., Hviid, S.F., Madsen, M.B., and Olsen, M., 2000. Magnetic enhancement on the surface of Mars. *Journal of Geophysical Research*, **105**(E1): 1819–1827.

Hood, L., and Huang, Z., 1991. Formation of anomalies antipodal to lunar impact basins: Two dimensional model calculations, *Journal of Geophysical Research*, **96**: 9837–9846.

Hood, L.L., Richmond, N.C., Pierazzo, E., Rochette, P., 2003. Distribution of crustal magnetic fields on Mars: Shock effects of basin-forming impacts. *Geophysical Research Letters*, **30**(6): 1281, doi:10.1029/2002GL016657.

Houseley, R.M., Grant, R.W., and Patton, N.E., 1973. Origin and characteristics of Fe metal in lunar glass welded aggregates. *Geochimica et Cosmochimica Acta*, **35**, Supplement(4): 2737–2749.

Kirschvink, J.L., Maine, A.T., and Vali, H., 1997. Paleomagnetic evidence of a low temperature origin of carbonate in the Martian meteorite ALH84001. *Science*, **275**: 1629–1638.

Kivelsen, M., Bargatgze, L.F., Khurana, K.K., Southwood, D.J., Walker, R.J., and Coleman, P.J., 1993. Magnetic field signatures near Galileo's closest approach to Gaspra. *Science*, **271**: 331–334.

Kletetschka, G., Wasilewski, P.J., and Taylor, P.T., 2000a. Hematite vs. magnetite as the signature for planetary magnetic anomalies? *Physics of the Earth and Planetary Interiors*, **119**: 259–267.

Kletetschka, G., Wasilewski, P.J., and Taylor, P.T., 2000b. Mineralogy of the sources for magnetic anomalies on Mars. *Meteoritics and Planetary Science*, **35**: 895–899.

Kletetschka, G., Wasilewski, P.J., and Taylor, P.T., 2002. The role of hematite-ilmenite solid solution in the production of magnetic anomalies in ground- and satellite-based data. *Tectonophysics*, **347**: 167–177.

Lanoix, M., Strangway, D.W., and Pearce, G.W., 1978. The primordial magnetic field preserved in chondrules of the Allende meteorite. *Geophysical Research Letters*, **5**: 73–76.

Lin, R.P., Anderson, K.A., and Hood, L.L., 1988. Lunar surface magnetic field concentrations antipodal to young large impact basins. *Icarus*, **74**: 529–541.

Lucey, P.G., Taylor, G.J., and Malareet, E., 1995. Abundance and distribution of iron on the moon. *Science*, **268**: 1150–1153.

McSween, H.Y., 2000. *Meteorites and their Parent Planets.* Cambridge: Cambridge University Press.

Mitchell, D.L., Lillis, R., Lin. R.P., Connerney, J., and Acuna, M., 2003. Evidence for Demagnetization of the Utopia Impacet Basin on Mars, *Eos, Transactions, American Geophysical Union*, **84**, 46, ABS., GP22A-08.

Morden, S.J., and Collinson, D.W., 1992. The implications of the magnetism of ordinary chondrite meteorites. *Earth and the Planetary Science Letters*, **109**(1–2): 185–204.

Nagata, T., Fisher, R.M., and Schwerer, F.C., 1972. Lunar rock magnetism. *The Moon*, **4**: 160–186.

Nagata, T., and Funaki, M., 1981. The comparison of natural remanent magnetization of an Antarctic chondrite ALH 76009 L6. *Proceedings of the Lunar Planetary Science Conference*, **12B**: 1229–1241.

Nagata, T., and Sugiura, N., 1977. Paleomagnetic field intensity derived from meteorite magnetization. *Physics of the Earth and Planetary Interiors*, **13**: 373–379.

Özdemir, O., 2000. Chemical remanent magnetization-possible source for the magnetization of Martian crust (abstract), American Geophysical Union Spring Meeting GP31A-05.

Özdemir, O., and Dunlop, D.J., 2002. Thermoremanence and stable memory of single-domain hematites. *Geophysical Research Letters*, **29**, No. 18 10.1029/2002GL015597.

Pearce, G.W., Williams, R.J., and McKay, D.S., 1972. The magnetic properties and morphology of metallic iron produced by sub-solidus reduction of synthetic Apollo 11 composition glasses. *Earth and Planetary Science Letters*, **17**: 95–104.

Richter, L., Brinza, D.E., Cassel, M., Glassmeir, K.-H., Kunhke, F., Musman, G., Ohtmer, C., Schwingenschu, and Tsurutani, 2001. First direct field measurements of an asteroidal magnetic field: DSI at Braille. *Geophysical Research Letters*, **28**(10): 1913–1916.

Robinson, P., Harrison, R.J., McEnroe, S.A., and Hargraves, R.B., 2000. Lamellar magnetism in the hematite-ilmenite series as an explanation for strong remanent magnetization. *Nature*, **418**: 517–520.

Rochette, P., Lorand, G., Fillion, G., and Sautter, V., 2001. Pyrrhotite and the remanent magnetization of SNC meteorites: a changing perspective on martian magnetism. *Earth and Planetary Science Letters*, **190**: 1–12.

Runcorn, S.K.R., 1975. An ancient lunar magnetic dipole field. *Nature*, **253**: 701–703.

Russell, C.T., Weiss, H., Colema, P.J., Soderblom. L.A., Stuart-Alexander, D.E., and Wilhelms, D.E., 1975. Geologic-magnetic correlations on the Moon: sub-satellite results, *Proceeedings of the eight Lunar Conference*. *Geochimica et Cosmochimica Acta*, **41**, Supplement 8: 1171–1185.

Scott, E., and Fuller, M., 2004. A possible source for the martian crustal magnetic field, EPSL., 220, 83–90.

Shaw, J., 1974. Anew method of determining the magnitude of the paleomagnetic field. *Geophysical Journal of the Royal Astronomical Society*, **15**: 205–211.

Shaw, J., Hill, M.J., and Openshaw, S.J., 2001. Investigating the martian magnetic field using microwaves. *Earth and Planetary Science Letters*, **190**: 103–109.

Smethurst, M. T., and Herrero-Bervera, E., 2002. Paleomagnetic analysis of Calcium-Aluminium Inckusions (CAI's) from the Allende meteorite EOS Trans. AGu, 83(47) Fall meet. Suppl., Abstract GP72A-0989.

Srnka, L.J., Martelli, G., Newton, G., Cisowski, S.M., Fuller, M., and Schaal, R.B., 1979. Magnetic field and shock effects and remanent magnetization in a hypervelocity impact experiment. *Earth and Planetary Science Letters*, **42**: 127–137.

Solomon, S. C., Aharonson, O., Banerdt, W. B., Dombard, A. J., Frey, H. V., Golombek, M. P., Hauck, III, S. A., Head, III, J. W., Johnson, C. L., McGovern, P. J. Phillips, R. J., Smith, D. E., and Zuber, M. T., 2003. Why are there so few magnetic anomalies in Martian Lowlands and Basins?, Abstract, *Lunar Planetary Science*, XXXIV #1382, CD-ROM.

Stacey, F.D., Lovering, J.F., and Parry L.G., 1961. Thermomagnetic properties natural magnetic moments and magnetic anisotropies of some chondritic meteorites. *Journal of Geophysical Research*, **66**: 1523–1534.

Stegman, D.R., Jellinek, A.M., Zatman, S.A., Baumgardnerk, J.R., and Richards, M.A., 2003. An early lunar Core dynamo driven by thermochemical mantle evolution. *Nature*, **451**: 146.

Stevenson, D.J., 2001. Mars' core and magnetism. *Nature*, **412**: 214–219.

Strangway, D.W., Larson, E.E., and Perce, G.W., 1970. Magnetic studies of Lunar samples, breccias and fines, *Proceedings of the Apollo 11, Lunar Science Conference. Geochimica et Cosmochimica Acta*, Supplement **1**: 2435–2451.

Strangway, D.W., Pearce, G.W., Gose, W.A., and McConnell, R.K., 1973. Lunar magnetic anomalies and the Cayley Formation. *Nature*, **246**: 112–114.

Thomas-Keprta, K.L., Bazylinski, D.A., Kirschvink, J.L., Clement, S.J., McKay, D.S., Wentworth, S.J., Vali, H., Gibson, Jr. E. K., and Romanek, C.S., 2000. Elongated prismatic magnetite crystals in ALH84001 carbonate globules: Potential Martian magnetofossils. *Geochimica et Cosmochimica Acta*, **64**: 4049–4081.

Wasilewski, P.J., 1988. Magnetic characterization of the new mineral tetrataenite and its contrast with isochemical taenite. *Physics of the Earth and Planetary Interiors*, **52**(1–2): 150–158.

Wasilewski, P.J., and Fuller, M., 1975. Magnetochemistry of the Apollo landing sites. *The Moon*, **14**: 79–101.

Wasilewski, P.J., Acuna, M.H., and Kletetschka, G., 2002. 433 Eros, problems with the meteorite magnetism record in attempting an asteroid match. *Meteoritics and Planetary Science*, **37**: 937–950.

Weiss, B.P., Kirschvink, J.L., Baudenbacher, F.J., Vali, H., Peters, N.T., Macdonald, F.A., and Wikswo, J.P., 2000. A low temperature transfer of ALH84001 from Mars to Earth. *Science*, **290**: 791–795.

PALEOMAGNETISM, OROGENIC BELTS

Orogenic belts are the key signature of Plate Tectonics at the sites of plate convergence. At these margins the consumption of ancient ocean basins culminates in the collision of blocks of continental crust and this is responsible for deforming broad tracts of crust on either side of the site of collision (*suture*). The deformed rocks are mostly marine

sediments and the products of the preceding phases of ocean development. After collision they are squeezed into increasingly tight folds that may ultimately become overfolded and develop shear planes along which wedges of crust are transported horizontally for large distances as *nappes*. Slices of young, light, and buoyant ocean crust may also become incorporated in this process and emplaced (*obducted*) into the deformed crust as *ophiolites* instead of being subducted back into the mantle.

Orogenic deformation is concentrated mainly within the rock wedges accreted to the peripheries of the continents during the preceding phase of ocean growth, which deform in a semiplastic way. The ancient, relatively cold metamorphic and igneous basements to the continental crust act as the rigid indenters and the inherited shapes of these blocks of old hard crust ultimately control the shape of the orogenic belt. Further from the site of the suture, the sedimentary covers on the continents may be deformed by collision into open folds with amplitudes and wavelengths declining away from the collisional zone. This cover is typically folded independently of the underlying basement by slipping along detachment zones (*decollements*). Such detachments are also developed within the orogenic belt where rocks deform by contrasting mechanisms controlled by their ductility and bedding. This deformation is constrained between the limiting *parallel* case where the folding layers in the rock section preserve their thickness but not their shape, and the *similar* case where they preserve their shape but not their thickness.

The compressional phases of orogenic deformation lead in turn, to crustal thickening, isostatic rebound and uplift. The thickened wedge of deformed rocks becomes topographically unstable and flows outwards as a viscous medium on a geological timescale in a secondary phase of plate collision known as *orogenic collapse.* Compressional deformation then gives away to extensional deformation that may be regarded as a later phase of a single Plate Tectonic cycle. The development of the Basin and Range Province in western North America during Tertiary times for example, followed compression and crustal thickening during the Laramide Orogeny in Late Cretaceous times. Extensional deformation in the continental crust can occur by two mechanisms. Pure shear attenuates a viscous crust (McKenzie 1978) leading to a change in shape with little or no rotation. In contrast, deformation by *simple shear* develops a low-angle detachment zone through the crust (Wernicke *et al*., 1987). As this crust attenuates, the changing thickness balance of crust to mantle lithosphere causes partial uplift of the basement and rotation of blocks above the detachment about horizontal axes; the upper zone (*hanging wall*) may dissect into fault blocks that rotate about horizontal axes in a domino fashion and, if the detachment extends right through the crustal section, both upper and lower (*footwall*) sections may rotate with respect to each other.

Following continental collision, the rate of convergence of the two converging continents decelerates but relative movements may not cease altogether. One continental margin may then drive under, and uplift, the orogenic belt as in the case of India beneath Tibet. If the indenter has an irregular shape, or there is ocean basin to one side, blocks of the orogen defined by major vertical faults are extruded laterally by *tectonic escape.* This latter phenomenon also occurs when the subduction of ocean crust is oblique to the orogenic margin. It is responsible for the tectonics of the Cordilleran margin of western North America where terranes are slipping differentially northwards along the continental margin until they become locked into a dumping ground in Alaska. In the orthogonal continent-continent collision of the Alpine-Himalayan Belt the tectonic escape defines the last phase of the orogenic cycle.

The ability of rocks to record the direction of the ancient magnetic field provides the key quantitative information for unraveling tectonic deformation in orogenic belts. Geological indicators such as bedding directions, stratigraphic variations and dyke intersections can be used only rarely to provide data of comparable significance, and they are unconstrained to a paleogeographic orientation. The orogenic environment, however, causes specific problems to the analysis of the magnetism in rocks due to the effects of strong deformation and temperature increase. Rocks in this environment are more likely to have their primary magnetism partially or completely overprinted by magnetizations linked to the deformation. Partially set against this disadvantage, the deformed nature of the rocks means that the paleomagnetic fold test is more readily applied to constrain the geological ages of the magnetizations than would be possible in less deformed settings. The study of rock-units may include fault flakes up to a few kilometers in size rotating within fault zones, thrust sheets in interior zones of strong deformation and blocks of crust on a 10–100 km scale bounded by major near vertical faults called *terranes*; only if the terrane extends to the base of the continental lithosphere can it properly be referred to as a *microplate*.

Paleomagnetic analysis assumes that the mean direction of magnetization recovered from the rock-unit is a record of the time averaged dipole field source at the time of magnetization. The cumulative deformation can then be resolved by comparing this direction with the predicted direction at the study location at the time of magnetization. These predicted directions are usually calculated from the *apparent polar wander paths* (*APWPs*) of the adjoining continental indenter. In the case of the Alpine-Himalayan orogenic belt for example, they would be calculated from APWPs of continental Africa, Arabia, India, or Eurasia. Usually the difference is the resultant of more than one episode of deformation and in favorable circumstances it can be decomposed using geological evidence or from studying the paleomagnetism of rocks of different ages.

The angular deformation is usually considered in terms of differences of declination and inclination with respect to the reference direction from the stable plate. The difference between the observed and expected directions is described in terms of rotation and flattening. A difference in declination implies rotation (R) of a crustal block about a quasivertical axis and is usually calculated by the method of Beck (1980). Both observed and reference directions have confidence limits (ΔD and ΔD_{ref}, respectively) and Beck (1980) proposed a confidence limit on R' defined by $\Delta R' = \sqrt{\left(\Delta D^2 + \Delta D_{\text{ref}}^2\right)}$. From a statistical analysis of this proposed confidence limit, Demarest (1983) concluded that this value overestimates errors and showed that, provided α_{95} is small and preferably less than 10°, a standard correction factor is applicable. For a direction derived from $n \geq 6$ or more samples, the correction factor lies between 0.78 and 0.80. Then $\Delta R'$ is derived from the equation $\Delta R' = 0.8\sqrt{(\Delta D^2 + \Delta D_{\text{ref}}^2)}$ and only, if $R' > \Delta R'$ can tectonic rotation be regarded as significant.

A difference in inclination(I), or flattening(F), is also subject to error limits (ΔI and ΔI_{ref}, respectively). Following Demarest (1983) it is given by $\Delta F = 0.8\sqrt{\left(\Delta I^2 + \Delta I_{\text{ref}}^2\right)}$ but provided that $F > \Delta F$ the flattening may be regarded as significant. F has two possible explanations. Firstly, it could result from rotation of crustal blocks about near horizontal axes. This contribution can usually be isolated if references to the paleohorizontal, such as sedimentary bedding, are present. Secondly, the continental block could have moved through latitude since the time of magnetization. This latter interpretation of F has proved more contentious than the interpretation of R, in part because there is often structural or paleogeographic evidence with which the paleomagnetic analysis can be tested independently. It has been found that inclination differences within the Alpine-Himalayan Belt are often too large to be attributed to continental movement through latitude alone. The anomalies are more important in sedimentary rocks and imply that inclination shallowing during compaction and lithification is a factor here (Bazhenov and Mikolaichuk, 2002). However, Tertiary inclinations from igneous rocks also appear to be too shallow to be accommodated solely by latitudinal movement (Beck *et al*., 2001). The difference is probably to be explained in terms of small departures from the geocentric axial dipole assumption and a full explanation for this anomaly currently limits the usefulness of flattening in tectonic analysis.

The values of F and R need to be interpreted in terms of the scale of the crustal blocks undergoing deformation and temporal setting of the deformation within the orogenic cycle. Two examples from the

Anatolian sector of the Alpine-Himalayan orogenic belt illustrate contrasts in scale (see Figures P39, P40). Figure P39 shows an example of rotation across an intracontinental transform, the North Anatolian Fault Zone, separating the Eurasian and Anatolian plates. The crust on either side of this fault zone shows comparable regional anticlockwise rotation. This occurred before the initiation of the transform plate boundary in Late Pliocene times. Within the transform fault zone, small fault blocks <10 km in size are being rotated clockwise in ball bearing fashion between master faults at rates of the order of 1° per 10 ka. Figure P40 shows a large-scale example of deformation in which blocks on a scale of ~50–200 km are being rotated as Anatolian crust is being extruded outwards to the west by the impingement of the Arabian indenter into a collage of terranes accreted to the Eurasian margin during closure of the Tethyan Ocean in Mesozoic and Early Tertiary times. Most of these rotations are concentrated within the last few millions of years and are thus a record of the last phase of orogenic development (tectonic escape) following continental collision and crustal thickening. Both these examples illustrate deformation during late stages of orogenic deformation following collision, folding and crustal thickening. Within the Alpine-Himalayan Belt, they fall into the timescale of postcollisional events described as *neotectonic* to distinguish it from the pre and syn collisional history described as *paleotectonic*.

In principle there are two aspects to the earlier history of orogenesis that paleomagnetic study can aim to quantify. Firstly, there is the phase of ocean closure in which latitudinal convergence of the two continental margins is recorded by a decline in the difference between paleomagnetic inclinations from either margin. In the Anatolian case, for example, this is identified by progressive reduction in flattening as the Afro-Arabian crust has moved northwards to close the Tethyan Ocean (Kaymakci *et al*., 2003). Secondly, the plastic deformation associated with continental collision is responsible for nappe emplacement and R is a measure of the differential rotation between the nappe and the footwall beneath the thrust. Figure P41 shows directions of magnetization resolved from Late Cretaceous rocks, mostly passive margin limestones, in the overthrust front of the Apenninic and Silcilian nappes of southern Italy (Channell *et al*., 1980). The distribution of declinations is a composite of rotation during nappe emplacement and of differential rotations during the opening of the Tyrrhenian Sea to form the Calabrian arc of southern Italy.

The large-scale deformation shown in Figures P40, P41 producing a radial distribution of paleomagnetic directions over hundreds of kilometers of continental crust is often referred to as "orogenic bending." One of the best documented examples is the Japanese Arc (see Figure P42) where magnetic declinations in north east Japan are rotated anticlockwise and directions in south west Japan are rotated clockwise. The relative rotation between these two regions appears to have occurred over a relatively short interval of time (~16–20 Ma) during the opening of the Japan Sea by back-arc spreading (Otofuji *et al*., 1985). However, the actual deformation mechanisms operating in such arcs are certainly complex (Randall, 1998). They no doubt vary from region to region and are likely to involve both small block rotations

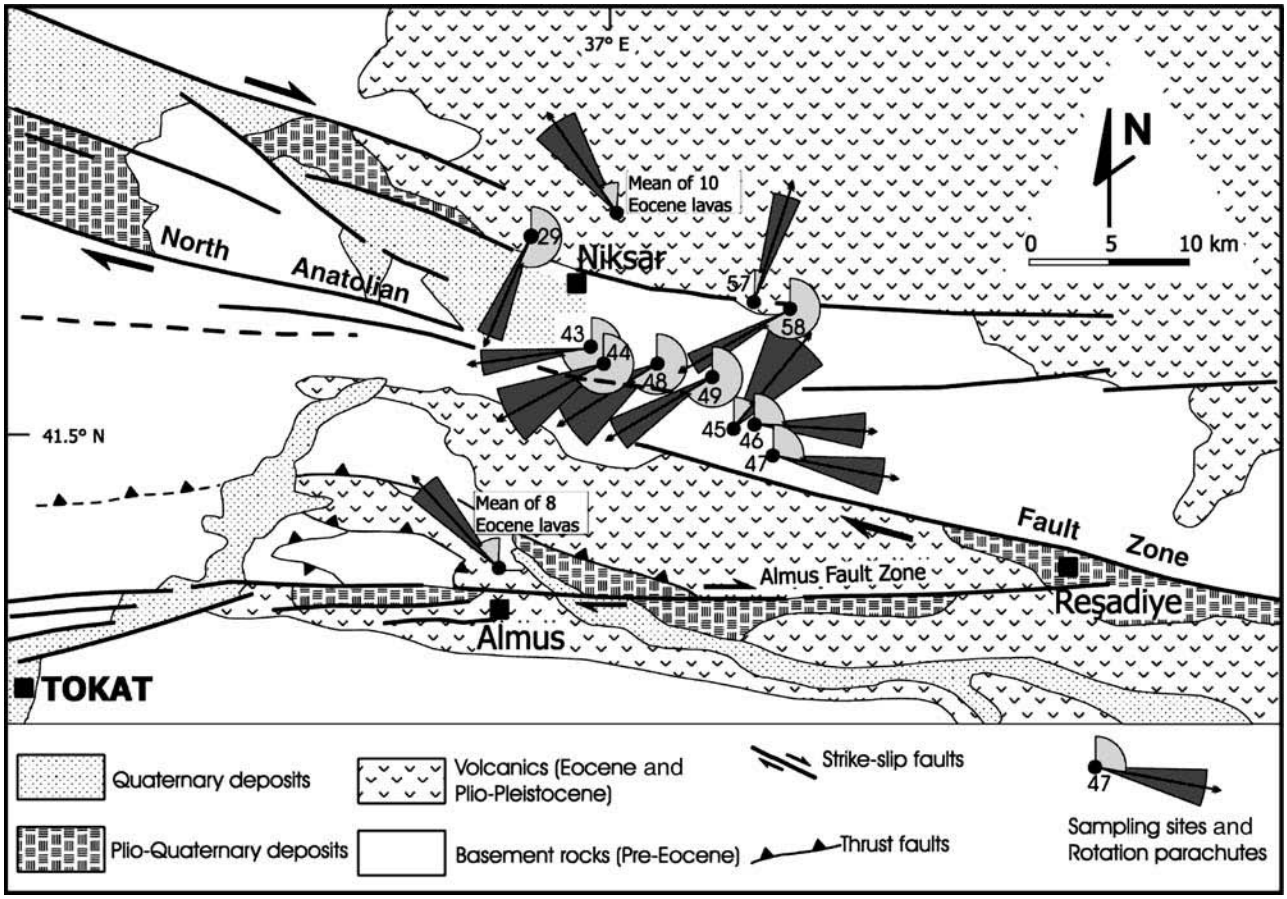

Figure P39 Deformation across an intracontinental dextral transform in the Niksar sector of the North Anatolian Fault Zone in northern Turkey. The arrows with 95% confidence cones are normal polarity directions. Rapid clockwise rotation of small blocks between the master faults is identified in Brunhes chron lava units with ages defined by high-precision K-Ar dating at ca. 520 ka. After Piper *et al*. (1997).

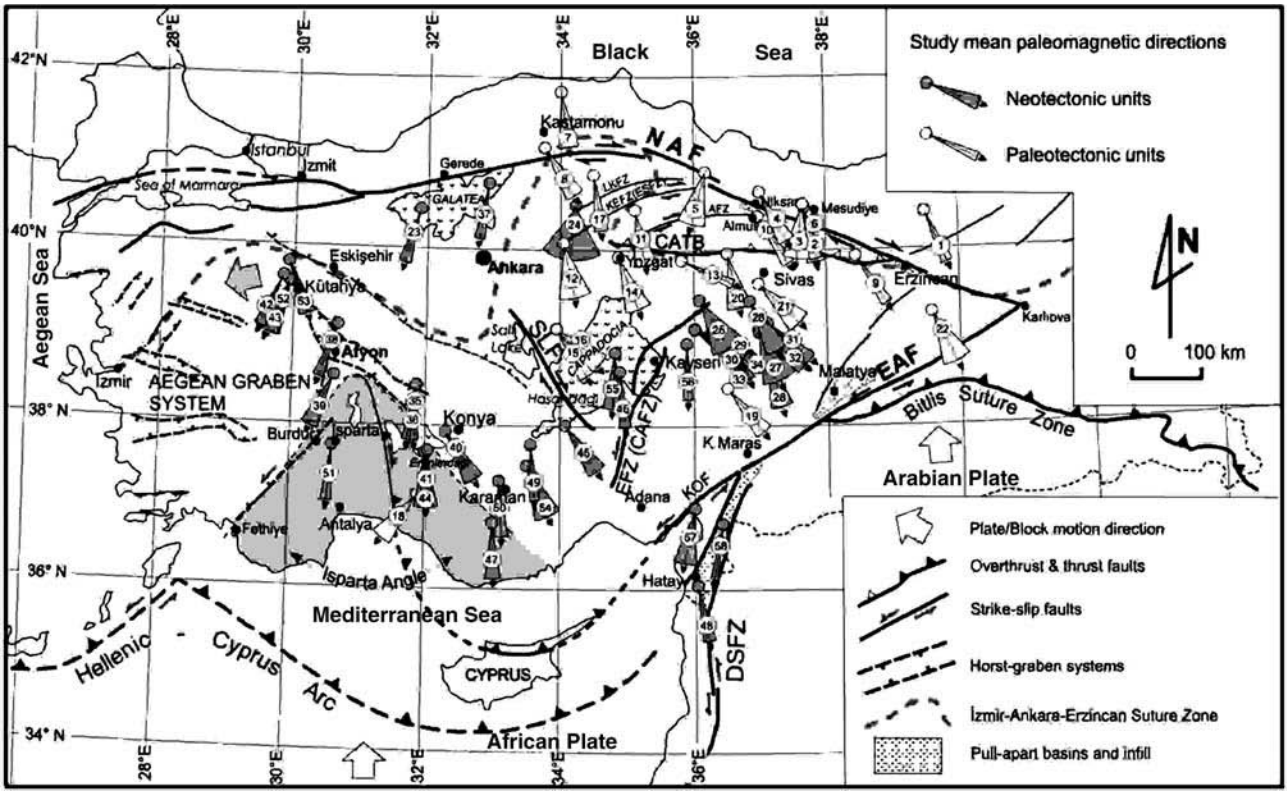

Figure P40 Rotation of blocks within the accretionary collage in central Anatolia formed by closure of the Neotethys Ocean prior to the termination of suturing ~12 Ma ago and defined by paleomagnetic directions (here shown with common reversed polarity). The neotectonic magnetizations are less than 12 Ma in age and the rotations are an expression of block rotation during tectonic escape to the west as the Arabian indenter is continuing to impinge into the weak continental crust of Anatolia and the Eurasian margin in the east. After Piper *et al.* (2003).

and differential slip along major lineaments such as the "D" zones in the Calabrian example shown in Figure P41a.

Rotation can occur within an orogenic belt either during translation of nappes over a low-angle thrust (Figure P41) or in response to strike slip fault movement within the seismogenic upper crust. The stress conditions for strike slip faulting occur when the maximum (σ_1) and minimum (σ_3) principal stresses are in the horizontal plane. Whilst this ideally generates two sets of subvertical faults that are conjugate to one another, one fault set always becomes dominant over time. Vertical axis rotation is demonstrably a major component of crustal deformation within orogenic belts although the kinematics of *in situ* vertical axis rotations in the upper crust is still controversial due to uncertainties relating to the ways in which continental crust deforms. Limiting models consider the deformation to be *continuum* or *discrete* with the division between them based on the driving mechanism for the rotation rather than the type of deformation produced. In continuum models, the rotating blocks are considered to be significantly smaller than the size of the deforming zone and occur passively in response to motion of a ductile lower crust. Shear is distributed across a wide zone with creep and diffusive mass transfer accommodating the deformation. Paleomagnetic directions will be rotated by an amount that diminishes away from the main fault (McKenzie and Jackson, 1983).

In the discrete case the strain is localized into bands and deformation involves the rotation of rigid blocks with slip between them accommodated by fault movement. The blocks themselves are internally undeformed although space constraints imply that they may be expected to undergo tectonic erosion at some peripheries and *spheochasm* formation to open conduits to the lower crust at others. Whilst the evidence indicates that continental lithosphere as a whole deforms on a large scale as a fluid medium with a behavior that can be modeled as a thin viscous sheet (England and Jackson, 1989), pervasive deformation in the upper crust can only occur if there is a sufficient high-level heat source to promote ductile deformation and permit diffusive mass transfer so that strain is not focused. As Figure P39 demonstrates, this condition does not pertain in the brittle upper crust, even adjacent to intracontinental transform faults. Deformation here takes the form of intense rotation confined between master faults and realistic models to explain rotations must therefore invoke a discrete mechanism. The base of this upper crust is evidently decoupled from a viscous lower crust obeying power law behavior. This detachment is defined by an abrupt reduction in seismicity in the depth range 10–20 km over most of the continental crust. It correlates with the combined effects of increase in temperature and in relatively weak pyroxene and plagioclase feldspar mineral assemblages, which combine to produce a rapid reduction in the strength of the crust below this level.

In discrete models the deformation is taken up on rigid crustal blocks with a length comparable to the width of the deforming zone (Figure P43). The rotation and deformation is the response to shear applied along the edges of the blocks by strike slip faults. All blocks and block bounding faults within the same fault domain will rotate by the same amount in the same direction. An exception to this rule will occur when the strike slip faults form two domains and the sense of rotation will then be opposite within each domain (Ron *et al.*, 1984). It is usually considered that rotation will be clockwise in regions of net right lateral shear and anticlockwise in regions of net left lateral shear (Nelson and Jones, 1987) as shown in Figure P43a. However, the sense of fault motion on the block bounding faults controlling the rotation need not necessarily be the same as the motion sense on the system

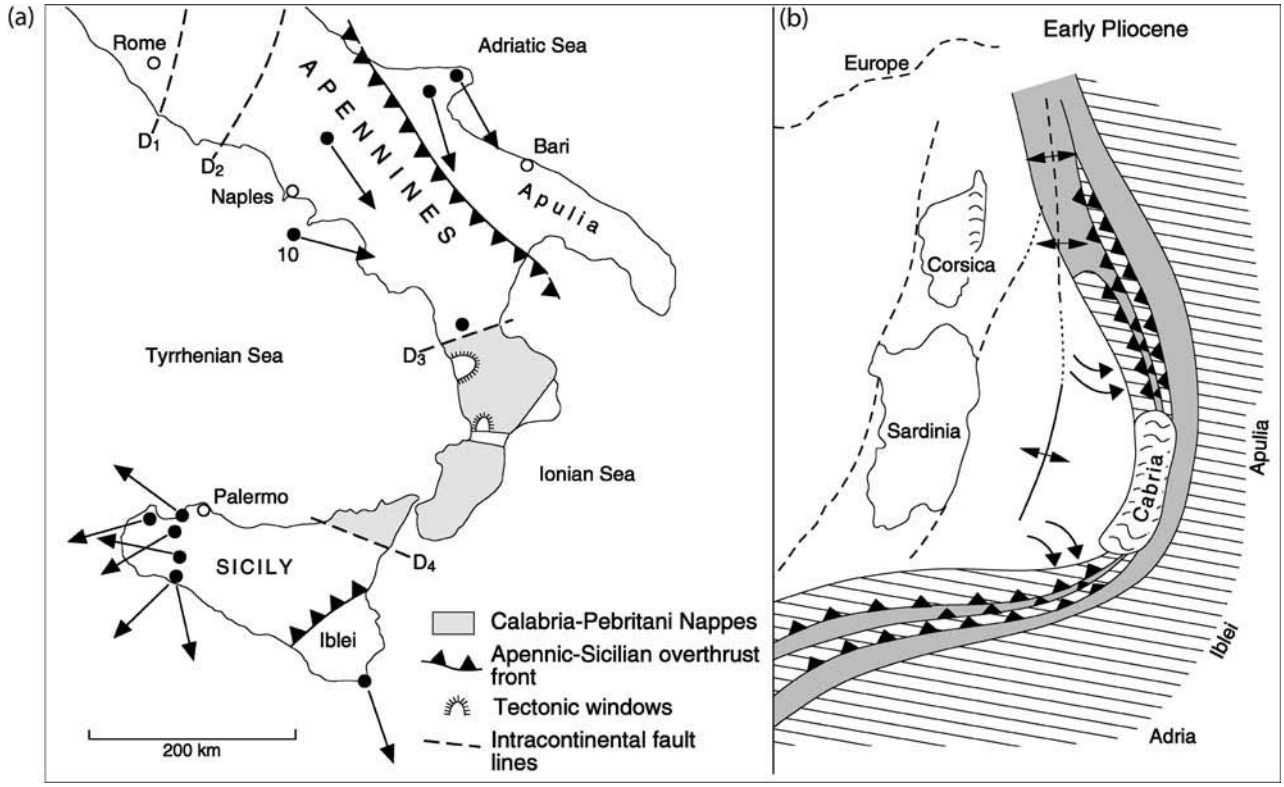

Figure P41 (a): Mean directions (reversed polarity) in Late Cretaceous rocks of the Apenninic and Sicilian nappes and the bordering autochthonous zones of Apulia and Iblei in southern Italy. (b) Schematic reconstruction showing the opening of the Tyrrhenian Sea in Early Pliocene times responsible for the large-scale regional differences in magnetic declination in (a) Compiled from Channell *et al.* (1980).

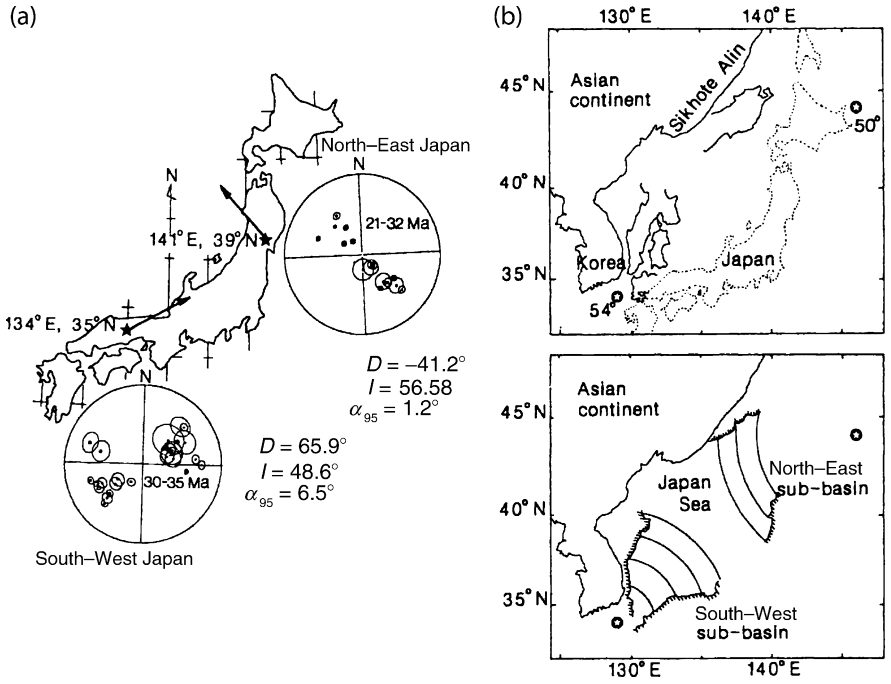

Figure P42 (a): Mean paleomagnetic field directions from rock-units older than 20 Ma in age in northeast and southwest Japan. (b) Explanation for the difference between the regional directions shown in (a) in terms of rotation of the two sectors of Japan away from the Asian margin as a result of the fan-shaped opening of the Japan Sea. After Otofuji *et al.* (1985).

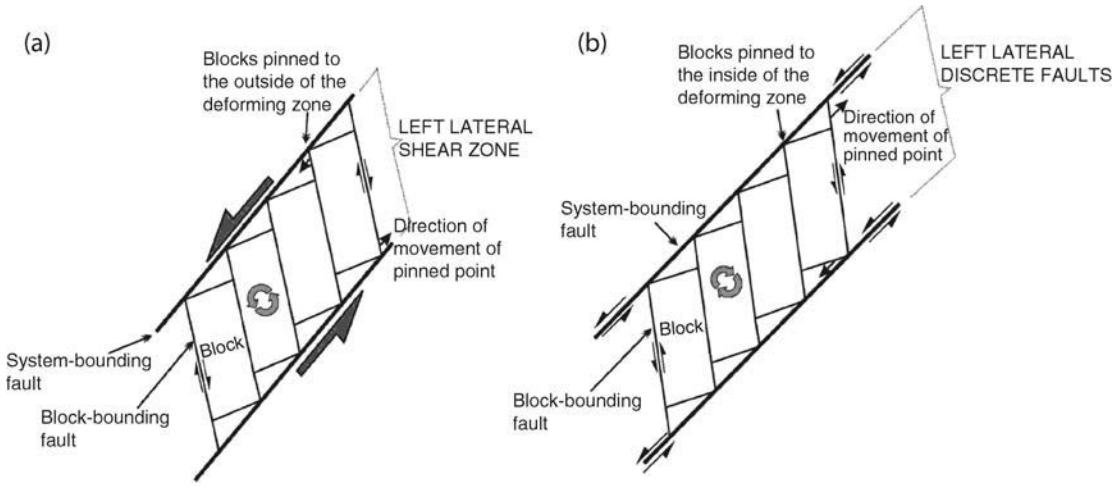

Figure P43 The origin of clockwise and anticlockwise rotations defined by paleomagnetic study of small blocks influenced by major vertical faults cutting through the thickness of the seismogenic upper crust when the deformation is (a) distributed and (b) discrete. Adapted from Randall (1998) and Tatar *et al*. (2004).

bounding faults (Randall, 1998). The sense of rotation is controlled by the initial orientation of the block bounding faults with respect to the system bounding faults, and whether the system bounding faults are acting as the margins of a wide shear zone (Figure P43a) or as discrete faults either side of the rotating blocks (Figure P43b). If the block bounding faults have the same sense of motion to the discrete system bounding faults (Figure P43b) the blocks rotate in the direction opposite to that suggested by the bulk shear on the deformation zone. Examples of both types of rotation have been reported from application of paleomagnetism to orogenic belts and are evidently a signature of the distributed or discrete character of the causative major strike slip zones.

In general there are two scales of tectonic rotation observed in orogenic belts. Large and rapid rotations are present within, or adjacent to, the intracontinental transform faults defining the conservative boundaries of the plates; Figure P39 is an example of this kind of deformation. More modest and slower rotations are present where terranes are being pushed laterally by oblique subduction or tectonic escape, or nappes are being emplaced by an advancing fold belt. Figures P39 (remote form the intracontinental transform) and P40 are examples of this scale of deformation.

A further important aspect of orogenic paleomagnetism is the study of remagnetization events directly related to orogenesis. A burial related heating that partially or completely remagnetizes preexisting ferromagnetic minerals may cause these overprints. More commonly they reside in chemical remanent magnetizations (CRMs) carried by new minerals that have either been transformed from the preexisting minerals (*diagenesis*) or have been precipitated from fluids (*authigenesis*). Comparison of the pole position with the APWP of the adjoining indenters may then allow diagenetic and authigenic events to be dated. In addition progressive unfolding of remagnetized rocks within fold structures can constrain this event within a pre, syn or postfolding timeframe. The most commonly invoked mechanism for regional CRMs in the vicinity of orogenic belts is lateral migration of preexisting connate brines within the deforming rock assemblage as it is loaded and heated within the orogenic belt. Forced migration of these orogenic fluids along ancient aquifers under a temperature and pressure gradient is considered to be a plausible explanation for the widespread distribution of CRMs away from some orogenic belts such as the Appalachians, although evidence for the link is still in part circumstantial (Elmore *et al*., 2000). Precipitation of new ferromagnetic minerals will be controlled by the availability of ions, and the temperature, pH and Eh of the ambient environment. Oxidizing conditions will favor precipitation of hematite whereas alkaline and mildly reducing environments favor precipitation of magnetite. In more strongly reducing conditions, the ferromagnetic pyrrhotite is precipitated and can produce important late stage CRMs within the orogenic belt where abundant mudrocks originally containing pyrite are present or where mineralizing fluids have been able to permeate. Thus, in addition to applications of the primary or early tectonic paleomagnetic record for resolving the scale of deformation, the study of chemical magnetic overprints can constrain the age and regional extent of important later events in the development of orogenic belts.

John D.A. Piper

Bibliography

Bazhenov, M.L., and Mikolaichuk, A.V., 2002. Palaeomagnetism of Palaeogene basalts from the Tien Shan, Kyrgystan: rigid Eurasia and dipole geomagnetic field. *Earth and Planetary Science Letters*, **195**: 155–166.

Beck, M.E., 1980. Palaeomagnetic record of plate margin processes along the western edge of North America. *Journal of Geophysical Research*, **87**: 7115–7131.

Beck, M.E., Burmester, R.F., Kondopoulou, P., and Atzemoglou, A., 2001. The palaeomagnetism of Lesbos, NE Aegean, and the eastern Mediterranean inclination anomaly. *Geophysical Journal International*, **145**: 233–245.

Channell, J.E.T., Catalano, R., and D'Argenio, B., 1980. Palaeomagnetism and the deformation of the Mesozoic continental margin in Sicily. *Tectonophysics*, **61**: 391–407.

Demarest, H.H., 1983. Error analysis for the determination of tectonic rotation from palaeomagnetic data. *Journal Geophysical Research*, **88**: 4321–4328.

Elmore, R.D., Kelley, J., Evans, M., and Lewchuk, M., 2000. Remagnetization and Orogenic Fluids: Testing the hypothesis in the central Appalachians. *Geophysical Journal International*, **144**: 568–576.

England, P.C., and Jackson, J., 1989. Active deformation of the continents. *Annual Review of Earth and Planetary Science*, **17**: 197–226.

Kaymakci, N., Duermeijer, C.E., Langereis, C., White, S.H., and Van Dijk, P.M., 2003. Palaeomagnetic evolution of the Cankiri Basin (Central Anatolia, Turkey): implications for oroclinal bending due to indentation. *Geological Magazine*, **140**: 343–355.

King, G., Oppenheimer, D., and Amelung, F., 1994. Block versus continuum deformation in the western United States. *Earth and Planetary Science Letters*, **128**: 55–64.
McKenzie, D.P., 1978. Some remarks on the development of sedimentary basins. *Earth and Planetary Science Letters*, **40**: 25–32.
McKenzie, D.P., and Jackson, J.A., 1983. The relationship between strain rates, crustal thickening, palaeomagnetism, finite strain and fault movements within a deforming zone. *Earth and Planetary Science Letters*, **65**: 182–202.
Nelson, M.R., and Jones, C.H., 1987. Palaeomagnetism and crustal rotations along a shear zone, Las Vegas Range, Southern Nevada. *Tectonics*, **6**: 13–33.
Otofuji, Y.-O., Matsuda, T., and Nohda, S., 1985. Opening mode of the Japan Sea inferred from the palaeomagnetism of the Japan Arc. *Nature*, **317**: 603–604.
Piper, J.D.A., Tatar, O., and Gürsoy, H., 1997. Deformational behaviour of continental lithosphere deduced from block rotations across the North Anatolian fault zone in Turkey. *Earth and Planetary Science Letters*, **150**: 191–203.
Piper, J.D.A., Gürsoy, H., and Tatar, O., 2001. Palaeomagnetism and magnetic properties of the Cappadocian ignimbrite succession, central Turkey and Neogene tectonics of the Anatolian collage. *Journal of Volcanology and Geothermal Research*, **117**: 237–262.
Randall, D.E., 1998. A new Jurassic-Recent apparent polar wander path for South America and a review of central Andean tectonic models. *Tectonophysics*, **299**: 49–74.
Ron, H., Freund, R., Garfunkel, Z., and Nur, A., 1984. Block rotation by strike slip faulting: structural and palaeomagnetic evidence. *Journal of Geophysical Research*, **89**: 6256–6270.
Tatar, O., Piper, J.D.A., Gürsoy, H., Heimann, A., and Kocbulut, F., 2004. Neotectonic deformation in the transition zone between the Dead Sea Transform and the East Anatolian Fault Zone, Southern Turkey: a palaeomagnetic study of the Karasu Rift Volcanism, *Tectonophysics*, **385**: 17–43.
Wernicke, B.P., Christiansen, R.L., England, P.C., and Sonder, L.J., 1987. Tectonomagmatic evolution of Cenozoic extension in the North American Cordillera. In Coward, M.P., Dewey, J.F., and Hancock, P.L. (eds.), *Continental Extensional Tectonics*. Geological Society of London Special Publication, **28**: 203–221.

PARKINSON, WILFRED DUDLEY

Twentieth century scientist

Wilfred Dudley Parkinson (see Figure P44) was an internationally prominent geomagnetician of the 20th century (Barton and Banks, 2002). His origins in geomagnetism were classical, and he was active through the remarkable period that saw observing apparatus change from mechanical to modern electronic, and recording methods change from paper chart and photographic paper to electronic memory. Data analysis methods changed from graphical and hand-calculated to the full range of numerical, modeling and inversion methods, which were possible with electronic computers by the end of the century. Parkinson was a dedicated and effective teacher at the University of Tasmania, and his book *Introduction to Geomagnetism* (Parkinson, 1983) reflected the benefits of being based on an excellent lecture course.

His research contributions, together, thus very much appear as a period piece of his time. The International Geophysical Year (IGY), which spanned the 18 months from July 1, 1957 to December 31, 1958 (Bates *et al*., 1982) promoted the observation of the geomagnetic time-varying field at an enhanced density of observatories relative to the then standard global network, and focussed attention on the spatial pattern of these time-varying fields. It was from an analysis of the fluctuating fields observed at Australian stations that Parkinson first observed the "coast effect" for which he became well known, and which he characterized by graphically constructed "Parkinson vectors" (also called "Parkinson arrows" see induction arrows).

The time of his activity, plus his natural skills, meant Parkinson led in pioneering much Australian geophysics. In pursuits promulgated by his national government employer, the Bureau of Mineral Resources, he was a pioneer in the construction of magnetic maps of the Australian continent, in developing the aeromagnetic survey method for Australia, and in instituting geomagnetic measurements in Antarctica.

However he is best known for his widely used "Parkinson arrow" contribution.

Brief biography

Parkinson was born in 1919 into a family active in geomagnetism, as his father worked for the Carnegie Institution of Washington (CIW), and was assistant observer at the Watheroo Observatory in Western Australia. Parkinson thus traveled extensively with his family in connection with geomagnetic activities. He received his first degree (BSc hons in mathematics) from the University of Western Australia, and then following service with the CIW at Huancayo Observatory in Peru he studied for his PhD at Johns Hopkins University in the United States of America. After some time in USA, he returned to Australia in 1954 to join the then Bureau of Mineral Resources. In 1967 he joined the Department of Geology at the University of Tasmania. He was promoted to Reader in Geophysics and spent the rest of his career at that university, traveling internationally to other places active in geomagnetism during his sabbatical leave periods.

Hobart and environs had been significant in the history of geomagnetism and Parkinson played an important role both in the celebration of the bicentenary of the year 1792 D'Entrecasteaux expedition (Lilley and Day, 1993), and in ensuring appropriate recognition of the site and history of the 1840 Rossbank Magnetic Observatory.

As a leader in Australian geomagnetism, he was an important figure at four Australian Geomagnetic Workshops which were convened in Canberra by C.E. Barton and F.E.M. Lilley in the years 1985, 1987, 1993, and 2000. It was appropriate that he was the invited guest speaker at the last workshop he was to attend, in 2000—the year before his death in 2001.

Dudley Parkinson, as he was widely known, was survived by his wife Mary, two sons Charles and Richard, and four grandchildren.

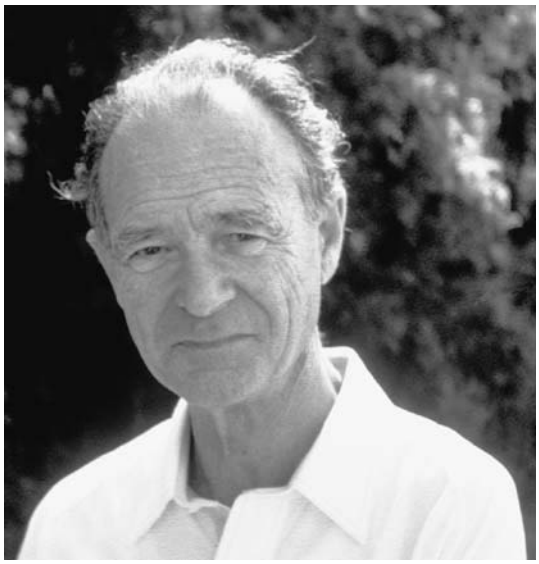

Figure P44 Wilfred Dudley Parkinson 1919–2001 (photo taken 1990, by F.E.M. Lilley).

Recognition of the coast effect, Parkinson arrows, and crustal conductivity structure

From his familiarity with magnetic observatory data, in the 1950s Parkinson had noticed that commonly for coastal observatories the vertical component of the fluctuating field had an evident correlation, best seen during magnetic storm activity, with the onshore horizontal component. Parkinson realized that from some starting point, the vectors of magnetic field change, reckoned at intervals of say half-an-hour, tended to lie on a plane in space. Parkinson called this plane the "preferred plane."

In investigating the phenomenon, Parkinson developed a graphical method for determining the plane at a particular observatory. To characterize the effect he plotted the horizontal projection of the (unit-length) downwards normal to the plane on a map, at the observatory site. The plane became known as the "Parkinson plane," and the horizontal projection of the downwards normal became known as the "Parkinson vector."

Subsequently, usage of the term Parkinson arrows was adopted to avoid any implication that Parkinson vectors of structures considered in isolation could necessarily be added vectorially to produce the effect of the structures in combination. Later Parkinson supported use of the term "Induction arrow", out of respect for others who had developed similar ideas.

Remote from a coastline, such arrows generally point to the high conductivity side of any conductivity structure present in the regional geology. (Note that in some conventions, such as that attributed to Wiese, the arrows are plotted in the opposite direction.) Plotted for an array of stations, the arrows demonstrated that electrical conductivity contrasts within continents, as well as at continent-ocean boundaries, could thus be mapped. The realization that the phenomenon was controlled by Earth electrical conductivity structure guided much of Parkinson's research for the rest of his career.

Chronicle of publications

Parkinson's published work provides a representative chronicle in geomagnetic research for the later half of the 20th century. Thus Parkinson (1959) describes recognition of the "preferred plane," and Parkinson (1962) introduces the Parkinson vector technique. In Parkinson (1964) a laboratory model comprising copper sheeting for the seawater of the world's oceans is described—Parkinson's "terrella"—in an attempt to test whether induction in the seawater alone is sufficient to account for the coast effect. The coast effect is reviewed further in Parkinson and Jones (1979).

Parkinson (1971) addresses an analysis of the Sq variations recorded during the IGY. These observations had been a prime objective of the IGY global network of observatories, and Parkinson's analysis was one of the first to exploit the power of electronic computers, which were developing rapidly in the 1960s. This thread is picked up again in Parkinson (1977), Parkinson (1980) and Parkinson (1988).

Dosso *et al*. (1985), Parkinson *et al*. (1988), and Parkinson (1989) see attention given again to local induction, and the discovery of the Tamar conductivity anomaly in northeast Tasmania. The Australian island State proved a productive field area for Parkinson and his students, based in Hobart. In Parkinson (1999) several earlier pursuits are brought together, in addressing the influence of time-variations on aeromagnetic surveying. Parkinson and Hutton (1989) is a major review, bringing together threads of earlier research contributions.

F.E.M. Lilley

Bibliography

Barton, C., and Banks, M., 2002. Wilfred Dudley Parkinson: Obituary. *Preview (Newsletter of the Australian Society of Exploration Geophysicists)*, **96**: 11.

Bates, C.C., Gaskell, T.F., and Rice, R.R., 1982. *Geophysics in the Affairs of Man.* New York: Pergamon Press.

Dosso, H.W., Nienaber, W., and Parkinson, W.D., 1985. An analogue model study of electromagnetic induction in the Tasmania region. *Physics of the Earth and Planetary Interiors*, **39**: 118–133.

Lilley, F.E.M., and Day, A.A., 1993. D'Entrecasteaux 1792: celebrating a bicentennial in Geomagnetism. *Eos, Transactions, American Geophysical Union*, **74**: 97 and 102–103.

Parkinson, W.D., 1959. Directions of rapid geomagnetic fluctuations. *Geophysical Journal of the Royal Astronomical Society*, **2**: 1–14.

Parkinson, W.D., 1962. The influence of continents and oceans on geomagnetic variations. *Geophysical Journal of the Royal Astronomical Society*, **6**: 441–449.

Parkinson, W.D., 1964. Conductivity anomalies in Australia and the ocean effect. *Journal of Geomagnetism and Geoelectricity*, **15**: 222–226.

Parkinson, W.D., 1971. An analysis of the geomagnetic diurnal variation during the International Geophysical Year. *Gerlands Beitrage Zur Geophysik*, **80**: 199–232.

Parkinson, W.D., 1977. An analysis of the geomagnetic diurnal variation during the International Geophysical Year. *Bureau of Mineral Resources, Geology and Geophysics, (Australia)*, **173**.

Parkinson, W.D., 1980. Induction by *Sq*. *Journal of Geomagnetism and Geoelectricity*, **32**(Supplement I): SI 79–SI 88.

Parkinson, W.D., 1983. *Introduction to Geomagnetism.* Edinburgh: Scottish Academic Press.

Parkinson, W.D., 1988. The global conductivity distribution. *Surveys in Geophysics*, **9**: 235–243.

Parkinson, W.D., 1989. The analysis of single site induction data. *Physics of the Earth and Planetary Interiors*, **53**: 360–364.

Parkinson, W.D., 1999. The influence of time variations on aeromagnetic surveying. *Exploration Geophysics*, **30**: 113–114.

Parkinson, W.D., and Hutton, V.R.S., 1989. The electrical conductivity of the Earth. In Jacobs, J.A. (ed.) *Geomagnetism.* London: Academic Press, vol. 3, pp. 261–321.

Parkinson, W.D., and Jones, F.W., 1979. The geomagnetic coast effect. *Reviews of Geophysics and Space Physics*, **17**: 1999–2015.

Parkinson, W.D., Hermanto, R., Sayers, J., and Bindoff, N.L., 1988. The Tamar conductivity anomaly. *Physics of the Earth and Planetary Interiors*, **52**: 8–22.

Cross-references

Coast Effect of Induced Currents
Electromagnetic Induction (EM)
Geomagnetic Deep Sounding

PEREGRINUS, PETRUS (FLOURISHED 1269)

Virtually nothing is known of the life or wider circumstances of the Frenchman Peter, Pierre, or Petrus Peregrinus, beyond what he wrote in his *Epistola Petri Peregrini de Maricourt*, from the camp of the army besieging Lucera in Apulia, Italy, and dated August 8, 1269. Most probably, he was a native of Méharicourt, Picardy, in north-east France, and from his fascination with all kinds of machines and self-acting devices, he could have been a military engineer. His honorific title "Peregrinus," no doubt stemming from the Latin *peregrinator*, or wanderer, could have derived from his having been on pilgrimage or Crusade, though there is no evidence to back the legend that he was a monk or priest. Whether he was the same "Master Peter" referred to as a mathematician of brilliance by his English contemporary Friar Roger Bacon is uncertain but possible.

Peter's historical importance, however, derives from his being the first significant author on magnetism. His *Epistola* of 1269 was widely circulated across Europe in manuscript form, and in the 16th century

was acknowledged by no less a figure than William Gilbert in *De Magnete* (1600). The *Epistola* recounts that magnetic phenomena was already familiar to Europeans by 1269 (for knowledge of the compass, originally obtained from China, had already been used for direction finding in the West for about 100 years by Peter's time), along with new experiments and insights, which could well have been Peter's own. What Peter does, however, is producing a coherent treatise that surveys the current state of magnetic knowledge in Europe by 1269, before going on to describe his own experiments.

Peter experimented with different types of magnets, including elongated pieces of magnetite stone, with what seem to have been spherical magnets (probably carved from blocks of magnetite) and with the transfer of magnetism from the natural stone to pieces of iron or steel. While there was some conjecture amongst scholars as to whether he was the first person to use the term "pole" with relation to magnetism, he was certainly familiar with the concept of the north and south terminations of all magnetic bodies. When using what seems to have been a spherical magnet, for instance, he describes employing the natural orientation of needles upon its surface to trace lines that would converge in polar points.

He also conducted experiments in the breaking in two of natural magnets, and found that when a piece of magnetic stone was so divided, the ends of the two broken pieces suddenly acquired north and south polar characteristics of their own. Yet if one rejoins the broken pieces and cemented them together, then the two magnetic fields seemed to recombine and form one magnet again. Peter's experiments showed that like poles repel and unlike poles attract. Heavy pieces of magnetite with an apparently homogenous composition were more powerful attractors of iron than the light-weighted and less pure pieces of the stone.

Needles and pieces of iron (or steel), under the right conditions and by bringing them into contact with natural magnets, themselves become magnetic, and display all the characteristics of the natural magnets from which they were derived.

Peter Peregrinus described several experiments with floating magnets which he had placed in cups that were then made to float in water—the pieces of magnetite, indeed, being like passengers in a boat. He found that when placed in an unrestricted environment of this kind, the magnets always oriented themselves north-south by the Earth's own astronomical poles. An advancement on this experiment was made when he encased an elongated piece of magnetite in wood, so as to make it float. First, he proposed that if the rim of the water-containing vessel was divided into the cardinal points and the whole vessel into 360°, then one had an instrument which would allow an observer or navigator at sea to determine the exact rising and setting points of astronomical bodies on the horizon, with reference to the north pole. Next Peter proposed a dry compass, where instead of water, the balanced needle rotated upon a vertical pin, but which still allowed astronomical bearings to be read off against a graduated edge. This would have been a very early version of a marine azimuth compass.

But in addition to his more practical experimental work, Peter was interested in the source of the magnet's power. First, he dismissed what seem to have been a series of folk myths about magnetism. For instance, magnetism could *not* have been a uniquely north-polar phenomenon because the north pole is too cold to be inhabited and hence there can be no people there to mine the magnetite familiar to scholars. Peter reminds us that magnetite deposits occur in many places in Europe that are many degrees south of the north polar regions, while—let us not forget—the needle also points south. And while Peter, like all educated medieval men who were heirs to the classical tradition, knew that the Earth itself was a sphere. In 1269 no European knew anything for certain about the nature, inhabitants, or geography of the Southern Hemisphere.

As an educated man who had clearly received some training in the classical sciences of astronomy, geometry, and arithmetic, and had no doubt encountered the increasingly influential ideas of Aristotle (all of which were part of the undergraduate *Quadrivium* of Europe's universities in the 13th century), he would have taken it as axiomatic that the Earth rested motionless at the center of the universe and that the heavens revolved about it. In this way of thinking, the Earth was associated with cosmological stability, whereas the heavens were imbued with motion. So it was probably this line of reasoning which led Peter to attribute the motion inducing capacity of the magnet to the heavens. This also prompted him to suggest the devising of a piece of apparatus to demonstrate the phenomenon. He proposed that if a spherical magnet were mounted upon its polar points in some sort of bearing, and the north and south poles exactly oriented to correspond with those of the Earth (in what would now be called an Equatorial Mount), then the sphere would rotate of its own accord. It would do so in accordance with the natural rotation of the heavens, the sphere's own magnetism simply responding to its celestial source. Peter never reported any success with this experiment as the reasons seem to be obvious.

But Peter's obvious interest in inventions next led him to join that band of medieval men who were fascinated with perpetual motion. Yet whereas his 12th-century fellow-Frenchman, Villard de Honnecourt, and others like him saw their machines as powered by arrangements of falling weights, Peter's proposed perpetual motion machine was set in train by an oval magnet the north-seeking properties of which actuated the teeth of a denticulated wheel.

What is so tantalizing about Peter is that we know nothing of him beyond his *Epistola* of August 8, 1269. His very fleeting passage across the pages of history, therefore, begs more questions than it answers. For how many educated men were there in medieval Europe who traveled, possibly crusaded, worked as military engineers, and were fascinated by mechanical invention? And let us not forget that the *Epistola* was sent not to a Bishop or university corporation, but to "*Sygerum de Foucaucourt, Militem*", or "Sygerus... the *Soldier*". Did ingenious military engineers conduct experiments into magnetism and investigate astronomy and other branches of science on those long tedious days in camp, when they were not supervising storming engines? Indeed, 13th- and 14th-century Europe was vibrant with mechanical invention: improved wind and water mills, iron founding machinery, daring Gothic cathedrals, early gun founding and explosives manufacture, the ship's rudder, and soon after 13th century the first geared mechanical clocks, many of which possessed elaborate automata. To see medieval Europe as technologically primitive is just as much a myth of our own time as was Peter's refutation of the existence of a great lump of ironstone at the north pole. And it was this ingenious culture, which produced the first experimentally based treatise on magnetism.

Allan Chapman

Bibliography

For English edition of Epistola, see Silvanus P. Thompson, Epistle of Petrus Peregrinus of Maricourt, to Sygerus of Foucaucourt, Soldier, Concerning the Magnet (London, 1902).

Grant, E., 1972. Peter Peregrinus, *Dictionary of Scientific Biography* New York: Scribner's. Grant's bibliographical essay on Peter is exhaustive.

Hellmann, G., Rara Magnetica, Neudrucke von Schriften und Karten über Meteorologie und Erdmagnetismus, no. 10 (Berlin, 1898).

PERIODIC EXTERNAL FIELDS

Definition

The lines of force of the Earth's magnetic field extend upwards from the surface of the Earth to the magnetopause, which is the boundary at great altitudes within which the solar wind confines the Earth's magnetic field. At an altitude of 100 km the atmospheric pressure is low and

molecules dissociate to form a conducting layer called the ionosphere. When lower layers of the atmosphere are heated by sunlight and caused to move, the motion is propagated in all directions. Electromotive forces are formed everywhere in the moving atmosphere, where from Lenz's law, $E = \mathbf{v} \times B$. In the electrically conducting ionosphere, electrical currents flow, and the magnetic field of these currents forms the external periodic magnetic variation. On magnetically quiet days this variation is called the solar quiet day variation, denoted Sq.

In every month of the calendar, five days are denoted as disturbed days, and another five as quiet days. The difference between the magnetic field, hour after hour, on the quiet and disturbed days, is called the disturbance daily variation, denoted SD, and it is another periodic field of external origin.

The gravitational force of the Sun and the Moon causes tidal movements in the oceans, the atmosphere and the solid Earth. The tidal movements of the ionosphere caused by the Moon lead to the lunar magnetic daily variations. Solar tides are much smaller than lunar tides and the corresponding solar tidal magnetic effect is difficult to discern from the magnetic variation arising from solar heating of the atmosphere.

The deep oceans in tidal movement also give rise to magnetic variations. The separation of oceanic and ionospheric components in the analysis of solar and lunar daily magnetic variations is based on the assumption that there is no ionospheric current flow at local midnight.

Because of their ionospheric origin, the regular daily variations at the surface of the Earth have an external component that is greater than the corresponding induced internal component, and the results are used for the modeling of the distribution of electrical conductivity within the Earth's interior land eigenmodes of atmospheric oscillation.

Magnetograms

In geomagnetism, the declination, denoted D, refers to the angle between the direction of the compass needle and true north, positive towards the east. The horizontal intensity, H, of the magnetic field is that component of the field in the direction of true north, and the vertical intensity, Z, is the vertically downwards component. Magnetic variations are recorded in these three elements at magnetic observatories throughout the world. Satellite magnetic data from low-Earth-orbiting satellites at an altitude of approximately 400 km, above the ionosphere, record the main field components and the determination of daily variations from satellite magnetic data has only just begun.

Magnetograms of the declination of the Earth's magnetic field recorded at Canberra magnetic observatory are given in Figure P45 with one calendar month to each row and 12 monthly rows for the year 1999. The most prominent feature of the daily magnetograms is the regular daily change that occurs on each day throughout the year, with a daily range that is smaller in local winter months.

The monthly mean values of the magnetic elements show a small annual, one cycle per year, external, periodic variation of the order of 10 nT, and it is necessary to use several years of data to get a significant result. This variation is thought to arise from the seasonal displacement of the ring current from the equatorial plane. The accurate analysis of long-period terms such as the annual variation and the 11 year cycle, is plagued by a number of difficulties, amongst which are baseline problems arising from small errors in instrument calibration.

Hourly mean values

For many years the daily variations in the magnetic field were given as hourly mean values that had been prepared manually from magnetogram photographic traces, and given in Universal Time centered midway between the hours. The results were published in yearbooks, usually three elements, month by month, after a long delay, often of some years. With modern three component vector magnetometers (see *Magnetometers*) providing samples every 10 s with a resolution of 0.1 nT, it is now possible to have 1-min values transmitted within minutes via the Intermagnet program. In 2001 about half of the world's magnetic observatories contributed to the Intermagnet program, and since that time the number of observatories contributing has increased.

Fourier analysis

The Fourier analysis of solar and lunar magnetic tides from observatory hourly mean values has a number of technical difficulties, such as noncyclic variation, but in every case, harmonic analyses of either 24-hourly mean values or 1440 one-minute values are required. The fast Fourier transform can be used, although for relatively small calculations the Goertzel algorithm (Goertzel, 1958) is useful and easily programmed. For the analysis of lunar magnetic tides, each day is "tagged" with an integer, usually from 1 to 12, called a "character number," based on a linear combination of the astronomical parameters denoted s, h, and p, by Bartels (Bartels, 1957, 747, see *Bartels, Julius*). These represent the east longitudes of the Moon, the Sun and the Moon's perigee respectively, from January 1, 1900. For the lunar variations, the character number is determined from the angular measure of $2s - 2h$, and seasonal sidebands are determined using character numbers $2s - h$ and $2s - 3h$. Hourly values from days with the same tag provide an average daily sequence, and the 12 groups are called "group sum sequences."

The Chapman-Miller (Chapman and Miller, 1940), (see *Chapman, Sydney*) method analyses the 12 groups of 24 values, by a modified two-dimensional Fourier analysis, with adjustments for the daily noncyclic variation. By using the variability of Fourier coefficients determined for the 12 groups, reasonable estimates of standard deviations for computed coefficients are obtained. The Chapman-Miller method has the great advantage of being able to deal effectively with missing days of data, or the rejection of days because of magnetic disturbance.

The Chapman-Miller method can be adapted (Malin, 1970) to separate the lunar magnetic variations into parts of ionospheric and oceanic origin.

The Fourier analysis of the elements X, Y, and Z, being the northward, eastward, and vertically downward components, respectively, of the Earth's magnetic field, over a sphere of radius a, leads to the following Fourier series:

$$
\begin{aligned}
X(a,\theta,\phi) &= \sum\nolimits_{M=1}^{4} [C_{XM}(\theta,\phi)\cos Mt + D_{XM}(\theta,\phi)\sin Mt],\\
Y(a,\theta,\phi) &= \sum_{M=1}^{4} [C_{YM}(\theta,\phi)\cos Mt + D_{YM}(\theta,\phi)\sin Mt],\\
Z(a,\theta,\phi) &= \sum_{M=1}^{4} [C_{ZM}(\theta,\phi)\cos Mt + D_{ZM}(\theta,\phi)\sin Mt].
\end{aligned}
\qquad \text{(Eq. 1)}
$$

Spherical harmonic analysis of the Fourier coefficients C_{XM}, C_{YM}, and C_{ZM} gives internal field coefficients $g_{NCi}^{mM}, h_{nCi}^{mM}$, and external field coefficients $g_{NCe}^{mM}, h_{nCe}^{mM}$, in the potential function $V_C^M(r,\theta,\phi)$, where

$$
\begin{aligned}
V_C^M(r,\theta,\phi) = a\sum_n \sum_m \Bigg[&\left(\frac{a}{r}\right)^{n+1} \left(g_{nCi}^{mM}\cos m\phi + h_{nCi}^{mM}\sin m\phi\right)\\
&+ \left(\frac{r}{a}\right)^{n} \left(g_{nCe}^{mM}\cos m\phi + h_{nCe}^{mM}\sin m\phi\right)\Bigg] P_n^m(\cos\theta).
\end{aligned}
\qquad \text{(Eq. 2)}
$$

It is the usual practice to do a spherical harmonic analysis of the Fourier coefficients D_{XM}, D_{YM}, and D_{ZM}, giving the two sets of spherical

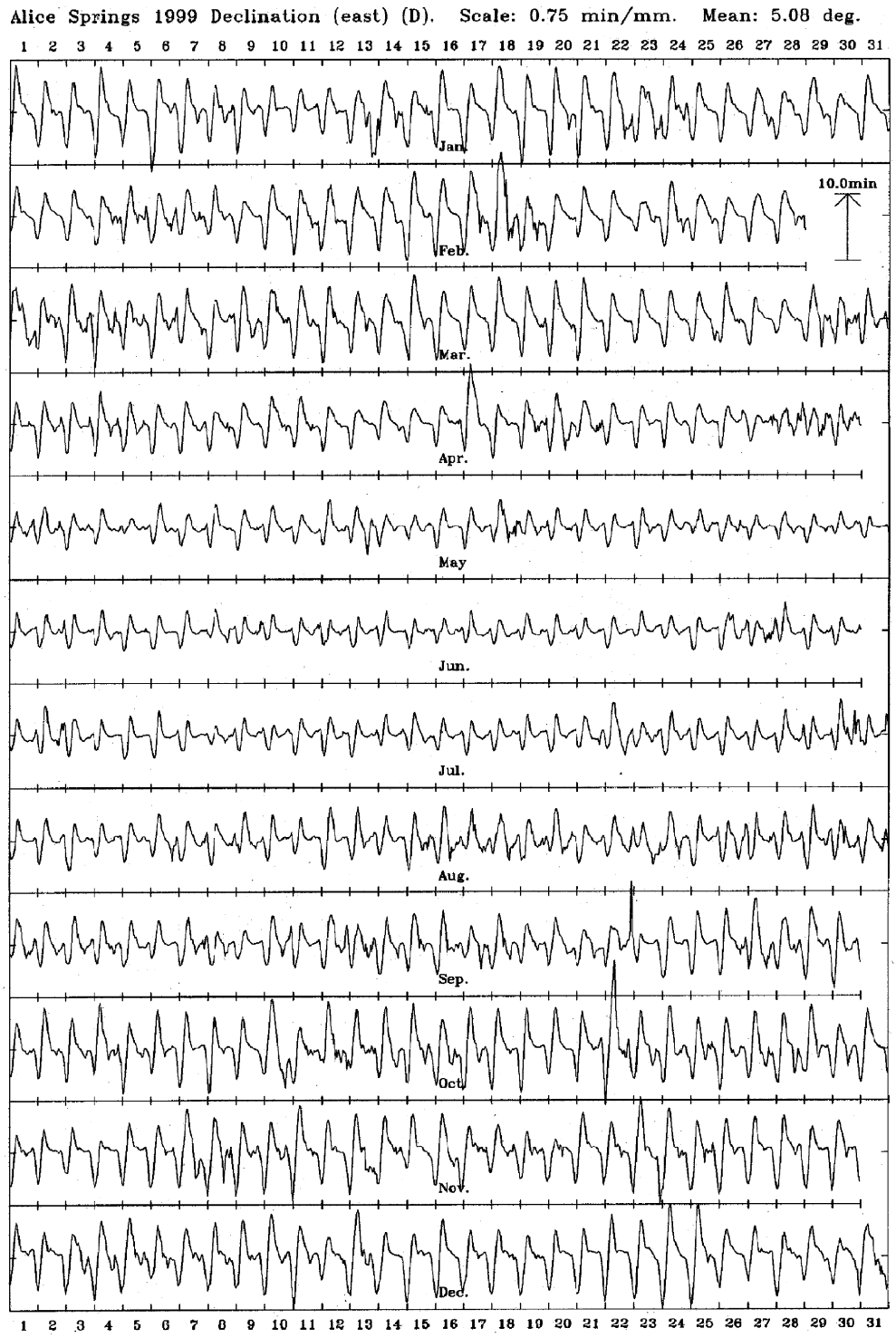

Figure P45 Daily change of the compass needle at Alice Springs, 1999. The daily range is smaller in local winter months, the lunar changes appear as a small, fortnightly modulation. (From the Australian Geomagnetism Report, 1999. Magnetic Observatories, vol. 47, Part 1, 2001).

harmonic coefficients, but leaving the researcher with the difficult task of deciding which coefficient is which, and of separating the westward and eastward moving terms.

However, by using the g and h coefficients from $V_C^M(r,\theta,\phi)$ to represent the potential $V_D^M(r,\theta,\phi)$ for the D coefficients in the form:

$$V_D^M(r,\theta,\phi) = a\sum_n\sum_m \left[\left(\frac{a}{r}\right)^{n+1}\left(h_{nCi}^{mM}\cos m\phi - g_{nCi}^{mM}\sin m\phi\right) + \left(\frac{r}{a}\right)^{n}\left(h_{nCe}^{mM}\cos m\phi - g_{nCe}^{mM}\sin m\phi\right)\right] P_n^m(\cos\theta) \quad \text{(Eq. 3)}$$

the potential function based on both $V_C^M(r,\theta,\phi)$ and $V_D^M(r,\theta,\phi)$, namely

$$V_C^M(r,\theta,\phi)\cos Mt + V_D^M(r,\theta,\phi)\sin Mt = a\sum_{n=1}^{N}\sum_{m=0}^{n}\left\{\left(\frac{a}{r}\right)^{n+1}\left[g_{nCi}^{mM}\cos(m\phi+Mt)+h_{nCi}^{M}\sin(m\phi+Mt)\right] + \left(\frac{r}{a}\right)^{n}\left[g_{nCe}^{mM}\cos(m\phi+Mt)+h_{nCe}^{M}\sin(m\phi+Mt)\right]\right\}P_n^m(\cos\theta) \quad \text{(Eq. 4)}$$

consists entirely of westward moving terms. The actual numerical analysis is based on Eqs. (2) and (3) together. The terms for which $m = M$ are local time terms. It is a simple matter to construct an expression corresponding to Eq. (3), which will give the results for eastward moving terms, which analysis shows to be much smaller than the westward moving terms.

Amplitudes and phase angles for internal and external fields are needed for conductivity studies, so that results of Eq. (4) should be provided in the form

$$a\sum_{n=1}^{N}\sum_{m=0}^{n}\left\{\left(\frac{a}{r}\right)^{n+1}A_{nCi}^{mM}\cos(m\phi+Mt+\epsilon_{nCi}^{mM}) + \left(\frac{r}{a}\right)^{n}A_{nCe}^{mM}\cos(m\phi+Mt+\epsilon_{nCe}^{mM})\right\}P_n^m(\cos\theta). \quad \text{(Eq. 5)}$$

Note particularly that the phase angles ϵ_{nCi}^{mM} and ϵ_{nCe}^{mM} in Eq. (5) are given for cosine functions.

No general method of analysis for periodic external variations from satellite magnetic data is available. Significant orbital drift through local time is required, and the more rapid the drift, the better.

Ionospheric current systems

It is very convenient to represent the vector field of external (ionospheric) origin by a scalar "stream function" whose contours run parallel to the lines of flow of electrical currents in the thin conducting shell used to represent the ionosphere. This scalar function $W(\theta,\phi)$, A, in Eq. (6), is determined from the *external* field coefficients only. The surface current density $\mathbf{K}(\theta,\phi)$, A/m, is

$$\mathbf{K}(\theta,\phi) = \nabla\times[\mathbf{e}_r\Psi(\theta,\phi)] = -\mathrm{e}_r\times\nabla W(\theta,\phi), = \frac{1}{R}\left(\frac{1}{\sin\theta}\frac{\partial W}{\partial\phi}\mathrm{e}_\theta - \frac{\partial W}{\partial\theta}\mathrm{e}_\phi\right), \mathrm{A/m}. \quad \text{(Eq. 6)}$$

The current function $W(\theta,\phi)$, A, for a shell of radius R, relative to a reference sphere of radius a, is given by

$$W(\theta,\phi) = \sum_{n=1}^{N}\sum_{m=0}^{n}\left[W_{gn}^m\cos(m\phi+Mt) + W_{hn}^m\sin(m\phi+Mt)\right]P_n^m(\cos\theta) \quad \text{(Eq. 7)}$$

with coefficients W_{gn}^m and W_{hn}^m as given originally by Maxwell (Maxwell, 1873, p. 672),

$$W_{gn}^m = -a_{km}\frac{10}{4\pi}\frac{2n+1}{n+1}\left(\frac{R_{km}}{a_{km}}\right)^{n+1}(g_{nCe}^{mM})_{\mathrm{nT}},$$
$$W_{hn}^m = -a_{km}\frac{10}{4\pi}\frac{2n+1}{n+1}\left(\frac{R_{km}}{a_{km}}\right)^{n+1}(h_{nCe}^{mM})_{\mathrm{nT}}. \quad \text{(Eq. 8)}$$

Contours in kiloamperes of the current function for the solar quiet day variation are given in Figure P46.

Ionospheric dynamo theory

An article by Stewart (1883) in the 9th edition of the *Encyclopedia Britannica*—in a subsection of the article, "Meteorology"—proposed a dynamo in the upper atmosphere as the only plausible theory for the regular solar daily magnetic variation. Schuster (1889) analyzed Sq from four Northern Hemisphere observatories, and then used the theory of electromagnetic induction (see *Electromagnetic induction* and *Price, Albert Thomas*) in a uniformly conducting sphere as derived by Lamb (in an appendix to Schuster's 1889 paper) to determine the electrical conductivity models of the Earth's interior. The theory, for a uniformly conducting sphere, uses phase angle differences and amplitude ratios of internal and external components. Schuster (1908) took the process a step further, inferring upper atmosphere wind velocities from global representations of atmospheric pressure. In particular he represented the components of electric force by a potential function $S(\theta,\phi)$ and a stream function $T(\theta,\phi)$,

$$E_\theta = -\frac{1}{a}\left(\frac{\partial S}{\partial\theta} - \frac{1}{\sin\theta}\frac{\partial T}{\partial\phi}\right),$$
$$E_\phi = -\frac{1}{a}\left(\frac{1}{\sin\theta}\frac{\partial S}{\partial\phi} + \frac{\partial T}{\partial\theta}\right). \quad \text{(Eq. 9)}$$

Schuster included an analysis of the seasonal change of *Sq*. His theory provided a solid foundation for ionospheric dynamos, adapted in more recent times by using the eigenfunctions of the Laplace tidal equation to represent the forced and free atmospheric oscillations and wind velocities.

Chapman (1919) (see *Chapman, Sydney*) developed the ionospheric dynamo theory (see *Ionosphere*) of the magnetic daily variations, of solar and lunar origin, using atmospheric velocities given as the gradient of a scalar potential. Mathematical expressions for the lunar magnetic variations, and the Chapman-Miller method for their analysis developed gradually over many years.

In the following sections, r,θ,ϕ, will denote radial distance, colatitude, and east longitude in a spherical polar coordinate system. Subscripts will be used to denote the r,θ,ϕ, components of vectors. For wind movements in the high atmosphere, the radial component v_r is assumed to be negligibly small, relative to the horizontal components, v_θ and v_ϕ. In a magnetic field with magnetic flux density components (B_r,B_θ,B_ϕ), the dynamo electric field $\mathbf{v}\times\boldsymbol{B}$ has spherical polar components

$$E_r = v_\theta B_\phi - v_\phi B_\theta,$$
$$E_\theta = v_\phi B_r,$$
$$E_\phi = -v_\theta B_r. \quad \text{(Eq. 10)}$$

Consider the dipole term only in the geomagnetic potential, V, where

$$V = a\left(\frac{a}{r}\right)^2 g_1^0\cos\theta, \quad \text{(Eq. 11)}$$

so that the components of magnetic flux density from $\boldsymbol{B} = -\nabla V$ at $r = R$, are,

$$B_r = -\left.\frac{\partial V}{\partial r}\right|_{r=R} = 2G_1^0\cos\theta,$$
$$B_\theta = -\left.\frac{1}{r}\frac{\partial V}{\partial\theta}\right|_{r=R} = G_1^0\sin\theta,$$
$$B_\phi = -\left.\frac{1}{r\sin\theta}\frac{\partial V}{\partial\phi}\right|_{r=R} = 0, \quad \text{(Eq. 12)}$$

where $G_1^0 = (a/R)^3 g_1^0$.

With the Schuster representation of the electric field, in Eq. (9), the currents driven in the direction of the gradient of the function $S(\theta,\phi)$ will go towards maxima or minima of the function, which act as sinks or sources. In a conducting thin shell, these currents have nowhere to go and an electrostatic field is set up so that no current

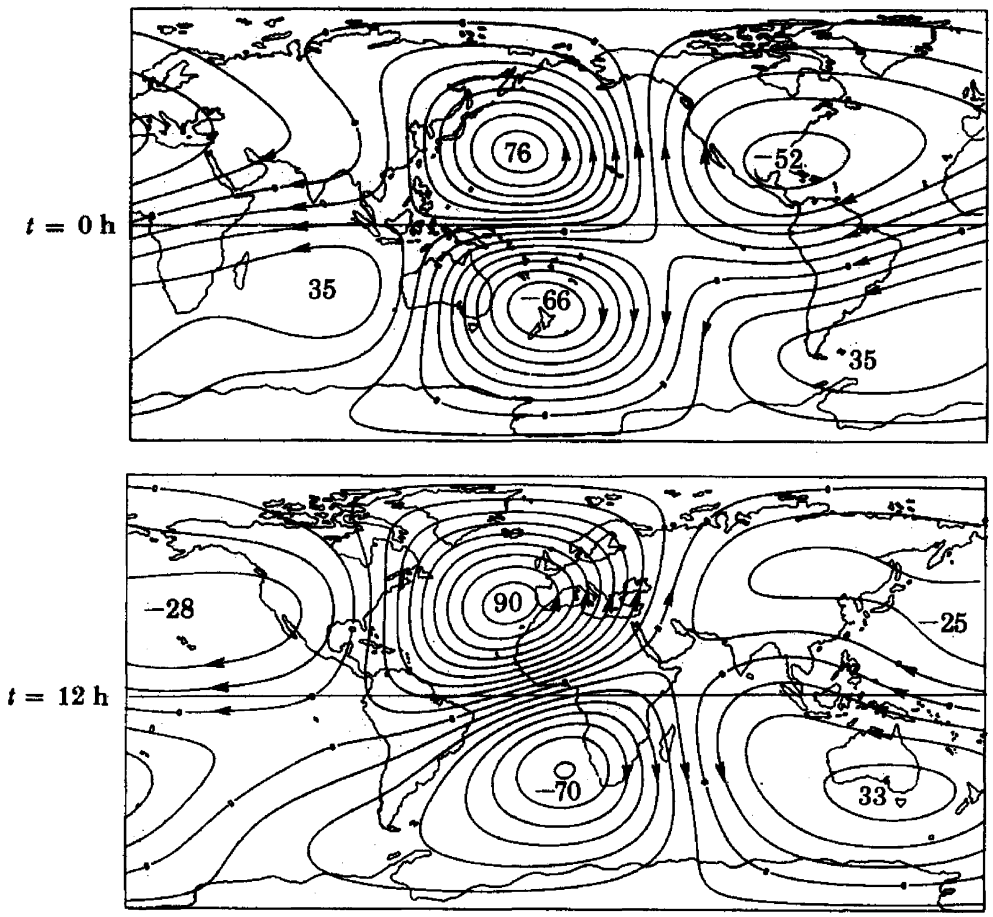

Figure P46 Equivalent external ionospheric current system for annual average Sq, 1964–1965. Contour interval and extrema in kiloamperes (from Winch, 1981).

flows. The stream function, or toroidal component $T(\theta,\phi)$, drives a stream function electrical current parallel to the contours of $T(\theta,\phi)$ in the thin spherical shell representing the ionosphere. Thus, backing off the electrostatic field from the dynamo field,

$$E_\theta + \frac{1}{R}\frac{\partial S}{\partial \theta} = \frac{1}{R\sin\theta}\frac{\partial T}{\partial \phi}, \quad E_\phi + \frac{1}{R\sin\theta}\frac{\partial S}{\partial \phi} = -\frac{1}{R}\frac{\partial T}{\partial \theta}. \qquad \text{(Eq. 13)}$$

From the current function $W(\theta,\phi)$, determined from observatory data, the components of surface current density are J_θ, J_ϕ, where

$$J_\theta = \frac{1}{R\sin\theta}\frac{\partial W}{\partial \phi}, \quad J_\phi = -\frac{1}{R}\frac{\partial W}{\partial \theta}. \qquad \text{(Eq. 14)}$$

Therefore, by Ohm's law in the form $\boldsymbol{E} = \boldsymbol{J}/\sigma(\theta,\phi)$,

$$\frac{1}{\sigma(\theta,\phi)R\sin\theta}\frac{\partial W}{\partial \phi} = \frac{1}{R\sin\theta}\frac{\partial T}{\partial \phi}, \quad \frac{1}{\sigma(\theta,\phi)R}\frac{\partial W}{\partial \theta} = -\frac{1}{R}\frac{\partial T}{\partial \theta}. \qquad \text{(Eq. 15)}$$

Therefore, from Eqs. (10) to (15), ignoring self-induction,

$$2v_\phi G_1^0\cos\theta - \frac{1}{R}\frac{\partial S}{\partial \theta} = \frac{1}{\sigma(\theta,\phi)R\sin\theta}\frac{\partial W}{\partial \phi}, \quad 2v_\theta G_1^0\cos\theta + \frac{1}{R\sin\theta}\frac{\partial S}{\partial \phi} = \frac{1}{\sigma(\theta,\phi)R}\frac{\partial W}{\partial \theta}. \qquad \text{(Eq. 16)}$$

Eliminating the electrostatic function $S(\theta,\phi)$ from Eq. (16) gives

$$\frac{2G_1^0}{\sin\theta}\left[\frac{\partial v_\phi}{\partial \phi}\cos\theta + \frac{\partial}{\partial \theta}(v_\theta\sin\theta\cos\theta)\right] = -\frac{1}{\sigma(\theta,\phi)R}\left[\frac{1}{\sin^2\theta}\frac{\partial^2 W}{\partial \phi^2} + \frac{1}{\sin\theta}\frac{\partial}{\partial \theta}\left(\sin\theta\frac{\partial W}{\partial \theta}\right)\right] - \frac{1}{\sigma^2(\theta,\phi)R}\left[\frac{\partial \sigma}{\partial \phi}\frac{1}{\sin\theta}\frac{\partial W}{\partial \phi} + \frac{\partial \sigma}{\partial \theta}\frac{\partial W}{\partial \theta}\sin\theta\right]. \qquad \text{(Eq. 17)}$$

In the special case of constant conductivity $\sigma(\theta,\phi) = \sigma$, Eq. (17) can be written

$$\frac{2G_1^0}{\sin\theta}\left[\frac{\partial v_\phi}{\partial \phi}\cos\theta + \frac{\partial}{\partial \theta}(v_\theta\sin\theta\cos\theta)\right] = -\frac{1}{\sigma R}\nabla_H^2 W(\theta,\phi), \qquad \text{(Eq. 18)}$$

where ∇_{H}^2 is the horizontal Laplacian operator,

$$\nabla_{\mathrm{H}}^2 W = \frac{1}{\sin\theta}\frac{\partial}{\partial \theta}\left(\sin\theta\frac{\partial W}{\partial \theta}\right) + \frac{1}{\sin^2\theta}\frac{\partial^2 W}{\partial \phi^2}. \qquad \text{(Eq. 19)}$$

Wind velocities in the upper atmosphere will be governed by the Laplace tidal equation, and the components of the equation can be used to simplify the expression on the left of Eq. (18).

Laplace tidal equation

Taylor, in his paper on oscillations of the atmosphere (Taylor, 1936), showed that when the temperature of the atmosphere is a function only of height above the ground, free oscillations are possible which are identical with those of a sea of uniform depth H, except that the amplitude of the oscillations is a function of the height.

Movements of the upper atmosphere are governed by the Laplace tidal equation, which includes Coriolis forces and conservative forces. In vectorial form

$$\frac{\partial \boldsymbol{v}}{\partial t} + 2\Omega \times \boldsymbol{v} = -\nabla F \qquad \text{(Eq. 20)}$$

If v_θ and v_ϕ denote the southward and eastward components of velocity relative to the surface of the rotating Earth of radius a, the horizontal components of Eq. (20) are

$$\begin{aligned} \frac{\partial v_\theta}{\partial t} - 2\Omega v_\phi \cos\theta &= -\frac{1}{R}\frac{\partial F}{\partial \theta}, \\ \frac{\partial v_\phi}{\partial t} + 2\Omega v_\theta \cos\theta &= -\frac{1}{R\sin\theta}\frac{\partial F}{\partial \phi}, \end{aligned} \qquad \text{(Eq. 21)}$$

The function F is the scalar potential of conservative forces,

$$F = \delta p/\rho + V. \qquad \text{(Eq. 22)}$$

With e^{iMt} time dependence, Eq. (21) can be written

$$\begin{aligned} iMv_\theta - 2\Omega v_\phi \cos\theta &= -\frac{1}{R}\frac{\partial F}{\partial \theta}, \\ iMv_\phi + 2\Omega v_\theta \cos\theta &= -\frac{1}{R\sin\theta}\frac{\partial F}{\partial \phi}. \end{aligned} \qquad \text{(Eq. 23)}$$

With $e^{im\phi}$ longitude dependence, the Laplace tidal equation in the form of Eq. (23) can be solved for v_θ and v_ϕ,

$$v_\theta = \frac{iM}{4R\Omega^2(f^2 - \cos^2\theta)}\left(\frac{\partial F}{\partial \theta} + \frac{m}{f}F\cot\theta\right), \qquad \text{(Eq. 24)}$$

$$v_\phi = \frac{-M}{4R\Omega^2(f^2 - \cos^2\theta)}\left(\frac{\cos\theta}{f}\frac{\partial F}{\partial \theta} + \frac{m}{\sin\theta}F\right) \qquad \text{(Eq. 25)}$$

where $f = M/2\Omega$.

From Eqs. (24) and (25), the divergence of the velocity is

$$\frac{1}{\sin\theta}\left[\frac{\partial v_\phi}{\partial \phi} + \frac{\partial}{\partial \theta}(v_\theta \sin\theta)\right] = \frac{iM}{4R\Omega^2}LF \qquad \text{(Eq. 26)}$$

where the operator L is defined by

$$\begin{aligned} LF = &\frac{1}{\sin\theta}\frac{\partial}{\partial \theta}\left(\frac{\sin\theta}{f^2 - \cos^2\theta}\frac{\partial F}{\partial \theta}\right) \\ &- \frac{1}{f^2 - \cos^2\theta}\left[\frac{m}{f}\frac{f^2 + \cos^2\theta}{f^2 - \cos^2\theta} + \frac{m^2}{\sin^2\theta}\right]F, \end{aligned} \qquad \text{(Eq. 27)}$$

where $f = M/2\Omega$. Eigenfunctions $F(\theta)$ of the operator L, are denoted $\Theta^M(\theta)$ and have $e^{im\phi}$ longitudinal dependence, and e^{iMt} time dependence,

$$L\Theta^M = -(4R^2\Omega^2/gh^M)\Theta^M. \qquad \text{(Eq. 28)}$$

For specific values of M, the eigenfunctions Θ^M form an orthogonal set. The eigenvalue $4R^2\Omega^2/gh^M$ is chosen to correspond to the theory of the oscillations of a shallow ocean of depth h^M on a rotating sphere of radius R.

Eliminating the scalar potential $F(\theta, \phi)$ in Eq. (23) leads to the remarkable simplification required in Eq. (18), namely

$$\begin{aligned} &\frac{1}{\sin\theta}\left[\frac{\partial v_\phi}{\partial \phi}\cos\theta + \frac{\partial}{\partial \theta}(v_\theta \sin\theta\cos\theta)\right] \\ &\quad = \frac{iM}{2\Omega}\frac{1}{\sin\theta}\left[\frac{\partial v_\theta}{\partial \phi} - \frac{\partial}{\partial \theta}(v_\phi \sin\theta)\right] \end{aligned} \qquad \text{(Eq. 29)}$$

Longuet-Higgins calculation

Longuet-Higgins (1968) used spectral analysis of tidal modes of "stream function" and "potential" function type for a shallow ocean on a rotating sphere. Tarpley (1970) pointed out the need to use wind velocities based on the Laplace tidal equation, and not just the gradient of a scalar potential. He showed the influence of the various tidal modes in the combinations of spherical harmonic coefficients obtained by analysis of global distributions of hourly mean values.

The horizontal components of velocity with potential and stream function components, Φ and Ψ, respectively, are

$$\begin{aligned} v_\theta &= \frac{\partial \Phi}{\partial \theta} + \frac{1}{\sin\theta}\frac{\partial \Psi}{\partial \phi}, \\ v_\phi &= \frac{1}{\sin\theta}\frac{\partial \Phi}{\partial \phi} - \frac{\partial \Psi}{\partial \theta}. \end{aligned} \qquad \text{(Eq. 30)}$$

In particular, the eigenvalues of the Laplace tidal equation yield eigenfunctions for Φ and Ψ simultaneously. It follows from Eq. (30) that

$$\frac{1}{\sin\theta}\left[\frac{\partial v_\phi}{\partial \phi} + \frac{\partial}{\partial \theta}(v_\theta \sin\theta)\right] = \nabla_H^2 \Phi, \qquad \text{(Eq. 31)}$$

$$\frac{1}{\sin\theta}\left[\frac{\partial v_\theta}{\partial \phi} - \frac{\partial}{\partial \theta}(v_\phi \sin\theta)\right] = \nabla_H^2 \Psi, \qquad \text{(Eq. 32)}$$

where ∇_H^2 is the horizontal Laplacian, defined in Eq. (19).

When $\Phi(\theta, \phi)$ and $\Psi(\theta, \phi)$ are represented as a series of associated Legendre functions,

$$\begin{aligned} \Phi(\theta, \phi) &= \sum_{n=m}^{\infty} A_n^m P_n^m(\cos\theta) e^{i(m\phi + Mt)}, \\ \Psi(\theta, \phi) &= \sum_{n=m}^{\infty} iB_n^m P_n^m(\cos\theta) e^{i(m\phi + Mt)}, \end{aligned}$$

then Eqs. (31) and (32) lead to the equations for the eigenvalues h^M, and eigenfunctions, namely, in which the coefficients A_n^m and B_n^m are calculated simultaneously.

From Eqs. (26), (28), and (31), for the horizontal divergence of the flow, the horizontal Laplacian of the potential flow is proportional to the eigenfunctions Θ^M

$$\nabla_H^2 \Phi = -\frac{iM}{4R\Omega^2}L\Theta^M = -\frac{iMR}{gh^M}\Theta^M. \qquad \text{(Eq. 33)}$$

From Eqs. (18), (29), and (32), the velocity stream function term $\Psi(\theta, \phi)$, is given in terms of the current function $W(\theta, \phi)$, which has been calculated by spherical harmonic analysis of geomagnetic data:

$$\nabla_H^2 \Psi = \frac{i\kappa\Omega}{aMG_1^0}\nabla_H^2 W(\theta, \phi). \qquad \text{(Eq. 34)}$$

Equations (33) and (34) are valid only for an ionosphere with constant conductivity, whereas the ionospheric conductivity will be small during nighttime hours and large during daylight hours. For this

particular approximation, Eq. (34) indicates that from the known current function $W(\theta,\phi)$, the coefficients B_n^m of the stream function component $\Psi(\theta,\Phi)$ of wind velocity can be obtained. These coefficients are determined by eigenvalue calculation at the same time as coefficients A_n^m of the potential function component $\Phi(\theta,\phi)$ of wind velocity and allow a direct determination of wind velocity modes from the magnetic field daily variation current function. See, for example, Winch (1981).

Ionospheric conductivity

The electrical conductivity of an ionized gas in the presence of a magnetic field is no longer uniform, but depends on the relative orientation of the applied electric field and the magnetic flux density $\boldsymbol{B}$. The electric field can be resolved into three components. Thus component of $\boldsymbol{E}$ parallel to $\boldsymbol{B}$ is denoted $\boldsymbol{E}_0$; the component of $\boldsymbol{E}$ perpendicular to $\boldsymbol{B}$ in the plane containing both $\boldsymbol{E}$ and $\boldsymbol{B}$ is denoted $\boldsymbol{E}_1$; the component of $\boldsymbol{E}$ in the direction $\boldsymbol{B}\times\boldsymbol{E}$ is denoted $\boldsymbol{E}_2$. The current density $\boldsymbol{J}$ is given by

$$\boldsymbol{J}=\sigma_0\boldsymbol{E}_0+\sigma_1\boldsymbol{E}_1+\sigma_2\boldsymbol{E}_2. \qquad \text{(Eq. 35)}$$

in which σ_0 is the longitudinal conductivity, σ_1 the Pedersen conductivity, and σ_2 the Hall conductivity.

Thus, if $\boldsymbol{b}$ is used to denote a unit vector in the direction of the magnetic flux density $\boldsymbol{B}$, then if χ is used to denote the magnetic dip, being the angle that the magnetic needle dips below the horizontal, the spherical polar components of the unit vector $\boldsymbol{b}$ are

$$\boldsymbol{b}=-\sin\chi\,\boldsymbol{e}_r-\cos\chi\,\boldsymbol{e}_\theta. \qquad \text{(Eq. 36)}$$

Spherical polar components of the electric field $\boldsymbol{E}_0,\boldsymbol{E}_1$and $\boldsymbol{E}_1$ are

$$\begin{aligned}
\boldsymbol{E}_0&=(\boldsymbol{E}\cdot\boldsymbol{b})\boldsymbol{b},\\
&=(E_r\sin\chi+E_\theta\cos\chi)\sin\chi\,\boldsymbol{e}_r+(E_r\sin\chi\\
&\quad+E_\theta\cos\chi)\cos\chi\,\boldsymbol{e}_\theta\\
\boldsymbol{E}_1&=\boldsymbol{E}-\boldsymbol{E}_0,\\
&=(E_r\cos\chi-E_\theta\sin\chi)\cos\chi\,\boldsymbol{e}_r-(E_r\cos\chi-E_\theta\sin\chi)\\
&\quad\times\sin\chi\,\boldsymbol{e}_\theta+E_\phi\boldsymbol{e}_\phi,\\
\boldsymbol{E}_2&=\boldsymbol{b}\times\boldsymbol{E},\\
&=-E_\phi\cos\chi\,\boldsymbol{e}_r+E_\phi\sin\chi\,\boldsymbol{e}_\theta+(E_r\cos\chi-E_\theta\sin\chi)\boldsymbol{e}_\phi.
\end{aligned} \qquad \text{(Eq. 37)}$$

The spherical polar components of current are

$$\begin{aligned}
J_r&=(\sigma_0\sin^2\chi+\sigma_1\cos^2\chi)E_r+(\sigma_0-\sigma_1)\sin\chi\cos\chi E_\theta\\
&\quad-\sigma_2\cos\chi E_\phi,\\
J_\theta&=(\sigma_0-\sigma_1)\sin\chi\cos\chi E_r+(\sigma_0\cos^2\chi+\sigma_1\sin^2\chi)E_\theta\\
&\quad+\sigma_2\sin\chi E_\phi,\\
J_\phi&=\sigma_2\cos\chi E_r-\sigma_2\sin\chi E_\theta+\sigma_1E_\phi.
\end{aligned} \qquad \text{(Eq. 38)}$$

At the dip equator, $\chi=0$, and Eq. 38 reduces to

$$\begin{aligned}
J_r|_{\chi=0}&=\sigma_1E_r|_{\chi=0}-\sigma_2E_\phi\big|_{\chi=0},\\
J_\theta|_{\chi=0}&=\sigma_0E_\theta|_{\chi=0},\\
J_\phi\big|_{\chi=0}&=\sigma_2E_r|_{\chi=0}+\sigma_1E_\phi\big|_{\chi=0}.
\end{aligned} \qquad \text{(Eq. 39)}$$

At the dip equator, the fluid velocity $\boldsymbol{v}$ and the magnetic flux density $\boldsymbol{B}$ are both horizontal, and the dynamo electric field $\boldsymbol{v}\times\boldsymbol{B}$ will be a purely radial field $E_r|_{\chi=0}$. By the first of Eq. (39), and electrostatic field $E_\phi\big|_{\chi=0}$ appears,

$$E_r|_{\chi=0}=\frac{1}{\sigma_1}J_r|_{\chi=0}+\frac{\sigma_2}{\sigma_1}E_\phi\big|_{\chi=0}. \qquad \text{(Eq. 40)}$$

Substitution of Eq. (40) into $J_\phi\big|_{\chi=0}$ of Eq. (39) gives

$$J_\phi\big|_{\chi=0}=\frac{\sigma_2}{\sigma_1}J_r|_{\chi=0}+\sigma_3E_\phi\big|_{\chi=0}$$

in which σ_3 is the Cowling conductivity, defined at the dip equator by

$$\sigma_3=\sigma_1+\frac{\sigma_2^2}{\sigma_1}=\frac{\sigma_1^2+\sigma_2^2}{\sigma_1}, \qquad \text{(Eq. 41)}$$

which is clearly greater than the Pedersen conductivity σ_1.

Equatorial electrojet

At observatories within one or two degrees of the magnetic equator, particularly at Huancayo in Peru, the regular daily variations in horizontal intensity are larger than at observatories further away from the magnetic equator. The section of the equivalent ionospheric current system that is responsible for this variation was first called the equatorial electrojet by Chapman (Chapman, 1951), and it is a narrow band of current flowing eastward along the magnetic dip equator in the sunlit section of the ionosphere. Baker and Martyn (Baker and Martyn, 1953) showed that "thin-shell" approximation, in which the radial component of current generated by the ionospheric dynamo is inhibited, leads to an effective enhancement of conductivity in a narrow band along the dip equator.

Vector component data from the Magsat satellite of 1980, in an orbit that remained on the dawn and dusk terminators in the ionosphere-magnetosphere region, allowed modeling of the morning and afternoon structure of the equatorial electrojet. The more recent CHAMP and Ørsted satellites, moving steadily through a range of local times, provide information on the longitudinal distribution and local time variation of the equatorial electrojet. Studies also continue at observatories in India, Africa, and Vietnam that are along, and in lines directly across the magnetic equator.

Thin-shell approximation

From the first of Eq. (38) use

$$\begin{aligned}
&(\sigma_0\sin^2\chi+\sigma_1\cos^2\chi)E_r\\
&\quad=J_r-(\sigma_0-\sigma_1)\sin\chi\cos\chi E_\theta+\sigma_2\cos\chi.
\end{aligned} \qquad \text{(Eq. 42)}$$

to eliminate E_r in Eq. (38) to obtain

$$\begin{aligned}
J_\theta&=\frac{(\sigma_0-\sigma_1)\sin\chi\cos\chi}{\sigma_0\sin^2\chi+\sigma_1\cos^2\chi}J_r+\sigma_{\theta\theta}E_\theta+\sigma_{\theta\phi}E_\phi,\\
J_\phi&=\frac{\sigma_2\cos\chi}{\sigma_0\sin^2\chi+\sigma_1\cos^2\chi}J_r-\sigma_{\theta\phi}E_\theta+\sigma_{\phi\phi}E_\phi.
\end{aligned} \qquad \text{(Eq. 43)}$$

The tensor conductivity components are

$$\begin{aligned}
\sigma_{\theta\theta}&=\frac{\sigma_0\sigma_1}{\sigma_0\sin^2\chi+\sigma_1\cos^2\chi},\\
\sigma_{\theta\phi}&=\frac{\sigma_0\sigma_2\sin\chi}{\sigma_0\sin^2\chi+\sigma_1\cos^2\chi},\\
\sigma_{\phi\phi}&=\frac{\sigma_0\sin^2\chi+\sigma_3\cos^2\chi}{\frac{\sigma_0}{\sigma_1}\sin^2\chi+\cos^2\chi}.
\end{aligned} \qquad \text{(Eq. 44)}$$

At the dip equator, $\chi=0$, the conductivity$\sigma_{\phi\phi}$ reduces to the Cowling conductivity,

$$\sigma_{\phi\phi}\big|_{\chi=0} = \sigma_3. \quad \text{(Eq. 45)}$$

In the ionosphere, $\sigma_0 \approx 800\sigma_1$, and this tends to keep the conductivity $\sigma_{\phi\phi}$ much smaller than the Cowling conductivity σ_3 in all regions except those where the magnetic dip is small. In a narrow band along the dip equator, corresponding to the equatorial electrojet, $\sigma_{\phi\phi}$ is approximately equal to the Cowling conductivity.

Disturbance daily variation

The disturbance daily variation is simply the daily variation that occurs when the Earth rotates about the geographic axis when it is surrounded by a ring current system symmetric about the geomagnetic axis.

Annual variation

Walker, in his Adam's Prize essay of 1866 (Walker, 1866) includes a chapter on the annual variation, recording that Cassini noted an annual variation in the direction of the compass needle in 1786. Modern analyses show that there are both annual and semiannual components. Spherical harmonic analysis shows that the annual term is dominantly a zonal quadrupolar term, and the semiannual term is a zonal dipolar term. Determination of these long period terms is difficult due to aliasing by shorter period variations. For example, a calculation based on midnight values only will detect the K1 tide, a sidereal time variation, as an annual term. The precise origin of these terms is still debated, but annual changes in the Sun-Earth geometry have been proposed, together with the corresponding changes in the influences of the solar wind on the Earth's magnetosphere and ring current.

Denis Winch

Bibliography

Baker, W.G., and Martyn, D.F., 1953. Electric currents in the ionosphere. I. The conductivity. *Philosophical Transactions of the Royal Society of London*, **246**A: 281–294.

Bartels, J., 1957. Geizeitenkräfte. *Handbuch der Physik*, **48**: 734–774.

Chapman, S., 1919. The solar and lunar diurnal variations of terrestrial magnetism. *Philosophical Transactions of the Royal Society of London*, **218**A: 1–118.

Chapman, S., and Bartels, J., 1940. *Geomagnetism.* Oxford: Clarendon Press.

Chapman, S., 1951. The equatorial electrojet as detected from the abnormal electric current distribution above Huancayo, Peru and elsewhere. *Archiv für Meteorologie Geophysik und Bioklimatologie, Serie A, Meteorologie und Geophysik*, **4**: 368–390.

Chapman, S., and Miller, J.C.P., 1940. The statistical determination of lunar daily variations in geomagnetic and meteorological elements. *Monthly Notices of the Royal Astronomical Society, Geophysical Supplement*, **4**: 649–659.

Goertzel, G., 1958. An algorithm for the evaluation of finite trigonometric series. *American Mathematical Monthly*, **65**(1): 34–35.

Longuet-Higgins, M.S., 1968. The eigenfunctions of Laplace's tidal equations over a sphere. *Philosophical Transactions of the Royal Society of London.* **262**A: 511–607.

Malin, S.R.C., 1970. Separation of lunar daily geomagnetic variations into parts of ionospheric and oceanic origin. *Geophysical Journal of the Royal Astronomical Society*, **21**: 447–455.

Maxwell, J.C., 1873. *A Treatise on Electricity and Magnetism.* Oxford: Clarendon Press.

Schuster, A., 1889. The diurnal variation of terrestrial magnetism. *Philosophical Transactions of the Royal Society of London*, **180**A: 467–518.

Schuster, A., 1908. The diurnal variation of terrestrial magnetism. *Philosophical Transactions of the Royal Society of London*, **208**A: 163–204.

Stewart, B., 1883. Terrestrial magnetism. *The Encyclopædia Britannica*, 9th ed, pp. 159–184.

Tarpley, J.D., 1970. The ionospheric wind dynamo–1. Lunar Tide. *Planetary and Space Science*, **18**: 2075–1090.

Taylor, G.I., 1936. The oscillations of the atmosphere. *Proceedings of the Royal Society of London*, **156**A: 318–326.

Walker, E., 1866. *Terrestrial and cosmical magnetism.* The Adams prize essay for 1865. Cambridge: Deighton, Bell and Co.

Winch, D.E., 1981. Spherical harmonic analysis of geomagnetic tides, 1964–1965. *Philosophical Transactions of the Royal Society of London*, **303**A: 1–104.

Cross-references

Bartels, Julius (1899–1964)
Chapman, Sydney (1888–1970)
Electromagnetic Induction (EM)
Ionosphere
Magnetometers
Ocean, Electromagnetic Effects
Price, Albert Thomas (1903–1978)

PLATE TECTONICS, CHINA

Our Earth is a layered planet with a dense iron core, a surficial crust of light rock, and between them, a solid silicate, convecting mantle. Plate tectonics is the surface manifestation of mantle convection. This activity gives rise to seafloor spreading, continental drift, earthquakes, and volcanic eruptions. Specifically, plate tectonics is the theory and study of plate formation, movement, interactions, and destruction, with seafloor spreading ridges, transform faults, and subduction zones as the plate boundaries. Today, many displaced continental blocks have been found in the world, and the original locations of some have yet to be worked out. Nevertheless, the concept of continental drift is now accepted as a necessary consequence of plate tectonics, and the complexity of mountain belts is well recognized as the product of the great mobility of lithospheric plates.

Paleomagnetism, which is the study of the ancient magnetism of the Earth, has played a central role in this developing view of the dynamic Earth. In the 1950s and early 1960s, scientists collected rocks on land all over the world and determined their magnetism and ages in order to reconstruct the history of the Earth's magnetic field. This worldwide effort led to the discovery of reversals of the geomagnetic field, and thus the realization that the seafloor acts as a tape recorder of the Earth's magnetic reversals, and polar wandering (McElhinny and McFadden, 2000). In particular, polar wandering is an interpretation given to the observation that the magnetic pole—and the geographic pole—has moved extensively in the geologic past. In the absence of any external influences, however, the direction of the Earth's axis of rotation cannot shift but remains fixed in space for all the time due to the law of conservation of angular momentum. The only way out of this dilemma is—the continents have to be moved relative to the axis of rotation. Thus, polar wandering is actually a manifestation of the mobility of the lithospheric plates. There are two principal ways of summarizing paleomagnetic data for a given region. One approach is to construct paleogeographic maps of the region for different geologic periods. These maps are mostly useful for comparison with relevant information, but not easy to view overall variations over different geologic time intervals. A much simpler and convenient way is to plot successive positions of paleomagnetic pole for a given continent from epoch to epoch on the present latitude-longitude grid. Such a path, traced out by the paleomagnetic poles and relative to the continent, is called the apparent polar wander path (APWP).

Fundamental principles in paleomagnetism

The first assumption of paleomagnetism is that the time-averaged geomagnetic field is produced by a single magnetic dipole at the center of the Earth and aligned with the Earth's rotation axis (McElhinny and McFadden, 2000). Thus, the calculated paleomagnetic pole coincides with the geographic pole. This geocentric axial dipole (GAD) hypothesis means that, when averaged over time, magnetic north is geographic north and there are simple relationships between the geographic latitude and the inclination of the field, which are the cornerstones of paleomagnetic methods applied to plate reconstruction and paleogeography. Paleomagnetic data can be used to find latitude and north-south orientation of the paleocontinents. Paleolatitude can be also checked with paleoclimate records (Irving, 1964). Although it is not possible to assign longitudinal position to the paleocontinents, the relative positions of the continents around the globe can often be pieced together by matching the shapes of apparent polar wander paths.

The configuration of the Earth's field today is modeled fairly closely by a geocentric dipole inclined at 11.5° to the rotation axis, but the field for most of the Tertiary, when averaged over periods of several thousand years, agrees well with the GAD model (Merrill *et al*., 1996). During the 1950s and early 1960s, many questioned the validity of the GAD hypothesis during the Paleozoic and Mesozoic. With the expansion of paleomagnetic data and development of plate tectonics studies, the validity of the GAD hypothesis as a good working approximation now appears to be on solid ground (McElhinny and McFadden, 2000). Rigorously selected paleomagnetic data are in quite good agreement with plate tectonic reconstructions and also internally self-consistent under the assumption of a GAD field (Besse and Courtillot, 2002). Moreover, paleolatitude changes calculated from paleomagnetic data are consistent with paleoclimatic changes: the distribution of various paleoclimatic indicators is latitude dependent (Irving, 1964; Ziegler *et al*., 1996).

The second assumption of paleomagnetism applied to plate tectonics is that one can use rocks as fossil compasses that record the Earth's ancient field. Study and experiments have proved that igneous and sedimentary rocks acquire primary magnetization when they were formed (McElhinny and McFadden, 2000). But determining whether the natural remanent magnetization of rocks is primary is often problematical and challenging. The original magnetization may be unstable to later physical or chemical processes and partially or completely overprinted over geologic time. Some sedimentary rocks have been shown to record paleomagnetic directions significantly shallower than the ancient field direction, a phenomenon termed inclination error (Tauxe, 1998, 2005). An important factor in making meaningful tectonic interpretations from volcanic rocks is the need to sample many separate flows that span many thousand years, a requirement that cannot always be fulfilled. The reason for this is the necessity of averaging out secular variation of the magnetic field, which typically produces a 10–20° angular dispersion of instantaneous directions, so as to obtain the time-averaged, GAD field direction (McElhinny and McFadden, 2000).

Supercontinent Gondwanaland and its dispersion

The past existence of the Gondwanaland supercontinent, a huge landmass comprised of over half of the world's present continental crust, is now clearly confirmed by paleomagnetic and paleobiogeographic data (Li, 1998). Late Precambrian to Early Paleozoic paleomagnetic data suggest that the Gondwanaland supercontinent had assembled just before the end of Early Cambrian (520 million years ago, Ma) as a result of collision between proto East Gondwanaland (Antarctica, India, Australia) and proto West Gondwanaland (Africa, Arabia, South America, and possibly Madagascar). For at least 100 Ma during the Late Devonian to Middle Carboniferous, Gondwanaland is thought to have remained over the south pole, as indicated by the available paleomagnetic data (Li and Powell, 2001) and southern cold-water fauna (Yin, 1988) and cool-climate flora (Runnegar and Cambell, 1976; Ziegler, 1990). By 320–310 Ma, Gondwanaland had collided with Laurussia to form a single supercontinent named Pangea, which stretched from pole to pole. The fragmentation of Pangea occurred as a result of plate tectonics and continental drift over Late Paleozoic, Mesozoic, and Cenozoic time to form the modern continents and oceans (Metcalfe, 1999).

Starting in Late Paleozoic time, fragmentation of Pangea (and former Gondwanaland continents) and the concomitant expansion of Eurasia have occurred repeatedly. The latest example is the addition of India to Eurasia in Early Cenozoic time (McElhinny and McFadden, 2000). Indeed, this global geographical reorganization is still in progress, as evidenced in part by the continued movement of Australia northward toward Asia (White, 1995). The ability of modern science to reconstruct this paleo-supercontinent is truly impressive. Earth scientists are continuing to sort out more details of this complex jigsaw puzzle, whose individual pieces change shape over geologic time.

Tectonic framework of China

China, which covers 9.6 million square kilometers (6.5% of the Earth's land surface) in eastern Asia, is complex and interesting from both tectonic and paleogeographic standpoints. In its simplest form, China consists of three large Precambrian continental cratons, namely, the Tarim, North China Blocks, and South China Blocks (NCB and SCB), separated by Paleozoic and Mesozoic accretionary belts, as well as several smaller blocks or terranes (Tibet, Junggar and Qaidam basins, and the Alashan/Hexi Corridor, see Figure P47). Several recent studies favor the hypothesis that these continental blocks and terranes were derived from Gondwanaland (Wang *et al*., 1999). A close biogeographic association of South China with Australia has been recognized for both the Cambrian and Devonian, suggesting that South China may have been part of Gondwanaland in Early and Middle Paleozoic time (Burrett and Richardson, 1980; Long and Burrett, 1989). Some paleontological data from Tarim show that Cambrian and Ordovician Bradoriida fossils are very similar to those of South China, which in turn would suggest that Tarim was also part of Gondwanaland in the Early Paleozoic (McKerrow and Scotese, 1990; Shu and Chen, 1991). But it is less clear whether North China belonged to Gondwanaland or not during this same period. Early Cambrian fauna from North China show affinity with Australia, but Ordovician benthic trilobite assemblages in North China show more similarity with those of Siberia and North America (Burrett *et al*., 1990). Comparative studies of the tectono-stratigraphy, paleontology, and structural geology of the various terranes in the Tibetan Plateau suggest that they were all derived directly or indirectly from Gondwanaland (Metcalfe, 1999) and added successively to the Eurasian plate during the Mesozoic and Cenozoic eras (Burg and Chen, 1984).

If, indeed, these Chinese blocks and terranes were associated with Gondwanaland during the Early Paleozoic, then the key questions would be, when and in what sequence did these blocks rift off from Gondwanaland and stitch as they are at present. As outlined below, geologic data germane to these questions are sparse and subject to conflicting interpretations (e.g., Klimetz, 1983; Mattauer *et al*., 1991; Hsu *et al*., 1988).

North China block

The North China block is bounded on the north by the Central Asian Fold Belt and on the south by the Qilian-Qingling-Dabie Shan ("shan" = mountain in Chinese). The Tancheng-Lujiang (more often referred to by the Chinese contraction "Tanlu") fault runs through the eastern part of the NCB, and sharply cuts the Qinling belt at its eastern end. There is considerable debate as to whether or not the fault represents the eastern boundary of the NCB, and its origin and history of development. The oldest basement rock was dated as 3670 ± 230 Ma, which is possibly the oldest age in China (Li and Cong, 1980). The oldest unmetamorphosed sedimentary cover has been dated at 1700 Ma (Wang, 1993).

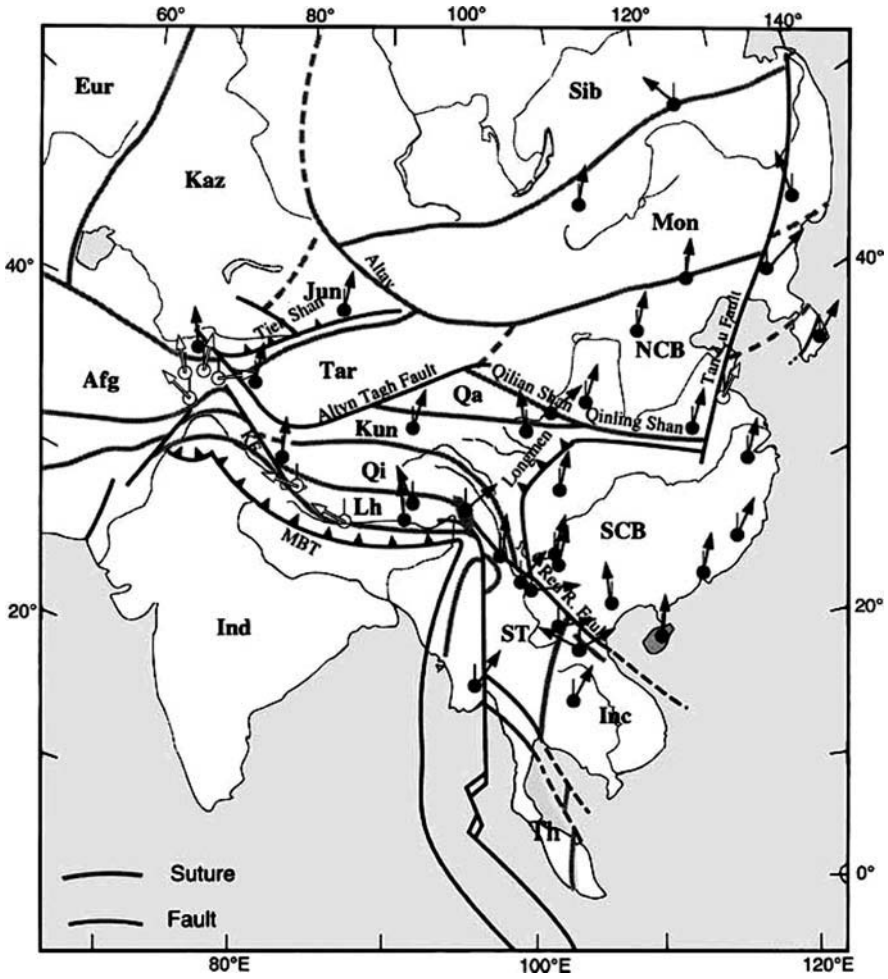

Figure P47 Simplified map (after Halim *et al.*, 2003) of Eastern Asia showing the main sutures and faults (KF, Karakorum fault; MBT, Main Boundary Thrust). The major blocks are: Afg, Afganistan; Eur, Eurasia; Inc, Indochina; Ind, India; Jun, Junggar; Kaz, Kazakhtan; Kun, Kunlun; Mon, Mongolia; NCB, North China block; Qa, Qaidam; Qi, Qiangtang; Sib, Siberia; SCB, South China block; ST, Shan Tai; and Tar, Tarim. Also indicated are the main locations where Cretaceous paleomagnetic data are available. Declination is indicated by arrows (a thin line indicates geographic north, it is vertical because of the projection selected). Open arrows are for areas suspected of major local scale deformation or unreliable paleomagnetic data. Solid arrows are thought to be representative of the individual blocks at a larger scale.

The Paleozoic sections of the NCB are dominated by Lower Paleozoic marine carbonates and characterized by a great sedimentary hiatus from the Late Ordovician through Early Carboniferous, although rare strata within this age span apparently exist on its western boundary. This remarkable hiatus has led many geologists to the conclusion that the NCB was separated from currently adjacent blocks during much of Paleozoic time. From the Late Permian onwards, its sediments are of continental origin.

The Korean Peninsula is situated east of the NCB. Traditionally, Korea has been incorporated with the NCB into a single craton (Sino-Korea) based on the close similarity of Paleozoic stratigraphy. Depending on the significance of Tanlu fault movement, it is possible that the Korean Peninsula (or part of it) was formerly located close to the South China Block, a question that is still intensively debated.

Geological estimates of the age of accretion of the NCB with Siberia to the north are also controversial. It is assigned a Middle Paleozoic age (end of Devonian and Hercynian Orogeny), while Klimetz (1983) ascribes it to the Mesozoic. By analyzing paleobiogeographic data, Laveine *et al*. (1989) argued that the Chinese blocks must have been close to Europe in the Late Carboniferous, as shown by plant migration routes.

South China block

The South China Block is bounded on the north by the Qinling and Dabie Shan, which mark the suture between the SCB and NCB (see Figure P47). Exposures of basement rocks are limited, but a U-Pb ziron date of 2860 Ma was reported for migmatitic granite in Guangxi province, indicating that the block may have formed in the late Archean. The basement of the SCB was finally consolidated around 850–800 Ma. The Paleozoic and Mesozoic strata consist mainly of marine carbonate and clastic sediments, with continental lava flows in the Late Permian. The Cenozoic strata are mainly red beds.

In the eastern part of the Qinling-Dabie Mountains, ultrahigh-pressure, coesite- and diamond-bearing metamorphic rocks crop out. Ages from U-Pb dating of zirons from eclogites range from 250 to 220 Ma, which correspond to the time when sedimentation in the SCB changed from marine to continental. This change was heralded by the

voluminous eruption of the Emeishan basalts in southwestern China around 250 Ma. Great quantities of Jurassic red beds in the Sichuan Basin indicate that large neighboring mountains were being eroded at that time. Northeast of the Dabie Shan in eastern Shandong Peninsula lies another ultrahigh-pressure coesite-bearing metamorphic suite. Similarities in mineralogy of the Shandong and Dabie Shan metamorphic assemblages suggest they were once part of the same belt that was later displaced about 500 km by the Tanlu fault in a left-lateral sense. There are widely different estimates on the timing of collision between the SCB and NCB based on geologic data. These estimates vary from the Precambrian and Middle Paleozoic to the end of the Paleozoic and earliest Mesozoic.

The SCB is commonly segregated into the Yangtze block to the northwest and mobile belts to the southeast. In general, the division between the Yangtze block and exotic terranes is demarcated south of the exposed Meso- to Neoproterozoic low-grade metamorphic rocks called the Jiangnan old land. Jiangnan rocks include ophiolite and thick argillaceous turbidites that extend for over 1000 km. Using Sm (samarium) and Nd (neodymium) isotopes, two laboratories have dated two of the ophiloite suites at 1024 ± 24 Ma and 935 ± 34 Ma, and 1034 ± 24 Ma and 935 ± 10 Ma, respectively. Li *et al*. (1995) and Li (1998) suggested that the Yangtze Block and fold belts to the southeast were amalgamated in the late Proterozoic at around 1000 Ma and are separated by a failed intracontinental rift activated during the breakup of Rodinia at around 700 Ma. There is no well-documented evidence of a Phanerozoic suture in the SCB. Hsu *et al*. (1988) proposed a Mesozoic age collision model based on the discovery of Mesozoic thrust structures in south China. This new interpretation of south China tectonics has since led intensive debate.

Tarim and Junggar basins

Tarim is a rhombic-shaped basin, bounded by the Tianshan, ("Celestial Mountains"), Kunlun and Altyn Tagh mountain ranges, with Precambrian basement (3.3 Ga) exposed along its periphery (Hu and Rogers, 1992), attesting to an extensive geologic history for the block. Tarim became an inland basin since the beginning of the Mesozoic and it is presently covered by the Takalamagan (Takla Makan) desert, with Paleozoic rocks occurring mostly along its northern and southern margins. Cambrian and Ordovician strata are distributed mainly along the northern periphery of the basin, whereas the Silurian, Devonian, Carboniferous and Permian are mainly distributed in the northwestern part of the basin (Keping area). The lithologies of these Paleozoic sequences are mainly dolomitic limestone and red and yellow siltstones. The Mesozoic and Cenozoic strata consist mainly of green sandstone and red mudstone and are distributed in the northeast part of the basin (Kuche depression). A late Paleozoic (Hercynian) orogeny was responsible for a general unconformity between Paleozoic and Mesozoic formations.

Of the three major blocks that compose the tectonic framework of China, Tarim, being the most inboard must have arrived at its present position at least as early as any of the more outboard blocks and terranes. There is no clear suture zone between Tarim and the NCB. Indeed, some geologists considered the NCB and Tarim to have formed a rigid block since the Neoproterozoic because an almost continuous—"Hexizoulang", equivalent to "Hexi Corridor"—of Precambrian and Paleozoic formations connects the NCB and Tarim. This idea has been abandoned because available paleomagnetic data suggest that these two blocks did not assume their present configuration for sometime in the Mesozoic.

The Junggar Basin, often considered to be the southeast extremity of the Kazakhstan Block, sits in a complicated region squeezed between the Tarim Basin on the south, the Kazakhstan Block on the west, and Siberia to the northeast. Unlike the Tarim Basin, there are no known exposures of Precambrian rocks along the Junggar Basin margins. However, some researchers have suggested that Junggar is underlain by Precambrian crystalline basement, based entirely upon gravimetrically determined depths to the Moho (e.g., Ren *et al*., 1987). Other workers believe that it is underlain by a basement of structurally imbricated Ordovician to Lower Carboniferous accretionary metasedimentary rocks and oceanic crustal fragments. The oldest rocks in this region are of Late Cambrian age (508 ± 60 Ma). Middle Devonian strata consist of spilitic pillow lavas interlayered with radiolarian cherts and associated limestone horizons. Carboniferous units consist mainly of marine to continental volcanic rocks interbedded with clastics. Potassium-rich granitic plutons and their extrusive equivalents, which have Permian K-Ar ages and Middle to Late Carboniferous U-Pb ages are common in west Junggar. Permian rocks are mainly continental clastics and volcanic extrusive. At many localities igneous dikes of Permian age intrude the Carboniferous formations. Triassic and Jurassic sequences are all continental clastics.

Collision between Tarim and Junggar along the Tianshan Range has been inferred to be Early Permian in age, based on geological features such as the termination of andesitic volcanism, the development of unconformitites between late Early Permian and underlying units, the intrusion of widespread syncollisional to postcollisional granites in the Tianshan and the mixture of Angaran and Cathaysian flora across the Tianshan.

Alashan/Hexi Corridor terrane

Situated west of Ordos, the Alashan/Hexi Corridor terrane is bounded on the north by Central Asian Fold Belt and is separated from the Qaidam terrane by the Qilian Shan fold belt to the south. The western boundary with the Tarim is not clearly delineated but is thought to be within the northern Qilian Shan.

The oldest rock of the Alashan/Hexi Corridor terrane is Precambrian (about 1850 Ma), as the Precambrian Longshoushan Formation in the southern part is intruded by granites 1789 Ma in age (Yang *et al*., 1986, p. 244). The first most recognized regional uncomformity in southern Alashan area is between Middle and Late Cambrian (the Xianshan Formation), which can be correlated to the coeval unconformity the Ordos basin, one of the most stable parts of the NCB. In contrast, this geologic pattern never penetrated into the Central Asian Fold Belt, indicating the latter indeed is the geologic/block boundary. Because of these geological observations, Alashan/Hexi Corridor terrane is believed to be part of the NCB at least since the Late Cambrian and was still receiving deposition while most other parts of the NCB were standing higher during Late Ordovician to Early Carboniferous time.

Tibet and Qaidam basin

Tibet is a collage of continental terranes that accreted onto Eurasia ahead of India. From north to south, the Tibetan terranes are the Kunlun, Songpan-Ganze, Qiangtang, Lhasa, and Himalaya terranes, the latter being actually part of the Indian subcontinent (see Figure P47). Geologic studies suggest that these terranes collided with Eurasia at times progressively younging southward (Dewey *et al*., 1988; Yin and Harrison, 2000; Davis *et al*., 2002). The amalgamation of the Kunlun and Songpan-Ganze terranes is marked by a broad Early Paleozoic arc on which was later superposed a Triassic arc (Burchfield *et al*., 1992). The Qiangtang terrane accreted to the Songpan-Ganze terrane along the Jinsha suture during the Late Triassic or Early Jurassic (Xiao *et al*., 2002), followed by the docking of the Lhasa terrane against the Qiangtang block along the Bangong-Nujiang suture during the Late Jurassic (Dewey *et al*., 1988), although the precise age of suturing and subsequent reactivation by other collisions are still debated. The Indian subcontinent in turn collided with these terranes along the Yarlung-Zangbo suture during Late Cretaceous to Eocene time (Murphy *et al*., 1997).

The Qaidam Basin is relatively a lower elevation region of the northeast Tibetan Plateau bounded by the Altyn Tagh fault to the northwest, the Kunlun fault to the south, and the Nan Shan fold-and-thrust belt to the northeast. The nature of Qaidam's basement is not known because it is buried under thick cover strata and still no sufficient

borehole or geophysical data are available. Cover strata consist of Cenozoic clastics of terrestrial facies. Tertiary continental sediments in the Qaidam Basin reach several kilometers and serve as the main oil producing layers in the basin. Qaidam's mountain ranges probably formed as ramp anticlines stacked upon a crustal-scale thrust fault. However, compared to complexly deformed surrounding areas, the Qaidam Basin shows only limited deformation of Cretaceous to Tertiary sedimentary cover.

In summary, these geological observations provide fundamental constraints on tectonics models of Chinese blocks. Although the geology of the fold belts between these major Chinese blocks and terranes has the potential of constraining the times of collisions more tightly than the geology of the blocks themselves, the complexity of these fold belts has led to widely different views of the tectonic history of the region. With Gondwanaland in high southern paleolatitudes during the Late Paleozoic and the Chinese blocks nowadays situated at mid-northern latitudes, paleomagnetism is obviously an ideal tool by which to test various Paleozoic paleogeographic models and to unravel the later northward relative motions of these blocks and terranes if they were part of Gondwanaland. As explored below, paleomagnetism offers an independent—and complementary—source of constraints in terms of the style of convergence and timing of amalgamation of individual continental blocks.

Paleomagnetic constraints on tectonic history of major chinese blocks

The tectonic relationship between crustal blocks can be constrained by comparison of their paleomagnetic poles. If reliable poles of the same age from two blocks are significantly different, one must conclude that the two blocks have moved relative to one another sometime after remanent magnetization was acquired. The converse is not necessarily true, since it is not possible to assign longitudinal position to the paleocontinents according to the GAD model.

Paleomagnetic investigation in China began in the early 1960s. Great development in the acquisition of paleomagnetic data has been made since early 1980s. In particular, the Cretaceous is well-studied paleomagnetically both in terms of data quality and area distribution (see Figure P47). The Global Paleomagnetic Data Base nowadays has included studies from the Chinese literature, but there is still a large variation in quality and reliability of the poles. Detailed reviews of paleomagnetic poles ("paleopoles" for short) for Chinese blocks have been given in several papers and books (e.g., Lin *et al*., 1985; Zheng *et al*., 1991; Enkin *et al*., 1992; Zhao and Coe, 1987; Van der Voo, 1993; Zhao *et al*., 1996, 1999; McElhinny and McFadden, 2000; Zhu and Tschu, 2001; Yang and Besse, 2001). Several additional paleopoles have become available since 2001. Up to 2003, a total of 415 paleomagnetic poles have been published for Chinese blocks and terranes. Some of these poles are still subject to debate and interpretation. Any serious use of paleomagnetic data from China should always involve independent evaluation and assessment of each study. Thus, our intention is not to list the detailed references for these 415 paleopoles and discuss exhaustively the significance of data. Readers are referred to the Global Paleomagnetic Data Base Version 4.6 (www.tsrc.uwa.edu.au/data_bases) for more information. These paleomagnetic poles, from both Chinese and English language journals and books, are briefly outlined below.

Paleomagnetic studies in the North China block (+Hexi Corridor and Korea): 118 Poles

Quaternary (3 poles)

The Quaternary is represented by only three paleomagnetic poles: two studies on the Chinese Loess Plateau in Shaanxi province and one study on basalt flows in Shandong province.

Tertiary (7 poles)

Little work has been done on Tertiary rocks in North China as well: Only a total of seven paleopoles have been reported from volcanic and sedimentary rocks from Inner Mongolia, Hebei, Shandong, Shanxi, and Gansu provinces. Most of the results passed reversal tests, although the reliability of some of the studies can still be argued. The scarcity of reliable paleomagnetic poles for these younger geologic time intervals seems to be a result of the low research priority given to them.

Cretaceous (16 poles)

Twelve Cretaceous paleopoles have been reported from Ningxia, Gansu, Shaanxi, Shanxi, Henan, Shandong, and Inner Mongolia of the NCB. In addition, four studies on Cretaceous rocks from South Korea have been published in the literature. These Cretaceous-aged poles obtained from widely separated regions are consistent with each other, suggesting that these areas occupied the same relative positions in terms of paleolatitudes since the Cretaceous. Clockwise vertical-axis block rotations of 30° of Korea relative to the NCB, however, are implied by the Cretaceous data for Korea.

Jurassic (12 poles)

Only one Early Jurassic pole is available from Shaanxi province. Four Late Jurassic poles have been published from three areas of Inner Mongolia and Shanxi provinces and six paleopoles are available for the Middle Jurassic that were derived from sedimentary rocks in Shaanxi and Shanxi provinces. One Late Jurassic pole was reported from Korea, again showing the region has rotated clockwise with respect to China. There is still a worldwide deficiency of Early Jurassic paleomagnetic poles, and North China is no exception.

Triassic (23 poles)

The Late Triassic in the NCB has only been studied in one region of Shanxi province (2 poles). Nine paleopoles were reported from Middle Triassic formations in Shaanxi and Shanxi provinces. Twelve paleopoles are available for the NCB from the Early Triassic sections in Liaoning, Shandong, Shanxi, and Shaanxi provinces, but five of them are clearly questionable.

Permian (26 poles)

A total of 19 Late Permian poles have been obtained from 14 sections distributed over Hebei, Shanxi, Shaanxi, and Inner Mongolia. There are also four Late Permian paleopoles available for Korea. In contrast, only three Early Permian paleopoles are available from Shaanxi and Shanxi province, which are significantly different from each other. Like the Early Triassic, the distribution of the Late Permian paleomagnetic poles is streaked along a small circle centered on the NCB, indicating significant internal deformation that has caused local rotations.

Carboniferous (6 poles)

Two studies have reported Middle-Late Carboniferous results from Shanxi and Shaanxi province for the NCB. None of them was considered reliable (Zhu and Tschu, 2001), underscoring that more paleomagnetic study of Carboniferous rocks should be a future research focus. Four preliminary Late Carboniferous paleomagnetic poles were reported from Korea.

Devonian and Silurian (5 poles)

Because of the great sedimentary hiatus during the Devonian and Silurian for the NCB, three studies were conducted in the Alashan/Hexi Corridor in the Ningxia Hui Autonomous region on Middle to Late Devonian and Silurian red beds. Two Middle to Late Devonian and

three Middle to Late Silurian paleopoles have been published from these studies.

Ordovician (10 poles)

Nine paleopoles have been obtained from Liaoning, Hebei, Shandong, Shaanxi provinces and the Ningxia Hui Autonomous region that are distributed along a small circle centered on the NCB, indicating local rotations. One Early Ordovician pole was obtained from Korea. There was a dispute on the magnetic polarity of the stable magnetization from the Ordovician rocks in China, which was resolved by a recent magnetostratigraphic study on rocks spanning the Cambrian/Ordovician boundary and into early Ordovician.

Cambrian (10 poles)

Ten Cambrian paleopoles have been reported for the NCB that were derived from rock formations from Liaoning, Shandong, Shanxi, Shaanxi, and Ningxia. These poles can be grouped into three clusters. One group (3 poles) is close to the Triassic pole of the NCB and without stability tests. These poles are suspicious because they may have been remagnetized in the Triassic. Poles in the second group fall near the equatorial area of the western Atlantic while those in the third group are in the eastern Atlantic. The scatter of paleopoles may result from the local rotation of sampling areas or unsatisfactory removal of a second magnetization component.

Paleomagnetic study in the South China block: 204 poles

Quaternary (5 poles)

Early Quaternary poles were obtained from a basalt formation in Jiangsu (1 pole) and clays from Yunnan (4 poles). No details concerning sampling sites and laboratory work were given.

Tertiary (24 poles)

Tertiary paleomagnetic data are numerous for the SCB. A total of 24 paleopoles are available for the SCB, which come from red beds and basalt formations in Yunnan, Guangdong, Sichuan, Hubei, Hunan, Zhejiang, and Jiangsu provinces.

Cretaceous (26 poles)

Of the 26 paleopoles determined for the Cretaceous, 12 come from sedimentary rocks in Sichuan province. The rest are obtained from red beds and mudstones in Guangxi, Fujian, Yunnan, and Guangxi provinces. There are two poles obtained from volcanic rocks in Zhejiang and Hong Kong, respectively.

Jurassic (31 poles)

Fourteen poles have been published for the Late Jurassic of the SCB, which were obtained from sandstone and mudstone formations in Zhejiang, Sichuan, Anhui, and Yunnan provinces. The Middle Jurassic is represented by 11 paleopoles that come from sedimentary and volcanic rocks from Guangxi, Hubei, Anhui, Sichuan, Guizhou, and Hong Kong. Six paleopoles from sandstone formations in Sichuan, Hubei, Anhui, Guangxi, and Yunnan are available for the Early Jurassic.

Triassic (49 poles)

Fifteen Late Triassic poles have been isolated from siltstone sites in Sichuan and Yunnan provinces. Nine Middle Triassic poles were reported from limestone and red sandstone in Hubei, Jiangsu, Guizhou, Sichuan, Hunan, and Guangxi provinces. Most of poles from the Early Triassic limestone formations are from Sichuan. It is important to note that Early Triassic poles from limestone and sandstone formations of Jiangsu and Zhejiang in the eastern extreme of the block are coherent with the poles from west (Sichuan), suggesting that the SCB has behaved more or less rigidly since at least this period.

Permian (30 poles)

Many high-quality paleomagnetic data for the Late Permian have been presented since McElhinny *et al.*'s (1981) pioneering paleomagnetic paper on the Emeishan Basalt from Sichuan. Those poles are now from both the Emeishan basalt from Yunnan and Guizhou provinces and red limestone and sandstone from Hubei, Zhejiang, Guangdong, and Sichuan. In contrast, only one Early Permian pole is reported from a limestone section in Hubei province. It is worth mentioning that, like many other fields in Earth sciences, progress in the paleomagnetic data of China has grown through repeated trials, criticisms, and improvements. Some studies may encompass entire lifetimes of devoted work. The debate on the age of magnetization of the Late Permian Emeishan Basalt from the SCB is a case in point. Debate has continued for the last 15 years as to whether the observed magnetic direction is primary or secondary. Although a reported positive conglomerate test by Huang and Opdyke (1995) effectively refuted the suspicion that the directions from the Emeishan Basalt may represent a remagnetization of Triassic or even Jurassic age, it may still require more extensive investigations to unequivocally settle the question.

Carboniferous (5 poles)

Out of the 5 Carboniferous poles published from limestone and mudstone formations in Zhejiang, Yunnan, and Fujian provinces, none of them, however, can demonstrate the age of magnetization with certainty, reflecting the still insufficient inventory of Chinese paleomagnetic data.

Devonian (5 poles)

Five poles of Devonian age for the SCB are reported from sandstone formations in Zhejiang, Jiangsu, Yunnan, and Sichuan. The data set is relatively small and also subject to debate. Only one pole was selected by McElhinny and McFadden (2000) to be included in their book.

Silurian (8 poles)

Silurian poles for the SCB were reported from red beds, sandstone, and limestone in Guizhou, Zhejiang, Hubei, Yunnan, and Sichuan provinces. These poles have been all determined using the modern methods and analytical techniques.

Ordovician (8 poles)

Eight Ordovician paleomagnetic poles have been reported for South China that were derived from limestone and sandstone in Zhejiang, Hubei, Yunnan, and Sichuan province. These poles generally have poor quality.

Cambrian (5 poles)

The collected Cambrian poles were derived from rocks from Zhejiang, Hubei, and Yunnan provinces. The poles are very different from Cambrian poles of the NCB, suggesting that North and South China were two different continental blocks during Cambrian.

Paleomagnetic study in the Tarim and Junggar basins: 52 poles

Quaternary (1 pole)

Only one study of Quaternary basalt from the southeast of the Tarim Basin has been published. The age of the basalt is still in dispute, but it seems reasonable for it to represent the Quaternary.

Tertiary (11 poles)

Tertiary paleomagnetic poles for Tarim were mainly obtained from the Aertushi region of western Tarim, the Kuche depression of northwest Tarim, and the Maza Tagh range in the central Tarim Basin. Up to 1990, the paleomagnetic database for Tarim was very sparse. The last 13 years saw a major increase in the number of paleomagnetic data for Tarim, which is rather fortunate because tectonic rotations caused by the Indian collision might be constrained by such data.

Cretaceous (10 poles)

Eight Cretaceous poles were reported for Tarim, all of them from the Kuche depression in northwestern Tarim. Of the eight poles, six were derived from red beds and two were from basalt formations in the Tuoyun area of western Tarim. Two Cretaceous poles were published for the Junggar basin, which are close to Cretaceous poles for Tarim.

Jurassic (4 poles)

One Late Jurassic and three Middle Jurassic pole are available for Tarim. Both were derived from red bed formations in southwestern Tarim. No coeval pole is available for the Junggar basin.

Triassic (3 poles)

The Triassic of Tarim is represented by three poles (one each in the Late, Middle, and Early Triassic). Among them, only the Late Triassic was well studied through a magnetostratigraphic investigation.

Permian (14 poles)

Permian paleomagnetic poles for Tarim are mainly from volcanic rocks in the Aksu, Keping, and Kuche areas of western Tarim, with 7 poles for Late Permian and 5 poles for the Early Permian. Two Late Permian poles have been reported for the Junggar Basin, which is concord with the Permian poles for Tarim. The number and quality of Permian paleopoles for Tarim is quite impressive, suggesting one should treat these poles seriously. No paleopoles older than Permian were reported from the Junggar basin.

Carboniferous (4 poles)

Four Carboniferous paleopoles are available for Tarim, which were all derived from sedimentary rocks (limestone and sandstone) from South western Tarim.

Devonian (3 poles)

Three Devonian paleomagnetic poles were reported for the Tarim, obtained from both the north and south rims of Tarim.

Silurian (3 poles)

There are three middle Silurian poles for Tarim. The magnetization is dominated by an extremely weak, recent-field component of magnetization that was carried by goethite. Clearly, these poles are unacceptable for tectonic study.

Ordovician (1 pole) and Cambrian (1 pole)

Although the number of poles for these two periods is extremely sparse, the reported poles each pass fold and reversal tests and place Tarim in low paleolatitudes during Cambrian and Ordovician.

Paleomagnetic studies in the Tibet and Qaidam basin: 38 poles

Since the early 1980s, paleomagnetic investigation has been an important aspect of all the major geologic expeditions conducted on the Tibetan plateau. While paleomagnetic investigations of the Cretaceous and younger rocks from the plateau have yielded useful constraints for the Lhasa and Qiangtang terranes (Achache *et al*., 1984; Lin and Watts, 1988; Otofuji *et al*., 1989; Huang *et al*., 1992; Chen *et al*., 1993), studies on the Paleozoic formations were often hampered by lack of favorable lithology, multiphase deformation, and metamorphism that has obliterated the primary magnetization (Lin and Watts, 1988; Otofuji *et al*., 1989; Huang *et al*., 1992). Triassic and Jurassic paleomagnetic directions also tend to be remagnetized (Chen *et al*., 1993). As a result, there are a total of 8 Tertiary and 13 Cretaceous paleomagnetic poles for Tibet.

Among the Late Cretaceous paleomagnetic results from Tibet, those reported from south Tibet (Achache *et al*., 1984), east Qiangtang (Huang *et al*., 1992), and west Qiangtang (Otofuji *et al*., 1989; Chen *et al*., 1993) appear to have high quality, each with positive fold test result. However, there is a serious problem in interpreting these Late Cretaceous data in terms of paleolatitude. The study on the Late Cretaceous Takena red beds and Paleocene andesites of the Lhasa Block yielded a paleolatitude of 15–20° N for Lhasa. It should be pointed out that the Paleocene Lingzizong volcanics in the Lhasa area give consistent result (with positive fold and reversal test) with the underlying Cretaceous strata (Achache *et al*., 1984) and provide a notable example that both red beds and volcanic rock in the Lhasa area recorded the same ancient magnetization. Lin and Watts (1988) sampled the Takena formation in the Linzhou area as well as Late Cretaceous volcanic units in Nagqu and Qelico. Their data pass a fold test and give slightly lower paleolatitudes ($7.6 \pm 3.5°$ N), but still similar to the results of Achache *et al*. (1984). If we use the mean of these three results, the paleolatitude of Lhasa in the Late Cretaceous would be about 12.5° N. A comparison of this value with that predicted by the reference pole (Besse and Courtillot, 1991) would confirm the conclusion of Achache *et al*. (1984, p. 10335) that crustal shortening of the order of 2000 km has occurred between Lhasa and Eurasia since the Late Cretaceous. Calculations of shortening using the Early Tertiary Linzizong volcanic rocks yield a similar amount of northward displacement of the Lhasa terrane. This is compatible with other geophysical and geological estimation that India has moved about 2500 km northward about 50 Ma (e.g., Dewey *et al*., 1988). However, when comparing the paleolatitude of Lhasa with that of west Qiangtang (Chen *et al*., 1993) and Tarim/Junggar (Li *et al*., 1988; Chen *et al*., 1991), the data suggest that there is no net crustal shortening between Lhasa and west Qiangtang/Tarim/Junggar from the Late Cretaceous to present. In other words, the entire 2000 km of northward displacement of the Lhasa block suggested by the Late Cretaceous paleomagnetic data would have to be taken up in the region to the north of Junggar. This would conflict with existing understanding of the formation of the Tibetan plateau by either the crustal shortening model (Dewey *et al*., 1988) or the tectonic extrusion model (Tapponnier *et al*., 2001), or a combination of the two (Harrison *et al*., 1992). In addition, there is no geologic evidence to suggest a candidate place between Siberia platform and Junggar/Tarim to accommodate crustal shortening of this magnitude in the Tertiary. If the configuration for most or all of the Tibetan plateau has been created by the India/Asia collision, then the Late Cretaceous paleomagnetic results from Lhasa and west Qiangtang /Tarim/Junggar cannot both be correct. Obviously, further work is badly needed to solve this problem, and a reliable paleomagnetic pole from central Qiangtang would provide a direct test.

For the Qaidam Basin, there are 5 Jurassic, 3 Cretaceous, and 9 Tertiary poles reported from paleomagnetic investigations of the basin. These studies were designed to detect possible clockwise rotation of Qaidam basin, as implied by extrusion models. Rotation within the Qaidam-Altyn Tagh region is very controversial, and existing paleomagnetic data are contradictory. Halim *et al*. (2003) presented one Late Jurassic pole from red beds in Huatugou of Qaidam basin. This pole indicates negligible northward convergence of the Qaidam block with respect to Tarim since Late Jurassic times, but implies a significant relative clockwise rotation of the studied area with respect to Tarim ($\sim$16°). Similarly, Chen *et al*. (2002) reported that three widely

spread areas in Qaidam exhibit 20° clockwise rotations during the Late Oligocene-Late Miocene time. However, recent study from the east end of the Altyn Tagh fault by Gilder *et al*. (2001) shows that area has rotated 27° ± 5° counterclockwise with respect to the Eurasian reference pole during the last 19 Ma. Otofuji *et al*. (1995) also suggest that their sampling sites along the Altyn Tagh fault showed 7.4° ± 5.2° counterclockwise rotation during the last 1.0 Ma. On the other hand, Dupont-Nivet *et al*. (2002, 2003) and Rumelhart *et al*. (1999) argue for no significant Neogene vertical-axis rotation in northern Tibet since Eocene. These results would contradict extrusion models which imply clockwise rotation of Qaidam basin at rates approaching 1°/Ma.

Paleo-positions of Chinese blocks

Although a great number of Late Mesozoic and Cenozoic paleomagnetic results are available, the current paleomagnetic data base for China is still limited to allow a satisfactory interpretation of the questions concerning the paleogeography of China and the implications for Gondwanaland. Because many studies are performed at a single locality or over a small region and are of variable quality, paleomagnetists must critically assess and update the previously published data from China and Eurasia in order to better understand the tectonic relationship between the Chinese blocks and their relative motions with respect to Eurasia (i.e., Europe, Siberia, and Kazakhstan) during the Phanerozoic. Basic criteria for an acceptable paleomagnetic pole determination should include (i) age of the magnetization; (ii) structural control; and (iii) paleomagnetic laboratory treatment (demagnetization) of sufficient samples.

After such evaluations and assessments of each published study, the current state of paleomagnetic knowledge can be synthesized as follows: during Early (~530 Ma) and early-middle Late Cambrian (505 Ma), the paleolatitudes of South China, Tarim, and Australia permit them to be next to each other. North China can be placed between Siberia and Australia. All these blocks were in the area around the equator. Between late Middle to early Late Cambrian (~505 Ma), Tarim, North and South China Blocks lay closer to Australia and shared close trilobite affinities until Late Cambrian (~490 Ma). The counterclockwise rotation of Gondwanaland during the Cambrian was reversed during the Ordovician. The change in sense of rotation occurred at the Cambro-Ordovican boundary. The North and South China Blocks, and Tarim, remained in low latitudes, and rotated sinistrally along the Cimmerian margin of Gondwanaland towards positions they are inferred to have occupied later on the basis of faunal relationships.

By Early Silurian time (430 Ma) Siberia remained in the vicinity of the equator but has moved slightly northward to a position north of the equator. Gondwanaland appears to have moved southward and rotated clockwise. North China may also have rotated clockwise and appears to be compatible with a position next to the northern margin of Australia, which also fits the distribution of freshwater fish fauna on the two continents. While South China remains in roughly the same position, Tarim appears to have rifted off the SCB by rapid clockwise rotation and northward displacement.

At Middle Devonian time (~380 Ma) the location of South China suggests that it may have rifted off Australia. Tarim is continuing its northward journey. Siberia has also drifted northward and rotated clockwise. North China, on the other hand, is still on the equator. The development of highly endemic vertebrate faunas on both the North and South China Blocks indicates that these two blocks were separated from Gondwanaland during Early-Middle Devonian.

Later at the Late Devonian time (~354 Ma), Gondwanaland began to drift rapidly across the south pole, and by mid-Carboniferous (320–310 Ma), it has collided with Laurussia to start assemblage the supercontinent Pangea. It was for the first time that Australia had been drifted close to the south pole during the Paleozoic. The major Chinese blocks remained in low and medium paleolatitudes and started to develop their distinctive Cathaysia flora. The Late Carboniferous poles for Tarim and Eurasia are in agreement, suggesting that these regions could have started the process of accretion by Late Carboniferous time.

The paleogeography of the Early Permian (~280 Ma) remained more or less the same as the mid-Carboniferous, except that Siberia collided with Laurussia along the Urals. Mongolian terranes accreted to the North China, the first phase of continental collision between the NCB and SCB at their eastern ends started soon. Supercontinent Pangea was complete at this time.

Pangea endured from ~280 Ma to ~175 Ma when the first seafloor spreading began in the North Atlantic Ocean. During this time, several Tibetan terranes (Kulun, Songpan-Ganze, and Qiangtang) accreted to Eurasia. The apparent polar wander paths for Eurasia and North and South China converge during the Late Jurassic (~150 Ma) and are tightly grouped throughout the Cretaceous and Tertiary, implying that large relative motion (translation and/or rotation) between the blocks was accomplished by Late Jurassic. On the other hand, although the paleolatitudes for Tarim and Eurasia have been similar since Carboniferous time, a close inspection reveals that there is a significant difference between the Late Permian, Early Triassic and Late Jurassic through Cretaceous poles for Eurasia/Siberia and Tarim, indicating relative motions between Tarim and Eurasia.

Tectonic models inferred by the paleomagnetic data

The paleomagnetic results available from China allow plausible tectonic models to be constructed for the amalgamation of the Chinese blocks with themselves and with Eurasia (Zhao and Coe, 1987; Zhao *et al*., 1996). The collision between Siberia/Eurasia and the Mongolia-NCB initially occurred in the Permian near the western end of their boundary in the Irtysh-Zaysan region (50° N, 75° E), which is near the edge of the Kazakhstan Block (in today's geographical frame). Suturing progressed eastward as the Mongolia-NCB rotated counterclockwise about 90° in relation to Eurasia during the Early Mesozoic with a scissors-like motion (see Figure P48). The amalgamation of North and South China took place in the Late Permian by a similar but antithetic mechanism, with collision first occurring near the eastern end (about 30° N, 120° E) of the Qinling Fold belt and diachronously suturing from east to west due to a clockwise rotation of 65° of South China relative to North China.

Early Triassic paleomagnetic poles for all continental blocks are very similar to those for the Late Permian, consistent with the same scissor model discussed above and reinforcing the tectonic model. Reliable Middle and Late Triassic paleomagnetic data for the NCB, SCB, and Eurasia are still relatively sparse. Little change appears to have taken place by Middle Triassic time, with about 65° of rotation still left between Eurasia and the NCB to reconcile their poles.

In the Early Jurassic, more than half of the Qinling Sea between the NCB and SCBs was subducted, and so was the Mongol-Okhotsk Ocean between Eurasia and the NCB. Therefore, paleomagnetic data suggest that most of the relative rotation between the Chinese blocks took place during the Late Triassic and Early Jurassic. By the Middle Jurassic, the Qinling Sea is almost completely closed, although this may not be entirely correct due to the relatively large uncertainty in the SCB poles. The Late Jurassic and Early Cretaceous paleomagnetic poles for the NCB and SCB are statistically indistinguishable at this time, suggesting that accretion between the two blocks was accomplished some time between the Middle and Late Jurassic. However, the Chinese blocks were still significantly south of Siberia, with ~1000 km of the Mongol-Okhotsk Ocean to be closed north of Mongolia. The final closure of the Mongol-Okhotsk Ocean took place sometime in Cretaceous.

The tectonic model mentioned above contradicted widely held views at the time that the NCB and SCB were joined by the Devonian at the latest and that the Central Asian Fold Belt, which runs across North China just north of 40° N, is the zone where China was sutured to Siberia in Permian time. Rather, the paleomagnetic evidence suggested that in both cases suturing was completed much later, in Mid-Mesozoic time,

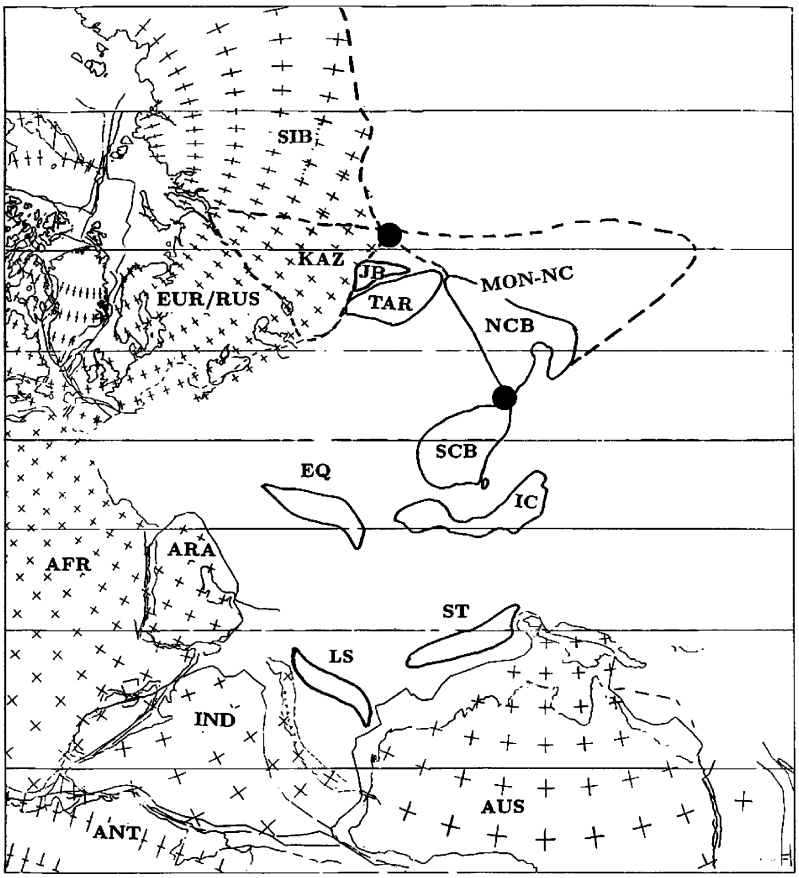

Figure P48 Schematic reconstruction of Mongolia-North China (MON-NC), Europe-Siberia-Kazakhstan (EUR-SIB-KAZ), Tarim (TAR), Junggar Basin (JB), South China block (SCB), Africa (AFR), Arabian Shield (ARA), India (IND), Australia (AUS), Antarctic (ANT), the East Qiangtang (EQ), Lhasa (LS), Indochina (IC), and Shan-Thai (ST) blocks in Late Permian time. Mecator Projection. After Zhao *et al.* (1990).

and that it was a composite Mongolia-North China plate, not the NCB, that became sutured to Siberia Mesozoic time in a zone much further north along what is termed the South Siberian Fold Belt. Furthermore, the paleomagnetic data suggested in both cases a very simple mechanism involving a scissors-like closing of the intervening ocean basins by antithetic senses of rotation about the points of initial collision at the eastern and western ends of the convergence zones of the southern and northern suture zones, respectively. These paleomagnetic models have been reinforced by many later studies and backed up by reinterpretation of relevant geological information, such as the propagation of abrupt regional and local changes from marine to continental basin deposition and of syncollisional to postcollisional alkalic granites in the collision zone. Therefore, here is a case where paleomagnetism has again provided first-order contributions in deciphering continental collision and amalgamation.

Paleomagnetic implications concerning tectonic controversies in China

Implications for the duration of continent-continent collisions

As noted above, the scissor model of NCB-SCB collision based on paleomagnetic data matches the change in sedimentary style from marine to continental on the northern margin of the SCB. Both paleomagnetic and geologic data agree that the onset of collision occurred in Permian to Triassic time. The data sets diverge, however, regarding the end (duration) of the collision, with the paleomagnetic data suggesting younger estimates (Middle Jurassic) than geological indicators (Late Triassic) by 20–30 Ma. Part of the discrepancy could be the lack of more reliable Late Triassic to Middle Jurassic paleomagnetic data from both blocks. Further studies could show that the paleomagnetic poles of Early Jurassic or Late Triassic age are indistinguishable, thereby bringing the paleomagnetic and geological data sets closer into agreement. On the other hand, it is possible that the rotation suggested by the paleomagnetic data also includes postcollisional shortening between the two blocks. Taking the ongoing India-Asia collision as an example of typical continent-continent collisions, deformation and shortening could continue at least 50 Ma after initial contact of the two plates. Such postcollision shortening could also potentially lead the age of initial India-Asia collision based on paleomagnetic data to be somewhat younger than those based on stratigraphic data.

Tertiary low-paleolatitude dilemma of western China

As the Chinese paleomagnetic database grows, several research teams are continuing to discover the outstanding regional disagreement between the observed and predicted Cenozoic paleomagnetic directions from red bed formations in western China. The inclinations of stable magnetization in Cretaceous red beds from Tarim and surrounding region's are somewhat shallower than expected using Besse and Courtillot (2002) APWP Cretaceous reference pole for Eurasia, whereas the Tertiary red beds are even more shallow using the corresponding Tertiary reference pole. The inclinations translate to anomalously low

paleolatitudes. If all these paleomagnetic data, the ages, and the GAD hypothesis were correct, then in the Cretaceous Tarim would have been somewhat further south with respect to Eurasia compared to its present situation, relatively even further south when the Tertiary red beds were magnetized, and then had to move to its present more northerly relative position after that time. This implies a southward (extensional) relative displacement away from Eurasia in the period between the times when the Cretaceous and Tertiary redbeds were magnetized, and significantly more northerly (compressional) relative displacement toward Eurasia after the Tertiary red beds were magnetized, a scenario that is geologically indigestible. Recent results from Cretaceous red beds in the Hexi-Corridor (central China) show that there is no evidence that red beds there suffered the same inclination shallowing as the neighborhood Cenozoic red beds to the west (Sun *et al*., 2001; Chen *et al*., 2002). A review of published poles also confirms previous analyses that red beds from South and North China do not reveal the shallow inclination and these blocks (plus Mongolia) and Siberia have not undergone very significant internal deformation since the Cretaceous (Besse and Courtillot, 2002). It appears that some red beds suffer from inclination error, and others do not. The task is thus to develop ways to identify which of the Tertiary red beds do and do not undergo inclination shallowing.

The most direct way would be to obtain reliable Tertiary paleomagnetic results from volcanic rocks and compare them with inclinations of coeval red beds in the same study area. Two such studies have reported contrasting results: (1) the Paleocene Lingzizong volcanics in the Lhasa area give consistent result (with positive fold and reversal test) with the underlying Cretaceous strata (Achache *et al*., 1984), providing a notable example that both red beds and volcanic rock in the Lhasa area recorded the same ancient magnetization; and (2) Early Cretaceous red beds and underlying basalt flows from Tarim and central Asia fold belt (Gilder *et al*., 2003) have directions that pass both fold and reversal tests, but the mean paleolatitude of the Early Cretaceous red beds is 11° lower than that of the Early Cretaceous basalts. Obviously, more studies should be conducted on Tertiary volcanic and red sedimentary rocks from the same area.

Tectonic affiliation of the Korean peninsula

The question about the Korean Peninsula's affinities with both the NCB and SCB is one of the highly charged controversies in Asian tectonics. The lack of knowledge about this question hampers our understanding concerning the models of collision of eastern Asian blocks and their paleogeographic settings. Pre-Cretaceous paleomagnetic poles for Korea are all different from each other and make it difficult to compare the coeval poles from the NCB and SCB. At first glance, Triassic and Jurassic paleomagnetic poles for Korea published prior to 1994 are indeed somewhat similar to coeval ones from the SCB, and this was perhaps the reason to lead some workers to suggest that Korea and South China may have behaved as a single tectonic block since the Triassic. However, all these poles that apparently correspond to the SCB poles were derived from rocks within the Okchon zone, which is known to be a site of severe deformation in the Mesozoic. In fact, Cretaceous remagnetization of Carboniferous rocks has been concluded for several previous published results. Although detailed structural analysis and mapping are still insufficient to unravel the kinematic history of the Okchon fold belt and assess its effects on these paleomagnetic poles, the proximity of these poles to the SCB poles may be a coincidence.

If one leaves out these poles derived from the Okchon zone and merely retains those poles derived from areas bordering the Okchon, a striking feature between the Korean and NCB poles emerges: the Late Permian, Early Triassic, and Late Jurassic poles for Korea are systematically displaced some 30° eastward with respect to the coeval poles of the NCB. A 30° clockwise rotation of Korea about a vertical axis brings these poles into general coincidence with those coeval poles for the NCB. Thus, paleomagnetic study suggests that the whole region was part of the North China landmass at least as early as Late Permian and rotated clockwise by about 30° with respect to the NCB during the Cretaceous (Zhao *et al*., 1999).

It is apparent that the rotated (or corrected) poles show large apparent polar wander motion of Korea between Early Triassic and Late Jurassic, replicating those found in the paleomagnetic results from the NCB. Late Jurassic paleomagnetic poles for the NCB, SCB, and Korea are statistically indistinguishable, reinforcing the hypothesis that the accretion of the NCB and SCB was finished at this time. Thus, the NCB-Korea connection is not only consistent with the majority geologic observations, suggesting affinities between the two blocks, but also consistent with the collisional tectonic history of the eastern Asian margin derived from paleomagnetic data.

Terrane accretion between east and west Qiangtang

Comparison of paleomagnetic data obtained from east and west Qiangtang shows a problem that obstructs our understanding of terrane accretion in Tibet. The Cretaceous paleolatitudes of Otofuji *et al*. (1989) and Huang *et al*. (1992) in the Markam area of east Qiangtang are similar to the expected paleolatitudes for the sampling locality. The data would suggest that east Qiangtang was 21° ± 10° farther north than expected for Lhasa and 22° ± 11° farther north than expected for western Qiangtang. Taken at face value, these data would suggest that no significant crustal shortening has taken place north of east Qiangtang since at least the Late Cretaceous. The 2000 km shortening of Lhasa must have been accommodated between the Qiangtang and Lhasa blocks in the Tertiary. On the other hand, west Qiangtang must be close to the Lhasa trerrane in Late Cretaceous time, so there should be a suture between east and west Qiangtang. Huang *et al*. (1992) interpreted their paleomagnetic observation in terms of a giant right-lateral transpressional zone advocated by Dewey *et al*. (1998). Chen *et al*. (1993), on the other hand, suggested that east Qiangtang may have belonged to South China or to a block that was separated from western Qiangtang.

Tectonic rotational history of northern Tibet

A closely related question is the tectonic rotational history of northern Tibet, which is often related to uplift and deformation. Magnetic declinations, which are not typically affected by depositional compaction, can be compared to expected magnetic directions to assess the extent to which regions within the northern Tibetan plateau have rotated about vertical axes with respect to stable Eurasia. In eastern Tibet, Cretaceous and Tertiary paleomagnetic data indicate large amounts—in the order of 40°—of clockwise rotation in the eastern Himalayan syntaxis (e.g., Achache *et al*., 1984; Huang *et al*., 1992), which is consistent with right-lateral simple shear and associated oroclinal bending. However, paleomagnetic data obtained from Cretaceous and Tertiary red sedimentary rocks of western Qiangtang (Chen *et al*., 1993) show no significant Neogene vertical-axis rotation in northern Tibet since the Late Cretaceous. Thus, all paleomagnetic data for tectonic rotations are not in agreement; some of them are apparently contradicting extrusion models that imply clockwise rotation of the region. These existing results, however, should be incorporated with forthcoming new results to advance our understanding of the growth history of the Tibetan plateau.

Summary

Plate tectonics views the whole Earth as a dynamic system in which the internal heat drives lithospheric plates in relative motion with respect to each other. Paleomagnetism enables geologists to view important aspects of continental movements in the past namely, changes in latitude and orientation relative to the geographic poles. It is important to realize the crucial role that paleomagnetic studies in China have played in providing the tectonic framework that guides geological investigation and interpretation. Until McElhinny *et al*.'s pioneering paleomagnetic paper in 1981 revealed discrepancies in Late

Permian paleolatitudes on the order of 20°, literally all geological interpretation concurred (incorrectly) that North and South China had been in place as part of the Eurasian landmass since the Early Permian or before. For some years after, with a notable exception (Klimetz, 1983), few geologists took these paleomagnetic results seriously enough to question the prevailing view. Meanwhile, additional paleomagnetic data began to accumulate in support of McElhinny *et al*.'s findings: discrepancies not only in Late Permian and but also in Early Mesozoic poles between South China and Siberia (Opdyke *et al*., 1986), between North and South China, and between North China (including Mongolia) and Eurasia (see Enkin *et al*., 1992 for references). It was on the basis of paleomagnetic evidence that the proposal was first made that South and North China collided at the eastern end of the Qinling belt at the close of the Permian and sutured progressively westward by relative rotation in the Mesozoic (Zhao and Coe, 1987), then backed up by reinterpretation of relevant geological information from the literature. Likewise, paleomagnetic evidence was the original basis of the similar mechanism of opposing sense (collision in the west followed by progressive rotation and suturing to the east) proposed for the incorporation of northern China into Eurasia in the Mesozoic (Zhao and Coe, 1989; Zhao *et al*., 1990).

Although paleomagnetism has already made a dramatic contribution to the tectonics of China, this is just the beginning. By carefully gathering the available paleomagnetic, geological, and geophysical data and integrating them, Earth scientists are testing new hypotheses about smaller scale, intracontinental deformation. The tectonics of China will continue as a fruitful focus in the study of the dynamics of the Earth.

Xixi Zhao and Robert S. Coe

Bibliography

Achache, J., Courtillot, V., and Zhou, Y.X., 1984. Paleogeographic and tectonic evolution of southern Tibet since middle Cretaceous time: New paleomagnetic data and synthesis. *Journal of Geophysical Research-Solid Earth*, **89**: 311–339.

Besse, J., and Courtillot, V., 1991. Revised and synthetic apparent polar wander paths of the African, Eurasian, North American and Indian plates, and true polar wander since 200 Ma. *Journal of Geophysical Research*, **96**: 4029–4050.

Besse, J., and Courtillot, V., 2002. Apparent and true polar wander and the geometry of the geomagnetic field in the last 200 Myr. *Journal of Geophysical Research*, **107**: 2300 doi:10.1029/2000JB000050.

Burchfiel, B.C., Chen, Z., Hodges, K.V., Liu, Y., Royden, L.H., *et al*., 1992. The south Tibetan detachment system, Himalayan orogen: extension contemporaneous with and parallel to shortening in a collisional mountain belt. *Geological Society of America Special Paper*, **269**: 1–41.

Burg, J.P., and Chen, G.M., 1984. Tectonics and structural zonation of southern Tibet, China. *Nature*, **311**: 219–223.

Burrett, C., and Richardson, R., 1980. Trilobite biogeography and Cambrian tectonic models. *Tectonophysics*, **63**: 155–192.

Burrett, C., Long, J., and Stait, B.,1990. Early-Middle Palaeozoic biogeography of Asian terranes derived from Gondwana. In Mckerrow, W.S. and Scotese, C.R. (eds.), *Palaeozoic Palaeogeography and Biogeography*, *Geological Society Memoir*, Bath, England. **12**: 163–174.

Chen, Y., Cogné, J.P., Courtillot, V., Avouac, J.P., Tapponnier, P., Buffetaut, E., Wang, G., Bai, M., You, H., Li, M., and Wei, C., 1991. Paleomagnetic study of Mesozoic continental sediments along the northern Tien Shan (China) and heterogeneous strain in central Asia. *Journal of Geophysical Research*, **96**: 4065–4082.

Chen, Y., Cogne, J.P., Courtillot, V., Tapponnier, P., and Zhu, X.Y. 1993. Cretaceous paleomagnetic results from western Tibet and tectonic implications. *Journal of Geophysical Research*, **98**(B10): 17981–17999.

Chen, Y., Gilder, S., Halim, N., Cogné, J.-P., and Courtillot, V. 2002. New Mezosoic and Cenozoic paleomagnetic data help constrain the age of motion on the Altyn Tagh fault and rotation of the Qaidam basin. *Tectonics*, **21**(5): 1042, doi:10.1029/2001 TC901030, 2002.

Davis, A.M., Aitchison, J.C., Zhu, B.D., and Huo, L., 2002. Paleogene Island arc collision related conglomerates, Yarlung Tsangpo suture zone, Tibet. *Sedimentary Geology*, **150**: 247–273.

Dewey, J.F., Shackleton, R.M., Chang, C.F., and Sun, Y.Y., 1988. The tectonic evolution of the Tibetan plateau, *Philosophical Transactions of the Royal Society of London Series A, Mathematical Physical and Engineering Sciences*, **327**: 379–413.

Dewey, J.F., Shackleton, R.M., Chang, C.F., and Sun, Y.Y., 1990. The tectonic evolution of the Tibetan plateau. In Sino-British Comprehensive Geological Expedition Team of the Qinghai-Tibet Plateau (ed.), *The Geological Evolution of the Qinghai-Tibet* (in Chinese). Beijing: Science Press, pp. 384–415.

Dupont-Nivet, G., Butler, R.F., Yin, A., and Chen, X., 2002. Paleomagnetism indicates no Neogene rotation of the Qaidam basin in north Tibet during Indo-Asian collision. *Geology*, **30**(3): 263–266.

Dupont-Nivet, G., Butler, R.F., Yin, A., and Chen, X., 2003. Paleomagnetism indicates no Neogene rotation of the Northeastern Tibetan Plateau. *Journal of Geophysical Research*, **108**(B8): 2386, doi:10.1029/2003JB002399, 2003.

Enkin, R.J., Yang, Z., Chen, Y., and Courtillot, V., 1992. Paleomagnetic constraints on the geodynamic history of the major blocks of China from the Permian to the Present. *Journal of Geophysical Research*, **97**: 13953–13984.

Gilder, S., Chen, Y., and Sen, S., 2001. Oligo-Miocene magnetostratigraphy and environmental magnetism of the Xishuigou section, Subei (Gansu Province, western China): Further implication on the shallow inclination of central Asia. *Journal of Geophysical Research-Solid Earth*, **106**: 30505–30521.

Gilder, S., Chen, Y., Cogne, J.P., Tan, X.D., Courtillot, V., Sun, D.J., and Li, Y.G., 2003. Paleomagnetism of Upper Jurrassic to Lower Cretaceous volcanic and sedimentary rocks from the western Tarim Basin and implications for inclination shallowing and absolute dating of the M-0 (ISEA?) chron. *Earth and Planetary Science Letters*, **206**: 587–600.

Halim, N., Chen, Y., and Cogné, J.P., 2003. A first palaeomagnetic study of Jurassic formations from the Qaidam basin, northeastern Tibet, China-tectonic implications. *Geophysical Journal International*, **153**: 20–26.

Harrison, T.W., Copeland, P., Kidd, W.S.F., and Yi, A., 1992. Raising Tibet. *Science* **255**: 1663–1670.

Hsu, K.J., Sun, S., Chen, H.H., Pen, H.B., and Sengor, AM.C., 1988. Mesozoic overthrust tectonics in south China. *Geology*, **16**: 418–421.

Hu, A.Q., and Rogers, G., 1992. Discovery of 3.3 Ga Archean rocks in north Tarim block of Xinjiang, western China. *Chinese Science Bulletin*, **37**: 1546–1549.

Huang, K., and Opdyke, N., 1995. A positive conglomerate test for the characteristic remanent magnetization of the Emeishan basalt from Southwest China. *Geophysical Research Letters*, **22**: 2769–2772.

Huang, K.N., Opdyke, N.D., Li, J., and Peng, X., 1992. Paleomagnetism of Cretaceous from eastern Qiangtang terrane of Tibet. *Journal of Geophysical Research*, **97**: 1789–1800.

Irving, E., 1964. *Paleomagnetism and its Application to Geological and Geophysical Problems*, New York: Wiley, 399 pp.

Klimetz, M.P., 1983. Speculations on the Mesozoic plate tectonic evolution of eastern China. *Tectonics*, **2**: 139–166.

Laveine, J.P., Zhang, S., and Lemoigne, Y., 1989. Global paleobotany, as exemplied by some Upper Carboniferous Pteridosperms. *Bulletin Societe Belge Geologique*, **98**: 115–125.

Li, Y.P., Zhang, Z., McWilliams, M., Nur, A., Li, Y., Li, Q., and Cox, A., 1988. Mesozoic paleomagnetic results of the Tarim Cration: Tertiary relative motion between China and Siberia. *Geophysical Research Letters*, **15**: 217–220.

Li, J.L., and Cong, B.L., 1980. A preliminary study on the early stage evolution of the Earth's crust in the North China fault block region.

In: *Formation and Development on the North China Fault Block Region,* Beijing, China: Publishing House of Academic, pp. 23–25.

Li, Z.X., Zhang, L., and Powell, C.McA., 1995. South China in Rodinia: part of the missing link beween Australia-East Antarctica and Laurentia? *Geology*, **23**: 407–410.

Li, Z.X.,1998. Tectonic history of the major east Asian lithospheric blocks since the mid Proterozoic—A synthesis. In Martin, F.J., Chung, S.-L., Lo, C.-J., and Lee, T.-Y. (eds.), *Mantle Dynamics and plate interactions in East Asia*, AGU Geodynamics Series **27**: Washington, DC: American Geophysical Union, pp. 221–243.

Li, Z.X., and Powell, C. McA., 2001. An outline of the palaeogeographic evolution of the Australasian region since the beginning of the Neoproterozoic. *Earth Science Reviews*, **53**: 237–277.

Lin, J.L., Fuller, M., and Zhang, W.Y., 1985. Preliminary Phanerozoic polar wander paths for the North and South China blocks. *Nature*, **313**: 444–449.

Lin, J., and Watts, D.R., 1988. Palaeomagnetic constraints on Himalayan-Tibetan tectonic evolution. *Philosophical Transactions of the Royal Society of London, Series A*, **326**: 177–188.

Long, J., and Burrett, C., 1989. Fish from the Upper Devonian of the Shan-Thai terrance indicate proximity to east Gondwana and south China terranes. *Geology*, **17**: 811–813.

Mattauer, M., Matte, P., Maluski, H., Qin, Z.Q., Zhang, Q.W., and Yong, Y.M., 1991. Paleozoic and Triassic plate boundary between North and South China, New structural and radiometric data on the Dabie-Shan (eastern China). *Comptes Rendus de l' Academie des Sciences—Series II*, **312**: 1227–1233.

McElhinny, M.W., Embleton, B.J., Ma, X.H., and Zhang, Z.K., 1981. Fragmentation of Asia in the Permian. *Nature*, **293**: 212–215.

McElhinny, M.W., and McFadden, P.L., 2000. *Paleomagnetism: Continents and Oceans International Geophysics Series* **73**, San Diego: Academic Press, 386 pp.

McKerrow, W.S., and Scotese, C.R., (eds.), 1990. Palaezoic paleogeography and biogeography. *Geology Society London Memoir* **12:** 435 pp.

Merrill, R.T., McElhinny, M.W., and McFadden, P.L., 1996. *The Magnetic Field of the Earth: Paleomagnetism, the Core, and the Deep Mantle.* San Diego: Academic Press, 541 pp.

Metcalfe, I., (ed.), 1999. *Gondwana Dispersion and Asian Accretion*, Final Results Volume for IGCP Project 321. Rotterdam: A.A. Balkema, VIII + 361 pp. ISBN 90 5410 446 5.

Murphy, M.A., Yin, A., Harrison, T.M., Durr, S.B., Chen, Z., Ryerson, F.J., Kidd, W.S.F., Wang, X., and Zhou, X., 1997. Did the Indo-Asian collision alone create the Tibetan plateau? *Geology*, **25**: 719–722.

Opdyke, N.D., Huang, K., Xu, G., Zhang, W.Y., and Kent, D.V., 1986. Paleomagnetic results from the Triassic of the Yangtze platform. *Journal of Geophysical Research*, **91**: 9553–9568.

Otofuji, Y., Funahara, S., Matsuo, J., Murata, F., Nishiyama, T., Zheng, X.L., and Yaskawa, K., 1989. Paleomagnetic study of western Tibet: Deformation of a narrow zone along the Indus Zangbo suture between India and Asia. *Earth and Planetary Science Letters*, **92**: 307–316.

Otofuji, Y., Matsuda, T., Itaya, T., Shibata, T., Matsumoto, M., Yamamoto, T., Morimoto, C., Kulinich, R.G., Zimin, P.S., Matunin, A.P., Sakhno, V.G., and Kimura, K., 1995. Late Cretaceous to early Paleogene paleomagnetic results from Sikhote-Alin, far eastern Russia: implications for deformation of East Asia. *Earth and Planetary Science Letters*, **130**: 95–108.

Otofuji, Y, Itaya, T., Wang, H., and Nohda, S., 1995. Paleomagnetism and K-Ar Dating of Pleistocene Volcanic-Rocks along the Altyn-Tagh Fault, Northern Border of Tibet. *Geophysical Journal International*, **120**(2): 367–374.

Ren, J.S., Jiang, C.F., Zhang, Z.K., and Qin, D.Y., 1987. *The Geotectonic Evolution of China.* Science Press. Springer-Verlag,

Rumelhart, P.E., Yin, A., Cowgill, E., Bulter, R., Zhang, Q., and Wang, X., 1999. Cenozoic vertical-axis rotation of the Altyn Tagh fault system. *Geology*, **27**: 819–822.

Runnegar, B., and Cambell, K.S.W., 1976. Late Palaeozoic faunas of Australia. *Earth Science Reviews*, **12**: 235–257.

Shu, D., and Chen, L., 1991. Paleobiogeography of Bradoriida and break-up of Gondwana. In Ren, J., and Xie, G. (eds.), *Proceedings of the 1st International Symposium on Gondwana Dispersion and Asia Accretion*. 314 pp., China University of Geosciences, Beijing, China, pp. 16–21.

Tapponier, P., Xu, Z.Q., Roger, F., Meyer, B., Arnaud, N.O., Wittlinger, G., and Yang, J.S., 2001. Oblique stepwise rise and growth of the Tibet Plateau. *Science*, **294**: 1671–1677.

Tauxe, L., 1998. *Paleomagnetic Principles and Practices.* Dordrecht: Kluwer Academic, 299 pp.

Tauxe, L., 2005. Inclination flattening and the geocentric axial dipole hypothesis. *Earth and Planetary Science Letters*, **233**: 247–261.

Van der Voo, R., 1993. *Paleomagnetism of the Atlantic, Tethys and Iapetus Oceans.* Cambridge: Cambridge University Press, 411 pp.

Wang, X.F., Xu, T., and Wei, C.S., 1999. Geodynamic and tectonic evolution of China and related Gondwana crustal fragments: Preface. *Gondwana Research*, **2**(4): 509–509.

Wang, S., 1993. The relationship between Ar and Cl in cherts and vein quartz and its significance on geochronology. *Acta Petrologica Sinica*, **9**: 319–328 (in Chinese).

White, M.C., 1995. Finding documents split of Indo-Australian plate. *EOS*, **76**: 337–343.

Xiao, W.J., Windley, B.F., Hao, J., and Li, J.L., 2002. Arc-ophiolite obduction in the Western Kunlun Range (China): implications for the Palaeozoic evolution of central Asia. *Journal of the Geological Society*, **159**: 517–528.

Yang, Z., and Besse, J., 2001. New Mesozoic apparent polar wandering path for south China: Tectonic consequences.. *Journal of Geophysical Research*, **106**: 8493–8520.

Yang, Z.Y., Cheng, Y.Q., and H.Z., Wang 1986. *The Geology of China.* Oxford: Clarendon Press.

Yin, A., and Harrison, T.M., 2000. Geologic Evolution of the Himalayan-Tibetan Orogen. *Annual Review of Earth and Planetary Science*, **28**: 211–280.

Yin, H.F., (ed.) 1988. *Paleobiogeography of China.* Beijing: Chinese University of Earth Sciences Press, 329 pp. (in Chinese).

Zhao, X., and Coe, R.S., 1987. Palaeomagnetic constraints on the collision and rotation of North and South China. *Nature*, **327**: 141–144.

Zhao, X., and Coe, R.,1989. Tectonic Implications of Permo-Triassic Paleomagnetic Results From North and South China. In Hillhouse, J.W. (ed.), Deep Structure and Past Kinematics of Accreted Terranes, Geophysical Monograph/International Union of Geodesy and Geophysics, **5**: 267–283.

Zhao, X., Coe, R.S., Zhou, Y.X., Wu, H.R., and Wang, J., 1990. New paleomagnetic results from northern China: collision and suturing with Siberia and Kazakhstan. *Tectonophysics*, **181**: 43–81.

Zhao, X., Coe, R.S., Gilder, S., and Frost, G., 1996. Palaeomagnetic constraints on palaeogeography of China: Implications for Gondwanaland, In Breakup of Rodinia and Gonwanaland and Assembly of Asia. *Special Issue of the Australian Journal of Earth Sciences*, **43**: 643–672.

Zhao, X., Coe, R.S., Chang, K.H., Park, S.O., Omarzai, S.K., Zhu, R. X., Gilder, S., and Zheng, Z., 1999. Clockwise rotations recorded in cretaceous rocks of South Korea: Implications for tectonic affinity between Korea Peninsula and North China. *Geophysical Journal International*, **139**: 447–463.

Zheng, Z., Kono, M., Tsunakawa, H., Kimura, G., Wei, Q.Y., Zhu, X.Y., and Hao, T., 1991. The apparent polar wander path for North China Block since the Jurassic. *Geophysical Journal International*, **104**: 29–40.

Zhu, R.X., and Tschu, K.K., 2001. *Studies on Paleomagnetism and Reversals of Geomagnetic Field in China.* Beijing: Science Press, 168 pp.

Zhu, X.Y., Liu, C., Ye, S.J., and Lin, J.L., 1977. Remanence of red beds from Linzhou, Xizang and the northward movement of the Indian plate (in Chinese with English abstract). *Scientia Geologica Sinica*, **1**: 44–51.

Ziegler, A.M., Rees, P.M., Rowley, D.B., Bekker, A., Li, Q., and Hulver, M.L., 1996. Mesozoic assembly of Asia: constraints from fossil floras, tectonics, and paleomagnetism, In An Yin and Harrison, M. (eds.), *The Tectonic Evolution of Asia.* Cambridge: Cambridge University Press, pp. 371–400.

Ziegler, A.M.,1990. Phytogeographic paterns and continental configurations during the Permian period. In McKerrow, W.S., and Scotese, C.R. (eds.), *Palaeozoic Palaeogeography and Biogeography.* Geological Society of London Memoir **12**, pp. 363–379.

Cross-references

Geomagnetic Polarity Reversals
Magnetosphere of the Earth
Paleomagnetism

POGO (OGO-2, -4 AND -6 SPACECRAFT)

The Polar Orbiting Geophysical Observatories (POGO) were the low altitude half of the Orbiting Geophysical Observatories (OGO) intended to carry a large number of instruments to observe the physical environment of the Earth's magnetosphere and outer ionosphere (Jackson and Vette, 1975). The characteristics of the three POGO spacecraft are shown in Table P1 and the spacecraft design is shown in Figure P49. The magnetometers were each a pair of optically pumped rubidium vapor units whose output signal strength had a $\sin\theta\cos\theta$ dependence, where θ is the angle between the optical axis and the observed magnetic field vector (Farthing and Folz, 1967). Each then had equatorial and polar "null zones" relative to their optical axes where the signals were too weak to measure. The equatorial ones were less than 7° half angle, and the polar zones less than 15°. The two instruments were mounted with their optical axes at 55° to each other so the combined output signal was available except for the two small angular areas where these zones overlapped.

The maximum altitude of the OGO-2 spacecraft was planned to be only 900 km but the tracking devices had lost its contact at launch due to the early morning fog, so it burned its full load of fuel to attain the high apogee seen in the table. The spacecraft also experienced problems soon after the operation began because its horizon sensors were found to be too sensitive; confusing temperature gradients in clouds with those at the horizon. It had utilized its full load of control gas within ten days of launch. It was then put into a slow spin mode. In April 1966 both batteries failed; so operation thereafter was limited to sunlit periods of the orbit. Nevertheless, there were some 306 days of observations. The OGO-4 spacecraft experienced far fewer problems and operated almost continuously until the tape recorders failed in January 1969. Because the orbits of both of these spacecraft drifted earlier in local time (5.5 min/day for OGO-2 and 6.1 for OGO-4) it was possible for the first time during September and early October 1967 to obtain magnetic field data simultaneously in two differing local time planes. OGO-6 was equally successful as OGO-4 though the data collection after August 1970 was sporadic. Having a lower inclination, the orbital drift with local time was higher—earlier by 8 min/day.

The magnetometer data from these three spacecrafts were the most accurate and continuous of any to that date, though the analysis was limited to use of the scalar field. A proposal to add vector instruments to OGO-6 by J.P. Heppner was not accepted by NASA, thus missing an opportunity to observe field-aligned currents in the polar regions for the first time. Initially, it was thought that accurate scalar observations would be sufficient to map the internal field as well as to study the *in situ* electrical currents. However, it was shown mathematically by Backus (1970) that there was one example of different vector

Table P1 The POGO spacecraft

Spacecraft	Dates of operation	Inclination (degrees)	Perigee (km)	Apogee (km)	Sample interval (s)
OGO-2	Oct 14, 1965-Oct 2, 1967	87.3	410	1510	0.5
OGO-4	July 28, 1967-Jan 19, 1969	86.0	410	910	0.5
OGO-6	June 5, 1969-June 1971	82.0	400	1100	0.288

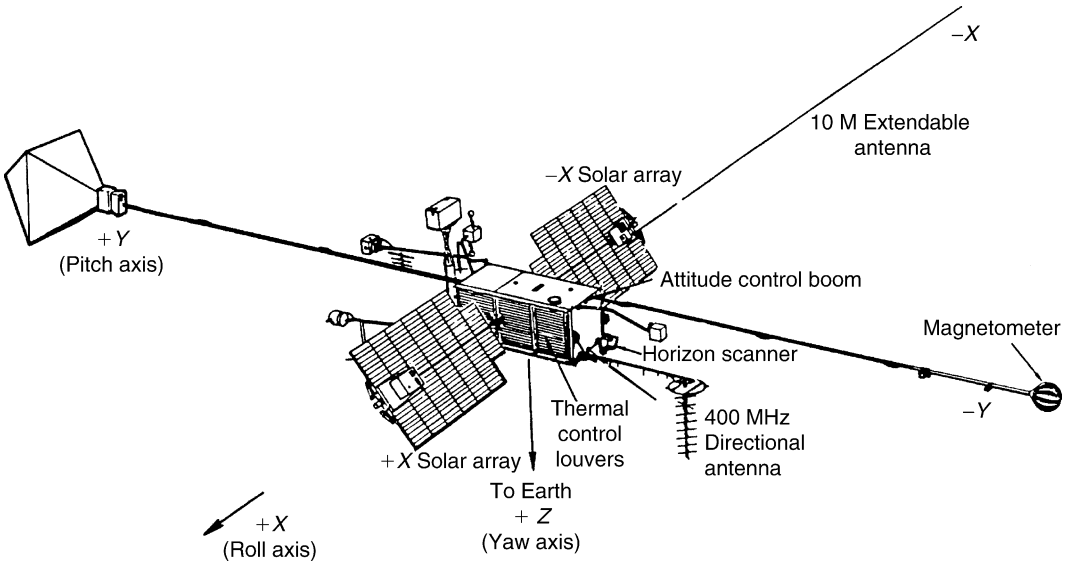

Figure P49 Typical OGO spacecraft in deployed configuration. The spacecrafts were of the order of 18 m long on the *Y*-axis. They were maintained in Earth orientation using gyroscopic reaction wheels with corrections as needed with gas jets. The *Z*-axis was toward the Earth and the direction of travel was along *X*-axis.

fields that could not be distinguished by observations of the scalar magnitude. Hurwitz and Knapp (1974) first demonstrated that models based only on scalar magnitude have larger vertical intensity errors in equatorial regions. Nevertheless, the data, especially for OGO-4, have been shown to be accurate to better than 4 nT, including the effects of orbital errors of position (Sabaka *et al*., 2004).

The data from OGO-2 were used as a standard in establishing the first International Geomagnetic Reference Field (IGRF) (Cain and Cain, 1971), and those from all three spacecrafts are the best control over the main field for the 1965–1971 epochs (Sabaka *et al*., 2004). Although Benkova *et al*. (1973) believed that Cosmos 49 measurements showed the presence of broad-scale magnetic anomalies, the noise in the data and orbital positions were too great to bring them out clearly. Until the POGO magnetic data were analyzed, the first accurate global magnetic anomaly map (Regan *et al*., 1975) could not be constructed.

The POGO data also allowed study of the field sources external to the Earth. Cain and Sweeney (1973) were the first to observe the equatorial electrojet from above the ionosphere. OGO-2 and OGO-4 were the first spacecrafts to operate simultaneously in different local time planes. Olsen *et al*. (2002) used data from a brief period in 1967 to show how such multispacecraft observations could help in obtaining a detailed picture of ionospheric current systems. Important contributions were also made to the understanding of high latitude external magnetic variations (Langel, 1974a) and their relation to the interplanetary field (Langel, 1974b) as well as the low energy plasma environment about the Earth (Langel and Sweeney, 1971).

Information about the POGO series spacecraft, experiments, and data sets can be obtained from the Master Catalog at the National Space Science Data Center Web site http://nssdc.gsfc.nasa.gov/nmc/sc-query.html by entering a query for the spacecraft name "pogo" and then following the response. Other internet sources include: http://www.spacecenter.dk/data/magnetic-satellites/ and http://core2.gsfc.nasa.gov/CM/.

Joseph C. Cain

Bibliography

Backus, G.E., 1970. Nonuniqueness of the external geomagnetic field determined by surface intensity measurements. *Journal of Geophysical Research*, **75**: 6339–6341.

Benkova, N.P., Dolginov, Sh., and Simonenko, T.N., 1975. *Journal of Geophysical Research*, **80**: 794–802.

Cain, J.C., and Cain, S.J., 1971. Derivation of the International Geomagnetic Reference Field [IGRF(1068)]. In Zmuda, A.J. (ed.), *The World Magnetic Survey* 1957–1969. pp. 163–166, 190–199, and 202–203, IAGA Bulletin, 28, Paris. Also published as *NASA Technical Note D–4527*, April, 1968.

Cain, J.C., and Sweeney, R.E., 1973. The POGO Data. *Journal of Atmospheric and Terrestrial Physics*, **35**: 1231–1247.

Farthing, W.H., and Folz, W.C., 1967. Rubidium vapor magnetometer for near Earth orbiting spacecraft. *Review of Scientific Instruments*, **38**: 1023–1030.

Hurwitz, L., and Knapp, D.G., 1974. Inherent vector discrepancies in geomagnetic main field models based on scalar F. *Journal of Geophysical Research*, **79**: 3009–3013.

Langel, R.A., 1974a. Near-earth magnetic disturbance in total field at high latitudes 1. Summary of data from OGO 2, 4, and 6. *Journal of Geophysical Research*, **79**: 2363–2371.

Langel, R.A., 1974b. Variation with interplanetary sector of the total magnetic field measured at the OGO 2, 4 and 6 satellites. *Planetary and Space Sciences*, **22**: 1413–1425.

Langel, R.A., and Sweeney, R.A., 1971. Asymmetric ring current at twilight local time. *Journal of Geophysical Research*, **76**: 4420–4427.

Jackson, J.E., and Vette, J.I., 1975. *OGO Program Summary*, NASA, SP–7601.

Olsen, N., Moretto, T., and Friis-Christensen, E., 2002. New approaches to explore the Earth's magnetic field. *Journal of Geodynamics*, **33**: 29–41.

Regan, R.D., Cain, J.C., and Davis, W.M., 1975. A global magnetic anomaly map. *Journal of Geophysical Research*, **80**: 794–802.

Sabaka, T.J., Olsen, N., and Purucker, M.E., 2004. Extending comprehensive models of the Earth's magnetic field with Ørsted and CHAMP. *Geophysical Journal International*, **159**: 521–547, 10111/j.1365–246X.2004.942421.x.

Cross-references

CHAMP, Ørsted, Magsat
Langel, Robert A. (1937–2000)
Magnetic anomalies, Long-wavelength
Magnetometers, Laboratory

POLARITY TRANSITION, PALEOMAGNETIC RECORD

Early work on the Matuyama-Brunhes transition field

The last change of geomagnetic polarity, bringing about an end to the Matuyama Reverse Chron and the onset of the Brunhes Normal Chron, occurred between 790 and 780 ka. This age was determined by both orbital tuning of marine sediment records (e.g., Tauxe *et al*., 1996) and by $^{40}Ar/^{39}Ar$ age determinations on transitionally-magnetized lavas (e.g., Singer and Pringle, 1996). Being the most youthful field reversal, it has always been associated with the largest number of available paleomagnetic records (see e.g., Love and Mazaud, 1997). One reason for this is that sedimentary records, often obtained from marine cores, penetrate this reverse-to-normal (R-N) polarity change before all others. It is no wonder then that the Matuyama-Brunhes (M-B) reversal was the first polarity transition to be associated with the availability of synchronous records from distant sites. These multiple recordings facilitated an initial attempt to better understand global characteristics of a transitioning field and the dynamo process that causes field reversal.

In 1976 the path of the virtual geomagnetic pole (VGP)—that is, the north geomagnetic pole position calculated by assuming each recorded paleodirection to be associated with a geocentric dipole–from a M-B record recovered from the dry sediments at Lake Tecopa, California, was compared by Hillhouse and Cox to the detailed, exposed marine sediment record published five years earlier (Niitsuma, 1971) from the Boso Peninsula, Japan. What was found was that the two VGP paths traced quite distinct tracks over Earth's surface from the geographic south polar region to the north polar region (see Figure P50), an observational finding that suggested for the first time that the transitioning field becomes largely nondipolar during, at least, this particular polarity change. On the other hand, if the two VGP tracks were quite similar, such a finding would be compatible with a transitioning field that remained dominantly dipolar. However, for this case, the VGP paths were found in the Atlantic and the west Pacific, respectively. Much later, the Lake Tecopa sediments became the focus of a second study by Valet *et al.* (1989) that attempted to confirm the earlier findings. This study found a far more complex VGP path, one that encompassed a significant portion of the central-to-east Pacific. Although these later findings still suggested a significant nondipole contribution to the transitioning M-B field, this study made clear that a complete understanding of even the most basic aspects of field geometry during such events would require a much larger database of contemporaneous records.

As the number of reversal records associated with the M-B transition steadily grew, so did the number of analyses that attempted to better define the structure of the transitional field. In 1981 a phenomenological model (Hoffman, 1981) was applied to available M-B datasets, an approach that assumed a reversal to begin at a particular locality within the core and then proliferate, or "flood," this "reversed" magnetic flux throughout the dynamo until completion of the process. This flooding model appeared to generally account for the M-B VGP paths that were available at the time.

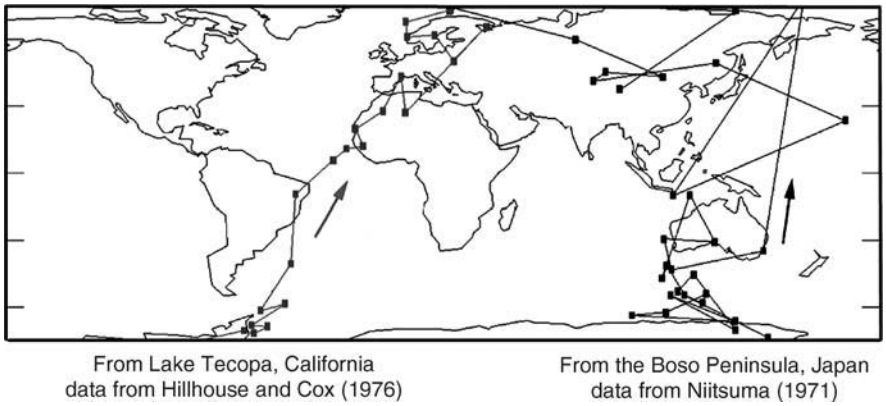

Figure P50 The path of the virtual geomagnetic pole (VGP) corresponding to the first two acquired paleomagnetic records of the Matuyama-Brunhes transition. Given the very different pathways, Hillhouse and Cox (1976) concluded that the M-B transition field was predominantly nondipolar.

Questions regarding the role of Earth's mantle

A decade later research regarding the last reversal took a new and exciting turn: Clement (1991) found that VGP paths associated with M-B records contained in a more complete database of published results displayed a significant bimodal distribution of transitional poles in geographic longitude. More specifically, the M-B VGPs appeared to preferentially lie within two particular antipodal bands, one running through the Americas, the other through East Asia and Australia (Figure P51a). This finding nearly coincided with another study—the results of which can be seen on the cover of a 1991 issue of *Nature* magazine—which found the same geographical bandings of transitional VGPs associated with several records of paleomagnetic reversals going back in time into the Miocene (Laj *et al.,* 1991).

This rather surprising result implied that, for the last several millions of years, and, in particular, during the time of the M-B event, transitional VGPs ran along "preferred" pathways. This, for the first time,

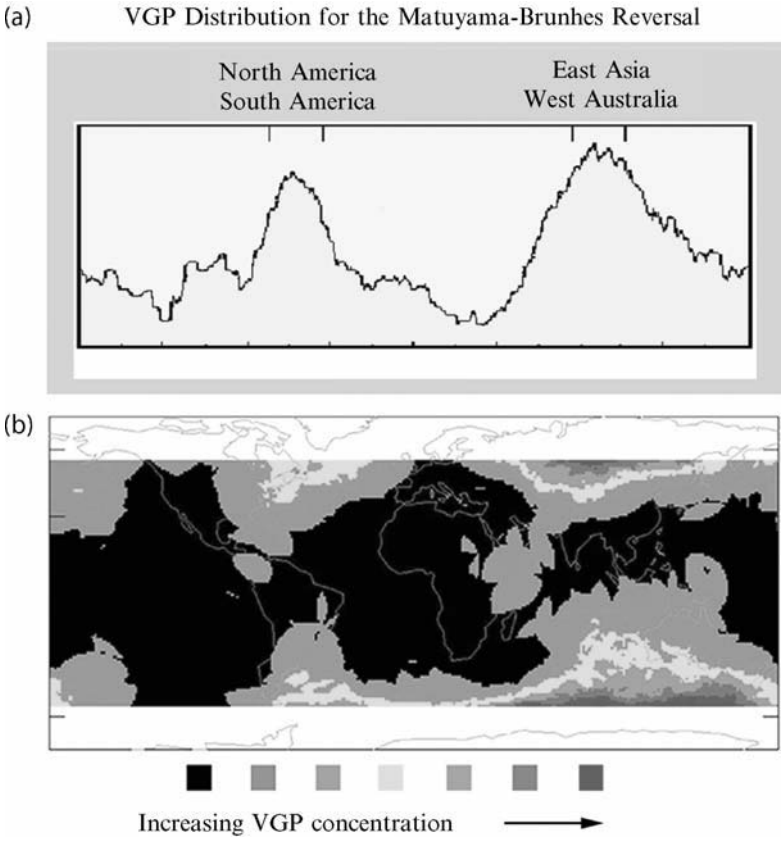

Figure P51 Geographical distribution of M-B transitional VGPs. (a) *after* Clement's (1991) finding of a bimodal distribution in longitude. (b) *after* Hoffman's (2000) global histogram.

suggested that Earth's mantle was intimately involved in the process of field reversal. That is, it was argued that such recurrence of field behavior had to be tied to physical conditions about the lowermost mantle, the variations of which imposing a control on the manner in which magnetic flux can emerge from the fluid outer core during reversals. Since the time of these two seminal papers by Clement (1991) and Laj *et al.* (1991), the question as to whether or not field behavior during successful reversals as well as during other transitional events—like, say, an aborted attempt—is largely influenced by such lower mantle heterogeneities, has been hotly debated (see e.g., Jacobs, 1994; Merrill and McFadden, 1999).

An alternative explanation put forward was that the apparent preferential behavior—rather than having a geomagnetic basis—was, in fact, an artifact related to limitations in the way sediments acquire their remanent magnetization (e.g., Rochette, 1990; Valet *et al.,* 1992; Langereis *et al*., 1992). However, during the following year an analysis (Hoffman, 1992) of transitional field behavior recorded in volcanic sequences having ages running back to the Miocene—rocks that, typically, provide the most accurate spot recordings of the paleofield vector—showed, not preferred banding of VGP paths, but rather preferred groupings, or clusters. Interestingly, these clusters resided within the hypothesized preferred longitudinal bands. Hence, this "preferred patch" finding implied virtually the same geomagnetic basis as proposed for sediment records. Yet, the correspondences and differences between what was observed in distinct rock types broadened the debate, while raising it to a new level. If preferred VGP behavior is assumed to be a manifestation of a dynamo process controlled by the lower mantle, could the apparent discrepancy observed in sediment and lava records—that is, preferred bands and preferred patches, respectively—be explained through the known differences in the manner these two types of rocks become magnetized? And, if so, could long-lived transitional field states during which time the field direction at a given site, although transitional, remained essentially stationary, produce both observations?

The MBD97 database

In 1997, the first rigorous attempt was made (Love and Mazaud, 1997) to distinguish which records of the full M-B database may be considered reliable, and, hence, worthy of inclusion in a robust analysis. Nearly 62 M-B records from sites about the globe were found in the literature, and each was subjected to a number of strict reliability criteria. Of these records only 11 satisfied this scrutiny and were admitted to the so-called *MBD97* database. These records now separated from less reliable records, were analyzed in an attempt to answer the primary question regarding the existence or not of preferential VGP behaviour during the last geomagnetic reversal. The findings by the authors of the *MBD97* database suggested a statistically significant answer in the affirmative. Specifically, they argued that the distribution of transitional M-B VGPs showed some degree of preferred longitudinal behavior compatible with the hypothesis that the bias was, in fact, a real geomagnetic phenomenon.

Other analyses of the *MBD97* database followed. One study (Gubbins and Love, 1998) raised the point that the VGP behavior, when viewed in a global sense, was associated with a dependence on the site of observation, and that each individual VGP path was compatible with inferred symmetry conditions within the core dynamo. Still another investigation of the *MBD97* database (Hoffman, 2000) produced a global histogram of transitional M-B VGPs (Figure P51b). This analysis, although again confirming a longitudinal bimodal nature of virtual poles, demonstrated that very few VGPs existed in the database at low latitudes near the equator. From this result it was argued that during the M-B transition considerable time was spent by the reversing field in particular configurations. Specifically, clusters of sequential VGPs near Australia, and in the South Atlantic, were found to exist in the database-data that was observed in records from sequences of lavas as well as sediments. Yet, the question regarding whether or not the VGP migrated across the equator along preferred longitudinally-confined pathways, remained unresolved.

Further work

Since the construction of the *MBD97* database, records of the Matuyama-Brunhes obtained from deep-sea sediments in the West Pacific (Oda *et al*., 2000) and the North Atlantic (Channell and Lehman, 1997; Channell *et al*., 2004), have found their way to publication. In particular, the several parallel records from North Atlantic high deposition-rate drift deposits are particularly noteworthy (see examples shown in Figure P52). These data sets, all displaying remarkably similar,

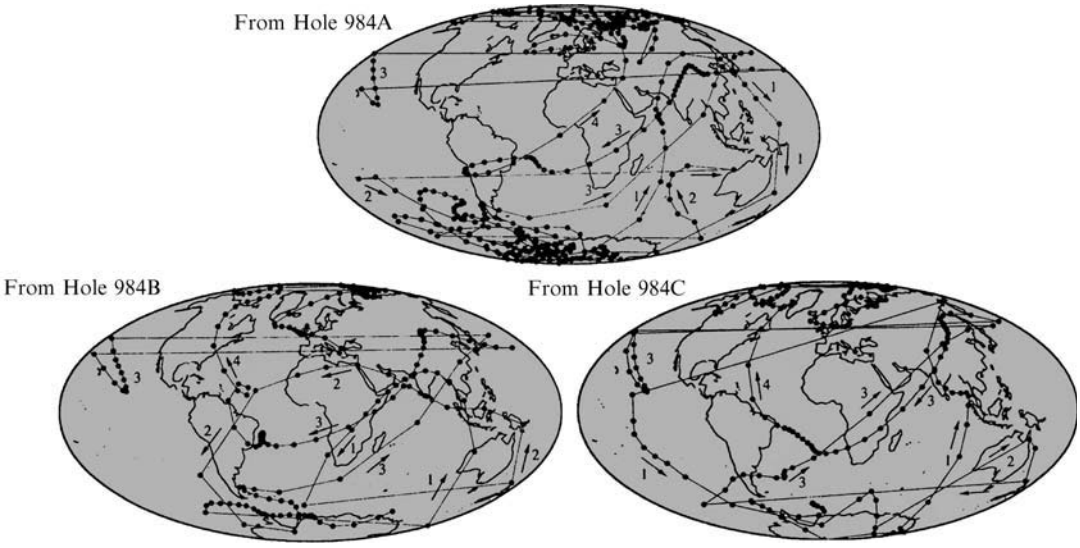

Figure P52 Three examples of VGP paths associated with parallel M-B marine sediment core records from the North Atlantic. Note the remarkable similarity of detail. After Channell and Lehman (1997).

though complex, field behavior, are arguably the most detailed and complete records of the M-B reversal presently available. In some contrast to the most reliable records obtained from mid-latitudes, these high latitude North Atlantic records show little in the way of VGP clustering near Australia, yet contain clusters both in the South Atlantic and northeast Asia (Channell and Lehman, 1997; Channell *et al*., 2004). If it is the case that VGP cluster localities are dependent on the site of observation, then the associated long-held field states must be largely nondipolar.

Constable (1992) was the first to show a link between preferred VGP path behavior and the modern-day geomagnetic field. Specifically, it was shown (see Figure P53, *top*) that if a polarity reversal simply involved the decay, vanishing, and reemergence of the axial dipole having opposite sign—keeping the remainder of the field constant—VGP pathways for sites from around the globe would preferentially lie along the same antipodal longitudinal bands proposed by Laj *et al.* (1991) and Clement (1991). The field configuration for which only the axial dipole has been removed is commonly termed the nonaxial dipole or, *NAD*-field (although it is sometimes also called the *sans*-axial dipole, or *SAD*-field, translated from French as to be "without" the axial dipole). Such a field state must occur during a successful change in polarity. That is, the axial dipole must vanish before it can change sign.

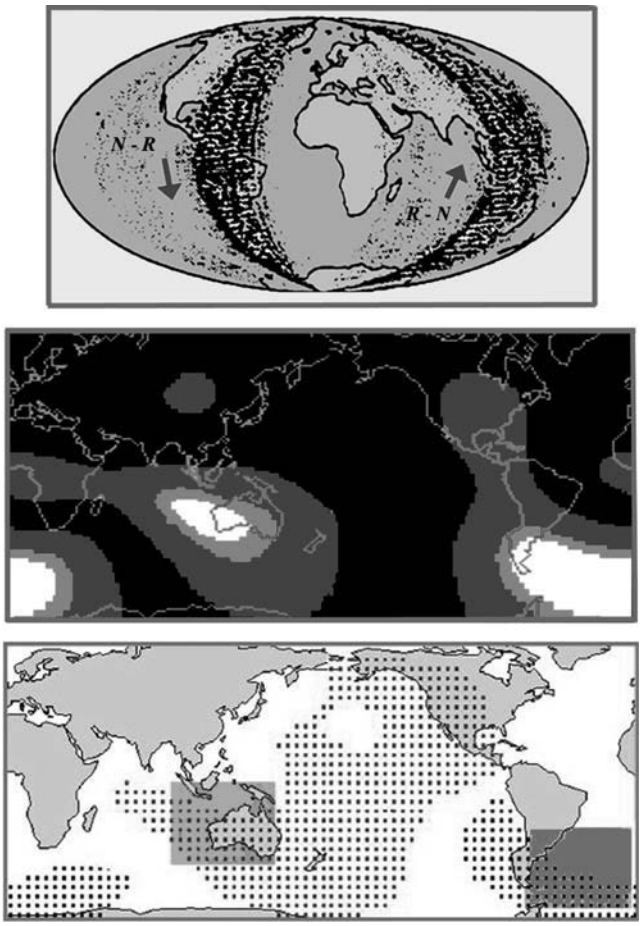

Figure P53 Aspects of the modern-day field. *(Top)* VGP pathways associated with numerous sites from about the globe for simulated normal-to-reverse (N-R) and reverse-to-normal (R-N) polarity transitions in which only the axial dipole is assumed to be involved in the process. After Constable (1992). *(Middle)* Intensity of the vertical component of the field at Earth's surface following synthetic removal of the axial dipole from the modern-day field (hence, the *NAD*-field). The two locations in white—near west Australia and in the South Atlantic—are the most intense, having at least 90% of the most intense value found. *(Bottom)* Two grids of sites defining regions that, when subjected to the modern-day *NAD*-field, would possess paleomagnetic directions corresponding to VGPs found in either of the two shaded localities (also found to be areas of the most intense *NAD*-field). The smaller and larger grids correspond to north-VGPs in the South Atlantic and south VGPs in the west Australian shaded regions, respectively *after* Hoffman and Singer (2004).

Interestingly, the primary locations of observed M-B clustered VGPs from available paleomagnetic records near western Australia, in the southwest Atlantic, and within Siberia, are not only sites within the two proposed preferred bands, but also correspond to the three locations at Earth's surface which possess the most intense vertical component of the modern-day field after synthetic removal of the axial dipole (i.e., the *NAD*-field) from the calculated spherical harmonic analysis (Figure P53 *middle*). Moreover, if VGPs are calculated for sites from around the globe when assumed to be experiencing the modern-day *NAD*-field, one finds that in the Southern Hemisphere, the very same Australian and South Atlantic localities are the most preferred regions (Figure P53 *bottom*). Thus, available paleomagnetic transition data appear to be linked to the field of today, suggesting that primary features of the modern-day *NAD*-field remain virtually stationary over times in order of 10^6 or, perhaps, 10^7 years (Hoffman and Singer, 2004). If so, this is a definite sign of a controlling influence by the lowermost mantle on flux emerging from the fluid outer core.

Duration of the Matuyama-Brunhes transition

Recently, the duration of the M-B transition has been under study. The investigation of paleodirectional records obtained from several marine sediment cores (Clement, 2004) found a clear dependence of reversal time on the latitude of the site of observation. Specifically, the duration varied from about 2000 years at low latitudes to 10000 years at high latitude sites. However, the complete temporal process of field reversal appears from other studies to be rather complex and require a significantly longer span of time: an earlier analysis by Hartl and Tauxe (1996) of several marine sediment cores that recorded the M-B found a significant decrease in field strength some 15 ka prior to a second weakening associated with the actual change in polarity. The first decrease of this "double-dip" in intensity was explained by the authors as a precursory geomagnetic event to the subsequent successful reversal.

Following this finding, a recent geochronological study in which several precise $^{40}Ar/^{39}Ar$ ages were determined for transitionally magnetized M-B lavas from volcanic sequences at four mutually distant sites found a bimodal age distribution consistent with such a precursor (Singer *et al.,* 2005). The initial instability, associated with the first of the two decreases in field intensity, was found to have occurred 18 ka prior to the polarity switch. The Australian and South Atlantic VGP clustering (Figure P54) appears now to be associated with the precursor, and thus suggests that the beginning of the period of dynamo instability may be simply explained by a process which essentially destroys the axial dipole, leaving the transitional field to have the configuration of the *NAD*-field at that time. Singer *et al.* (2005) further suggest that it is such a two-stage process that may be required for a given reversal attempt to be successful. Whether these characteristics of the M-B, the last reversal of Earth's magnetic field, are common to earlier polarity transitions (see e.g., Coe and Glen, 2004), and hence, typical of a fundamentally systematic process, requires the availability of considerably more paleomagnetic reversal data.

Kenneth A. Hoffman

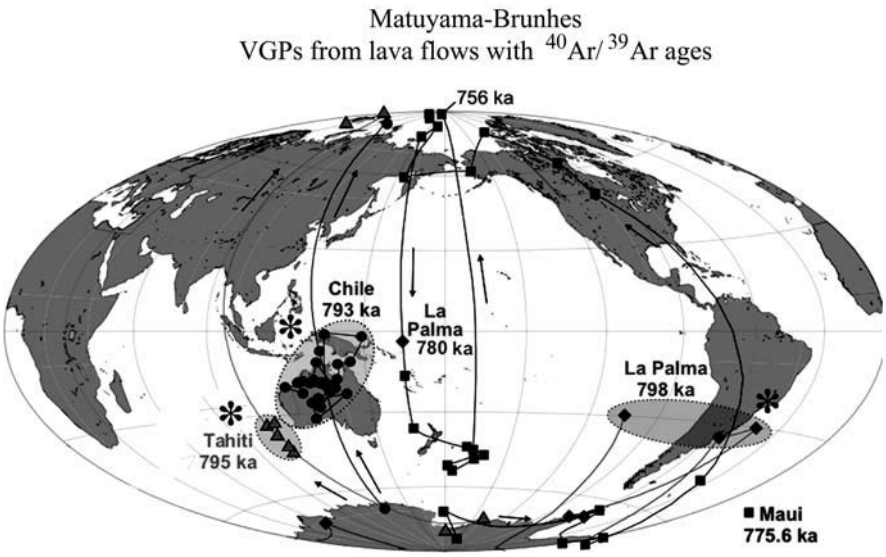

Figure P54 Matuyama-Brunhes VGPs and precise $^{40}Ar/^{39}Ar$ ages for sequences of transitionally-magnetized lavas from each of four mutually distant sites. Note that those sites associated with VGP clusters near Australia and the South Atlantic/South American regions (indicated with an asterisk) correspond to lavas that were erupted some 18 ka prior to the actual change in polarity that was recorded on Maui, Hawaii. After Singer *et al.* (2005).

Bibliography

Channell, J.E.T., and Lehman, B., 1997. The last two geomagnetic polarity reversals recorded in high-deposition-rate sediment drifts. *Nature*, **389**: 712–715.

Channell, J.E.T., Curtis J.H., and Flower, B.P., 2004. The Matuyama-Brunhes boundary interval (500–900 ka) in North Atlantic drift sediments. *Geophysical Journal International*, **158**: 489–505.

Clement, B.M., 1991. Geographical distribution of transitional VGPs: evidence for non-zonal equatorial symmetry during the Matuyama-Brunhes geomagnetic reversal. *Earth and the Planetary Science Letters*, **104**: 48–58.

Clement, B., 2004. Dependence on the duration of geomagnetic polarity reversals on site latitude. *Nature*, **428**: 637–640.

Constable, C., 1992. Link between geomagnetic reversal paths and secular variation of the field over the last 5 Ma *Nature*, **358**: 230–233.

Gubbins, D., and Love, J.J., 1998. Preferred VGP paths during geomagnetic polarity reversals: Symmetry conditions. *Geophysical Research Letters*, **25**: 1079–1082.

Hartl, P., and Tauxe, L., 1996. A precursor to the Matuyama/Brunhes transition-field instability as recorded in pelagic sediments. *Earth and the Planetary Science Letters*, **138**: 121–135.

Hillhouse, J., and Cox, A., 1976. Brunhes-Matuyama polarity transition. *Earth and the Planetary Science Letters*, **29**: 51–64.

Hoffman, K.A., 1981. Quantitative description of the geomagnetic field during the Matuyama-Brunhes polarity transition. In: *Proceedings of Symposium 10 "Dynamics of Core and Mantle"*, XVII General Assembly IUGG, Canberra, Australia, *Physics of the Earth and Planetary Interiors*, **24**: 229–235.

Hoffman, K.A., 1992. Dipolar reversal states of the geomagnetic field and core-mantle dynamics. *Nature*, **359**: 789–794.

Hoffman, K.A., 2000. Temporal aspects of the last reversal of Earth's magnetic field. *Philosophical Transactions of the Royal Society of London series A*, **358**: 1181–1190.

Hoffman, K.A., and Singer, B.S., 2004. Regionally recurrent paleomagnetic transitional fields and mantle processes. In Channell, J.E.T., Kent, D.V., Lowrie, W., and Meert, J. (eds.), *Timescales of the Internal Geomagnetic Field.,* Geophysical Monograph, Washington, DC: American Geophysical Union, pp. 233–243.

Jacobs, J.A., 1994. *Reversals of the Earth's Magnetic Field*, 2nd edn, Cambridge: Cambridge University Press.

Langereis, C.G., van Hoof, A.A.M., and Rochette, P., 1992. Longitudinal confinement of geomagnetic reversal paths as a possible sedimentary artefact. *Nature*, **358**: 226–229.

Laj, C., *et al.,*1991. Geomagnetic reversal paths. *Nature*, **351**: 447.

Love, J.J., and Mazaud, A., 1997. A database for the Matuyama-Brunhes magnetic reversal. *Physics of the Earth and Planetary Interiors*, **103**: 207–245.

Merrill, R.T., and McFadden, P.L., 1999. Geomagnetic polarity transitions. *Reviews of Geophysics* **37**: 201–226.

Niitsuma, N., 1971. Detailed study of the sediments recording the Matuyama-Brunhes geomagnetic reversal., *Science Reports of the Tohuku University Second Series (Geology)*, **43**: 1–39.

Oda, H., Shibuya, H., and Hsu, V., 2000. Paleomagnetic records of Brunhes/Matuyama polarity transition from Ocean Drilling Program Leg 124 (Celebes and Sulu Seas). *Geophysical Journal International*, **142**: 319–338.

Rochette, P., 1990. Rationale of geomagnetic reversals versus remanence recording processes in rocks: a critical review. *Earth and the Planetary Science Letters*, **98**: 33–39.

Singer, B.S., *et al.,* 2005. Structural and temporal requirements for geomagnetic field reversal deduced from lava flows. *Nature*, **434**: 633–636.

Singer, B.S., and Pringle, M.S., 1996. The age and duration of the Matuyama-Brunhes geomagnetic polarity reversal from $^{40}Ar/^{39}Ar$ incremental heating analyses of lavas. *Earth and the Planetary Science Letters*, **139**: 47–61.

Tauxe, L., *et al.,*1996. Astronomical calibration of the Matuyama-Brunhes boundary: consequences for magnetic remanence acquisition in marine carbonates and the Asian loess sequences. *Earth and the Planetary Science Letters*, **140**: 133–146.

Valet, J.P., Tauxe, L., and Clark, D.R., 1988. The Matuyama-Brunhes transition recorded from Lake Tecopa sediments (California). *Earth and the Planetary Science Letters*, **87**: 463–472.

Valet, J.P., *et al*. Palaeomagnetic constraints on the geometry of the geomagnetic field during reversals. *Nature*, **356**: 400–407.

Cross-references

Geomagnetic Polarity Reversals
Geomagnetic Polarity Reversals, Archives
Geomagnetic Polarity Reversals, Observations
Polarity Transitions: Radioisotopic Dating

POLARITY TRANSITIONS: RADIOISOTOPIC DATING

The Plio-Pleistocene Geomagnetic Polarity Time Scale (GPTS) developed beginning in the early 1960s as Cox *et al*. (1963) and McDougall and Tarling (1963) used K-Ar ages and magnetic remanence data from volcanic rocks to propose a sequence of normal and reverse polarity "epochs" now called Chrons (Opdyke and Channell, 1996). A large set of K-Ar ages were acquired, mainly from lavas, that defined the lengths of Chrons, but if few, these lavas showed transitional directions of remanent magnetization, the timing of the polarity reversals between the Chrons had to be interpolated. This was done using the chronogram method (Cox and Dalrymple, 1967) to minimize the error function of K-Ar ages near the polarity boundary relative to assumed ages for the boundary. In addition to the polarity Chrons, that are periods on the order of 10^6 year in length, K-Ar ages and magnetic data from widely dispersed locations began to delineate several $10^4 - 10^5$ year long subchrons including the Jaramillo, Olduvai, and Reunion subchrons (Opdyke and Channell, 1996).

Still shorter-lived geomagnetic events or Cryptochrons, that include excursions, aborted reversal attempts, or rapid back-to-back reversals, were also detected magnetically in sediments and volcanic rocks. K-Ar dating of normally magnetized basalt flows in Iceland (McDougall and Wensink, 1966) and a transitionally magnetized rhyolite in California (Mankinen *et al*.,1978) provided the first radioisotopic ages for events within the Matuyama reversed Chron, named the Gilsa and Cobb Mountain events. In the Brunhes normal chron, several transitionally magnetized lavas in the Massif central, France that recorded the Laschamp event have been K-Ar dated, but these ages are imprecise and scatter between 60 and 15 ka (Guillou *et al*., 2004). In a remarkable study, Hall and York (1978) obtained both K-Ar and $^{40}Ar/^{39}Ar$ ages from these lavas and concluded that the Laschamp event occurred about 47 ka; it marked the first use of the $^{40}Ar/^{39}Ar$ method to date lavas this young. The K-Ar age of 565 ± 28 ka (uncertainties herein are $\pm 2\sigma$ analytical errors) determined from two of four transitionally magnetized lava flows found in Idaho by Champion *et al*. (1988) provided a precise radioisotopic date for an event during the Brunhes normal chron which was named the Big Lost event for a nearby river. Notably, Champion *et al*. (1988) discussed the evidence from sediments and volcanic rocks globally that at least 10 geomagnetic events of short duration had occurred during the last 1 Ma.

More recently, as directional excursions associated with brief periods of low relative paleointensity were revealed in sediments worldwide, many of these geomagnetic events have been verified, and new ones proposed (Langereis *et al*., 1997; Guyodo and Valet, 1999; Channell, 1999; Channell *et al*., 2002). It is the promise of an accurate, high resolution correlation of these events globally that sparked considerable interest and debate concerning their number and precise timing. There are at least two reasons for this: First, marine and terrestrial sediments contain a rich, quasi continuous, archive of major climate changes that have shaped the Earth's surface over the past several Ma. An accurate calendar of changes in climate is crucial to determining the underlying driving mechanisms in the oceans and atmosphere. Second, theoretical arguments and numerical models have used the frequency and duration of reversals and excursions to infer magnetic or thermal interactions between the liquid outer core and either the solid inner core, or the lowermost mantle, that act to control the stability of the geodynamo (e.g., Gubbins, 1999; see *Geodynamo, numerical simulations; Core-mantle coupling, thermal*). Thus, an accurate accounting of spatial temporal instabilities of the magnetic field, from excursions to reversals, is critical in advancing the next generation of geodynamo models (Singer *et al*., 2002, 2005).

In sediments, the timing of an event may be estimated by astronomical tuning of oxygen isotope, or other variations that proxy for orbitally-driven changes in climate (e.g., Langereis *et al*., 1997; Channell *et al*., 2002). However, not all marine core is amenable to oxygen isotope measurements, few geomagnetic records have been astronomically tuned, and even the sediment that accumulates at the highest rates may contain hiatuses leading to underestimates of the amount of time actually recorded. In detail, magnetic recordings in sediment are further complicated by postdepositional processes, including lock-in of the magnetic remanence, such that an accurate chronology may be elusive (Merrill and McFadden, 1999). Alternatively, $^{40}Ar/^{39}Ar$ dating of lava flows or tuffs that rapidly lock in a thermal magnetic remanence during cooling has recently made it possible to obtain precise radioisotopic ages for at least 14 reversals and excursions, including previously unrecognized events that occurred during the past 2.2 Ma (Singer *et al*., 2002, 2004).

$^{40}Ar/^{39}Ar$ variant of K-Ar dating

Until the early 1990's K-Ar dating was the preferred method for determining ages of volcanic rocks. The $^{40}Ar/^{39}Ar$ variant offers many advantages over K-Ar dating and coupled with more sensitive measurement capabilities in such a way it has eclipsed K-Ar dating as the method of choice. The history, theory, and application of these techniques are summarized by McDougall and Harrison (1999), Renne (2000), and Kelley (2002); hence only a brief outline, drawn from these sources, is presented here. Both methods rely on the radioactive decay of naturally occurring ^{40}K to ^{40}Ar, which is proportional at any time t to the N number of ^{40}K atoms present:

$$\frac{dN}{dt} = -\lambda N \qquad \text{(Eq. 1)}$$

where λ is the total decay of ^{40}K. A large fraction, 89.52%, of ^{40}K decays to ^{40}Ca via beta emission ($\lambda_\beta = 4.962 \times 10^{-10}$ year), whereas 10.48% decays to ^{40}Ar via electron capture ($\lambda_\epsilon = 5.808 \times 10^{-11}$ year) so that the total decay constant ($\lambda = 5.543 \times 10^{-10}$ year) corresponds to a half-life of 1.25×10^9 year, Solving the differential equation (1) yields the age equation for the K-Ar isotope system:

$$t = \left(\frac{1}{\lambda}\right) \cdot \ln\left[1 + \left(\frac{\lambda}{\lambda_\epsilon}\right) \cdot \left(\frac{^{40}Ar^*}{^{40}K}\right)\right] \qquad \text{(Eq. 2)}$$

where $^{40}Ar^*$ is radiogenic argon, distinguished from other sources such as the atmosphere. The ratio of modern $^{40}K/K$ is constant, hence measurement of K and Ar concentrations (in mol/g), and isotope ratios of Ar, allow the age to be calculated. In practice, the sample is completely fused, the gas released is purified and spiked with a known amount of ^{38}Ar tracer, then its isotopic composition is measured in a mass spectrometer. K is a salt and must be measured independently on a separate aliquot of the same sample. Alternatively, $^{40}Ar^*$ may be measured directly by using a unique mass spectrometer which functions as a sensitive manometer able to distinguish minute quantities of radiogenic argon from the large atmospheric component found in most lavas (e.g., Guillou *et al*., 2004).

One of the more important assumptions of any radioisotopic dating system, including the K-Ar and $^{40}Ar/^{39}Ar$ methods, is that the rock or mineral has remained closed to loss or gain of parent and daughter nuclides. For example, loss of Ar or gain of K can yield spuriously young dates, whereas gain of Ar or loss of K may give spuriously old dates. From a K-Ar age determination alone, it is impossible to assess the validity of this assumption. Another limitation of K-Ar dates is their precision, which includes the compound uncertainty of two different analytical procedures used to measure separately the absolute contents in mol/g of Ar and K.

The $^{40}Ar/^{39}Ar$ method is based on the same radioisotopic decay system as the K-Ar method, but instead of measuring K in a separate aliquot of the sample, it is measured by creating ^{39}Ar from ^{39}K via neutron activation. The ^{39}Ar is produced by fast neutron bombardment in a nuclear reactor, and because the ratio of ^{39}K to ^{40}K is constant, it becomes a proxy for ^{40}K that allows the $^{40}Ar^*/^{40}K$ ratio to be calculated simply from the measurement of the ratio of two Ar isotopes $^{40}Ar/^{39}Ar$.

Production of ^{39}Ar atoms is given by

$$^{39}\mathrm{Ar} = {}^{39}\mathrm{K}\Delta\int\phi(\mathrm{E})\sigma(\mathrm{E})\mathrm{d}E \qquad \text{(Eq. 3)}$$

where ^{39}K is the number of atoms originally present, Δ the duration of irradiation, $\phi(E)$ the neutron flux density at energy, E, and $\sigma(E)$ the neutron capture cross section of ^{39}K for neutrons of energy E in the $^{39}K(n,p)^{39}Ar$ reaction. Solving Eq. (2) for $^{40}Ar^*$ and combining with Eq. (3) yields:

$$\left(\frac{^{40}\mathrm{Ar}^*}{^{39}\mathrm{K}}\right) = \frac{\left(\frac{^{40}\mathrm{K}}{^{39}\mathrm{K}}\right)\left(\frac{\lambda_\epsilon}{\lambda}\right)\left(\frac{1}{\Delta}\right)(\mathrm{e}^{\lambda t}-1)}{\Delta\int\phi(\mathrm{E})\sigma(\mathrm{E})\mathrm{d}E} \qquad \text{(Eq. 4)}$$

This can be simplified by defining a dimensionless irradiation parameter J:

$$J = \left(\frac{^{39}\mathrm{K}}{^{40}\mathrm{K}}\right)\left(\frac{\lambda}{\lambda_\epsilon}\right)\Delta\int\phi(\mathrm{E})\sigma(\mathrm{E})\mathrm{d}E \qquad \text{(Eq. 5)}$$

which allows Eq. (4) to be written as

$$\left(\frac{^{40}\mathrm{Ar}^*}{^{39}\mathrm{Ar}}\right) = \frac{(\mathrm{e}^{\lambda t}-1)}{J} \qquad \text{(Eq. 6)}$$

and rearranged to yield the age equation for $^{40}Ar/^{39}Ar$ dating:

$$t = \left(\frac{1}{\lambda}\right)\ln\left[1 + J\cdot\left(\frac{^{40}\mathrm{Ar}^*}{^{39}\mathrm{Ar}}\right)\right] \qquad \text{(Eq. 7)}$$

The value for the neutron fluence parameter J is determined by irradiating a standard mineral of known age t together with the samples, measuring its $^{40}Ar^*/^{39}Ar$ ratio, and solving Eq. (6) for J. In this sense, the $^{40}Ar/^{39}Ar$ method is a relative dating technique that relies on high-quality, homogenous standards that are available widely. There are many neutron fluence standards in use, however, not all laboratories use the same standards, nor does each use identical ages for some standards. Therefore, it is critical when comparing $^{40}Ar/^{39}Ar$ ages determined in various laboratories to normalize the ages to a common value, based on intercalibration of several standards (see Renne, 2002). For example, all the $^{40}Ar/^{39}Ar$ ages discussed below are calculated or normalized relative to an age of 28.02 Ma for the widely used and intercalibrated Fish Canyon Tuff sanidine standard.

The amount of $^{40}Ar^*$ measured must be corrected for the presence of atmospheric argon which has a $^{40}Ar/^{36}Ar$ ratio of 295.5. This is done using the relationship $(^{40}Ar^*/^{39}Ar) = (^{40}Ar^*/^{39}Ar)_m - 295.5(^{36}Ar/^{39}Ar)_m$, where the subscript m denotes the measured ratio. Other corrections for Ar isotopes produced by undesirable nuclear reactions during irradiation are also important, particularly for Plio-Pleistocene samples (Renne, 2000).

The fundamental difference between the K-Ar and $^{40}Ar/^{39}Ar$ dating methods is that the latter allows calculation of an age based solely on the isotopic composition of Ar in the sample, rather than absolute abundances of Ar and K, thereby eliminating major sources of potential error. The $^{40}Ar^*/^{39}Ar$ ratio is determined using highly sensitive mass spectrometry, thus the total fusion age for a Plio-Pleistocene sample of 10 mg of basalt groundmass or a single 1 mg phenocryst of sanidine can be determined to a precision of ~1–2%. Systematic uncertainties, including a potential uncertainty in the ^{40}K decay constant currently in use, may be important when comparing $^{40}Ar/^{39}Ar$ ages with those determined by other methods. This contribution to the total uncertainty associated with a particular age determination may be small, amounting to only a few hundred to a few thousand years for Pleistocene lava flows, but may be important when comparing $^{40}Ar/^{39}Ar$ ages of geomagnetic excursions or reversals to those obtained astronomically from marine sediment (Guillou *et al*., 2004).

Age spectra

Because measurement of the $^{40}Ar^*/^{39}Ar$ ratio does not require absolute abundances, another powerful aspect of the $^{40}Ar/^{39}Ar$ method is that rather than totally fusing an irradiated sample, it can be incrementally degassed by stepwise heating to higher temperatures using a controllable furance or laser. The apparent ages of each successive gas increment are monitored for consistency by plotting the ages vs. the cumulative release of ^{39}Ar, as a proxy for the parent isotope ^{40}K (see Figure P55). If successive gas increments yield consistent ages, the spectrum is concordant Figure P55a, reflecting an internally homogenous distribution of $^{40}Ar^*/^{39}Ar$, thereby providing evidence against mobility of K and Ar. The "plateau" age is commonly defined as the

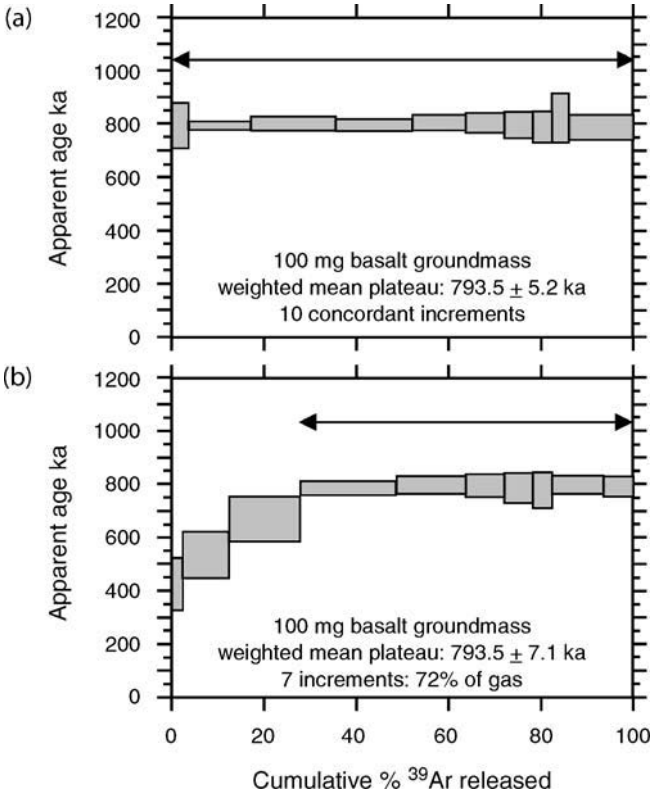

Figure P55 Age spectrum diagrams for two basaltic lava flows erupted during the Matuyama-Brunhes transition. Vertical height of each gas step gives the 2σ analytical uncertainty. (a) Concordant age spectrum. The ten gas steps were released by successively raising the temperature of a resistance furnace in 50°C increments between 700 and 1200°C. (b) Discordant age spectrum produced by the same procedure used in A. The plateau age is calculated from seven contiguous steps that comprise 72% of the gas released. The gas released at lower temperatures gives ages younger than the plateau, possibly reflecting argon loss during weathering. In both A and B, the isotopic composition of the plateau steps may be used to calculate an isochron (Figure P56).

mean of the concordant step ages, each step being weighted by its inverse variance. Though arbitrary, most definitions of a plateau specify that it must include at least three successive increments that comprise $\geq 50\%$ of the ^{39}Ar released that are concordant in age at the 95% confidence level. Weighting each plateau increment (or individual total fusion age) by its inverse variance $(1/\sigma_i^2)$, reduces the uncertainty of the mean age t according to

$$\sigma_t = \sqrt{\sum\left(\frac{1}{\sigma_i^2}\right)} \qquad \text{(Eq. 8)}$$

In this manner, the plateau age may approach a precision of 0.2%, depending on the number of concordant increments and the $^{40}Ar^*$ content of the material.

It is common, particularly with Plio-Pleistocene lavas, that age spectra are discordant. Notwithstanding, discordant spectra may yield a plateau, and depending on the nature of the disturbance, may provide important evidence for mobility of Ar or K. Figure P55b illustrates an example from a Pleistocene basalt interpreted to have lost a small fraction of $^{40}Ar^*$ due to low temperature weathering of the matrix.

Isochrons

It is routine in the $^{40}Ar/^{39}Ar$ method to measure five isotopes of Ar including ^{36}Ar, ^{39}Ar, ^{40}Ar, ^{37}Ar, ^{38}Ar; the latter two are required to correct for undesirable quantities of ^{40}Ar and ^{36}Ar produced artificially from K and Cl in the sample during irradiation. The other three isotopes facilitate isochron analysis; the most commonly used isochron is the plot of $^{36}Ar/^{40}Ar$ vs. $^{39}Ar/^{40}Ar$ where the intercepts yield reciprocals of $^{40}Ar^*/^{39}Ar$, hence age (from Eq. (7)), and $(^{40}Ar/^{36}Ar)_i$ which gives the initial or trapped component (see Figure P56). Isochrons are calculated by a least squares method that weights individual measurements by their inverse variance. Incremental heating experiments on Plio-Pleistocene volcanic rocks are particularly amenable to isochron analysis. In some instances isochrons are more powerful than the age spectrum approach, because no *a priori* assumption regarding the $(^{40}Ar/^{36}Ar)_i$ is made, which can be important for the small number of lavas or tuffs that may contain initially a nonatmospheric (or excess) component of argon (e.g., Singer and Brown, 2002). Indeed, the ability to use incremental heating data to test the assumptions of (1) closed system behavior and (2) an initial $(^{40}Ar/^{36}Ar)_i$ ratio corresponding to the atmosphere, makes it the preferred method for precisely dating lavas and tuffs thought to record geomagnetic reversals and events.

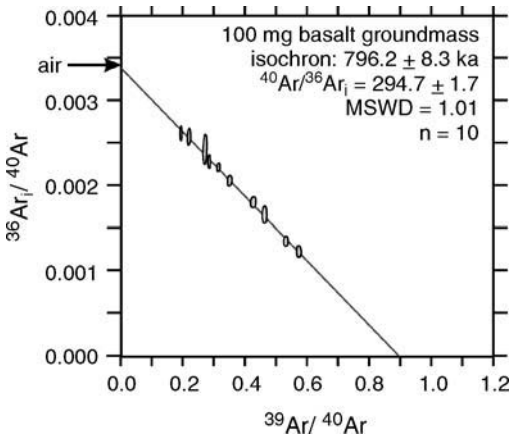

Figure P56 Isotope correlation or isochron diagram. Intercepts of the isochron in this diagram give the reciprocal of $^{40}Ar/^{39}Ar$ and $^{40}Ar/^{36}Ar_i$. Hence the isochron is a mixing line between the radiogenic argon and the initial or trapped component. The data points shown correspond to the ten gas increments in Figure P55a. In this example, the trapped component is indistinguishable from air argon. MSWD is the mean square weighted deviation, which indicates the magnitude of scatter about the isochron. A value of 1.0 means that the analytical uncertainties account for most of the error in the age which is calculated using least squares regression that weights each data point by the inverse of its variance.

Direct $^{40}Ar/^{39}Ar$ dating of polarity transitions and excursional events

Matuyama-Brunhes transition

The first direct radioisotopic date for the Matuyama-Brunhes polarity transition corresponding to the last reversal of Earth's magnetic field is based on $^{40}Ar/^{39}Ar$ isochrons from four incremental heating experiments by Baksi *et al.* (1992) on three lavas at Haleakala volcano on the island of Maui that possess transitional directions of magnetic remanence. Baksi *et al.*'s age of 795 ± 16 ka is ca. It was 65 ka older than the K-Ar based age for this reversal, but within error of the astronomical estimate of 780 ka. Singer and Pringle (1996) incrementally heated groundmass separates from eight basaltic to andesitic lavas that erupted during the M-B transition at volcanoes in Chile, and on the islands of Tahiti, La Palma, and Maui, including several replicate experiments to improve precision of the isochrons. Although Singer and Pringle (1996) determined the weighted mean age of these eight lavas at 791 ± 4 ka, they also emphasized that the 12 ka difference in age between the Chilean lavas and those from Maui may reflect the duration of this reversal. To further investigate the duration and structure of the M-B transition, Singer *et al.* (2005a) obtained 71 $^{40}Ar/^{39}Ar$ incremental heating experiments on 23 of the transitionally magnetized lavas from the four volcanoes above. Surprisingly, the mean $^{40}Ar/^{39}Ar$ ages of the lava sequences on La Palma, Tatara San Pedro, and Tahiti were found to cluster at 793 ± 3 ka, whereas the age of the lavas at Haleakala, 776 ± 2 ka, is about 18 ka younger. Singer *et al.* (2005a) propose that the older lavas record the onset of geodynamo instability and nondipolar field behavior, which persisted for a long enough period of time that magnetic flux diffused out of the solid inner core, thereby weakening its stabilizing effect and allowing the field to reverse itself at 776 ± 2 ka. This interpretation is bolstered, in part, by the paleointensity records from marine sediments, in which are observed a pronounced drop in intensity about 15 ka prior to the intensity low associated with the field reversal itself. Singer *et al.* (2005a) argue that these lava flows provide the first observational evidence in support of Gubbins' (1999) hypothesis that the solid inner core may control the frequency of excursions and probability of full field reversals.

Dating other reversals and events toward a geomagnetic instability timescale (GITS)

The K-Ar age of the Cobb Mountain event, 1120 ± 40 ka (Mankinen *et al.*, 1978), was revised to 1194 ± 12 ka on the basis of $^{40}Ar/^{39}Ar$ laser fusion and furnace incremental heating experiments on sanidine by Turrin *et al.* (1994). The 6% to 7% increase in age was attributed to incomplete degassing of sanidine during the K-Ar experiments, a problem that may have biased many K-Ar dates used to develop the original GPTS, including those used in the chronogram estimate of 730 ka for the M-B transition.

Isochron ages for 18 lavas within long basalt flow sequences at Punaruu Valley, Tahiti, and Haleakala volcano, Maui, known to record several polarity transitions and events were determined using the $^{40}Ar/^{39}Ar$ incremental heating method on groundmass separated by Singer *et al.* (1999). The results indicate that an event recorded 1122 ± 10 ka at Tahiti, which was originally correlated with the Cobb Mountain event on the basis of K-Ar dating, is actually a previously

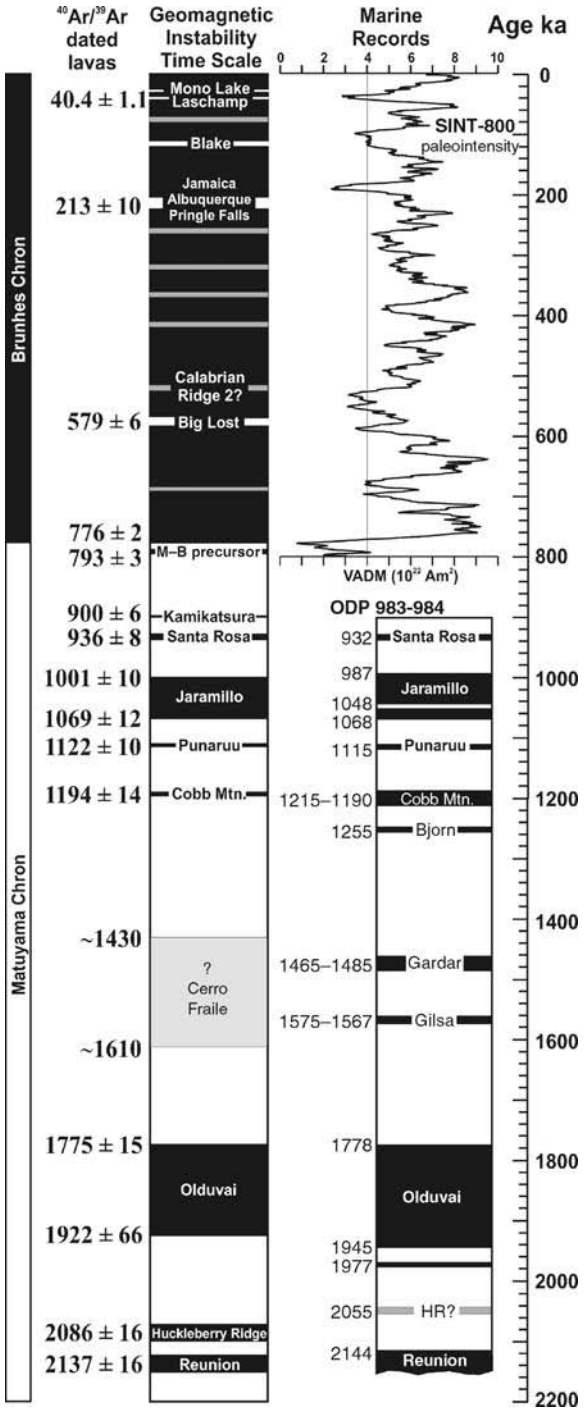

Figure P57 A Geomagnetic Instability Time Scale (GITS) for the Matuyama reversed and Brunhes normal Chrons. The ^{40}Ar/^{39}Ar ages of transitionally magnetized lava flows or tuffs recording reversals or excursional events are from Singer *et al.* (1999, 2002, 2004, 2005a,b), Singer and Brown (2002), and references therein. Postulated events in grey are undated, imprecisely dated, or less well documented magnetically (Singer *et al.*, 2002). The astronomically-dated record of reversals and excursions includes SINT-800, a global compilation of geomagnetic field intensity from 33 marine sediment records over the last 800 ka (Guyodo and Valet, 1999), and the composite record from sediment cored at Ocean Drilling Program sites 983 and 984 (Channell *et al.*, 2002). In the latter, paleointensity lows that correspond with equator crossing shifts in the direction of the virtual geomagnetic pole are dated using an astronomical age model of oxygen isotope variations in the cores. Note that several paleointensity lows in SINT-800 do not readily correlate to events that have been radioisotopically dated or assigned astronomical ages elsewhere. Similarly, although many radioisotopically dated events match those found in the ODP 983 and 984 cores, several paleointensity lows, including some not shown here, have yet to be found in lavas that have been ^{40}Ar/^{39}Ar dated. Note that all ^{40}Ar/^{39}Ar ages are calculated relative to an age of 28.02 Ma for the Fish Canyon tuff sanidine standard.

unrecognized event, now named the Punaruu event. The results of Singer *et al.* (1999) also provided for the first time,the direct radioisotopic ages for the onset and termination of the Jaramillo normal subchron at 1069 ± 12 and 1001 ± 10 ka, respectively, which are in agreement with astronomical estimates (see Figure P57). Between the Jaramillo subchron and the M-B boundary, eight transitionally magnetized lavas from Tahiti and Halekala yielded a common weighted mean ^{40}Ar/^{39}Ar age of 900 ± 6 ka, corresponding to Champion *et al.*'s (1988) Kamikatsura event (Singer *et al.*, 1999; Figure P57).

Singer *et al.* (1999) suggested that the Kamikatsura event shortly postdated another previously unrecognized event recorded by the Santa Rosa I rhyolite dome in the Valles Caldera, New Mexico. To verify this, Singer and Brown (2002) undertook ^{40}Ar/^{39}Ar laser fusion and incremental heating experiments on sanidine from the transitionally magnetized Santa Rosa I rhyolite dome and determined its age to be 936 ± 8 ka; that is, the Santa Rosa event is 37 ka older than the Kamikatsura event and 65 ka younger than the reversal that terminated the Jaramillo Subchron Figure P57. At Cerro del Fraile in southern Argentina, Singer *et al.* (2004) have ^{40}Ar/^{39}Ar dated a sequence of 10 basaltic lavas that, in concert with dates from lavas elsewhere, provide precise radioisotopic ages for geomagnetic events marking termination of the Reunion Subchron at 2137 ± 16 ka, plus the onset and termination of the Olduvai Subchron at 1922 ± 66 and 1175 ± 15 ka. A single transitionally magnetized lava gave a discordant age spectrum that, together with a K-Ar age determination, indicate an age between about 1610 and 1430 ka (Figure P57). The termination of the Reunion Subchron is temporally distinguished by about 50 ka from the Huckleberry Ridge event recorded in tuff at Yellowstone national park, Wyoming (Singer *et al.*, 2004).

The paleomagnetic and ^{40}Ar/^{39}Ar data of Singer *et al.* (2002) revealed that two geomagnetic events, including the one that preceded the M-B reversal by 18 ka, and a younger event dated at 580 ± 8 ka are recorded in lavas on the northeast flank of La Palma island. The latter correspond to the Big Lost event that was K-Ar dated in Idaho at 565 ± 28 ka by Champion *et al.* (1988). Moreover, Hoffman and Singer (2004) discovered a third recording of the Big Lost event in lavas at Tahiti, clearly demonstrating the global nature of this excursion at 579 ± 6 ka (Figure P57). Lava flows of the Albuquerque Volcanoes, New Mexico along with a sequence of lacustrine sediments and volcanic ash at Pringle Falls, Oregon, that both record excursional field behavior have been ^{40}Ar/^{39}Ar dated at 217 ± 17 and 211 ± 13 ka, respectively (Singer *et al.*, 2005b). The common age from the two sites suggests that they record the same period of geomagnetic instability with a weighted mean age of 213 ± 10 ka. Using both ^{40}Ar/^{39}Ar and unspiked K-Ar methods, two lava flows in the Massif Central, France that record the Laschamp excursion have recently been dated to 40.4 ± 1.1 ka, which is about 10% younger than previous estimates discussed earlier (Guillou *et al.*, 2004). This new age is indistinguishable from that of a prominent paleointensity low at 40.9 ka found in marine sediments of the North Atlantic Ocean whose history has been calibrated using an age model based on oxygen isotopes and annual varve counting in the Greenland Ice Sheet Project II (GISP2) ice core. Thus, despite uncertainties in the decay constant for ^{40}K, which may be as large as 2.4%, the ^{40}Ar/^{39}Ar method is capable of determining ages with

an accuracy and precision of between 1% and 2% for virtually the entire Pleistocene (Guillou *et al*., 2004).

Comparison of these radioisotopically dated events with more continuous records of paleointensity and paleodirection recovered from marine sediments has helped to (1) verify that excursions mark frequent instability of the geodynamo, (2) test the astronomical age estimates of many events, and (3) better interpret long-term temporal changes in the field. Perhaps the highest resolution recording of the field during the Matuyama reversed Chron comes from drift sediment deposited at high rates at Ocean Drilling Program (ODP) sites 983 and 984 in the Iceland basin (Channell *et al*., 2002). Hydraulic piston cores from these sites revealed changes in the direction of the magnetic field corresponding to at least seven excursional events and six reversals bounding subchrons (Figure P57). Each of these directional shifts is associated with a low in the relative intensity of the magnetic field, but there are also other paleointensity lows not associated with prominent directional excursions (Channell *et al*., 2002). ODP 983 and 984 cores record paleointensity lows corresponding to the Santa Rosa and Punaruu events, and to reversals bounding the Jaramillo, Cobb Mountain, Olduvai, and Reunion subchrons, each with an astronomical age that is within an error of the radioisotopic ages (Figure P57). Alternatively, a few events found in the ODP 983 and 984 cores, for example the Bjorn, Gardar, and Gilsa events, have yet to be $^{40}Ar/^{39}Ar$ dated in lavas, although the transitionally magnetized lava from Cerro del Fraile that is poorly dated between 1610 and 1430 ka may correspond to one of the latter two events (Figure P57). In the site 983 core, a paleointensity low accompanying an equator crossing of the virtual geomagnetic pole direction was not highlighted by Channell *et al*. (2002), but the astronomically estimated age of 2055 ka is close to the $^{40}Ar/^{39}Ar$ age of the Huckleberry Ridge event (Figure P57).

For the Brunhes normal Chron we have the global compilation of paleointensity data known as SINT-800 that indicates at least eight periods when the virtual axial dipole moment (VADM) is dropped below about 4×10^{22} Am^2 (Guyodo and Valet, 1999). Three of these events, astronomically dated at ca. 590, 190, and 40 ka, broadly correspond to the Big Lost, Jamaica, and Laschamp excursions. However, closer inspection reveals that the $^{40}Ar/^{39}Ar$ ages for the Big Lost and Albuquerque Volcanoes/Pringle Falls excursions are several ka older than first-order intensity lows recorded in the sediment (Figure P57). The SINT-800 paleointensity record is based on 33 sediment cores, no two of which preserve identical patterns of paleointensity (Guyodo and Valet, 1999). Given uncertainties associated with generating astrochronologic age models, and a limited understanding of how magnetic remanence acquisition may be delayed or distorted in marine sediments, these temporal mismatches suggest that caution be used when attempting to correlate the major paleointensity lows across the globe. Alternatively, dating of transitionally magnetized lava flows relies upon well understood process of radioisotopic decay and thermal magnetic remanence.

$^{40}Ar/^{39}Ar$ dating of lava flows which directly record brief periods of geomagnetic field instability, coupled with recognition of these events in marine sediment, indicate that both excursions and reversals reflect intrinsic behavior of the geodynamo. Singer *et al*. (2002) proposed that when the stability of the geodynamo is considered, rather than the lengths of polarity chrons, an alternative approach to the GPTS is needed. Hence, a new $^{40}Ar/^{39}Ar$-based Geomagnetic Instability Time-Scale (GITS) for the last 2.2 Ma is under construction (Figure P57). Experience suggests that many geomagnetic events remain to be discovered or verified as more lava flow sequences are studied in detail.

Brad S. Singer

Bibliography

Baksi, A.K., Hsu, V., McWilliams, M.O., and Farrar, E., 1992. $^{40}Ar/^{39}Ar$ dating of the Brunhes-Matuyama geomagnetic field reversal. *Science*, **256**: 356–357.

Champion, D.E., Lanphere, M.A., and Kuntz, M.A., 1988. Evidence for a new Geomagnetic reversal from lava flows in Idaho: Discussion of short polarity reversals in the Brunhes and Late Matuyama Polarity Chrons. *Journal of Geophysical Research*, **93**: 11667–11680.

Channell, J.E.T., 1999. Geomagnetic paleointensity and directional secular variation at Ocean Drilling Program (ODP) Site 984 (Bjorn Drift) since 500 ka: Comparisons with ODP Site 983 (Gardar Drift). *Journal of Geophysical Research*, **104**: 22937–22951.

Channell, J.E.T., Mazaud, A., Sullivan, P., Turner, S., and Raymo, M.E., 2002. Geomagnetic excursions and paleointensities in the Matuyama Chron at Ocean Drilling Program Sites 983 and 984 (Iceland Basin). *Journal of Geophysical Research*, **107**, doi: 10.1029/2001JB000491.

Cox, A., Doell, R.R., and Dalrymple, G.B., 1963. Geomagnetic polarity epochs and Pleistocene geochronometry. *Nature*, **198**: 1049–1051.

Cox, A., and Dalrymple, G.B., 1967. Statistical analysis of geomagnetic reversal data and the precision of potassium-argon dating. *Journal of Geophysical Research*, **72**: 2603–2614.

Gubbins, D., 1999. The distinction between geomagnetic excursions and reversals. *Geophysical Journal International*, **137**: F1–F3

Guillou, H., Singer, B.S., Laj, C., Kissell, C., Scalliet, S., and Jicha, B.R., 2004. On the age of the Laschamp Event. *Earth and Planetary Science Letters*, **227**: 331–343.

Guyodo, Y., and Valet, J.-P., 1999. Global changes in intensity of the Earth's magnetic field during the past 800 ka. *Nature*, **399**: 249–252.

Hall, C.M., and York, D. 1978. K-Ar and $_{40}Ar/_{39}Ar$ age of the Laschamp geomagnetic polarity reversal. *Nature*, **274**: 462–464.

Hoffman, K.A., and Singer, B.S., 2004. Regionally recurrent paleomagnetic transitional fields and mantle processes. In Channell, J.E.T., Kent, D.V., Lowrie, W., and Meert, J., (eds.), *Timescales of the Paleomagnetic Field, American Geophysical Union,* Geophysical Monograph, **145**: 233–243.

Kelley, S., 2002. K-Ar and Ar-Ar Dating. In Porcelli, D.P., Ballentine, C.J., and Wiele, R. (eds.), *Noble Gases*. *Reviews in Mineralogy and Geochemistry*, The Mineralogical Society of America, Washington, DC, **47**: 785–818.

Langereis, C.G., Dekkers, M.J., de Lange, G.J., Paterne, M., and van Santvoort, P.J.M., 1997. Magnetostratigraphy and astronomical calibration of the last 1.1 Ma from an eastern Mediterranean piston core and dating of short events in the Brunhes. *Geophysical Journal International*, **129**: 75–94.

Mankinen, E.A., Donnelly, J.M., and Gromme, C.S., 1978. Geomagnetic polarity event recorded at 1.1 Ma B.P. on Cobb Mountain, Clear Lake volcanic field, California. *Geology*, **6**: 653–656.

McDougall, I., and Tarling, D.H., 1963. Dating of reversals of the Earth's magnetic fields. *Nature*, **198**: 1012–1013.

McDougall, I., and Wensink, J., 1966. Paleomagnetism and geochronology of Pliocene-Pleistocene lavas in Iceland. *Earth and Planetary Science Letters*, **1**: 232–236.

McDougall, I., and Harrison, T.M., 1999. *Geochronology and thermochronology by the $^{40}Ar/^{39}Ar$ method.* New York: Oxford University Press.

Merrill, R.T., and McFadden, P.T., 1999. Geomagnetic polarity transitions. *Reviews of Geophysics*, **37**: 201–226.

Opdyke, N.D., and Channell, J.E.T., 1996. *Magnetic Stratigraphy.* San Diego:Academic Press.

Renne, P.R., 2000. K-Ar and $^{40}Ar/^{39}Ar$ dating. In Noller, J.S., Sowers, J.M., and Lettis, W.R., (eds.) *Quaternary Geochronology: Methods and Applications.* American Geophysical Union Reference Shelf 4. Washington, DC: American Geophysical Union, pp. 77–100.

Singer, B.S., and Pringle, M.S., 1996. Age and duration of the Matuyama-Brunhes geomagnetic polarity reversal from $^{40}Ar/^{39}Ar$ incremental heating analyses of lavas. *Earth and Planetary Science Letters*, **139**: 47–61.

Singer, B.S., Hoffman, K.A, Chauvin, A., Coe, R.S., and Pringle, M.S., 1999. Dating transitionally magnetized lavas of the late Matuyama Chron: Toward a new $^{40}Ar/^{39}Ar$ timescale of reversals and events. *Journal of Geophysical Research*, **104**: 679–693.

Singer, B.S., Relle, M.R., Hoffman, K.A., Battle, A., Guillou, H., Laj, C., and Carracedo, J.C., 2002. Ar/Ar ages from transitionally

magnetized lavas on La Palma, Canry Islands, and the Geomagnetic Instability Timescale. *Journal of Geophysical Research*, **107**: 2307, doi: 10.1029/2001JB001613.

Singer, B., and Brown, L.L., 2002. The Santa Rosa Event: $^{40}Ar/^{39}Ar$ and paleomagnetic results from the Valles Rhyolite near Jaramillo Creek, Jemez Mountains, New Mexico. *Earth and Planetary Science Letters*, **197**: 51–64.

Singer, B.S., Brown, L.L., Rabassa, J.O., and Guillou, H., 2004. $^{40}Ar/^{39}Ar$ chronology of Late Pliocene and early Pleistocene geomagnetic and glacial events in southern Argentina. In Channell, J.E.T., Kent, D.V., Lowrie, W., and Meert, J. (eds.), *Timescales of the Paleomagnetic Field, American Geophysical Union*, Geophysical Monograph **145**: 175–190.

Singer, B.S., Hoffman, K.A., Coe, R.S., Brown, L.L., Jicha, B.R., Pringle M.S., and Chauvin, A., 2005a. Structural and temporal requirements for geomagnetic field reversal deduced from lava flows. *Nature*, **434**: 633–636.

Singer, B.S., Jicha, B.R., Kirby, B.T., Zhang, X., Geissman, J.W., and Herrero-Bervera, E., 2005b. An $^{40}Ar/^{39}Ar$ age for geomagnetic instability recorded at the Albuquerque Volcanoes and Pringle Falls, Oregon. *EOS, Transactions of the American Geophysical Union* 86 (52), abstract GP21A–0019.

Turrin, B.D., Donnelly-Nolan, J.M., and Hearn, B.C. 1994. $^{40}Ar/^{39}Ar$ ages from the rhyolite of Alder Creek, California: Age of the Cobb Mountain Normal-Polarity Subchron revisited. *Geology*, **22**: 251–254.

Cross-references

Core-Mantle Coupling, Thermal
Geodynamo, Numerical Simulations
Geomagnetic Excursion

POLE, KEY PALEOMAGNETIC

Introduction

Using paleomagnetism to reconstruct continents in the Precambrian has proven to be exceedingly difficult despite a database of many hundreds of paleomagnetic poles from around the world. The most serious problem involves the large age uncertainties associated with most Precambrian paleopoles. This is due to a number of factors, most notably the poor age constraints on the rock-units from which the paleopoles are derived and magnetic overprinting during metamorphic events.

Roy (1983) first pointed out that most Precambrian paleopoles were too poorly dated, with uncertainties of tens or even hundreds of millions of years, to be of use in defining apparent polar wander paths (APWPs). Buchan and Halls (1990) suggested rigorous criteria to identify individual paleopoles that are sufficiently well defined and well dated that they are useful for defining apparent polar wander paths or reconstructing paleocontinents. Such paleopoles were termed "key paleopoles" by Buchan *et al*. (1994).

Criteria of a key paleomagnetic pole

The following basic criteria for a key paleomagnetic pole are adapted from Buchan and Halls (1990) and Buchan *et al*. (2001).

(a) *Age of the paleopole*: The paleopole should be demonstrated to be primary and the rock-unit precisely and accurately dated.
(b) *Quality of the paleopole*: The primary paleomagnetic remanence should be properly isolated, secular variation averaged out, and, where necessary, correction made for crustal tilting.

The critical importance of the age criterion cannot be overemphasized; *only* well dated paleopoles should be considered as key paleopoles. Field tests are required to demonstrate that the remanence is primary. For example, igneous rocks can be shown to carry a primary remanent magnetization using the baked contact test (see *Baked contact test*). A Precambrian rock-unit must have a radiometric age with an uncertainty of $< \pm 20$ Ma (Buchan *et al*., 2001). At present, only U-Pb and Ar-Ar dating meet this requirement. In the future, with improved analytical techniques it should be possible to strengthen this criterion and require age uncertainties $< \pm 5$ Ma.

It is important to ensure that the age and the paleomagnetic remanence are actually derived from the same geological unit. Thus, the geochronological and paleomagnetic studies should be integrated and carried out at the same sampling localities wherever possible (e.g., Buchan *et al*., 1994).

The direction of the paleomagnetic remanence used to calculate the paleomagnetic pole must accurately represent the direction of the Earth's magnetic field. In particular, the paleopole itself must be properly isolated to ensure that secondary magnetizations have been eliminated. This requires the use of stepwise alternating field and thermal demagnetization techniques. Secular variation must be averaged out. For example, in the case of rapidly cooling igneous units such as volcanic flows, several different units must be sampled. The paleopole must be corrected if crustal tilting has occurred since remanence acquisition.

Apparent polar wander path method vs. comparison of key paleomagnetic poles

The standard practice of comparing APWPs for different continental blocks in order to determine their relative movements often breaks down in the Precambrian. At present, there are simply too few key paleopoles from most continental blocks to allow meaningful APWPs to be constructed. In an attempt to circumvent this problem, it has been standard practice to make use of large numbers of poorly dated paleopoles. In some cases, the large uncertainties in the age of most of the paleopoles are disregarded. In other cases, "grand mean" paleopoles are calculated from the poorly constrained data and used as tie-points along the APWP. In still other cases, the APWP is simply interpolated over relatively long time intervals between existing individual paleopoles or grand mean paleopoles.

However, as noted above, most Precambrian paleopoles are too poorly dated to allow them to be properly sequenced along APWPs. Long time gaps in the paleopole record from a given continental block make it difficult to interpolate between them. In addition, interpolation between widely separated paleopoles is hindered by an ambiguity in magnetic polarity that results from the lack of continuous APWPs from the Precambrian to the Present. The unreliability of Precambrian APWPs based on poorly dated paleopoles was illustrated by Buchan *et al*. (1994), who used key paleopoles to demonstrate that the widely used Paleoproterozoic APWP for the Superior Province of the Canadian Shield was invalid.

The extent of the dating problem has been described in recent reviews by Buchan *et al*. (2000) and Buchan *et al*. (2001), who examined the Baltica-Laurentia database for the Proterozoic and the global database for the period 1700–500 Ma, respectively. They concluded that only a very few Proterozoic paleopoles are sufficiently well dated to pass the age criterion for a key paleopole. Although many paleopoles in the database are well defined, their ages are uncertain. Either they do not have a rigorous field test to determine that the remanence is primary, or the rock-unit from which they have been derived is undated or poorly dated. Most of the key paleopoles that were identified come from a single continental block, Laurentia. A few are available from Baltica. More recent work has yielded key paleopoles for Australia (e.g., Wingate and Giddings, 2000; Pisarevsky *et al*., 2003). Unfortunately, there are as yet no key Proterozoic paleopoles that can be used for reliable APWP construction from most other continental blocks.

The comparison of APWPs derived from different continental blocks is the ideal method of determining if continental blocks were drifting as a unit or separately. However, Buchan and Halls (1990) and Buchan *et al*. (1994) suggested that key paleopoles only be connected to form a segment of an APWP if their ages are within 30 Ma.

Instead, Buchan *et al*. (2000) proposed that, until enough key paleopoles are available to construct reliable APWPs, individual key paleopoles of the same age from different continental blocks should be directly compared in order to determine the relative position of the blocks. Of course, comparing key paleopoles of a single age would not yield a unique reconstruction, because of the longitudinal uncertainty inherent in the paleomagnetic method. However, as noted by Buchan *et al.* (2000, p. 185–186), a unique reconstruction may be possible if two (or more) ages of key paleopoles are compared and if the continental blocks in question moved as a unit and rotated through a significant angle during the period under study.

Conclusion

Reliable APWPs and continental reconstructions cannot be obtained from poorly dated paleomagnetic poles, no matter how many are used or how well defined are the paleopole themselves. Key paleopoles that are both well dated and well defined are a prerequisite for establishing reliable APWPs and producing robust paleocontinental reconstructions.

Kenneth L. Buchan

Bibliography

Buchan, K.L., and Halls, H.C., 1990. Paleomagnetism of Proterozoic mafic dyke swarms of the Canadian Shield. In Parker, A.J., Rickwood, P.C., and Tucker, D.H. (eds.), *Mafic Dykes and Emplacement Mechanisms.* Rotterdam: Balkema, pp. 209–230.

Buchan, K.L., Mortensen, J.K., and Card, K.D., 1994. Integrated paleomagnetic and U-Pb geochronologic studies of mafic intrusions in the southern Canadian Shield. *Precambrian Research*, **69**: 1–10.

Buchan, K.L., Mertanen, S., Park, R.G., Pesonen, L.J., Elming, S.-Å., Abrahamsen, N., Bylund, G., 2000. Comparing the drift of Laurentia and Baltica in the Proterozoic: the importance of key paleomagnetic poles. *Tectonophysics*, **319**: 167–198.

Buchan, K.L., Ernst, R.E., Hamilton, M.A., Mertanen, S., Pesonen, L.J., and Elming, S.-Å., 2001. Rodinia: the evidence from integrated palaeomagnetism and U-Pb geochronology. *Precambrian Research*, **110**: 9–32.

Pisarevsky, S.A., Wingate, M.T.D., and Harris, L.B., 2003. Late Mesoproterozoic (ca. 1.2 Ga) palaeomagnetism of the Albany-Fraser orogen: no pre-Rodinia Australia-Laurentia connection. *Geophysical Journal International*, **155**: 6–11.

Roy, J.L., 1983. Paleomagnetism of the North American Precambrian: a look at the data base. *Precambrian Research*, **19**: 319–348.

Wingate, M.T.D., and Giddings, J.W., 2000. Age and paleomagnetism of the Mundine Well dyke swarm, Western Australia: implications for an Australia-Laurentia connection at 755 Ma. *Precambrian Research*, **100**: 335–357.

Cross-references

Baked Contact Test

POTENTIAL VORTICITY AND POTENTIAL MAGNETIC FIELD THEOREMS

Theoretical studies of motions in the Earth's fluid (liquid) metallic outer core, where the main geomagnetic field is produced by self-exciting *dynamo* (*q.v.*) action, are based on the nonlinear partial differential equations (PDEs) of *magnetohydrodynamics (MHD)* (*q.v.*) that govern the flow of electrically conducting fluids. The equations are mathematical expressions of the laws of *mechanics*, *thermodynamics* and *electrodynamics* applied to a continuous medium.

The equations of electrodynamics are not needed when dealing with fluids of low electrical conductivity, for effects due to Lorentz forces associated with the flow of electric currents are then negligible, as in dynamical meteorology and oceanography. In these highly developed areas of geophysical fluid dynamics a key role is played by the concept of *potential vorticity* (PV). This pseudoscalar quantity—defined as the reciprocal of the density of the fluid multiplied by the scalar product of the vorticity vector and the gradient of any differentiable scalar quantity, such as the potential temperature or specific entropy of the fluid (see Eqs. (2), (17) below)—satisfies an elegant theorem (see Eq. (3)) due to Ertel (1942; see also Gill, 1982; Pedlosky, 1987).

In the words of Pedlosky (1987, p. 38) extolling the virtues of Ertel's theorem: "although the vorticity equation [which expresses the effects of torques associated with forces acting on a moving fluid element] is illuminating because it deals directly with the vector character of vorticity, it is more descriptive of how vorticity is changed than a useful constraint on that change. Kelvin's (circulation) theorem is more powerful, but (it) is an integral theorem dealing with a scalar and requires knowledge of the detailed evolution of material surfaces in the fluid. ... (The) beautiful and unusually useful theorem due to Ertel (governing the behavior of potential vorticity) ... provides a constraint on vorticity which is free from many of (these) difficulties..."

An analogous constraint (Hide, 1983) on the behavior of the magnetic field (rather than vorticity) in a moving electrically conducting medium follows directly from the equations of electrodynamics (see Eqs. (6), (7) below). The constraint involves the concept of *potential magnetic field* (PMF) (defined by Eq. (6)), the behavior of which is governed by the general expression given by Eq. (7), the electrodynamic analogue of the Ertel PV theorem (for recent references see Hide, 2002, 2004). The full set of mathematical equations obtained by incorporating into extended versions of these PV and PMF theorems (see Eqs. (8) and (9) below) the constraints that arise from thermodynamic considerations on *potential temperature* or *specific entropy* should facilitate future theoretical and numerical investigations of the *geodynamo* (*q.v.*) and other MHD phenomena encountered in theoretical geophysics and astrophysics; see Hide (1996). The rest of present article closely follows Hide (1996), material from which is reproduced here by kind permission of the Royal Astronomical Society and Blackwell Publishers.

Potential vorticity

Consider a continuous medium in which the mass density is $\rho(\boldsymbol{r},t)$ and Eulerian velocity relative to an inertial frame is $\boldsymbol{u}(\boldsymbol{r},t)$ at a general point P with position vector $\mathbf{r}$ at time t. Conservation of mass requires that

$$\frac{\mathrm{D}\rho}{\mathrm{D}t} + \rho\nabla\cdot\boldsymbol{u} = 0 \qquad \text{(Eq. 1)}$$

(where $\mathrm{D}/\mathrm{D}t \equiv \partial/\partial t + \boldsymbol{u}\cdot\nabla$), which reduces to $\nabla\cdot\boldsymbol{u} = 0$ when the medium is incompressible.

If by $\xi \equiv \nabla\times\boldsymbol{u}$ we denote the (absolute) vorticity and by

$$\rho^{-1}\xi\cdot\nabla H^* \qquad \text{(Eq. 2)}$$

the so-called "potential vorticity", where $H^* = H^*(\boldsymbol{r},t)$ is any continuous and differentiable function, then by a very slight extension of Ertel's theorem (see Gill, 1982; Pedlosky, 1987), we have

$$\frac{\mathrm{D}}{\mathrm{D}t}\left(\frac{\xi\cdot\nabla H^*}{\rho}\right) = \frac{\xi}{\rho}\cdot\nabla\frac{\mathrm{D}H^*}{\mathrm{D}t} + \nabla H^*\cdot\Psi \qquad \text{(Eq. 3)}$$

where

$$\Psi \equiv \rho^{-2}[\mathbf{g}\times\nabla\rho + \nabla\times(\boldsymbol{j}\times\boldsymbol{B}) + \nabla\times\boldsymbol{F}]. \qquad \text{(Eq. 4)}$$

Here $-\mathbf{g}$ is the acceleration due to gravity and $\boldsymbol{j} \times \boldsymbol{B}$ the, Lorentz ponderomotive force, if $\boldsymbol{j}(\boldsymbol{r},t)$ is the electric current density at P and $\boldsymbol{B}(\boldsymbol{r},t)$ is the magnetic field, which satisfies

$$\nabla \cdot \boldsymbol{B} = 0. \qquad \text{(Eq. 5)}$$

The term $\boldsymbol{F}$ in Eq. (4) represents the visco-elastic force acting on an element of material of unit volume which at time t is situated at P, reducing in the case of a fluid to the usual term representing the viscous force.

Potential magnetic field

Analogous to the derivation of Eq. (3) from the equations of dynamics, is the derivation from the equations of electrodynamics of an expression governing the behavior of the "potential magnetic field", defined as

$$\rho^{-1}\boldsymbol{B} \cdot \nabla G^* \qquad \text{(Eq. 6)}$$

(where G^*, like H^*, is any continuous and differentiable function of $\boldsymbol{r}$ and t), namely

$$\frac{\mathrm{D}}{\mathrm{D}t}\left(\frac{\boldsymbol{B} \cdot \nabla G^*}{\rho}\right) = \frac{\boldsymbol{B}}{\rho} \cdot \nabla \frac{\mathrm{D}G^*}{\mathrm{D}t} + \nabla G^* \cdot \Phi \qquad \text{(Eq. 7)}$$

(Hide, 1983). Here Φ comprises several terms, all of which vanish when the medium is a perfect conductor of electricity and thermoelectric, Hall, Nernst-Ettinghausen and other "nonohmic" effects are negligible. (Consistent with the neglect of relativistic effects, no account is taken of Maxwell displacement currents and electrostatic forces can be ignored in $\boldsymbol{F}$, see Eq. (4).)

Now make the successive substitutions $H^* = H$ and then $H^* = q'H$ in the potential vorticity Eq. (3) and combine the resulting two equations to obtain

$$\frac{\mathrm{D}}{\mathrm{D}t}\left[\frac{H}{\rho}\xi \cdot \nabla q'\right] = \left(\frac{\xi \cdot \nabla q'}{\rho}\right)\frac{\mathrm{D}H}{\mathrm{D}t} + \frac{H}{\rho}\left(\xi \cdot \nabla \frac{\mathrm{D}q'}{\mathrm{D}t}\right) + H\Psi \cdot \nabla q' \qquad \text{(Eq. 8)}$$

In the same way, substitute $G^* = G$ and then $G^* = qG$ in the potential magnetic field equation (7); hence

$$\frac{\mathrm{D}}{\mathrm{D}t}\left[\frac{G}{\rho}\mathbf{B} \cdot \nabla q\right] = \left(\frac{\mathbf{B} \cdot \nabla q}{\rho}\right)\frac{\mathrm{D}G}{\mathrm{D}t} + \frac{G}{\rho}\left(\mathbf{B} \cdot \nabla \frac{\mathrm{D}q}{\mathrm{D}t}\right) + G\Phi \cdot \nabla q \qquad \text{(Eq. 9)}$$

(The functions H, G, q, and q' are also arbitrary. see Hide, 1996.)

Equations (8) and (9) are useful extensions of the general results expressed by Eqs. (3) and (7) respectively, for each equation contains two arbitrary scalars, rather than just one. Suitable choices of these scalars lead directly to other general results, such as a relationship between forms of potential vorticity, helicity and superhelicity in hydrodynamics and its counterpart in electrodynamics (see Hide, 1989, 2002).

Some geophysical applications

As an application of these equations we set $G = \xi \cdot \nabla q'$ in Eq. (9) and H as a comparable function of $\boldsymbol{B}$ and q in Eq. (8) and subtract the resulting equations. Thus:

$$\frac{\mathrm{D}}{\mathrm{D}t}\left[\log\frac{\mathbf{B} \cdot \nabla q}{\xi \cdot \nabla q'}\right] = (\mathbf{B} \cdot \nabla q)^{-1}\left[\mathbf{B} \cdot \nabla \frac{\mathrm{D}q}{\mathrm{D}t} + \rho\Phi \cdot \nabla q\right] - (\xi \cdot \nabla q')^{-1}\left[\xi \cdot \nabla \frac{\mathrm{D}q'}{\mathrm{D}t} + \rho\Psi \cdot \nabla q'\right] \qquad \text{(Eq. 10)}$$

Equation (10) is particularly useful when q and q' are simply related to the coordinates of the general point P. Consider for example the case when spherical polar coordinates (r, θ, ϕ) are used and $q = q' = r$. Equation (10) then reduces to

$$\frac{\mathrm{D}}{\mathrm{D}t}\left[\log\left(\frac{\mathbf{B}_r}{\xi_r}\right)\right] = \frac{1}{B_r}(\hat{\mathbf{B}} \cdot \hat{\nabla} u_r + \rho\Phi_r) - \frac{1}{\xi_r}\left[\hat{\xi} \cdot \hat{\nabla} u_r + \rho\Psi_r\right] \qquad \text{(Eq. 11)}$$

where the subscript r denotes the r-component of the corresponding vector and the operators

$$\hat{\mathbf{B}} \cdot \hat{\nabla} \equiv \mathbf{B} \cdot \nabla - B_r\partial/\partial r \quad \text{and} \quad \hat{\xi} \cdot \hat{\nabla} \equiv \xi \cdot \nabla - \xi_r\partial/\partial r \qquad \text{(Eq. 12)}$$

Comparable relationships can be found by setting q and q' equal to θ and ϕ.

In geophysical and astrophysical fluid dynamics we are often interested in fluids for which the electrical conductivity is very high and "non-ohmic" effects (see Eq. (7)) are negligible, so that Alfvén's "frozen magnetic flux" (*q.v*) theorem holds. Then the vector $\Phi = 0$ in Eq. (7) (see also Eqs. (9), (10) (11)) which when $G^* = r$ and the fluid is incompressible (so that $\mathrm{D}\rho/\mathrm{D}t$, see Eq. (1)) gives

$$\frac{\mathrm{D}}{\mathrm{D}t}B_r = \mathbf{B} \cdot \nabla u_r \qquad \text{(Eq. 13)}$$

This equation has been put to good use by geophysicists in work on the determination of the flow just below the Earth's core-mantle interface from observations of the *geomagnetic secular variation* (*q.v.*); see Eq. (16) below.

Also of interest are studies of flows in rapidly rotating systems, where it is convenient to work in a frame of reference that rotates relative to an inertial frame with angular velocity $\Omega = (\Omega\cos\theta, -\Omega\sin\theta, 0)$ about the polar axis. Equations (1)–(11) hold in the new frame if we re-define ξ as being equal to $\nabla \times \boldsymbol{u} + 2\Omega$, include centripetal effects in $\mathbf{g}$ and add the term $\rho\boldsymbol{r} \times \mathrm{d}\Omega/\mathrm{d}t$ to $\boldsymbol{F}$ (see Eq. (4)). Such flows include those where to a first approximation buoyancy forces act in the radial direction and other forces and torques acting on individual fluid elements are in magnetostrophic balance which, when Lorentz forces are also negligible, reduces to geostrophic balance. Magnetostrophic balance is characterized here by setting

$$(\xi_r, \xi_\theta) = 2\Omega(\cos\theta, -\sin\theta) \quad \text{and} \quad \Psi = \rho^{-2}\boldsymbol{j} \times \boldsymbol{B}, \qquad \text{(Eq. 14)}$$

with $\Psi = 0$ in the geostrophic case. When combined with Eq. (14), Eq. (11) gives

$$\frac{\mathrm{D}}{\mathrm{D}t}\log\left(\frac{B_r}{\cos\theta_r}\right) = \left(\frac{\hat{\boldsymbol{B}} \cdot \hat{\nabla}}{B_r} - \frac{\hat{\xi} \cdot \hat{\nabla}}{2\Omega\cos\theta}\right)u_r - \frac{[\nabla \times (\boldsymbol{j} \times \boldsymbol{B})]_r}{2\rho\,\Omega\cos\theta} \qquad \text{(Eq. 15)}$$

In the case of geostrophic flow over a spherical surface where u_r is negligibly small in magnitude in comparison with u_θ and u_ϕ, it follows immediately from Eq. (15) that

$$\frac{\mathrm{D}}{\mathrm{D}t}(B_r\sec\theta) = 0 \qquad \text{(Eq. 16)}$$

implying the conservation of the quantity $B_r\sec\theta$ on moving fluid elements. This result is a familiar one in work on the determination of motions just below the Earth's core-mantle boundary from *geomagnetic secular variation* data (*q.v.*), where near-uniqueness can be secured by combining the assumption of geostrophy with Alfvén's

frozen magnetic flux theorem (see Eq. (13)). Conditions under which the result can be expected to apply are clearly exposed by its novel derivation here from the powerful general theorems governing the behavior of potential vorticity and potential magnetic field in magnetohydrodynamic flows.

The full equations of magnetohydrodynamics express not only the laws of mechanics (the basis of Eq. (3)) and of electrodynamics (the basis of Eq. (7)) but also the laws of thermodynamics governing, inter alia, the behavior of specific entropy $\Theta = \Theta(\boldsymbol{r},t)$. This quantity satisfies

$$\frac{D\Theta}{Dt} = Q \qquad \text{(Eq. 17)}$$

where $Q = Q(\boldsymbol{r},t)$ represents thermal conduction, radiation and other diabatic effects, including ohmic heating. We conclude this short note by observing that Eq. (10) with $q = q' = \Theta$ shows that isentropic flows, for which $Q = 0$ by definition, satisfy

$$\frac{D}{Dt}\left(\frac{\mathbf{B}\cdot\nabla\Theta}{\xi\cdot\nabla\Theta}\right) = 0 \qquad \text{(Eq. 18)}$$

in regions where Ψ^* and Φ are also negligibly small. According to Eq. (18), within such flows the ratio of the components of $\boldsymbol{B}$ and ξ in the direction of $\nabla\Theta$, the gradient of specific entropy, is (like Θ itself) conserved on moving fluid elements. A further result of geophysical and astrophysical interest is that Eq. (18) reduces to Eq. (16) in cases when approximate geostrophic balance obtains and the nonradial components of $\nabla\Theta$ are much weaker than its radial component.

Raymond Hide

Bibliography

Ertel, H., 1942. Ein neuer hydrodynamischer Wirbelsatz. *Meteorologische Zeitscrift*, **59**: 271–281.

Gill, A.E., 1982. *Atmosphere-Ocean Dynamics*. New York: Academic Press.

Hide, R., 1983. The magnetic analogue of Ertel's potential vorticity theorem. *Annales Geophysicae*, **1**: 59–60.

Hide, R., 1989. Superhelicity, helicity and potential vorticity. *Geophysical and Astrophysical Fluid Dynamics*, **48**: 69–79.

Hide, R., 1996. Potential vorticity and potential magnetic field in magnetohydrodynamics. *Geophysical Journal International*, **125**: F1–F3.

Hide, R., 2002. Helicity, superhelicity and weighted relative potential vorticity (and their electrodynamic counterparts): Useful diagnostics pseudoscalars? *Quarterly Journal of the Royal Meteorological Society*, **128**: 1759–1762.

Hide, R., 2004. Reflections on the analogy between the equations of electrodynamics and hydrodynamics. In Schröder, W. (ed.), *Hans Ertel: Gedenkschrift zum 100. Geburtstag*. Bremen: Deutscher Arbeitskreis Geschichte, Geophysik und Kosmische Physik, pp. 25–33.

Pedlosky, J., 1987 *Geophysical Fluid Dynamics*, 2nd edn. New York: Springer-Verlag.

Cross-references

Alfvén's Theorem and the Frozen Flux Approximation
Core Motions
Geodynamo
Geomagnetic Secular Variation
Magnetohydrodynamics
Proudman-Taylor Theorem

PRECESSION AND CORE DYNAMICS

The Earth is forced to precess by the gravitational action of the Sun, the Moon and the other planets of the solar system on its equatorial budge. Like a spinning top, the axis of rotation of the planet moves on a cone of semiangle 23.27° with a period of 26000 years, which is known from early astronomy as the precession of the Earth. The motions of the axis on smaller cones with shorter periods are known as nutations. The amplitudes and periods of the precession nutations are directly connected to the shape (ellipticity) and structure of the Earth. The presence of a liquid layer (the core) at the center of the planet introduces a differential precession between liquid and solid parts and their coupling sets the amplitude of this difference. After a first attempt by Kelvin, Hough (1895) and Poincaré (1910) were the first to model this problem in order to determine whether the interior of the Earth is liquid or solid. Considering an inviscid fluid, Poincaré suggested that the response of the fluid is rather simple as it is a solid body rotation and a gradient flow associated with the ellipticity of the solid boundary. More generally, Busse (1968) revealed an analogy between the core flow induced by precession and the one due to tidal bulge. Malkus (1968) envisioned the core motion associated with precession as a possible source for the geodynamo.

Position of the axis of rotation of the Core

The axis of rotation of the liquid core differs from the axis of rotation of the mantle and the torque balance on the fluid core gives the relative position of the two axes (Poincaré (1910) for the inviscid problem and Busse (1968) for the viscous correction). In Figure P58, the photograph illustrates this situation as the rotation axis of fluid is clearly off the axis of the container. It is worth noting that there is no differential rotation along the axis of rotation of the fluid while the flow

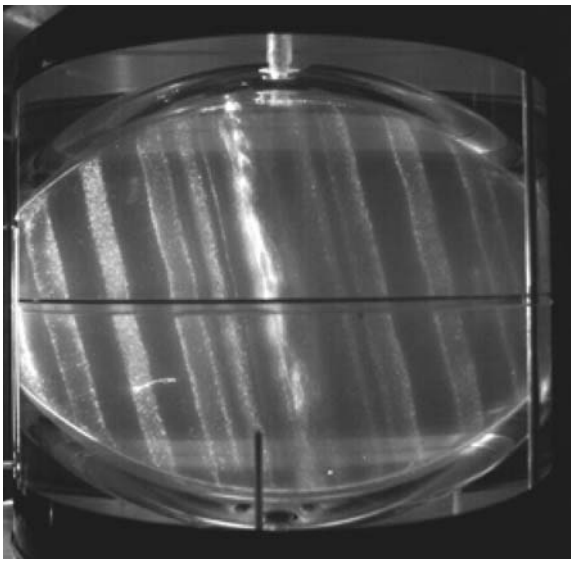

Figure P58 Precessional flow in a laboratory spheroid. Kalliroscope flakes dispersed in the fluid are illuminated by a beam of light in a plan containing both the rotation axis of the container and of the fluid. Any shear in the flow aligns the flakes. The obliquity angle is 20°. Experimental details can be found in Noir *et al.* (2003). Meridional cross sections of geostrophic cylinders aligned with the axis of the Poincaré mode are clearly seen. Oscillations (or instabilities?) of the axis are also visible.

induced by precession is not associated with a spin-up process, which would not preserve the geometry of the Poincaré mode (Greenspan, 1968). As the Earth's rotation decreases, the precessional and nutational forcings vary and the fluid response may match an eigenmode flow in the rotating core known as the "tilt-over mode" (Greenspan, 1968), generating a resonance in the core which may be related to the reversals frequency of the geomagnetic field or major geologic events (Greff and Legros, 1999). Noir *et al*. (2003) have observed this resonance in their experiment and showed its nonlinear implications from the torque balance; very large excursions of the axis of rotation of the fluid are predicted. It remains unclear how the presence of an inner core (with a different ellipticity) would influence these results.

Boundary layer singularities

A thin boundary layer develops at the core-mantle boundary to ensure continuity of the velocity field. Both magnetic (electromagnetic skin layer) and viscous (Ekman layer) effects form a layer a few hundreds meter in depth at the liquid core boundaries (see Core, boundary layers, Loper, 1975; Deleplace and Cardin, 2005). Because of their diurnal oscillations, the viscous boundary layer is singular at the critical latitudes ($\pm 30^\circ$) and diurnal jets or shear layers erupt in the bulk fluid along characteristic cones associated with inertial waves in the fluid core (Hollerbach and Kerswell, 1995; Noir *et al*., 2001). Asymptotic scaling (with no magnetic field) lead to diurnal motions in the core of amplitude $\approx 10^{-5}$ m/s, depending on the effective viscosity of the fluid outer core.

Geostrophic motions

Cylindrical motions have been observed in precession experiments (Malkus, 1968; Vanyo *et al*., 1995). In Figure P58, we clearly see axisymmetric geostrophic shear flows (Black and white lines parallel to the axis of rotation). Their source is associated with a nonlinear effect in the boundary layer at the critical latitude. These geostrophic motions have been retrieved in nonlinear calculations of precessing flows (Noir *et al.*, 2001). Malkus (1968) determined the amplitude of the velocities of the geostrophic cylinders and the recent numerical results agree qualitatively with his experimental findings. In the absence of magnetic field, an amplitude of 10^{-5} m/s of the geostrophic cylinders is predicted in the Earth's core.

Instabilities

In Figure P58 the central axis of rotation of the fluid shows a variation of the brightness. This modulation may be the signature of an elliptical or shear instability, which would result from the nonlinear interaction of two inertial waves and the Poincaré flow according to symmetry rules (Kerswell, 2002). Such an instability may lead to intermittency of small-scale turbulence (Malkus, 1989; Lorenzani and Tilgner, 2003; Lacaze *et al*., 2004). It is difficult to apply these results to planetary interiors as they are only partially understood in simple systems.

Dynamo action

In the past, energetic arguments based on the Poincaré mode alone, have been used to rule out precession as a source for the geodynamo (Loper, 1975). This result is invalid if we consider that the Poincaré mode transfers energy from the kinetic energy stored in the Earth's equatorial rotation (Malkus, 1968) to secondary motions within the core (geostrophic cylinders, instabilities) through nonlinear effects which have not been taken into account in Loper's approach.

The Poincaré flow cannot produce any dynamo action as it is mainly a solid body rotation. The erupted layers and connected inertial waves are diurnal and confined to very small regions; they may participate to a permanent dynamo only through a nonlinear and alpha-effect but no results have been reported according to our knowledge. Geostrophic motions and associated instabilities can produce a kinematic dynamo as Tilgner (2005) just proved, at least for a very viscous fluid. The importance of elliptical instabilities for the dynamo remains an open question even though Aldridge and Baker (2003) used them as a basis of an interpretation of the paleomagnetic reversals frequency.

Philippe Cardin

Bibliography

Aldridge, K., and Baker, R., 2003. Paleomagnetic intensity data: a window on the dynamics of Earth's fluid core? *Physics of the Earth and Planetary Interiors*, **140**: 91–100.

Busse, F.H., 1968. Steady fluid flow in a precessing spheroidal shell. *Journal of Fluid Mechanics*, **33**: 739–751.

Deleplace, B., and Cardin, P., 2005. Viscomagnetic torque at the core mantle boundary. submitted to *Geophysical Journal International*, GJI, 2006, **167**: 557–566.

Greenspan, H.P., 1968. *The Theory of Rotating Fluids.* Cambridge: Cambridge University Press.

Greff, M., and Legros, H., 1999. Core rotational dynamics and geological events. *Science*, **286**: 1707–1709.

Hollerbach, R., and Kerswell, R.R., 1995. Oscillatory internal shear layers in rotating and precessing flows. *Journal of Fluid Mechanics*, **298**: 327–339.

Hough, S.S., 1895. The oscillations of a rotating ellipsoidal shell containing fluid. *Philosophical Transactions of the Royal Society of London*, **186**: 469.

Kerswell, R.R., 2002. Elliptical instability. *Annual Review of Fluid Mechanics*, **34**: 83–113.

Lacaze, L., Le Gal, P., and Le Dizs, S., 2004. Elliptical instability in a rotating spheroid. *Journal of Fluid Mechanics*, **505**: 1–22.

Loper, D.E., 1975. Torque balance and energy budget for the precessionally driven dynamo. *Physics of the Earth and Planetary Interiors*, **11**: 43–60.

Lorenzani, S., and Tilgner, A., 2003. Inertial instabilities of fluid flow in precessing spheroidal shells. *Journal of Fluid Mechanics*, **492**: 363–379.

Malkus, W.V.R., 1968. Precession of the Earth as the cause of geomagnetism. *Science*, **160**: 259–264.

Malkus, W.V.R., 1989. An experimental study of global instabilities due to tidal (elliptical) distortion of a rotating elastic cylinder. *Geophysical and Astrophysical Fluid Dynamics*, **48**: 123–134.

Noir, J., Cardin, P., Jault, D., and Masson, J.-P., Experimental evidence of nonlinear resonance effects between retrograde precession and the tilt-over mode within a spheroid. *Geophysical Journal International*, **154**: 407–416.

Noir, J., Jault, D., and Cardin, P., 2001. Numerical study of the motions within a slowly precessing sphere at low Ekman number. *Journal of Fluid Mechanics*, **437**: 283–299.

Poincaré, H., 1910. Sur la précession des corps déformables. *Bulletin of Astronomical Society*, **27**: 321–356.

Tilgner, A., 2005. Precession driven dynamos. *Physics of Fluid*, **17**: 034104.

Vanyo, J., Wilde, P., Cardin, P., and Olson, P., 1995. Experiments on precessings flows in the Earth's liquid core. *Geophysical Journal International*, **121**: 136–142.

Cross-references

Core, Boundary Layers
Core, Magnetic Instabilities
Fluid Dynamics Experiments
Geodynamo, Energy Sources
Gravity-Inertio Waves and Inertial Oscillations

PRICE, ALBERT THOMAS (1903–1978)

An applied mathematician, born in Nantwich, Cheshire, Price is regarded as one of the founding figures in the development of geomagnetism, and was particularly concerned with the determination of the electrical properties of the Earth's interior. He pioneered methods for analyzing magnetic variations and for separating them into parts arising externally and internally to the Earth's surface. Treating the external part as an inducing field, he sought to explain the internal induced part by establishing theory for electromagnetic induction in spheres, in thin sheets and shells and in half-spaces. These had direct relevance to global problems of induction in the Earth, the oceans and the ionosphere, and to local problems of electromagnetic exploration. He sought mathematical theories to explain existing data and drove data acquisition programs to test mathematical theories.

A fundamental paper by Price and Chapman (1928) (see *Chapman, Sydney*) established that diurnal variations in the Earth's magnetic field are derivable from a scalar potential. In the 1930s, Price derived formal solutions to induction in uniformly conducting spheres by aperiodic inducing fields (Price, 1930) and included permeability (Price, 1931), complementing solutions of Lamb for periodic fields. This made him possible to investigate the conductivity of the Earth using both the periodic daily variation of the magnetic field on quiet days (S_q) and the aperiodic storm time variations (D_{st}) (see *Storms and substorms, magnetic* (*q.v.*)). He applied these theories, again with Chapman, establishing the validity of global electromagnetic induction and determining conductivity models for D_{st} (Chapman and Price, 1930) (see *Mantle, electrical conductivity, mineralogy*). The deeper penetrating storm time fields required a higher conductivity than was the case for S_q and this was early evidence that the Earth's electrical conductivity increases with depth. In a classic paper (Lahiri and Price, 1939), spheres in which the conductivity varied as a function of radius were considered. Analytic solutions were obtained for the special case of conductivity varying as a power of the normalized radius. These remain the only analytic solutions determined to date. Application of the theory jointly to both S_q and D_{st} revealed a rapid increase in conductivity around 600–700 km depth, a result of major importance in the study of the Earth. An additional requirement was the inclusion of a thin conducting shell at the Earth's surface, which was assumed to represent an effect of the conducting oceans.

Price provided theory for induction in nonuniform thin sheets and shells electrically insulated from their surroundings (Price, 1949), establishing what became known as Price's Equation (Parkinson, 1983). He provided analytic solutions for specific conductivity distributions and iterative schemes for obtaining numerical approximations for the general case. Through this he initiated two lines of research-induction in the ionosphere and induction in the oceans. Price's reappraisal of ionospheric current flow with Cocks (Cocks and Price, 1969) concluded that the prevalent theory of two-dimensional current flow was inadequate and that the external part of the S_q variations required a component of vertical current flow, now a well-established premiss in ionospheric studies (see *Ionosphere*). With Hobbs (Hobbs and Price, 1970) he derived a suite of surface integral formulae which found direct application in his iterative schemes for solving problems of induction in the nonuniformly distributed oceans. An intense period of thin-sheet oceanic induction studies followed until computing power in the 1980s was able to cope with a thin surface sheet electrically coupled to the underlying mantle (see *Ocean, electromagnetic effects*).

Price's continuing interest in S_q led to a new method of separating parts arising externally to the Earth from those arising from within the earth due to induction. The two-step method, proposed with Wilkins (Price and Wilkins, 1963), involved first determining values of a potential function on the Earth's surface representing the total magnetic variation field and then separating this total field into its external and internal parts using surface integrals. The potential function was determined by iteration, minimizing residuals of line integrals of the magnetic field around closed contours on the Earth's surface. Application of the surface integrals required establishing tables of values of integrands over worldwide tesseral elements. The new method was applied, using banks of mechanical calculators, to observations made during the International Polar Year (Price and Wilkins, 1963) and to the International Geophysical Year (1964). Price was instrumental, again with Chapman, in proposing and establishing S_q as a subject of study during the International Quiet Sun Year.

Price also provided theory for so-called local induction problems, whereby the Earth is represented as a half-space. In 1950 he gave complete solutions for induced and freely decaying modes and showed that induction in a half-space by a uniform field is an indeterminate problem (Price, 1950). In 1962 he presented formal theory for the magnetotelluric method including consideration of the dimensions of the source field (Price, 1962) (see *Magnetotellurics*). Work with Jones (Jones and Price, 1970) involved a detailed analysis of boundary conditions applicable to two-dimensional induction problems and showed how numerical solutions could be obtained for models that included inhomogeneous conducting regions. This paved the way for the interpretation of anomalies found in the rapidly expanding field of magnetotelluric surveys.

Summaries of much of his work, and that of others, are given in two valuable reviews (Price, 1967a,b). These reviews include observational material, theory, and applications together with physical and mathematical insights into geomagnetic phenomena. They are still useful works of reference.

In an academic career spanning of 43 years, Price held appointments at Queen's University, Belfast (1925); Imperial College, London (1926–1951); Royal Technical College, Glasgow (1951–1952) and University of Exeter (1952–1968). He was an IGY Research Associate at the National Academy of Sciences, Washington (1961–1962) and Chairman of Commission IV of IAGA on Magnetic Activity and Disturbances (1964–1968). The Gold Medal of the Royal Astronomical Society was awarded to Price in 1969 for his work on geomagnetism and especially for his studies of the electrical conductivity in the interior of the Earth. The Royal Astronomical Society awards the Price Medal for geomagnetism and aeronomy, in his honor.

Bruce A. Hobbs

Bibliography

Chapman, S., and Price, A.T., 1930. The electric and magnetic state of the interior of the Earth as inferred from terrestrial magnetic variations. *Philosophical Transactions of the Royal Society of London*, A**229**: 427–460.

Cocks, A.C., and Price, A.T., 1969. Sq currents in a 3-dimensional ionosphere. *Planetary and Space Science*, **17**: 471–482.

Hobbs, B.A., and Price, A.T., 1970. Surface integral formulae for geomagnetic studies. *Geophysical Journal of the Royal Astronomical Society*, **20**: 49–63.

Jones, F.W., and Price, A.T., 1970. Perturbations of alternating geomagnetic fields by conductivity anomalies. *Geophysical Journal of the Royal Astronomical Society*, **20**: 317–334.

Lahiri, B.N., and Price, A.T., 1939. Electromagnetic induction in nonuniform conductors and the determination of the conductivity of the Earth from terrestrial magnetic variations. *Philosophical Transactions of the Royal Society of London*, A**237**: 509–540.

Parkinson, W.D., 1983. *Introduction to Geomagnetism.* Edinburgh: Scottish Academic Press.

Price, A.T., 1930. Electromagnetic induction in a conducting sphere. *Proceedings of the London Mathematical Society*, [2], **31**: 217–224.

Price, A.T., 1931. Electromagnetic induction in a permeable conducting sphere. *Proceedings of the London Mathematical Society*, [2], **33**: 233–245.

Price, A.T., 1949. The induction of electric currents in nonuniform thin sheets and shells. *Quarterly Journal of Mechanics and Applied Mathematics*, **2**: 283–310.
Price, A.T., 1950. Electromagnetic induction in a semi-infinite conductor with a plane boundary. *Quarterly Journal of Mechanics and Applied Mathematics*, **3**: 385–410.
Price, A.T., 1962. Theory of magnetotelluric methods when the source field is considered. *Journal of Geophysical Research*, **67**: 1907–1918.
Price, A.T., 1967a. Electromagnetic Induction within the Earth. In Matsushita, S., and Campbell, W.H. (eds.), *Physics of Geomagnetic Phenomena.* London and New York: Academic Press, pp. 235–295.
Price, A.T., 1967b. Magnetic Variations and Telluric Currents. In Gaskell, T.F. (ed.), *The Earth's Mantle.* London and New York: Academic Press, pp. 125–170.
Price, A.T., and Chapman, S., 1928. On line-integrals of the diurnal magnetic variations. *Proceedings of the Royal Society of London*, A**119**: 182–196.
Price, A.T., and Stone, D.J., 1964. The quiet day magnetic variations during the IGY. In *Annals of the International Geophysical Year*, **35** Part III.
Price, A.T., and Wilkins, G.A., 1963. New methods for the analysis of geomagnetic fields and their application to the Sq field of 1932–1933. *Philosophical Transactions of the Royal Society of London*, A**256**: 31–98.

Cross-references:

Chapman, Sydney (1888–1970)
Ionosphere
Magnetotellurics
Mantle, Electrical Conductivity, Mineralogy
Ocean, Electromagnetic Effects
Storms and Substorms, Magnetic

PRINCIPAL COMPONENT ANALYSIS IN PALEOMAGNETISM

When studying the mean and variance of paleomagnetic data it is a common practice to employ principal component analysis (Jolliffe, 2002). The theory of this method is related to the mathematics quantifying the moment of inertia of a set of particles of mass about some reference point of interest. For the purposes of data analysis, principal component analysis was first promoted by Pearson (1901) and Hotelling (1933), and it also often associated with Karhunen (1947) and Loéve (1977). Principal component analysis is widely applied in crystallography (e.g., Schomaker *et al*., 1959). In paleomagnetism (e.g., Mardia, 1972; Kirschvink, 1980), it finds application in studies of the average paleofield, paleosecular variation, demagnetization, and magnetic susceptibility. Here we discuss and demonstrate principal component analysis in application to full paleomagnetic vectorial data and, separately, to paleomagnetic directional data.

Vectorial analysis

Consider a set of paleomagnetic vectors, with the ith vector $\mathbf{x}(i)$ having intensity, inclination, and declination values ($F(i)$, $I(i)$, $D(i)$). Their equivalent Cartesian expression is just

$$\begin{aligned} x_1(i) &= F(i)\cos I(i)\cos D(i),\\ x_2(i) &= F(i)\cos I(i)\sin D(i),\\ x_3(i) &= F(i)\sin I(i), \end{aligned} \qquad \text{(Eq. 1)}$$

where $\mathbf{x} = (x_1, x_2, x_3)$ represents the usual geographic components of (north, east, down). With N such vectorial data we can calculate their values relative to some fixed reference point $\mathbf{r} = (r_1, r_2, r_3)$

$$\delta\mathbf{x}(i) = \mathbf{x}(i) - \mathbf{r} \qquad \text{(Eq. 2)}$$

and with which we can calculate their covariance matrix,

$$\mathrm{C} = \frac{1}{N}\begin{pmatrix} \sum \delta x_1(i)^2 & \sum \delta x_1(i)\delta x_2(i) & \sum \delta x_1(i)\delta x_3(i) \\ \sum \delta x_2(i)\delta x_1(i) & \sum \delta x_2(i)^2 & \sum \delta x_2(i)\delta x_3(i) \\ \sum \delta x_3(i)\delta x_1(i) & \sum \delta x_3(i)\delta x_2(i) & \sum \delta x_3(i)^2 \end{pmatrix}. \qquad \text{(Eq. 3)}$$

This matrix can be reduced to diagonal form by an appropriate choice of axes, obtained by solving the eigenvalue problem

$$\mathrm{C}\mathbf{e}^m = \lambda_m \mathbf{e}^m, \qquad \text{(Eq. 4)}$$

where $\mathbf{e}^m$ is an eigenvector and λ_m is an eigenvalue (e.g., Strang, 1980). Three eigenvectors $\mathbf{e}^m$, for $m = 1, 2, 3$, and their corresponding eigenvalues λ_m can be found using standard numerical packages, such as LAPACK. The eigenvectors are orthogonal, and therefore

$$\mathbf{e}^m \cdot \mathbf{e}^n = 0, \quad \text{for} \quad m \neq n. \qquad \text{(Eq. 5)}$$

The eigenvectors only define directions; they are of arbitrary length. Here we choose to normalize the eigenvectors, so that

$$\mathbf{e}^m \cdot \mathbf{e}^m = 1. \qquad \text{(Eq. 6)}$$

The eigenvalues λ_m are real, but they have no particular ordering; we choose an ascending order here $\lambda_1 \leq \lambda_2 \leq \lambda_3$ for specificity.

Let us now examine transformations between geographic space $\mathbf{x}$ and eigen space, which we designate $\mathbf{z}$. A transformation matrix $\mathbf{E}$ can be constructed from a columnar arrangement of the eigenvectors $\mathbf{e}^m$. We choose to arrange the eigenvector columns in the order of their ascending eigenvalues,

$$\mathbf{E} = \begin{pmatrix} e_1^1 & e_1^2 & e_1^3 \\ e_2^1 & e_2^2 & e_2^3 \\ e_3^1 & e_3^2 & e_3^3 \end{pmatrix}. \qquad \text{(Eq. 7)}$$

The matrix $\mathbf{E}$ is orthonormal, and therefore its inverse is equal to its transpose,

$$\mathbf{E}^{-1} = \mathbf{E}^{\mathrm{T}}. \qquad \text{(Eq. 8)}$$

The matrix $\mathbf{E}$ rotates data from the eigenspace $\mathbf{z} = (z_1, z_2, z_3)$ into the original geographic space $\mathbf{x} = (x_1, x_2, x_3)$ through the transformation

$$\mathbf{x}(i) = \mathbf{E}\mathbf{z}(i). \qquad \text{(Eq. 9)}$$

The inverse transformation is given by

$$\mathbf{z}(i) = \mathbf{E}^{\mathrm{T}}\mathbf{x}(i). \qquad \text{(Eq. 10)}$$

The matrix $\mathbf{E}$ also diagonalizes the covariance matrix, so that

$$\mathbf{E}^{\mathrm{T}}\mathrm{C}\mathrm{E} = \Lambda, \qquad \text{(Eq. 11)}$$

where

$$\Lambda = \begin{pmatrix} \lambda_1 & 0 & 0 \\ 0 & \lambda_2 & 0 \\ 0 & 0 & \lambda_3 \end{pmatrix}. \qquad \text{(Eq. 12)}$$

All of these transformations are orthonormal, they are special cases of a more general similarity transformation, for which the trace is invariant, and so

$$\mathrm{tr}(\mathrm{C}) = \mathrm{tr}(\Lambda) = \sum_m \lambda_m. \quad \text{(Eq. 13)}$$

The eigenvectors and values have an important geometric interpretation. The variance of the data about the reference point $\mathbf{r}$ is an ellipsoid, which has the following simple expression in eigenspace

$$\frac{z_1^2}{\lambda_1} + \frac{z_2^2}{\lambda_2} + \frac{z_3^2}{\lambda_3} = 1. \quad \text{(Eq. 14)}$$

Depending on the relative sizes of the eigenvalues, different symmetries of the data distribution are revealed; a summary is given in Table P2. Note that each eigenvalue λ_m is the variance of the data along the direction defined by its corresponding eigenvector $\mathbf{e}^m$. If λ_3 is the largest eigenvalue, then the major axis is defined as the line segment joining the two points $\pm\sqrt{\lambda_3}\mathbf{e}^3$; the two other shorter minor axes are defined similarly. The eccentricity of each ellipsoidal equator is measured by

$$\epsilon_{mn} = \sqrt{1 - \frac{\lambda_m}{\lambda_n}}, \quad \text{for} \quad m < n. \quad \text{(Eq. 15)}$$

The overall anisotropy of the variance can be roughly quantified by the most eccentric ellipsoidal equator ϵ_{13}. Finally, it is important to recognize the fact that the line parallel to $\mathbf{e}^3(\mathbf{r})$ is, in a least-squares sense, the best fitting line to the data that passes through the reference point $\mathbf{r}$, with $\lambda_3(\mathbf{r})$ being a measure of the misfit to this line. Moreover, the plane normal to $\mathbf{e}^1(\mathbf{r})$, and which contains $\mathbf{e}^2(\mathbf{r})$ and $\mathbf{e}^3(\mathbf{r})$, is the least-squares, best fitting plane to the data that contains the reference point $\mathbf{r}$, with $\lambda_2(\mathbf{r}) + \lambda_3(\mathbf{r})$ functioning as a measure of misfit.

It is of interest to translate the eigenvalues into more conventionally interpretable quantities. For a prolate variance ellipsoid, Kirschvink (1980) has defined an approximate maximum angular deviation ($\mathrm{MAD_p}$) from the major axis $\mathbf{e}^3(0)$ by the conic angle determined by a projection of the minor ellipse onto the unit sphere

$$\mathrm{MAD_p} = \tan^{-1}\left[\sqrt{\frac{\lambda_1(0) + \lambda_2(0)}{\lambda_3(0)}}\right], \text{for} \quad \lambda_1 \simeq \lambda_2 \ll \lambda_3. \quad \text{(Eq. 16)}$$

For an oblate variance ellipsoid, we can also define a corresponding maximum angular deviation ($\mathrm{MAD_o}$) from the plane normal to the most minor axis along $\mathbf{e}^1(0)$,

$$\mathrm{MAD_o} = \tan^{-1}\left[\sqrt{\frac{\lambda_1(0)}{\lambda_2(0) + \lambda_3(0)}}\right], \quad \text{for} \quad \lambda_1 \ll \lambda_2 \simeq \lambda_3, \quad \text{(Eq. 17)}$$

which is somewhat different from the definition offered by Kirschvink. With respect to the maximum intensity deviation, if the variance ellipsoid about $\mathbf{r} = \bar{\mathbf{x}}$ is more or less spherical, then the maximum intensity deviation (MID) can be estimated as

Table P2 Eigenvalue classifications

Eigenvalues	Eigenvectors	Variance ellipsoid
$\lambda_1 = \lambda_2 = \lambda_3$	No preferred orientation	Spherical
$\lambda_1 = \lambda_2 < \lambda_3$	$\mathbf{e}^1$ and $\mathbf{e}^2$ have no preferred orientation	Prolate ellipsoid with rotational symmetry about $\mathbf{e}^3$
$\lambda_1 < \lambda_2 = \lambda_3$	$\mathbf{e}^2$ and $\mathbf{e}^3$ have no preferred orientation	Oblate ellipsoid with rotational symmetry about $\mathbf{e}^1$
$\lambda_1 \neq \lambda_2 \neq \lambda_3$	All eigenvectors have definite orientation	Scalene ellipsoid, with no axis of symmetry

Table P3 Principal component analysis of the Hawaiian data

Reference	Eigenvalue (μT^2)	Eigen direction $I(^\circ)$	Eigen direction $D(^\circ)$	Eccentricities ϵ_{12}	Eccentricities ϵ_{23}	Eccentricities ϵ_{13}	MID (μT)	$\mathrm{MAD_p}$ ($^\circ$)
			Past 5 Ma, Full vectors					
	34.4 (μT^2)	10.0	–96.4					
$r = 0$	65.6 (μT^2)	55.7	158.8	0.69				15.0
	1384.2 (μT^2)	32.5	0.1					
			Brunhes only, Full vectors					
	26.2 (μT^2)	12.5	–94.6					
$r = 0$	52.1 (μT^2)	54.2	157.5	0.71				12.8
	1505.4 (μT^2)	32.9	3.7					
	24.1 (μT^2)	11.4	–83.9					
$r = \bar{x}$	47.2 (μT^2)	44.3	174.7	0.70	0.81	0.91	11.8	
	138.4 (μT^2)	43.5	17.1					
			Past 5 Ma, Directions only					
	0.0304	–14.6	87.6					
$r = 0$	0.0601	–58.9	–48.4	0.71				17.6
	0.9088	31.1	–1.5					

Note: Results are shown for data recording a mixture of normal and reverse polarities over the past 5 Ma, as well as for normal Brunhes data only. Covariance is measured relative to the origin $\boldsymbol{r} = (0, 0, 0)$ and, for Brunhes data, relative to the vectorial mean $\bar{\boldsymbol{x}} = (31.3, 15.4, 19.7)\mu$T. The direction-only analysis utilizes unit vectors of the 5 Ma data set.

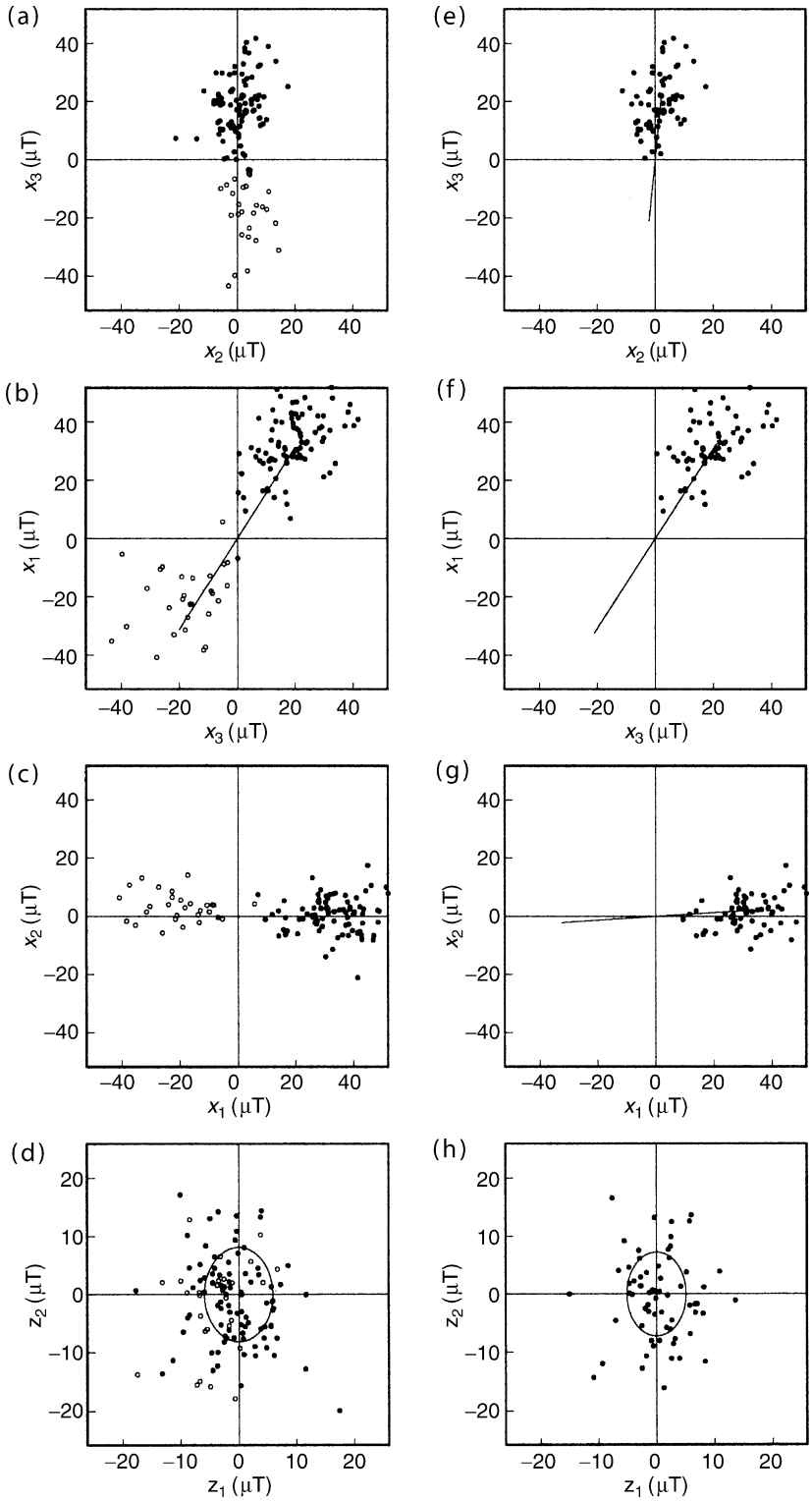

Figure P59 Projection of Hawaiian paleovector data onto the three geographic planes defined by (x_1,x_2,x_3) and onto the eigenplane $z_1 - z_2$ normal to the direction of the major axis defined by $\mathbf{e}^3$. (a-d) show data covering the past 5 Ma. (e-f) show data covering the normal Brunhes. In (a-c) and (e-f) we plot the major axis, and in (d) and (h) we plot the projection of the variance ellipse. Solid circles (disks) represent normal data, open circles represent reversed data.

$$\text{MID} = \sqrt{\frac{\lambda_1(\overline{\mathbf{x}}) + \lambda_2(\overline{\mathbf{x}}) + \lambda_3(\overline{\mathbf{x}})}{3}}, \quad \text{for} \quad \lambda_1 \simeq \lambda_2 \simeq \lambda_3. \tag{Eq. 18}$$

Otherwise, for aspherical dispersion, we need to consider the projection of the variance onto $\mathbf{e}^3(0)$,

$$\text{MID} = \sqrt{\sum_m \lambda_m(\overline{\mathbf{x}})[\mathbf{e}^m(\overline{\mathbf{x}}) \cdot \mathbf{e}^3(0)]^2}. \tag{Eq. 19}$$

Hawaiian bimodal vectors

Let us now illustrate the utility of principal component analysis with paleomagnetic data. For this example, we consider Hawaiian paleomagnetic vector data coming from lava flows emplaced over the past 5 Ma (Love and Constable, 2003), a period of time that encompasses several periods of normal and reverse field polarity. We consider only those flows that, upon sampling and subsequent measurement, have yielded complete triplets of intensity, inclination, and declination ($F(i)$, $I(i)$, $D(i)$), and which, therefore, represent the full ambient magnetic vector at the time of deposition. Calculating the covariance matrix about the origin, using $\mathbf{r} = 0$ in Eq. (3), we perform a principal component analysis to obtain the eigenvalues and corresponding eigenvectors; see Table P3. The major axis along $\mathbf{e}^3$ is orientated almost parallel to the mean direction found by others using other methodologies. This axis is shown in Figure P59a-P59c, where we see that it passes through both the zero point origin and the cloud of points defining the paleosecular variation. As a physical interpretation, it is this axis about which the geomagnetic field varies over time and, even, occasionally reverses its polarity. In Figure P59d we show the projection of the data onto the eigenplane $z_1 - z_2$, where we also plot the variance ellipse defined by the projection of the variance ellipsoid.

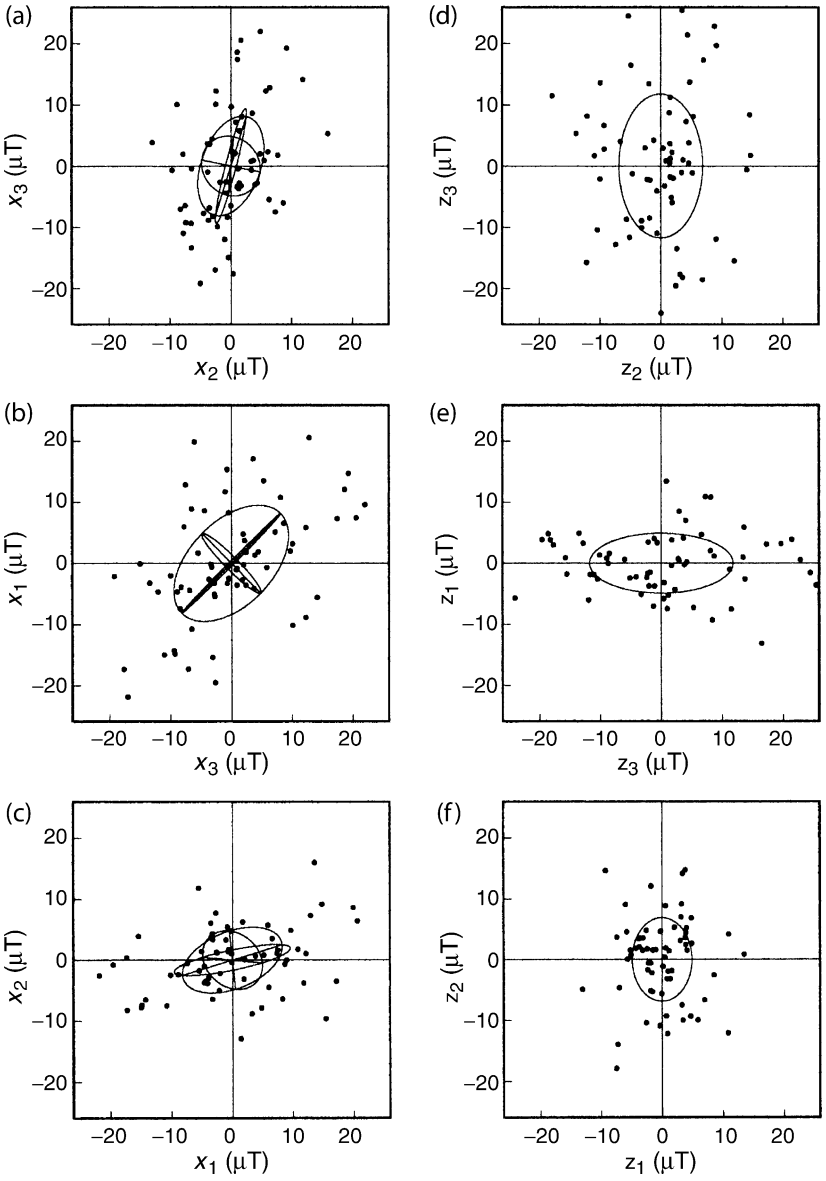

Figure P60 Projection of Brunhes Hawaiian paleovector secular-variation data (with mean vector having been subtracted) onto (a-c) the three geographic planes defined by (x_1, x_2, x_3) and onto (d-f) the three eigenplanes defined by (z_1, z_2, z_3). Also shown are the projections of the three equators of the variance ellipsoid in each coordinate system.

The slightly asymmetric form of the paleosecular variation about the major axis is to be noted.

Hawaiian unimodal vectors

Next, let us consider Brunhes normal data from Hawaii. Results of a principal component analysis of these data for reference point r = 0 are given in Table P3. In Figure P59e-P59g we plot the major axis defined by $\mathbf{e}^3$, and in Figure P59h we show the projection of the data onto the eigenplane $z_1 - z_2$, along with the corresponding variance ellipse. The results here are not dramatically different from the previous result, where we used data of mixed polarities, although some slight differences in the orientation of the major axis and variance size are noted. In order to better inspect the nature of the paleosecular variation at Hawaii during the Brunhes, we perform a principal component analysis of the covariance about the mean vector $\mathbf{r} = \overline{\mathbf{x}}$. In Table P3 we see that much of the secular variation is roughly parallel with the mean vector; the angular difference between the orientation of the two vectors is only 14.9°. The geometric form of the variance of the secular variation is shown in Figure P60, where we plot both the data and the variance ellipse in geographic and eigencoordinates. The utility of measuring the variance about the vectorial mean $\mathbf{r} = \overline{\mathbf{x}}$ and in the eigenspace $\mathbf{z}$ should now be obvious.

Directional analysis

Usually, paleomagnetists do not have complete vectorial data. Instead, directional data, consisting of inclination and declination values ($I(i)$, $D(i)$), are most commonly available. Therefore, let us consider a principal component analysis for directional-only data. The equivalent Cartesian expression of the data is

$$\begin{aligned}\hat{x}_1(i) &= \cos I(i) \cos D(i),\\ \hat{x}_2(i) &= \cos I(i) \sin D(i),\\ \hat{x}_3(i) &= \sin I(i).\end{aligned} \qquad \text{(Eq. 20)}$$

With N such directional data we can calculate their covariance about the defined origin $\mathbf{r} = (0, 0, 0)$

$$\hat{\mathbf{C}} = \frac{1}{N}\begin{pmatrix} \sum \hat{x}_1(i)^2 & \sum \hat{x}_1(i)\hat{x}_2(i) & \sum \hat{x}_1(i)\hat{x}_3(i) \\ \sum \hat{x}_2(i)\hat{x}_1(i) & \sum \hat{x}_2(i)^2 & \sum \hat{x}_2(i)\hat{x}_3(i) \\ \sum \hat{x}_3(i)\hat{x}_1(i) & \sum \hat{x}_3(i)\hat{x}_2(i) & \sum \hat{x}_3(i)^2 \end{pmatrix}. \qquad \text{(Eq. 21)}$$

As before, eigenvalues λ_m and eigenvectors $\mathbf{e}^m$ can be obtained for this matrix. Because all the data are unit vectors, the total variance measured relative to the origin is one and the trace of $\hat{\mathbf{C}}$ is unity:

$$\mathrm{tr}(\hat{\mathbf{C}}) = 1, \qquad \text{(Eq. 22)}$$

and so the sum of the three eigenvalues is determined,

$$\lambda_1 + \lambda_2 + \lambda_3 = 1. \qquad \text{(Eq. 23)}$$

This means that the eigenvalues have only two degrees of freedom. For a prolate variance ellipsoid, the approximate maximum angular deviation from the major axis along $\mathbf{e}^3$ is

$$\mathrm{MAD}_\mathrm{p} = \tan^{-1}\left[\sqrt{\frac{1-\lambda_3}{\lambda_3}}\right], \qquad \text{(Eq. 24)}$$

and for an oblate variance ellipsoid, the corresponding angular deviation from the plane normal to $\mathbf{e}^1$ is

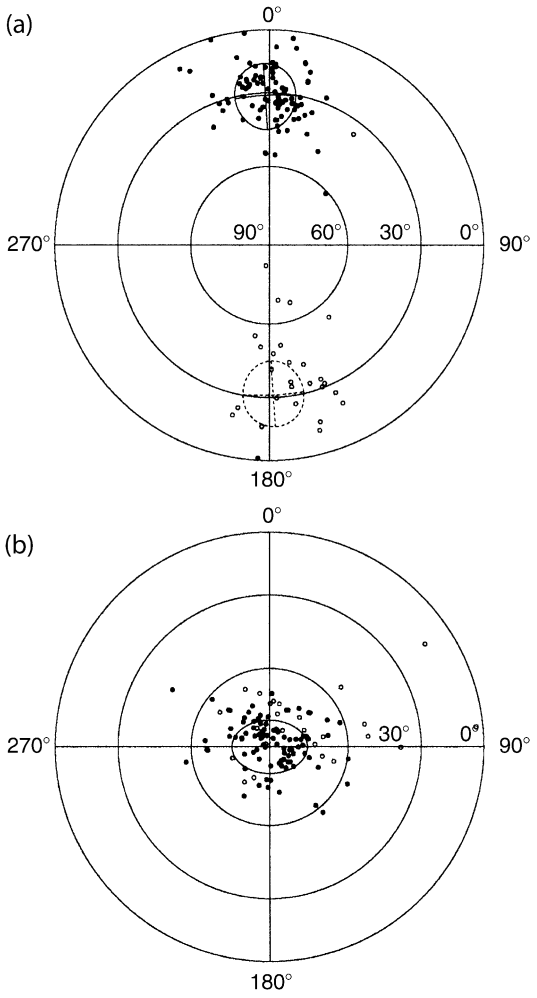

Figure P61 Equal-area projection of Hawaiian directional data, defined in (a) geographic coordinates and (b) eigen coordinates. Also shown are the projections of the variance minor ellipse, defined by λ_1 and λ_2. As is conventional, the azimuthal coordinate is declination (clockwise positive, 0°–360°), and the radial coordinate is inclination (from 90° in the center to 0° on the circular edge).

$$\mathrm{MAD}_\mathrm{o} = \tan^{-1}\left[\sqrt{\frac{\lambda_1}{1-\lambda_1}}\right]. \qquad \text{(Eq. 25)}$$

Hawaiian bimodal directions

As a final example, we return to the mixed polarity Hawaiian data covering the past 5 Ma, but this time we only consider the paleodirections $(I(i), D(i))$. Results of a principal component analysis of the corresponding unit vectors for reference point $r = 0$ are given in Table P3. In Figure P61a we plot the data, and the minor ellipse defined by λ_1 and λ_2, in an equal-area projection of geographic coordinates. After rotation into eigenspace (Figure P61b), we see, quite clearly, the asymmetric variance of paleodirections, thus, demonstrating the utility of inspecting directional data in the eigenspace $\mathbf{z}$.

Jeffrey J. Love

Bibliography

Hotelling, H., 1933. Analysis of a complex of statistical variables into principal components. *Journal of Educational Psychology*, **24**: 417–441, 498–520.

Jolliffe, I.T., 2002. *Principal Component Analysis*, 2nd edn. New York: Springer-Verlag.

Karhunen, K., 1947. Über lineare Methoden in der Wahrscheinlichkeitsrechnung. *Annales Academiae Scientiarum Fennocaeseries A1*, **37**: 3–79.

Kirschvink, J.L., 1980. The least-squares line and plane and the analysis of palaeomagnetic data. *Geophysical Journal International*, **62**: 699–718.

Loéve, M., 1977. *Probability Theory*, 4th edn. New York: Springer-Verlag.

Love, J.J. and Constable, C.G., 2003. Gaussian statistics for palaeomagnetic vectors. *Geophysical Journal International*, **152**: 515–565.

Mardia, K.V., 1972. *Statistics of Directional Data.* New York: Academic Press.

Pearson, K., 1901. On lines and planes of closest fit to systems of point in space. *Philosophical Magazine*, *series 6,* **2**: 559–572.

Schomaker, V., Wasser, J., Marsh, R.E. and Bergman, G., 1959. To fit a plane or a line to a set of points by least squares. *Acta crystallographica*, **12**: 600–604.

Strang, G., 1980. *Linear Algebra and Its Applications*, New York: Academic Press.

Cross-references

Bingham Statistics
Fisher Statistics
Magnetic Remanence, Anisotropy
Paleomagnetic Secular Variation
Statistical Methods for Paleovector Analysis

PROJECT MAGNET

Project Magnet is a comprehensive vector aeromagnetic surveying enterprise that spanned much of the last five decades. Under the direction of the United States Navy and management by the Naval Oceanographic Office, test flights began in 1951 and full operational capabilities were established in 1953. The project ran through 1994, ultimately contributing many thousands of track miles (see Figure P62) of geomagnetic data (Coleman, 1992). The data are available on CD-ROM through the National Geophysical Data Center (Hittelman *et al*., 1996).

The primary purpose of Project Magnet was to supply data in support of the World Magnetic Modeling (WMM) and charting program, which in turn supported civilian and military navigation requirements. The WMM has been incorporated into many global positioning system (GPS) receivers manufactured in the United States and has been used to control drift rates in inertial navigation systems. As a geophysical tool, the WMM has been useful as a reference measurement for Earth's core–mantle boundary field and as an aid in geophysical prospecting and resource evaluation.

Over the years, Project Magnet surveys have been performed using five different aircrafts, with each successive one improving in range, speed or altitude, navigational capabilities, and geophysical instrumentation. From 1953 to 1970 survey aircraft flew at 4615 m and most surveys were confined to remote ocean areas. Navigation methods in use at the time were periodic celestial fixes, LORAN, and dead reckoning. As a result, navigational accuracy was rather poor and was limited to about 5 nautical miles. Altitudes were determined using a baroclinic altimeter, with an uncertainty of ± 30 m. Observations of declination, inclination, and intensity (to an accuracy of ± 15 nT) were made using a self-orienting fluxgate magnetometer, while a towed, optically pumped metastable helium magnetometer measured field intensity to ± 4 nT. Until 1970, data acquisition systems consisted primarily of strip chart recorders and navigation logs. The majority of this data has been manually digitized.

The introduction of a new aircraft in 1970 permitted high level (over 4615 m) vector aeromagnetic surveying, usually conducted at altitudes between 6200 and 7700 m. During this era, the use of inertial navigation systems improved navigational accuracy to about 1 nautical mile, and in 1987, after the appearance of GPS, accuracies were further increased to several tens of meters, but only when a reliable signal was available. A baroclinic altimeter similar to the previous one was again the only source of altitude data. Improved magnetic measurements were facilitated by a fluxgate magnetometer, providing three vector components X, Y, and Z in the local reference frame to accuracies of ± 40 nT. An optically pumped metastable helium magnetometer mounted on a stinger extending from the rear of the aircraft measured intensity to ± 1 nT.

Major technological improvements arrived with the 1990s and by 1992 the Project Magnet aircraft had been fitted with an ASG-81 scalar magnetometer, a NAROD ring-core fluxgate vector magnetometer, and a ring-laser gyro (RLG) inertial system. The latter two instruments were mounted on a rigid beam in a magnetically clean area at the rear of the aircraft. The RLG was used primarily for attitude determination, while GPS, a radar system and a precision barometer were employed for altitude measurements, which were determined to a precision of less than 2 m. The GPS system was the primary navigational tool, with a circular error probability of 15 m. However, the accuracy of the magnetic measurements remained the same. Technological advancements also led to the incorporation of a number of other surveying capabilities, including gravity, ocean acoustics, and ocean temperature.

Survey data were calibrated by several low level "airswings" prior to and during the high level surveying. The airswings included straight and level passes as well as roll, pitch and yaw maneuvers in each cardinal direction at 1000 feet over a ground based observatory. The calibration data were used to model aircraft intrinsic magnetic fields that perturb the magnetometer data. The contaminating fields are due to: the permanently magnetized part of the aircraft; magnetization induced by the core field; and eddy currents driven by changes in the crustal and core fields as the aircraft passed through them. A compensation model, based on developments by Leliak (1961), involves a two-step iterative least squares solution for 21 coefficients, which characterize the contaminating fields, and three bias angles, which account for differences in the orientations of the vector magnetometer and the inertial navigation system. Measurements taken over all airswing maneuvers are then included in a least squares minimization of the difference between the magnitudes of the decontaminated aeromagnetic observations and the transformed ground based observations. This transformation involves upward continuation to aircraft altitude and rotation into the aircraft reference frame using roll, pitch and heading data.

The compensation model is imprecise in that it is based on the assumption that the coefficients are constant with respect to latitude and frequency of the airswing maneuvers. There have been attempts to account for these variations and the Project Magnet database includes compensation coefficients from repeated calibration flights at observatories over the globe. More importantly, Project Magnet orientation accuracy is insufficient to prevent contamination of the magnetic field vector components due to misalignment of the aircraft coordinate system (Parker and O'Brien, 1997). Because field intensity is immune from orientation errors, Parker and O'Brien (1997) show that simple spectral analysis of intensity and the three vector magnetic components as functions of along track distance may be used as a diagnostic for this contamination.

Although one of the primary goals of Project Magnet was to characterize the magnetic field generated in Earth's core, the majority of published studies exploiting Project Magnet data have been focused on the crustal part of the field, including numerous regional magnetic

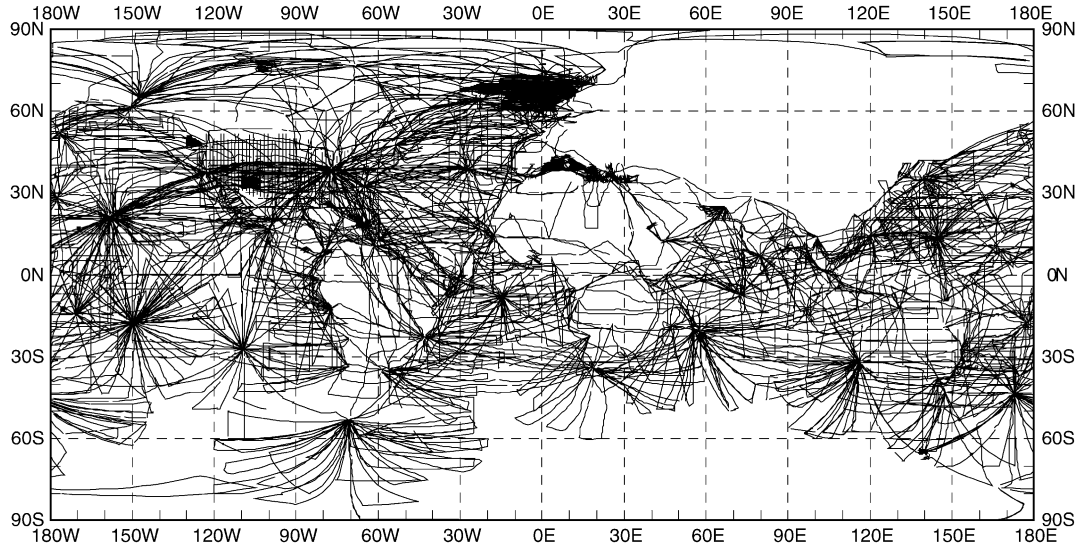

Figure P62 Coverage of Project Magnet aeromagnetic surveys, 1953–1994 (cylindrical equidistant projection). Reproduced by permission of the National Geophysical Data Center.

mapping efforts spread across the globe. These include sub-Saharan Africa (Green, 1976), South Georgia Island (Simpson and Griffiths, 1982), Iceland (Jonsson *et al*., 1991), and New Zealand (McKnight, 1996). A detailed study by Horner-Johnson and Gordon (2003) of short wavelength features (20–150 km) over the equatorial Pacific, suggests that magnetic anomalies associated with seafloor spreading are more clearly delineated by vector aeromagnetic data than by the traditional shipboard total field observations. O'Brien *et al*. (1999) developed a method, based on spectral analysis of Project Magnet data along great circle paths, to estimate the geomagnetic spatial spectrum of the oceanic crust for spherical harmonic degrees from $l \approx 60$ to 1200. Observational models based on satellite data had previously been limited to $l \approx 100$. Korte *et al*. (2002) observed that the agreement of the new model with satellite based observations was unsatisfactory for degrees $l < 100$, and found that O'Brien *et al*. had overcompensated for external magnetic field variations in their analysis. The improved model of Korte *et al*. (2002) achieves better agreement with theoretical and satellite based models of the spatial spectrum.

The advent of satellite based magnetic observations, in particular Magsat in the 1980s raised the question of agreement between aeromagnetic and spaced based geomagnetic observations. An early study by Won and Son (1982), using Project Magnet data spanning the continental US and upward continued to Magsat altitude, revealed agreement in gross features of the crustal field. Using an improved method for removing the core field (spherical harmonic degrees $l \leq 13$) and long wavelength external contributions, Wang *et al*. (2000) demonstrated excellent agreement between aeromagnetic and satellite data over the continental US, and suggest that an anomaly field derived from a combined dataset provides accurate estimates of the long wavelength crustal field.

David G. McMillan

Bibliography

Coleman, R.J., 1992. Project magnet high-level vector survey data reduction. In Langel, R.A., and Baldwin, R.T. (eds.), *Types and Characteristics of Data for Geomagnetic Field Modelling*. NASA Conference Publication 3153, pp. 215–248.

Green, A.G., 1976. Interpretation of project magnet aeromagnetic profiles across Africa. *The Geophysical Journal of the Royal Astronomical Society*, **44**: 203–228.

Hittelman, A.M., Buhmann, R.W., and Racey, S.W., 1996. *Project Magnet Data (1953–1994) CD-ROM User's Manual.* Boulder: National Geophysical Data Center.

Horner-Johnson, B.C., and Gordon, R.G., 2003. Equatorial pacific magnetic anomalies identified from vector aeromagnetic data. *Geophysical Journal International*, **155**: 547–556.

Jonsson, G., Kristjansson, L., and Sverrisson, M., 1991. Magnetic surveys of Iceland. *Tectonophysics*, **189**: 229–247.

Korte, M., Constable, C.G., and Parker, R.L., 2002. Revised magnetic power spectrum of the Oceanic crust. *Journal of Geophysical Research*, 107, EPM 6.

Leliak, P., 1961. Identification of magnetic field sources of magnetic airborne detector equipped aircraft. *IRE Transactions on Aerospace and Navigational Electronics*, **8**: 95–105.

McKnight, J.D., 1996. An updated regional geomagnetic field model for New Zealand. Institute of Geological and Nuclear Sciences Science Report: Report 96/4; M24/773; M24/774.

O'Brien, M.S., Parker, R.L, and Constable, C.G., 1999. Magnetic power spectrum of the Ocean crust on large scales. *Journal of Geophysical Research*, **104**: 29189–29201.

Parker, R.L., and O'Brien, M.S., 1997. Spectral analysis of vector magnetic profiles. *Journal of Geophysical Research*, **100**: 20111–20136.

Simpson, P., and Griffiths, D.H., 1982. The structure of the South Georgia Continental block. In Craddock, C. (ed.) *Antarctic Geoscience.* Madison, WI: University of Wisconsin Press, pp. 185–191.

Wang, B., Ravat, D., Sabaka, T., and Hildenbrand, T.G., 2000. Long-wavelength magnetic field for the conterminous US. from project magnet and magsat data. *Eos,Transactions of the American Geophysical Union*, **81**, GP71B-09.

Won, I.J., and Son, K.H., 1982. A preliminary comparison of the MAGSAT data and aeromagnetic data in the Continental US. *Geophysical Research Letters*, **9**: 296–298.

Cross-references

Aeromagnetic Surveying
Core-mantle Boundary
Electromagnetic Induction (EM)
Geomagnetic Spectrum, Spatial
Instrumentation, History of
Magsat
Upward and Downward Continuation

PROUDMAN-TAYLOR THEOREM

Geophysicists accept a suggestion traceable back to a paper by Elsasser (1939) that the near-alignment of the main geomagnetic field (see *Main field*) with the Earth's geographic polar axis is a manifestation of the influence on convective motions in the liquid, metallic outer *core* (*q.v.*) that is exerted by gyroscopic (Coriolis) forces associated with the Earth's diurnal rotation. Such forces render core motions anisotropic and highly sensitive to the mechanical and other (thermal and electromagnetic) boundary conditions imposed on the motions by the underlying solid inner *core* (*q.v.*) and the overlying *mantle* (*q.v.*) (for further references see Hide, 2000).

The influence of Coriolis forces on motions in spinning fluids is most pronounced in mechanically-driven flows satisfying the so-called Proudman-Taylor (PT) theorem. Stated in words, the theorem (see Eq. (5)) shows that "slow and steady hydrodynamical motion of an inviscid (and electrically insulating) fluid of constant density that is otherwise in steady "rigid-body" rotation will be the same in all planes perpendicular to the axis of rotation". Given in a paper by J. Proudman in 1916, the PT theorem was successfully tested by means of a laboratory experiment in which G.I. Taylor investigated the relative flow produced in a tank of water in rapid rotation about a vertical axis by the slow and steady horizontal motion of a solid body through the water (see Greenspan, 1968). In accordance with the theorem, the flow was highly two-dimensional nearly everywhere and the moving solid object carried with it a "Taylor column" of water extending axially throughout the whole depth of the tank.

We note here in passing (a) that the theorem had appeared much earlier in the literature, in a paper on tidal theory by S.S. Hough (Gill, 1982), and (b) that some writers find it convenient to refer to it as the "Proudman theorem" (Hide, 1977), to avoid confusion with another theorem, due to G.I. Taylor, concerning effects of Coriolis forces on fluid motions (see Greenspan, 1968; Hide, 1997).

Convective motions in the *core* (*q.v.*) cannot satisfy the PT theorem exactly because they are driven by buoyancy forces due to the action of gravity on density inhomogeneities, which give rise to axial variations of the horizontal components of the relative flow velocity (see Eq. (6)). Core motions are also influenced by Lorentz forces associated with electric currents and magnetic fields in the core, which in regions well below the *core-mantle boundary* (*q.v.*) may be comparable in strength with Coriolis forces (see Eqs. (1) and (2)). But—as in theoretical work in dynamical meteorology and oceanography, see e.g., Gill, 1982; Pedlosky, 1987—certain basic dynamical processes and phenomena can be elucidated by means of simplified theoretical models in which axial variations of the nonaxial components of the relative flow velocity are neglected in the first instance.

Characteristic shear waves that occur in fluids subject to Coriolis and/or Lorentz forces—such as Rossby waves, Alfvén (*magnetohydrodynamic waves* (*q.v.*)) and related hybrid waves (one important type of which may underlie the *geomagnetic secular variation* (*q.v.*))—have been investigated in this way. And so have other phenomena, such as torsional oscillations of the core-mantle system associated with angular momentum transfer within the Earth's core (Hide *et al.*, 2000) and differential rotation produced in a rapidly rotating spherical fluid annulus by *potential vorticity* (*q.v.*) mixing (Hide and James, 1983).

Geostrophic and magnetostrophic flows

Flows satisfying the PT theorem belong to a wider class of "geostrophic" flows (see Gill, 1982; Pedlosky, 1987), for which the horizontal component of the local pressure gradient, **grad** p, is closely balanced by the horizontal component of the Coriolis force (per unit volume), $2\rho\boldsymbol{\Omega}\mathbf{x}\boldsymbol{u}$ (see Eq. (1)), but torques produced by buoyancy forces associated with horizontal density gradients give rise to systematic axial variations in the horizontal components of $\boldsymbol{u}$ (see Eqs. (5) and (6)).

Consider a moving element of fluid of density ρ which at time t is located at a general point P with vector position $\boldsymbol{r}$ in a frame of reference that rotates with angular velocity $\boldsymbol{\Omega}$ relative to an inertial frame. Newton's second law is conveniently expressed as follows (see Hide, 1971):

$$2\rho\boldsymbol{\Omega}\mathbf{x}\boldsymbol{u} + \mathbf{grad}\, p + \rho\, \mathbf{grad}\, V + \boldsymbol{A} = 0 \qquad \text{(Eq. 1)}$$

where the Eulerian flow velocity at P and the corresponding pressure and the potential due to gravitational plus centripetal effects are denoted by $\boldsymbol{u}$, p, and V respectively. The "ageostrophic" term, $\boldsymbol{A}$, in Eq. (1) is defined as follows:

$$\boldsymbol{A} = \rho[\partial\boldsymbol{u}/\partial t + (\boldsymbol{u}.\mathbf{grad})\boldsymbol{u} - \boldsymbol{r}\mathbf{x}\mathrm{d}\boldsymbol{\Omega}/\mathrm{d}t] + \mathbf{curl}\,(\nu\rho\boldsymbol{\omega}) - \boldsymbol{j}\mathbf{x}\boldsymbol{B} \qquad \text{(Eq. 2)}$$

if $\boldsymbol{\omega} = \mathbf{curl}\,\boldsymbol{u}$, the relative vorticity vector at P, and ν denotes the coefficient of kinematic viscosity. The term $\boldsymbol{j}\mathbf{x}\boldsymbol{B}$ in Eq. (2) is needed when dealing with electrically conducting fluids; it represents the Lorentz force per unit volume acting on the fluid element if $\boldsymbol{j}$ is the electric current density and $\boldsymbol{B}$ the magnetic field at P.

The flow is said to be *geostrophic* in regions where $\boldsymbol{A}$ is negligible in comparison with other terms in Eq. (1). Within the Earth's *core* (*q.v.*), such regions probably arise in its upper reaches (LeMouël, 1984; Hide, 1995) where the toroidal part of the *geomagnetic field (q.v.)* is no stronger than the poloidal part and the corresponding Lorentz term is typically no more than a few parts percent of the Coriolis term in magnitude. On the other hand, the flow is said to be in "*magnetostrophic"* (rather than geostrophic) balance in any regions where the Lorentz force provides the main contribution to $\boldsymbol{A}$ and is comparable in magnitude with $2\rho\boldsymbol{\Omega}\mathbf{x}\boldsymbol{u}$**.** Such regions probably arise at depth within the core, where the toroidal part of the magnetic field may be an order of magnitude stronger than the poloidal part.

Following Hide, 1971, now consider the balance of torques acting on the moving fluid element by taking the **curl** of Eq. (1), thereby obtaining the so-called "vorticity" equation in the useful form

$$2\boldsymbol{\Omega}.\mathbf{grad}\,(\rho\boldsymbol{u}) + \mathbf{grad}\, V \,\mathrm{x}\, \mathbf{grad}\,\rho + \mathbf{curl}\,\boldsymbol{A} + 2\boldsymbol{\Omega}C = 0. \qquad \text{(Eq. 3)}$$

Here $C = \partial\rho/\partial t$ which, by the mass continuity equation, satisfies

$$\mathbf{div}\,(\rho\boldsymbol{u}) + C = 0. \qquad \text{(Eq. 4)}$$

The PT theorem follows immediately from Eq. (3), for when the conditions $\boldsymbol{A} = 0$, **grad** $\rho = 0$ and $C = 0$ are satisfied, the equation reduces to

$$(2\boldsymbol{\Omega}.\mathbf{grad})\,\boldsymbol{u} = 0. \qquad \text{(Eq. 5)}$$

The above equation implies that all three components of $\boldsymbol{u}$ are independent of the axial coordinate. When the restriction to cases of fluids of constant density is relaxed we have

$$2\boldsymbol{\Omega}.\mathbf{grad}\,(\rho\boldsymbol{u}) + \mathbf{grad}\, V\,\mathbf{x}\,\mathbf{grad}\,\rho = 0, \qquad \text{(Eq. 6)}$$

in place of Eq. (5).

Flow patterns satisfying Eqs. (5) or (6) are constrained by Coriolis forces to have no circulation in (meridian) planes containing the axis of rotation. But by Eq. (6) the horizontal component of $\boldsymbol{u}$ is not independent of the axial direction, except in regions where **grad** ρ has no horizontal component. We note here in passing (a) that the s*pecific helicity,* $\boldsymbol{u}.\boldsymbol{\omega}$,—a quantity of importance in *dynamo theory* (*q.v.*)—of flows satisfying Eq. (6) is generally nonzero (Hide, 1976), and (b) that with certain geometrical simplifications Eq. (6) leads to the meteorologist's "*thermal wind*" equation (*q.v.*) relating the rate of increase

of the speed and direction of the geostrophic wind with height in the atmosphere to the horizontal gradient of temperature.

Ageostrophic effects and detached shear layers

The full expression of the laws of mechanics given by Eq. (1) is, of course, *prognostic,* in the sense that when solved simultaneously with the full equations of thermodynamics and electrodynamics under all the relevant boundary conditions the equation gives the fields of all the dependent variables, p, $\boldsymbol{u}$, ρ, $\boldsymbol{j}$, $\boldsymbol{B}$ etc. But the expression for geostrophic flow to which Eq. (1) reduces in regions where the ageostrophic term, $\boldsymbol{A}$, is negligible is *diagnostic* (rather than prognostic), in the sense that it provides useful relationships between $\boldsymbol{u}$, p and ρ, but it cannot give full solutions satisfying all the relevant boundary conditions.

It follows that flows in real systems cannot be geostrophic everywhere. Regions of ageostrophic flow involving length scales so short that $\boldsymbol{A}$ is comparable in magnitude with $2\rho\boldsymbol{\Omega}\boldsymbol{x}\boldsymbol{u}$ must be present not only on bounding surfaces (in Ekman-Hartmann and Stewartson boundary layers (see core, boundary layers)) but also within the main body of the fluid, in "detached shear layers". It is within such regions, where effects due to Coriolis forces are countered by strong ageostrophic effects, that meridional circulation can occur. Detached shear layers formed the "walls" of the so-called "Taylor column" of fluid that remained attached to the moving solid body in G. I. Taylor's experiment. Geophysical examples of ageostrophic detached shear layers embedded in geostrophic flows are the jet streams and their associated frontal systems seen in the Earth's atmosphere and "western boundary" currents such as the Gulf Stream in the Atlantic Ocean and the Kuroshio Current in the Pacific Ocean (see Gill, 1982; Pedlosky, 1987).

Amongst the various laboratory investigations that were stimulated directly by the original "Taylor column" experiment were several studies of the effect of the inner spherical boundary on patterns of mechanically-driven (Greenspan, 1968; Hide, 1977) and buoyancy-driven flows in a rotating spherical annulus of fluid. These studies clearly demonstrated what general arguments based on Eq. (5) or (6) predict, namely that near the imaginary "tangent cylindrical surface" (see Inner core tangent cylinder) in contact with the equator of the inner spherical surface and extending axially throughout the fluid, a detached shear layer would form inhibiting mixing of fluid in the "polar" regions inside the cylinder with fluid in the "equatorial" region outside the cylinder. Such behaviour is thought to bear on core dynamics and the influence of the solid inner core on structure of the geomagnetic field (for further references see Hide, 2000 and Hide, 1966a,b).

Raymond Hide

Bibliography

Elsasser, W.M., 1939. On the origin of the Earth's magnetic field. *Physical Reviews*, **55**: 489–497.

Gill, A.E., 1982. *Atmosphere-Ocean Dynamics.* New York: Academic Press.

Greenspan, H.P., 1968. *The Theory of Rotating Fluids.* Cambridge: Cambridge University Press.

Hide, R., 1966a. The dynamics of rotating fluids and related topics in geophysical fluid dynamics. *Bulletin of the American Meteorological Society*, **47**: 873–885.

Hide, R., 1966b. Free hydromagnetic oscillations of the Earth's core and the theory of the geomagnetic secular variation. *Philosophical Transactions of the Royal Society of London*, **A259**: 615–647.

Hide, R., 1971. On geostrophic motion of a nonhomogeneous fluid. *Journal of Fluid Mechanics*, **49**: 745–751.

Hide, R., 1976. A note on helicity. *Geophysical (Astrophysical) Fluid Dynamics*, **7**: 157–161.

Hide, R., 1977. Experiments with rotating fluids; Presidential address. *Quarterly Journal of the Royal Meteorological Society*, **103**: 1–28.

Hide, R., 1995. The topographic torque on the rigid bounding surface of a rotating gravitating fluid and the excitation of decadal fluctuations in the Earth's rotation. *Geophysical Research Letters*, **22**: 1057–1059.

Hide, R., 1997. On the effects of rotation on fluid motions in containers of various shapes and topological characteristics. *Dynamics of Atmospheres and Oceans*, **27**: 243–256.

Hide, R., 2000. Generic nonlinear processes in self-exciting dynamos and the long-term behaviour of the main geomagnetic field, including superchrons. *Philosophical Transactions of the Royal Society of London*, **A358**: 943–955.

Hide, R., Boggs, D.H., and Dickey, J.O., 2000. Angular momentum fluctuations within the Earth's core and torsional oscillations of the core-mantle system. *Geophysical Journal International*, **143**: 777–786.

Hide, R., and James, I.N., 1983. Differential rotation produced by large-scale potential vorticity mixing in a rapidly-rotating fluid. *Geophysical Journal of the Royal Astronomical Society*, **74**: 301–312.

Le Mouël, J.-L., 1984. Outer core geostrophic flow and the secular variation of the Earth's magnetic field. *Nature*, **311**: 734–735.

Pedlosky, J., 1987. *Geophysical Fluid Dynamics*, 2nd edn. New York: Springer-Verlag.

Cross-references

Core, Boundary Layers
Core Convection
Core-Mantle Boundary
Core Motions
Equilibration of Magnetic Field, Weak and Strong Field Dynamos
Geodynamo
Geomagnetic Secular Variation
Inner Core Tangent Cylinder
Length of the Day Variations, Decadal
Magnetohydrodynamic Waves
Oscillations, Torsional
Potential Vorticity and Potential Magnetic Field Theorems
Thermal Wind